uOttawa

L'Université canadienne
Canada's university

FACULTÉ DES ÉTUDES SUPÉRIEURES ET POSTOCTORALES

uOttawa

L'Université canadienne
Canada's university

FACULTY OF GRADUATE AND POSDOCTORAL STUDIES

Julio Angel Infante Sedano
AUTEUR DE LA THÈSE / AUTHOR OF THESIS

Ph.D. (Civil Engineering)
GRADE / DEGREE

Department of Civil Engineering
FACULTÉ, ÉCOLE, DÉPARTEMENT / FACULTY, SCHOOL, DEPARTMENT

A Modified Ring Shear Test Device for Testing Hydro-mechanical Behaviour of Saturated Soils
TITRE DE LA THÈSE / TITLE OF THESIS

Sai Vanapalli
DIRECTEUR (DIRECTRICE) DE LA THÈSE / THESIS SUPERVISOR

Vinod Garga
CO-DIRECTEUR (CO-DIRECTRICE) DE LA THÈSE / THESIS CO-SUPERVISOR

EXAMINATEURS (EXAMINATRICES) DE LA THÈSE / THESIS EXAMINERS

Erman Evgin

Serge Leroueil

Mamadou Fall

Tim Law (Absent)

Gary W. Slater
Le Doyen de la Faculté des études supérieures et postdoctorales / Dean of the Faculty of Graduate and Postdoctoral Studies

A Modified Ring Shear Test Device For Determining The Hydro-Mechanical Behaviour Of Unsaturated Soils

Julio Ángel Infante Sedano

A Dissertation
Submitted to School of Graduate Studies
Under the joint supervision of

Dr. Vinod K. Garga, P.Eng., F. EIC.
and
Dr. Sai K. Vanapalli, P.Eng.

in partial fulfillment of the requirements for the degree of

Doctor of Philosophy in Civil Engineering

Department of Civil Engineering
Université d'Ottawa/University of Ottawa
Ottawa,Ontario
Canada K1N 6N5

May 2006

The Doctor of Philosophy in Civil Engineering is a joint program between Carleton University and University of Ottawa, which is administered by the Ottawa-Carleton Institute for Civil Engineering.

Your file Votre référence
ISBN: 978-0-494-18586-5
Our file Notre référence
ISBN: 978-0-494-18586-5

Abstract

This thesis presents the design details of an automated modified ring shear apparatus for the testing of unsaturated soils using the axis translation technique. The system is fully automated and it can be used for conducting Constant Load and constant Suction (CLS) shear tests, Constant Volume and constant Suction (CVS) shear tests, Constant Load and constant Water content (CLW) shear tests as well as Constant Volume and constant Water content (CVW) shear tests. In addition to shear tests, the soil-water retention curve (SWRC) can also be generated for the same specimen in the same testing device. The principal advantages of the device include its ability to shear unsaturated soils to very large deformations as well as conducting tests under constant volume conditions. Analysis of the experimental data using these characteristics suggests that the volumetric changes of the sheared specimen are not the only factor affecting the changes of its water content under constant matric suction conditions. In addition, the experimental evidence suggests that shear deformations much greater than those typically used in the testing of unsaturated soils are required if an ultimate water content equilibrium condition is to be reached. Such an equilibrium condition is required if critical state data is to be determined for unsaturated soils.

The thesis also presents the design and use of additional equipment utilised for testing unsaturated soils. This includes the use of an electronic balance to measure the change in water volume of the specimen, and provides details on how the readings of the balance can be stabilized to remove the noise caused by the connection of the tubes to the overflow jar. A simple technique relying solely on the measurement of the water volume change to determine the volume of diffused air removed by the flushing operations is also presented. The other pieces of equipment described include a volume gauge/air trap that can be used to measure the water volume changes of unsaturated soil specimens, and a simple, robust, and precise pressure gauge.

Résumé

Cette thèse présente les détails de conception d'un appareil de cisaillement annulaire modifié pour l'étude des sols non-saturés, utilisant la technique de translation de l'axe. Le système est entièrement automatisé et peut être utilisé pour effectuer des essais de cisaillement à Charge et à Succion Constantes (CSC), des essais de cisaillement à Volume et à Succion Constants (VSC), des essais de cisaillement à Charge et à teneur en Eau Constantes (CEC), ainsi que des essais de cisaillement à Volume et à teneur en Eau Constants (VEC). De plus, la courbe de rétention d'eau (CRE) d'un sol non-saturé peut être déterminée dans le même appareil. Parmi les principaux avantages de l'appareil se trouvent la possibilité de soumettre un échantillon de sol non-saturé à de très grandes déformations de cisaillement, ainsi qu'à la possibilité d'effectuer des essais dans des conditions de volume constant. L'analyse de résultats expérimentaux tirant profit de ces caractéristiques suggère que les changements volumétriques des échantillons soumis à un effort de cisaillement ne sont pas seuls responsables du changement de la teneur en eau de l'échantillon dans des conditions de succion constante. Les résultats suggèrent également que des déformations de cisaillement bien supérieures aux valeur normalement atteintes peuvent s'avérer nécessaires afin d'atteindre un état d'équilibre de la teneur en eau lors du cisaillement. Il est nécessaire d'atteindre un tel état d'équilibre pour étudier l'état limite des sols non-saturés.

La thèse présente aussi les détails de conception et d'utilisation de pièces d'équipement utilisées lors de la recherche. Celles-ci comprennent l'utilisation d'une balance électronique pour mesurer le changement de volume d'eau du spécimen. La procédure de stabilisation des données rendue nécessaire par le raccordement de tubes au récipient de mesure est aussi décrite en détail. Une technique n'utilisant que la mesure du volume d'eau pour déterminer le volume d'air dissout est également présentée. Les autres pièces d'équipement comprennent une jauge de volume/trappe à bulles d'air pouvant être utilisée pour mesurer le changement de volume d'eau d'un spécimen non-saturé, ainsi qu'une jauge de pression d'air robuste, précise, et de fabrication simple.

Acknowledgments

I would first thank for their ever presence and support my parents, who have provided continuous encouragement and assistance. I would also like to thank my two co-supervisors, Dr. Vinod Garga, and Dr. Sai Vanapalli, for their guidance and mentorship. Great thanks also to the Geotechnical technician at Ottawa U. Richard Moore, who has provided immeasurable assistance not only in the development of the laboratory equipment, but also in the transmission of the knowledge and insight that have made my own personal contributions to the lab equipment more valuable. Many thanks also to the great support staff, and in particular to the staff from the machine shop, most notably Brent for not only producing the parts required, but for actively ensuring that the design specs made sense in light of practical limitations, and for catching the little mistakes that can creep up in the drawings. I would also like to thank my fellow graduate students in the geotechnical program, and in particular Kenton Power, who has given me great assistance in some of the most labour intensive aspects of the program, as well as Elizabeth Garven and Cevat Çatana for their help in the last minute preparations for final submission.

Table Of Contents

1 Introduction....2
1.1 Background....2
1.2 Scope of Research....3
1.3 Research objectives....4
1.4 Outline of thesis....5
2 Literature review....7
2.1 Introduction....7
2.2 Modelling the shear strength of unsaturated soils....7
2.2.1 Single stress-state variable approach....7
2.2.2 Two stress-state variable approach....8
2.2.3 Shear strength prediction methods....9
2.2.4 Critical state....13
2.2.5 Critical state frameworks....14
2.3 Determining the shear strength of unsaturated soils....19
2.3.1 Modified triaxial tests....19
2.3.2 Modified direct shear tests....21
2.4 Water Content Measurement and Air Diffusion....23
2.5 Concluding remarks....26
2.6 Figures....27
3 Axis Translation Equipment....46
3.1 Introduction....46
3.2 Compressible air column pressure gauge....46
3.2.1 Theoretical Concept....47
3.2.2 Application....50
3.2.3 Graduated gauge scale....51
3.2.4 Calibration....52
3.2.5 Effect of Atmospheric Pressure....52
3.2.6 Limitations of the air pressure gauge....53
3.2.7 Typical Result....54
3.3 Integrated Volume Gauge and Air Trap....55
3.3.1 Operation of the Device....56
3.3.2 Air Phase Isolators....57
3.4 Conclusion....58
3.5 Figures....59
4 Modified Ring Shear Cell....79
4.1 Introduction....79
4.2 The Cell....80
4.2.1 Cell base....81
4.2.2 End platens....81

4.2.3 Cell Cover....82
4.2.4 Torque Arm....82
4.3 Flushing system and water volume measurement....83
4.4 Automation....85
4.4.1 Instrumentation....86
4.4.2 Pneumatic Control Systems....86
4.5 Compaction....87
4.5.1 Compaction Equipment....87
4.5.2 Specimen compaction procedure....88
4.6 Types of Tests....88
4.6.1 Constant Load with Constant Suction (CLS) Tests....89
4.6.2 Constant Volume with Constant Suction (CVS) Tests....89
4.6.3 Constant Load with Constant Water content (CLW) Tests....89
4.6.4 Constant Volume with Constant Water Content (CVW) Tests....90
4.6.5 Soil-Water Retention Curve (SWRC)....90
4.7 Summary....91
4.8 Figures....93
5 Experimental results....110
5.1 Introduction....110
5.2 Soil Characterization....111
5.2.1 Conventional soil properties....111
5.2.2 Static Compaction....112
5.2.3 Saturated shear strength....113
5.2.4 SWRC....114
5.3 Testing program....115
5.4 Specimen preparation....117
5.5 Consolidation Phase....117
5.6 Suction increment Stage....118
5.6.1 Correcting for air infiltration....118
5.6.2 Correcting for evaporation/condensation....122
5.7 CLS Test Results....123
5.8 CVS Test Results....127
5.9 Critical State....129
5.10 Average skeleton stress....132
5.11 Summary....134
5.12 Figures....135
6 SWRC and Shear Strength....185
6.1 Introduction....185
6.2 Dhanauri clay....186
6.3 Indian Head till....190
6.4 Summary....196
6.5 Figures....197
7 Summary and Conclusions....222
7.1 Summary....222
7.2 Conclusions....223
7.3 Suggestions for further research....225

8 References..227

1 Introduction

1.1 Background

Shear strength and volume change form important engineering properties in the design of geotechnical and geo-environmental structures such as earth dams, retaining walls, pavements, soil liners, and soil covers. Many of these soil structures are typically in a state of unsaturated condition and often do not attain fully saturated conditions during their design life period.

The shear strength of an unsaturated soil can be determined using modified direct shear or modified triaxial shear testing devices [Escario (1980), Escario and Jucá (1989), Gan et al. (1988), Vanapalli et al. (1996), Caruso and Tarantino (2004)]. Experimental studies related to determination of the shear strength of unsaturated soils are time consuming and require extensive laboratory facilities.

In recent years, several semi-empirical procedures were proposed to predict the shear strength of unsaturated soils [Vanapalli et al. (1996), Fredlund et al. (1996), Khalili and Khabbaz (1997), Öberg and Sällfors (1997), Bao et al. (1998), Xu and Sun (2001), Tekinsoy *et al.* (2004)]. These procedures use the effective shear strength parameters (c', ϕ') along with the soil-water retention curve (SWRC) data to predict the shear strength of unsaturated soils. The SWRC defines the relationship between the soil suction and gravimetric or volumetric water content, or the degree of saturation. The prediction procedures use the SWRC as a tool as there is a strong relationship between water content and the shear strength of a soil. The information of the geometry and distribution of the water in the liquid phase and the stress within the pore water is derived from the SWRC and used in the prediction of the shear strength unsaturated soils [Barbour (1998)].

The soil-water retention curves are conventionally measured using Tempe cell or the pressure plate apparatus on specimen that are typically 50 mm in diameter and 20 mm in height. The volume change of the soil specimen is not commonly measured while determining the soil-water retention curves. In several cases, the shear strength of an unsaturated soil is predicted using the soil-water retention curve measured without the application of any loading (i.e., conventional SWRC). In other words, the soil-water retention curve is measured without taking into account the influence of loading and the resulting volume change. The volume change with respect to soil suction is also ignored assuming it to be relatively small. From a practical perspective, the soil will be subjected to some loading and there will be volume change both during the loading and as well as the shearing stage.

None of the procedures available in the literature have addressed the influence of the volume change behaviour on the prediction of the shear strength of unsaturated soils. Analysis of available data suggests significant differences are possible in the SWRC obtained from sheared and unsheared specimens [Infante Sedano et al. (2002), Vanapalli et al. (2003)]. This in turn can affect appreciably the predicted shear strength of the soil, and the error in shear strength values increases with the matric suction.

1.2 Scope of Research

Through this thesis an attempt is made to understand the strengths and weaknesses of using the SWRC as tool in the determination of the shear strength of unsaturated soils. For example, the shear strength of compacted soils is predicted using the SWRC measured on a compacted specimen. The influence of stress history and volumetric changes are commonly not considered in the prediction of the shear strength of unsaturated soils. Therefore, there can be significant differences between the measured and predicted values of shear strength if the appropriate SWRC is not used. For this reason, the rationale for the choice of the SWRC should therefore be explored for better understanding the limitations of the presently used prediction procedures.

More recently, several investigators [Alonso et al (1990), Wheeler & Sivakumar (1995), Cui & Delage (1996), Rampino et al. (2000)] have developed critical state models for unsaturated soils. For development of such models high quality experimental data of soils in unsaturated conditions is required. This is only possible with the use of modified equipment triaxial or direct shear test devices. Such devices, however, allow for limited deformations, and may not always be adequate for the study of the critical state behaviour of unsaturated soils, which can sometimes require very large deformations to be achieved.

In addition, it is also important to collect all the data of volume change and shear strength precisely with the application of corrections with respect to diffusion, absorption and evaporation. Many of the commercially available equipment do not have the capabilities to gather the above data. Through this thesis, a conventional ring shear apparatus is modified for the purpose of testing the shear strength of unsaturated soils applying all these corrects.

Conventionally, the SWRC are developed using Tempe cells or pressure plate apparatus are not particularly convenient for applying pressures in the low suction range. Simple and economical equipment for the measurement of SWRC both for coarse and as well as fine-grained soils is required.

1.3 Research Objectives

The research program undertaken aims to modify a ring shear device to perform tests on unsaturated soils. This device would be uniquely suited for investigating the hydro-mechanical properties of unsaturated soils. It will allow for very large shear deformations to be applied, under controlled load or controlled volume conditions under either controlled suction or controlled water content conditions.

The study also aims to verify the shear strength envelope at large deformations with respect to matric suction. There currently exists only limited data in the literature on the critical state conditions for unsaturated states. In particular, the test data should provide measurements of the water content changes of the specimen, together with its stress state and volumetric changes to allow for a complete analysis.

As such, this research also aims to study the changes in water content occurring in specimen sheared under constant volume conditions and its implication regarding the SWRC of the specimen. This change in SWRC is also important in determining the true relationship between water content and shear strength of the unsaturated soil.

Finally, it will be necessary to examine the validity of some predictive methods for predicting the shear strength of unsaturated soils based on the SWRC properties of the soil.

The research program undertaken involves the following key objectives:

- To design and test a modified ring shear apparatus for determining shear strength of unsaturated soils under different loading conditions with volume change measurements applying various corrections.
- To conduct a series of controlled load and controlled suction (CLS) tests to investigate the influence of the volume changes during the shearing stage on the SWRC and its influence on the shear strength of an unsaturated soil.
- To conduct a series controlled volume and controlled suction tests (CVS) to assess the influence of the non-volumetric effects of the shearing process on the SWRC.
- To develop simple and precise measuring techniques for the determination of the matric suction and water content of unsaturated soil specimens.
- To examine the use of the SWRC as a tool in the prediction of the critical state strength of an unsaturated soil.

1.4 Outline of Thesis

Chapter 2 presents a review of the literature of the shear strength of unsaturated soils. The focus was mainly directed towards the testing techniques for the measurement of shear strength, critical-state frameworks for interpreting unsaturated soil behaviour and summarizing some of methods used for predicting the shear strength of unsaturated soils using the SWRC.

Chapter 3 describes the design details of the modified ring shear apparatus. The modifications to the body of the cell, as well as the attached components are presented.

Chapter 4 describes the development of equipment which include simple and precise measuring techniques for the determination of the matric suction and water content of unsaturated soil specimens.

Chapter 5 presents the shear strength results and analysis obtained from the modified ring shear tests. It also describes the correction methods, and corresponding analysis of data, applied to the water content change readings.

Chapter 6 presents a rigorous approach to the determination of shear strength of unsaturated soils using the SWRC.

Chapter 7 presents the conclusions of the study and recommendations for further research and development.

Appendix A presents drawings of the various components of the modified ring shear test device.

Appendix B presents a computer program for the generation of pressure gauge scales.

Appendix C describes the comparative analysis technique of shear strength data from the triaxial and direct shear tests.

2 Literature Review

2.1 Introduction

Several investigators studied the shear strength behaviour of unsaturated soils since 1960 [Bishop and Donald (1961), Blight (1967), Satija (1978), Fredlund et al. (1978), Escario and Sáez (1986), Wheeler (1988), Alonso et al. (1990), Toll (1990), de Campos and Carrillo (1995), Maatouk et al. (1995), Vanapalli et al. (1996), Öberg and Sällfors (1997), Rassam and Williams (1999), Herkal et al., (1999), Murray (2002), Blatz and Graham (2003), Chiu and Ng (2003), Yin (2003), Tarantino and Tombolato (2005)]. However, there are few studies reported in the literature where both the mechanical and flow behaviour results were reported in an integrated approach to better understand the engineering behaviour of unsaturated soils. There is still little experimental evidence of the effect of hydro-mechanical coupling on the shear strength of unsaturated soils [Tarantino and Tombolato (2005)].

2.2 Modelling the Shear Strength of Unsaturated Soils

Modelling of the shear strength of unsaturated soils requires a good understanding of the several factors that influence the shear strength. The main factor affecting the shear strength of the unsaturated soils, other than the applied net normal stress (which is defined as the difference of the net normal stress σ_n, and the pore air pressure, u_a, $(\sigma_n$-$u_a)$), is the stress state variable matric suction, $(u_a - u_w)$. This variable is defined as the difference between the pore air pressure, u_a, and the pore water pressure, u_w

2.2.1 Single stress-state variable approach

Several investigators have attempted to extend the use of a single stress state variable of saturated soils introduced by Terzaghi to study the shear strength of unsaturated soils [Aitchison and Donald (1956), Bishop and Donald (1961), Bishop and Blight (1963), Burland (1965)].

Bishop (1959) expressed the shear strength of unsaturated soil in terms of a modified effective stress variable that integrated both the matric suction, $(u_a - u_w)$ and the net normal stress, $(\sigma - u_a)$.

$$\sigma' = (\sigma - u_a) + \chi (u_a - u_w) \qquad [2.1]$$

where:

σ = total normal stress

u_a = pore air pressure

u_w = pore water pressure

χ = empirical parameter

Jennings and Burland (1962) expressed reservations about the use of the modified effective stress principle. Although the modified effective stress equation appeared to explain the shear strength behaviour of unsaturated soils, it could not explain simultaneously the shear strength and volume change behaviour (i.e., mechanical behaviour). Morgenstern (1979) commented that the equation would have little impact in practice due to the fact that χ was different when determined for volume change in comparison to shear strength.

2.2.2 Two stress-state variable approach

Further studies eventually led to the use of the two stress-state variables. This approach permits the formulation of constitutive equations to describe separately the shear strength and volume change behaviour of unsaturated soils without having to find a single-valued effective stress equation [Fredlund and Rahardjo (1993)].

Fredlund and Morgenstern (1977) proposed that any pair of the following stress fields could be considered:

$(\sigma - u_a)$ and $(u_a - u_w)$

$(\sigma - u_w)$ and $(u_a - u_w)$

or

$(\sigma - u_a)$ and $(\sigma - u_w)$

The choice of using as the two stress state variables, the matric suction $(u_a - u_w)$ and the excess of total stress above the air pressure, $(\sigma - u_a)$, or net normal stress has special advantage as calculating the stress state of typical field conditions where pore-air pressure, u_a is assumed to be atmospheric (i.e., 0) is equal to the total normal stress. The net normal stress variable is therefore readily calculated as the total overburden stress.

Fredlund et al. (1978) proposed an extension to the Mohr-Coulomb failure criterion which incorporated both stress state variables and a new friction angle ϕ^b relating the changes in shear strength to the changes in matric suction $(u_a - u_w)$.

$$\tau = c' + (\sigma - u_a)\tan\phi' + (u_a - u_w)\tan\phi^b \qquad [2.2]$$

where c' and ϕ' are the saturated effective stress parameters.

Based on limited data, this friction angle, ϕ^b was originally assumed to be constant thus describing a failure plane in tri-dimensional space. It was later demonstrated from increased experimental evidence that the failure envelope was nonlinear with respect to matric suction [Escario & Sáez (1986), Fredlund et al. (1987)].

2.2.3 Shear strength prediction methods

The single stress state variable approach proposed by Bishop (1959) had the limitation to couple together matric suction and net normal stress using a soil parameter, χ. This relationship was useful to highlight the influence of degree of saturation and the contribution of the matric suction to the shear strength of unsaturated soils.

Different methods have been investigated in recent years for the prediction of unsaturated shear strength based on parameters readily obtained from common tests.

Vanapalli et al. (1996) proposed a general, non-linear function for predicting the shear strength of an unsaturated soil using the soil-water retention curve and the saturated shear strength parameters (i.e., c' and ϕ'). The shear strength function is given below:

$$\tau = c' + (\sigma - u_a)\tan\phi' + \Theta^{\kappa}(u_a - u_w)\tan\phi' \qquad [2.3]$$

where:

Θ = $\dfrac{\theta}{\theta_s}$

θ = volumetric water content

θ_s = volumetric water content at saturation

κ = fitting parameter.

An equation similar in form was also proposed by Fredlund et al. (1996), based on theoretical studies proppsed by Vanapalli (1994). This is based on the Fredlund et al. (1978) equation; however, the term *tan* ϕ^b is replaced by a composite term $\Theta^{\kappa}\tan\phi'$. The value of Θ is equal to the degree of saturation. This method is conceptually different from Bishop's method which combines net normal stress and matric suction into a single effective stress state variable. In this approach both the stress state variables are kept rigorously separated. However, mathematically, they take a similar form, where the expression Θ^{κ} replaces the parameter χ. Studies have shown that κ parameter can be expressed as a function of plasticity index Vanapalli and Fredlund (2000) (Figure 2.1).

The parameter κ is equal to 1 for non-plastic soils but becomes larger as the plasticity of the soil increases. This relationship makes the shear strength function (Equation 2.3) all the more useful as a prediction tool since the plasticity index is a parameter readily available from any geotechnical investigation.

Vanapalli et al. (1996) also presented an alternate equation for the prediction of shear strength as given below:

$$\tau = c' + (\sigma - u_a)\tan\phi' + \left(\frac{\theta - \theta_r}{\theta_s - \theta_r}\right)(u_a - u_w)\tan\phi' \qquad [2.4]$$

where θ_r represents a residual volumetric water content SWRC.

Öberg & Sällfors (1997), extended the original expression of shear strength used by Bishop (1959).

$$\tau = c' + \left((\sigma - u_a) + \chi(u_a - u_w)\right)\tan\phi' \qquad [2.5]$$

with $\chi = S$

where S is the degree of saturation. The rationale for setting χ equal to the degree of saturation was the same as in the case of Vanapalli et al. (1996). In this equation, however, the value is expressed as the relative ratio of pore space occupied by water to that of air, thus reducing the influence of the suction with decreased degree of saturation.

Khalili & Khabbaz (1998) avoided the use of the degree of saturation altogether. Their formulation is also based on the Bishop equation, but in this case the expression for χ is expressed simply as a function of the matric suction. Their interpretation of the experimental data suggested that when the matric suction was normalized with the bubbling pressure (i.e., air-entry value) of the soil, a unique relationship could be established for all the compacted soils studied. This relationship takes the form of:

$$\chi = \left[\frac{(u_a - u_w)}{(u_a - u_w)_b}\right]^{-0.55} \qquad [2.6]$$

Rassam and Cook (2002) proposed an equation which is based on a power additive function that is used to describe the tri-dimensional shear strength envelope of saturated-unsaturated sands and silts only [Rassam and Williams (1999)].

$$\tau_s = \alpha + \sigma \tan\phi' + \psi \tan\phi' - (\psi - \psi_e)^\beta (\gamma + \lambda\sigma) \qquad [2.7]$$

where:

τ = the shear strength

σ = net normal stress

ψ = matric suction

ψ_e = air entry value

ϕ' = effective stress friction angle for saturated conditions.

α, β, γ, λ are fitting parameters

Rearranging the expression, Rassam and Cook expressed the contribution of matric suction to the shear strength of the soil as:

$$\tau_s = \tau - \sigma \tan\phi' - \alpha = \phi \tan\phi' - \phi(\psi - \psi_e)^\beta \qquad [2.8]$$

where τ_s is the contribution of matric suction to the shear strength of the soil, and ϕ replaces the term (γ + $\lambda\sigma$) since σ is assumed constant. A visual description of the terms of the equation is provided in Figure 2.2.

The values of ϕ and β can be obtained from the following relationships:

$$\phi = \frac{\psi_r \tan\phi' - \tau_{sr}}{(\psi_r - \psi_e)^\beta} \qquad [2.9]$$

$$\beta = \frac{\tan\phi'(\psi_r - \psi_e)}{\psi_r \tan\phi' - \tau_{sr}} \qquad [2.10]$$

where:

ψ_r = residual suction

τ_{sr} = contribution of matric suction to shear strength at residual state.

Thus, only one unsaturated shear strength test need be undertaken to obtain the shear strength parameters. It is still necessary to know the air entry value and residual suction, and therefore the SWRC must also be determined.

2.2.4 Critical state.

Casagrande (1936), working with sands, suggested that the ultimate strength and density of a soil were independent of its initial condition. Furthermore, the ultimate conditions remain unchanged during continued shearing. The density at which this condition was achieved was called the *critical density*. Further research in this field led to the development of the *Critical State Framework* [Roscoe et al, (1958)]. They provided the following definition for critical state:

> *In a drained test, the critical void ratio state can be defined as that ultimate state of a sample at which any arbitrary further increment of shear distortion will not result in any change of voids ratio. In any series of drained tests the set of critical void ratio points so defined can be expected to lie in or near a line on the drained yield surface.*
>
> *In an undrained test, the sample remains at a constant void ratio, but the effective stress will alter to bring the sample into an ultimate state such that the particular void ratio, at which it is compelled to remain, during shear, becomes a critical void ratio. In any series of undrained tests the set of critical void ratio points so defined can be expected to lie in or near a line on the undrained shear surface.*

Castro and Poulos (1977) defined the steady state of deformation as the state in which a soil will flow under constant shear stress at constant effective minor principal stress and at a constant volume. Poulos (1981) added the requirement for constant velocity.

Poorooshab (1989) indicated that the *critical state* as originally intended and the term *steady state of deformation* are identical. He also recommended that the term *Ultimate State* might be used instead since all specimens sheared far enough would tend to this terminal or *ultimate* state.

The implication of the critical state framework is that regardless of the stress history and soil structure of the soil, its ultimate condition during shearing tends towards a unique line which is formed by the intersection of two yield surfaces through which the stress path cannot pass. It can be used to couple the strength and volumetric change behaviour of the soil.

The critical state framework has originally been applied only to saturated soils, but attempts have been made to adapt it to the requirements of the mechanics of unsaturated soils. Ridley (1995) studies show that at any particular level of matric suction, a well defined and linear set of ultimate states exist. The slope and zero total stress intercept of the ultimate relationship are, however, both non-linear functions of the soil suction. Some studies were also undertaken by Croney and Coleman (1954) prior to the studies of Ridley (1995). These studies showed that clay specimens would reach an ultimate suction state when sheared at a constant moisture content. They called this line the *continuously disturbed line.* Furthermore, the continuously disturbed line was independent of the initial fabric of the soil.

Ridley (1995) conducted a series of unconfined compression tests on kaolin. The unconfined compression test is a constant water content test and it was therefore possible to study the suction at failure. From the test results obtained (Figure 2.3), it was found that the continuously disturbed line was parallel to the critical state line with respect to matric suction, but that it lied below that line.

2.2.5 Critical state frameworks

During the last fifteen years, more emphasis has been placed on the modelling of the critical state conditions in an unsaturated soil. Critical state concepts allow for the determination of ultimate failure criterion for soils. As such they are useful in establishing lower bound shear strength values for soils, but most importantly in developing comprehensive models of the shear strength behaviour of soils from initial loading conditions to its ultimate state. A few of the developments in this field are presented in the current section to underscore the need for the generation of quality critical state data for the calibration and validation of such models.

Alonso et al. (1990) presented a constitutive model coupling both the strength and volumetric deformation of unsaturated soils. Their model was based on a critical line with slope M (in p, q space). As a first hypothesis, the cohesion intercept of this line was set to increase with suction in a linear manner (Figure 2.4 and Figure 2.5). Based on Figure 2.4, the intercept of the CSL at suction, s would be equal to $M \cdot k \cdot s$. The critical state framework presented resulted in the following equations:

$$q = M \cdot p + M \cdot k \cdot s \qquad [2.11]$$

$$\upsilon = N(s) - \lambda(s) \ln(p/p_{at}) \qquad [2.12]$$

where:

p = average net normal stress

p_{at} = atmospheric pressure.

q = deviatoric stress

M = slope of critical state line.

k = constant (Figure 2.4)

$N(s)$ and $\lambda(s)$ are functions of the matric suction.

Toll (1990) also presented a critical state framework, where the critical state was represented by the following equations:

$$q=M_a(p-u_a)+M_w(u_a-u_w) \quad [2.13]$$

$$\upsilon=\Gamma_{aw}-\lambda_a \ln(p-u_a)-\lambda_w \ln(u_a-u_w) \quad [2.14]$$

where M_a, M_w, Γ_{aw}, λ_a and λ_w are functions of the degree saturation and soil fabric. It was also assumed that:

$$\Gamma_{aw}=1+\frac{\Gamma_s-1}{S_r} \quad [2.15]$$

where:

Γ_s = intercept of the critical state line at saturation

S_r = degree of saturation

Wheeler (1991), based on the data presented by Toll (1990) pointed out that there was no simple critical state relationship linking the specific volume, υ, to the stress state variables $(p-u_a)$ and $(u_a - u_w)$. It was proposed instead to use the specific water volume, υ_w, which can be expressed as:

$$\upsilon_w=eS_r+1=(\upsilon-1)S_r+1 \quad [2.16]$$

If the soil fabric consists of saturated packets separated by large air-filled voids, then υ_w can be thought of as being the specific volume of the packets [Wheeler (1991)].

Murray (2002), proposed using a coupling stress, p'_c, for the analysis of critical state data for unsaturated soils. This coupling stress, is expressed as:

$$p'_c=(p-u_a)+\alpha(n_w+n_s)(u_a-u_w) \quad [2.17]$$

where:

n_a = air porosity (V_a/V)

n_w = water porosity (V_w/V)

n_s = volume of soils/ total volume (V_s/V)

(n_w+n_s) = represents the total volume of the saturated packets per unit volume of soil.

α = is a dimensionless parameter

The value of α is equal to 1 for dry and saturated soils, and is smaller than 1 for intermediate degrees of saturation. It can however be assumed to remain equal to 1 with a small error which decreases with increasing matric suction, $(u_a - u_w)$ value [Murray (2002)].

The analysis of data reported by Toll (1990) and Wheeler and Sivakumar (1991), using p'_c as the controlling stress appears to provide a more consistent and logical trends [Murray (2002)] (Figure 2.6). Murray also remarks that normalizing q and p'_c with respect to $s=(u_a-u_w)$ helps in an understanding of volumetric influence on soil strength.

More recently, Gallipoli et al. (2003) proposed an elasto-plastic model using Bishop's effective stress equation (Equation 2.1). The parameter χ was considered to be equal to the degree of saturation, S. In other words, this variable is equivalent to the average stress acting in the soil skeleton. This incorporates the irreversible reduction of specific volume occurring during drying of an unsaturated soil and corresponding increase in suction, but not irreversible compression due to the wetting of the soil or the increase of the preconsolidation pressure with an increase in matric suction.

Gallipoli et al. (2003) also introduced a new state parameter, ξ that would represent the stabilizing effect of the normal force exerted at the inter-particle contact by meniscus lenses of water at negative pressures (Equation 2.18). This parameter should allow the consideration of the bonding and de-bonding effect due to the formation and vanishing of the menisci that cannot be considered exclusively on the basis of the average skeleton stresses.

$$\xi = f(s)(1-S_r) \qquad [2.18]$$

where:

S_r = degree of saturation of water

$(1 - S_r)$= degree of saturation of air

$f(s)$ = the function of suction

The factor $(1 - S_r)$ accounts for the fraction of water menisci per unit volume of the solid fraction. The assumption of a unique relationship for $(1 - S_r)$ is rigorously true only for the case of a rigid soil where the dimension and shape of the voids does not change with particle rearrangement. The explicit relationship between the number of water menisci and $(1 - S_r)$ was not specifically defined in this model since it is implicit in the function e/e_s to the bonding parameter ξ.

$$\frac{e}{e_s}=1-a[1-\exp(b\cdot\xi)] \qquad [2.19]$$

where a and b are fitting parameters.

The function $f(s)$ varies monotonically between 1 and 1.5 for suction values in the range of zero and infinity. It represents the ratio of the stabilizing force at a given suction with respect to a suction of zero for the ideal case of a water meniscus located at the contact between two identical spheres [Gallipoli et al. (2003)]. The specific shape of the function depends on the size of the spheres. The authors used a value 1 μm to represent the kaolin that was used in the analysis (Figure 2.7). The relationship between the bonding factor and the ratio e/e_s was found to be in good agreement both for the isotropic virgin loading and the critical state. The main limitation of the method is that the function $f(s)$ has been developed strictly for a soil composed of spheres of equal size.

Tarantino and Tombolato (2005), noted that the ultimate strength of Speswhite Kaolin could be modelled considering only the effect of the average skeleton stress, without invoking the contribution of the water menisci. This suggests that the contribution of the water menisci to the ultimate shear strength is small compared with the contribution of the average skeleton stress.

2.3 Determining the Shear Strength of Unsaturated Soils

The laboratory testing of unsaturated soils requires several modifications to the testing equipment as compared to conventional testing procedures used for saturated soils. The main requirement is in the measurement or control of the matric suction since it is a state variable that influences the unsaturated soils behaviour.

Problems associated with the measurement of water tension in unsaturated soils are alleviated through use of the axis-translation technique [Hilf (1956)]. In this technique, a positive air pressure is applied to the specimen such that the difference between the pore-air and pore-water pressures achieves the desired value of $(u_a - u_w)$. The total confining pressures must be modified accordingly so that $(\sigma - u_a)$ corresponds to the desired net normal stress.

2.3.1 Modified triaxial tests

The triaxial tests are versatile and allow the measurement, or control of confining stresses, deviator stresses, pore water pressures and matric suction

In a typical shear test of an unsaturated soil, the pore air pressure is applied to the top of the specimen while the water is allowed to drain at the bottom of the specimen. An important consideration in the triaxial testing of unsaturated soils is the accurate measurement of the volume and water content change of the specimen since both of these parameters are used to calculate the degree of saturation of the specimen, which itself controls the contribution of the matric suction to the shear strength of unsaturated soils.

An instinctive approach is to measure the volume of water entering and leaving the triaxial cell while taking into account the change in volume due to the immersion of the ram shaft to calculate the volume change of the specimen. Such an approach was used by Satija (1978) when testing Dhanauri clay. A major concern using this approach is the expansion of triaxial cell under the application of the net normal stress. While this expansion can be calibrated, it can be substantial with respect to the volume changes of the specimen thus raising concerns about the errors in measurement. This consideration prompted Satija to brace the cell wall with metallic strips to reduce the expansion of the acrylic and conduct the tests.

This concern about the expansion of the triaxial cell prompted the development of triaxial cells with dual chambers. The idea behind the approach of using two chambers in triaxial cell is to maintain an equal pressure on the outside and inside of the chamber containing the specimen to eliminate the stretching of the wall due to the pressure differential. Any volume change due to the compression of the acrylic under pressure would be much smaller and cause a minor error.

One such application of a dual chamber approach was developed by Bishop and Donald (1961) is shown in Figure 2.8. In their device, the inner cell contents were not separated from the outer cell, but instead connected by an opening at the top. The inner cell was filled with mercury which completely surrounded the specimen. A steel ball floating on the mercury was used as a reference point to detect the changes in volume of the specimen.

Another triaxial cell based on a similar principle has been developed by Ng et al. (2002). Here again the inner cell is not sealed but opened to the outer cell. Much like in the cell by Bishop and Donald (1961), this design depends on the movement of the interface between two fluids. Instead of using water and mercury, however, this system depends on the interface between water and air. A precise differential pressure transducer, connected to the water of the inner cell and a reference water column is used to measure any movement of the water surface in the inner cell (Figure 2.9).

Another approach, which has been more widely used in the triaxial testing of unsaturated soils is the dual chamber technique developed by Wheeler (1988) (Figure 2.10). Despite the double chamber layout to counteract the applied pressure and prevent expansion of the cells, it was still necessary to calibrate for the remaining small sources of volume change, namely compression of water in the cell, expansion of the short lengths of connecting tubes, and a slight flexure of the top and bottom cell plates. It was also necessary to calibrate for the absorption of water by the acrylic cylinder. Strict temperature control was also required for the entire duration of the tests. To avoid leaks between the cell and the air at atmospheric pressure at the entry point of the loading ram, a rolling diaphragm was used to seal the ram.

Similar designs have been used in recent years to adapt triaxial cell to the needs of unsaturated soil testing. Yin (2003), suggested improvements to the design by Wheeler (1988). In this design, the inner chamber is fully enclosed within the outer chamber, rather than sharing a common top plate. A result of this approach is that a large pressure differential at the entry point of the ram is avoided, and leaks are therefore less likely.

All the cells previously described were based on designs using the axis translation technique to apply controlled matric suction. The design by Blatz and Graham (2003) relies on a vapour equilibrium system to apply the matric suction and measure the same using psychrometers.

The use of vapour equilibrium systems to control the suction can be useful in the laboratory since the axis translation technique only allows the application of suction around 1500 kPa, after which water movement occurs predominantly in the gaseous phase. A similar but fully automated system was used by Likos and Lu (2003), to control the suction applied to a specimen for the determination of the SWRC. Although the use of different salts is commonly used technique in the laboratory in the measurement of the SWRC, such a use of a computer controlled system of controlling suctions osmotically makes it possible to conduct other types of tests at high controlled suctions.

2.3.2 Modified direct shear tests

The modified direct shear test has the distinct advantage of simplicity and can be used to obtain the shear strength characteristics of unsaturated soils [Escario and Sáez (1986), Gan and Fredlund (1988), de Campos and Carrillo (1995)].

The net normal stress on the plane of failure is always controlled and hence a failure envelope at a given net normal stress can easily be generated. In contrast, typical tests in triaxial devices allow control of the net confining pressure ($\sigma_3 - u_a$). This produces failure envelopes with respect to suction that are not perpendicular to the τ vs ($\sigma - u_a$) plane but instead cross it diagonally. This makes it necessary, when comparing test results from triaxial tests, to compare only the contribution of the shear strength due to suction. Controlling the net normal stress on the plane of failure in triaxial tests is possible with stress path controlled devices, but it is more easily achieved in the modified direct shear box.

Most modified shear devices use the axis-translation technique to apply controlled suctions on the specimen. Like other axis-translation devices, the specimen must be contained within a pressurized enclosure. Because shear box is divided in two equal halves, the entire box must be enclosed, with the specimen inside. The bottom platen on which the specimen is placed comprises a high air entry value ceramic disc to prevent the movement of free air into the measurement system. Below the disc, a spiral groove connects the water phase to a volume gauge in order to measure the water movement to and from the specimen. The water content of the specimen can therefore be computed throughout the test. Samplės of such modified direct shear devices are shown in Figures 2.11, and 2.12.

Caruso and Tarantino (2004) have presented another type of modified direct shear box. Rather than applying the axis-translation technique, the matric suction is measured directly using high-suction tensiometers. These devices, similar to the device used by Ridley (1993) (Figure 2.13) make use of the tensile strength of water to measure matric suctions of up to 1500 kPa (15 bar). An advantage of this approach is that the direct shear box does not require to be contained in a pressurized enclosure. The modifications made to the testing equipment therefore need not be as cumbersome (Figure 2.13). This approach to testing of unsaturated soils could make it more easily applicable in conventional geotechnical laboratories.

2.4 Water Content Measurement and Air Diffusion

It is common practice in geotechnical laboratories to measure the water volume changes within a specimen using a twin burette system. The advantage of a twin burette arrangement over a single burette is that the valve may be setup in different configurations allowing the water coming from the specimen to flow in one direction, then in the other when the limit has been reached in the original direction (Figure 2.14). The effective capacity of the system can therefore be increased indefinitely without loss of precision by simply changing the valve configuration.

When used for measuring the movement of water to and from unsaturated specimens, the conventional twin burette device must be modified to provide the greater accuracy that is required due to the small water volume changes associated with unsaturated soils [Fredlund and Rahardjo (1993)]. The modification consists in using a burette with a smaller inner diameter and accordingly smaller capacity. The twin burette systems commonly used in unsaturated soils laboratories have a nominal capacity of 10 ml with a precision of 0.01 ml.

When testing unsaturated soils, although a high air entry ceramic disc is placed between the soil specimen and the measuring system to resist the passage of air, some air will still diffuse through the water in the disc [Bishop and Donald (1961)]. The accumulation of air bubbles below the discs may break the continuity of the water column resulting in an incorrect evaluation of the pore water pressure. Even before the continuity of the water phase is broken, however, the continuous accumulation of air will result in incorrect measurements of water volume changes within the specimen. The air bubbles that form and grow below the ceramic disc occupy a finite volume which would otherwise have been filled solely by water. The water displaced by the formation and growth of the air bubbles is therefore measured and incorrectly interpreted as water expelled from the specimen.

For the accurate measurement of the pore water pressure and the water volume changes, it is necessary to flush the air bubbles that accumulate under the ceramic discs and to provide a means of quantifying their impact on the measurement of the water volume changes. This makes it possible to correct the water volume change readings accordingly.

All flushing systems require that a groove with openings at both extremities be provided below the ceramic disc. The groove should cover as much of the surface area of the disc as possible. Most frequently, the groove is given a spiral shape to achieve this. Water is made to flow from one end of the groove to the other by creating a pressure gradient between them. The groove as well as the tubing used in the system must be sufficiently narrow for the water flow to force the air bubbles to move along. If the conduit is too wide, water will flow around the air bubbles which will adhere to the solid surfaces.

Somewhere within the closed circuit a vertical tube, or chamber, with a wider diameter will be used as an air trap. The diameter of this chamber must be sufficiently large to allow the air bubbles to float freely to the surface of the water and accumulate at the apex of the air trap. In many systems the air trap is in line with the measurement system. This is how the diffused air is taken account using pressure plate extractors (Figure 2.15).

This was also the case in the flushing system with diffused air indicator presented by Bishop and Donald (1961). Figure 2.16 (a) shows a view of this system where the two lines connected to the groove under the ceramic disc are connect to the air trap. A gradient is caused between the two ends of the lines by tilting the pressure gauge is shown in Figure 2.16 (b). The air bubbles accumulate in the air trap which has a capacity of 5 ml. The air trap allows the measurement of the diffused air after each flushing. The volume indicated by the water volume gauge is not affected since the air remains in the system. The water volume readings must therefore later be adjusted to take into account the effect of the accumulation of the dissolved air.

Fredlund (1975) used a different type of diffused air volume indicator (DAVI). This one is kept isolated from the volume measuring system during the volume measurement phase. It is only connected when a flushing operation is performed. Figure 2.17 shows a schematic layout of the device. The diffused air volume indicator consists of a 10 cm^3 graduated burette and an acrylic (Lucite) exit tube placed inside a 80 mm acrylic cylinder. A vent at the top of the burette is opened when filling the burette with water. It must remain closed, however during operation of the device. Both the burette and exit tube are sealed inside the acrylic cylinder.

A *U* tube is used to connect the exit tube to the burette. The other extremity of the exit tube is exposed to the air pressure inside the acrylic cylinder. This air pressure is set at a constant value to establish a pressure gradient relative to the controlled water pressure below the ceramic disc of the testing device. When measuring the volume of the diffused air it is necessary to take into account the air pressure existing inside the acrylic cylinder as well as the pressure in the base plate (Figure 2.18).

Using Boyle's law for gases, under isothermal conditions the diffused air volume, V_{fa}, is given by:

$$V_{fa} = \frac{(u_{a1} h_{a2} - u_{a2} h_{a1}) A}{u_{fa}} \quad [2.20]$$

where:

u_{a1} = absolute initial air pressure in the burette (i.e., $u_{a1} = u_{atm} + u_{ab} + (h_{a1} - d)\rho_w g$)

h_{a1} = initial reading of the water level in the burette

h_{a2} = final reading of the water level in the burette

u_{fa} = absolute diffused air pressure in the base plate (i.e., $u_{fa} = u_{atm} + u_c$)

A = cross-sectional area of the burette

u_{atm} = atmospheric pressure (i.e. 101.3 kpa)

u_{ab} = applied gauge air pressure in the acrylic cylinder

d = height difference between the burette and the exit tube

ρ_w = density of water

g = acceleration due to gravity

u_c = water gauge pressure in the base plate

Using the data from the DAVI, it is possible to then correct the water change readings by subtracting the rate of air diffusion. Romero (1999, 2001) discussed in depth the physical aspects of the air diffusion, as well as the evaporation phenomena. He also suggested a procedure to detect and correct their effects on the water volume change measurements of the specimen. This procedure is based on the consideration of the steady state water flow regime at the end of each step of the wetting or drying paths. As the volumetric changes induced by a change of matric suction decrease with time toward an horizontal plateau, the change in water volume will tend towards an asymptote. If the asymptote is not horizontal it represents the combined effect of external factors such as air diffusion and evaporation. Airò Farulla and Ferrari (2005), applied this technique to correct for both the air diffusion and the evaporation simultaneously. Since the air diffusion occurs at a constant rate, then both effects combine linearly. Subtracting this final rate from the original data results in the corrected curve (Figure 2.19).

2.5 Concluding Remarks

The mechanics related to the engineering behaviour of unsaturated soils are still in their infant stages and still have to make their way into practice. To achieve this goal, a number of approaches have been developed during the recent years, . From the early Bishop equation where stress states and volumetric behaviour were coupled into the χ parameter, to the following era of the strict separation of the stress state and material parameter, new models are emerging with the goal of unifying the concepts of strength and volumetric behaviour in the same way it has been done for saturated soils. Many recent models require the use of a stress state parameter representing the coupling of the strength and volumetric behaviour, such as the coupling stress, p_c, used by Murray (2002) or the average skeleton stress used by Gallipoli et al. (2003). These trends show the strong dependence of the shear strength behaviour of unsaturated soils on their fabric and therefore on the volume change behaviour. A specimen that is being sheared will undergo volume changes and structure rearrangements that will in turn affect the stresses that it is subjected to, and its shear strength .

2.6 Figures

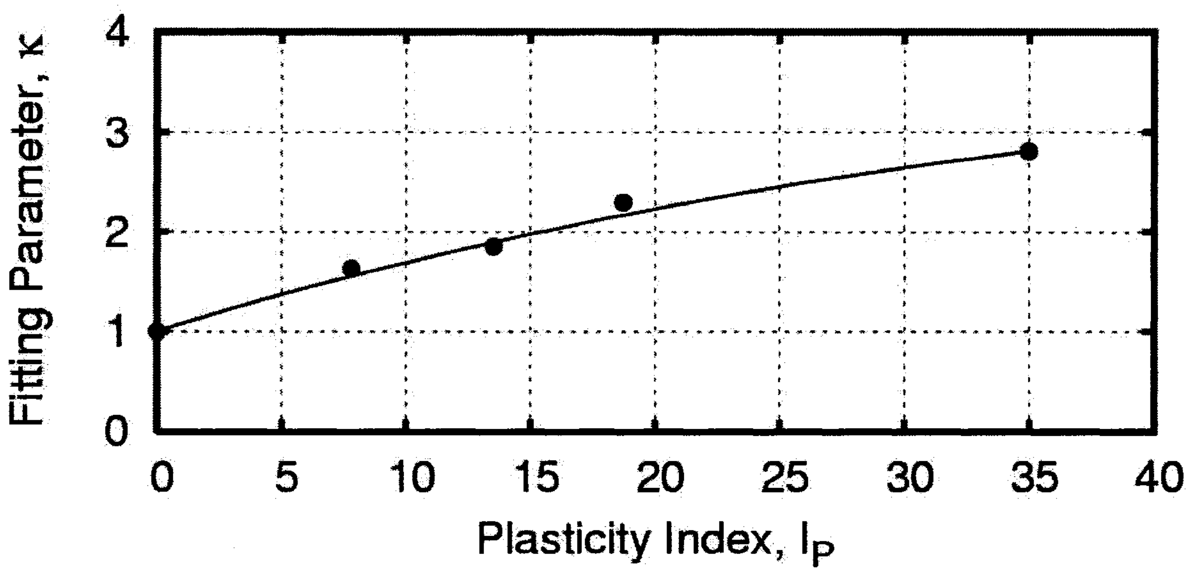

Figure 2.1 Relationship between the fitting parameter κ and the plasticity index of a soil [from Vanapalli and Fredlund (2000)].

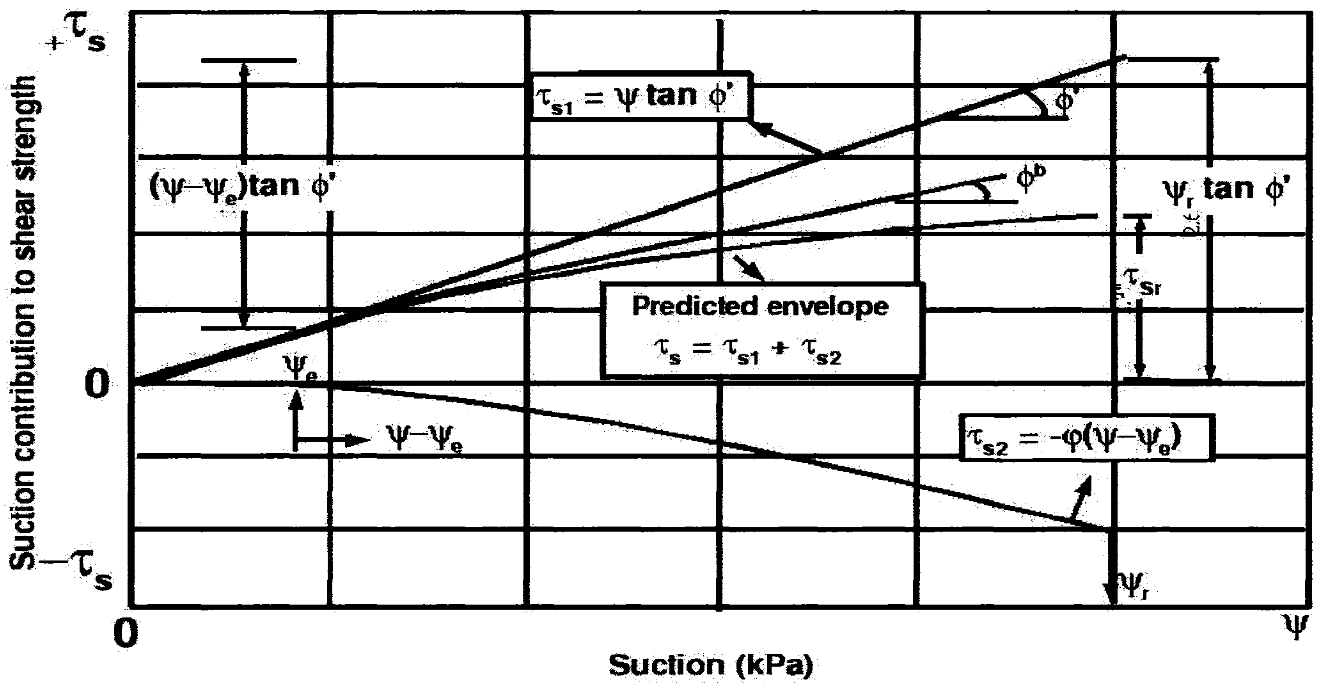

Figure 2.2 Graphical representation of Eq. 2.7 [from Rassam and Cook (2002)].

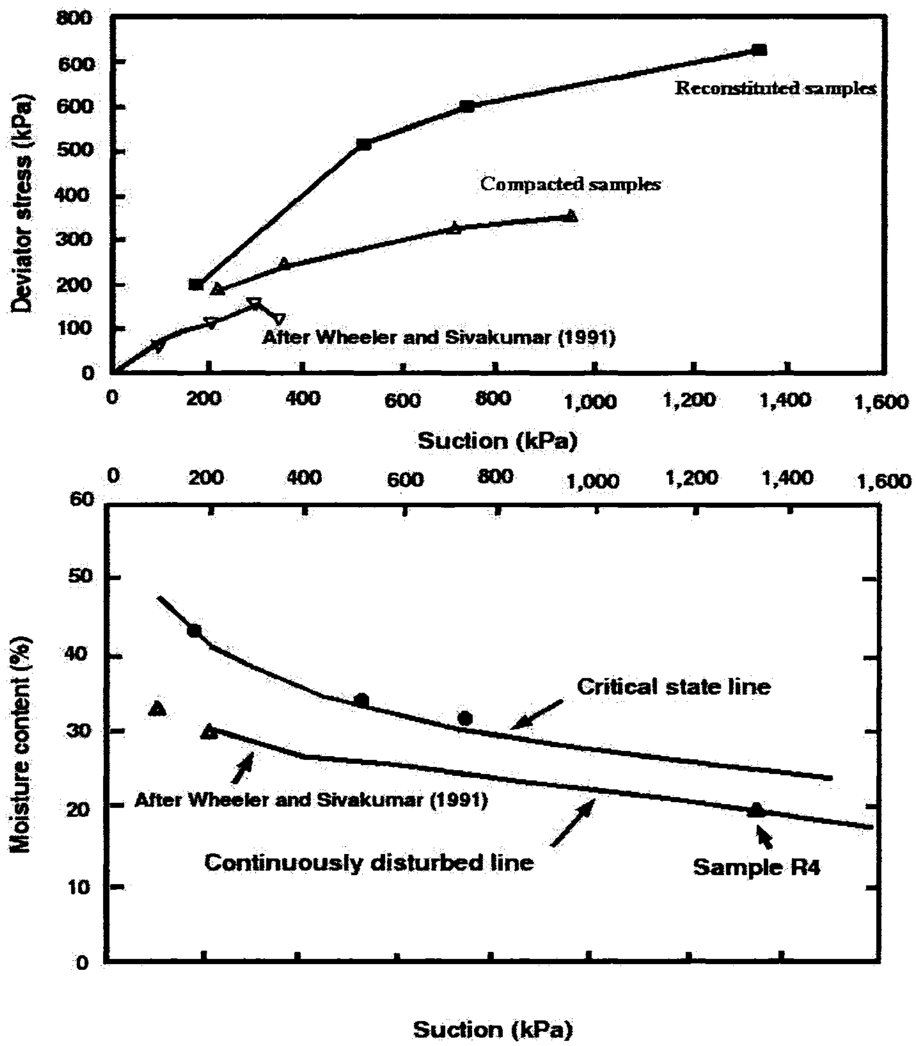

Figure 2.3 Strength -suction-moisture condition of kaolin at failure [from Ridley(1995)].

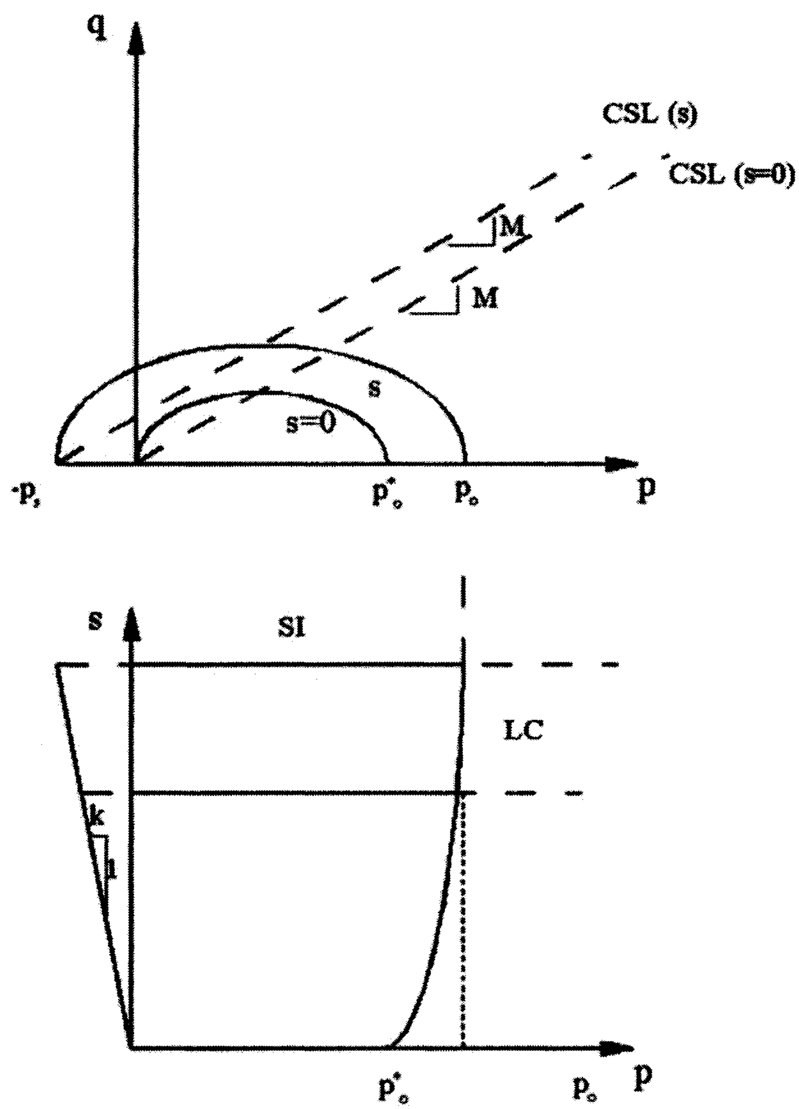

Figure 2.4 Yield surfaces in (p,q,s) space [from Alonso et. Al (1990)].

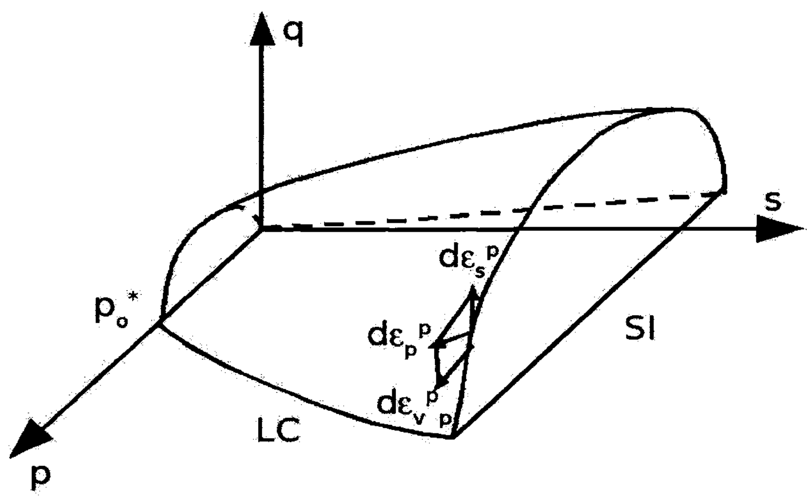

Figure 2.5 Three-dimensional view of the yield surfaces in (p, q, s) stress space [from Alonso et. al (1990)]

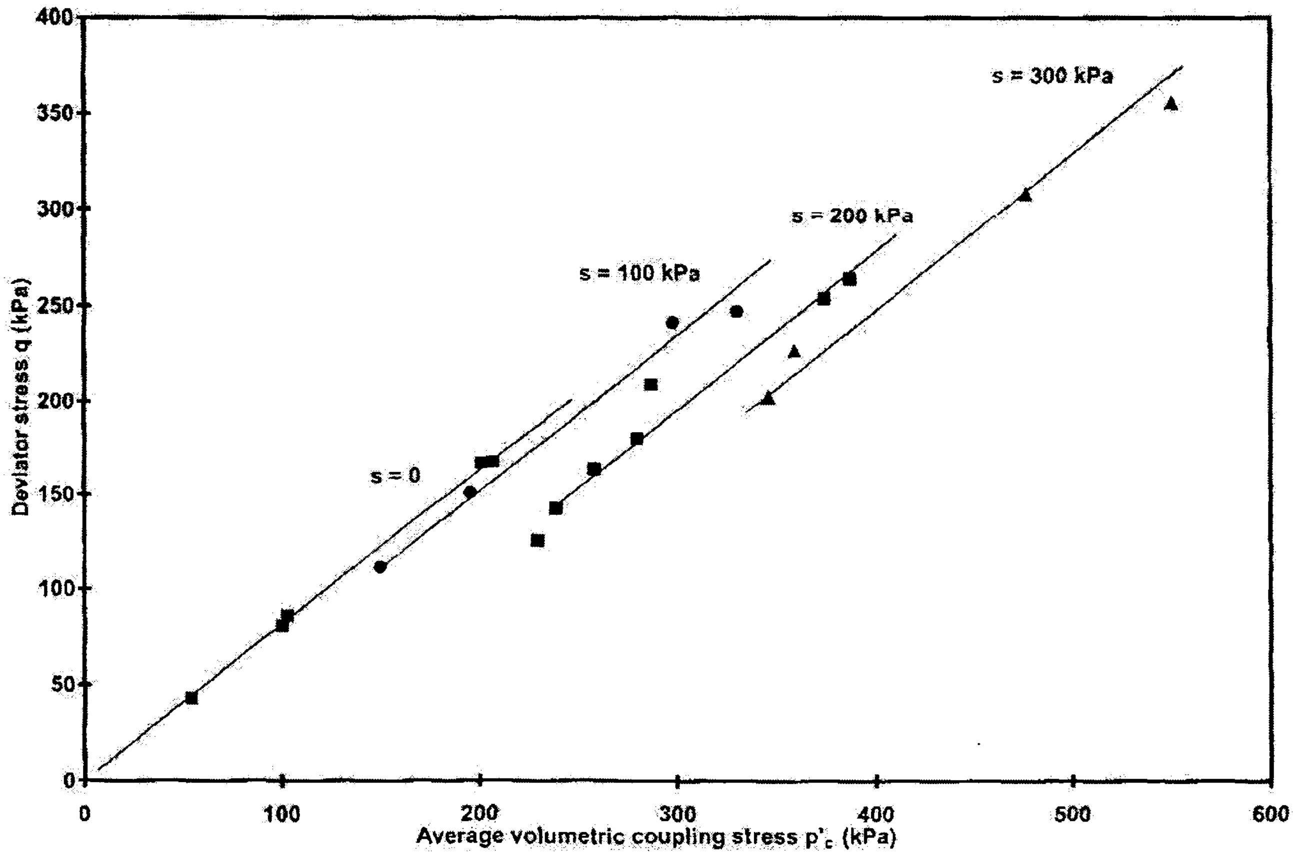

Figure 2.6 Plots of q versus p'_c at critical states from the data of Wheeler and Sivakumar (1995) [from Murray (2002)]

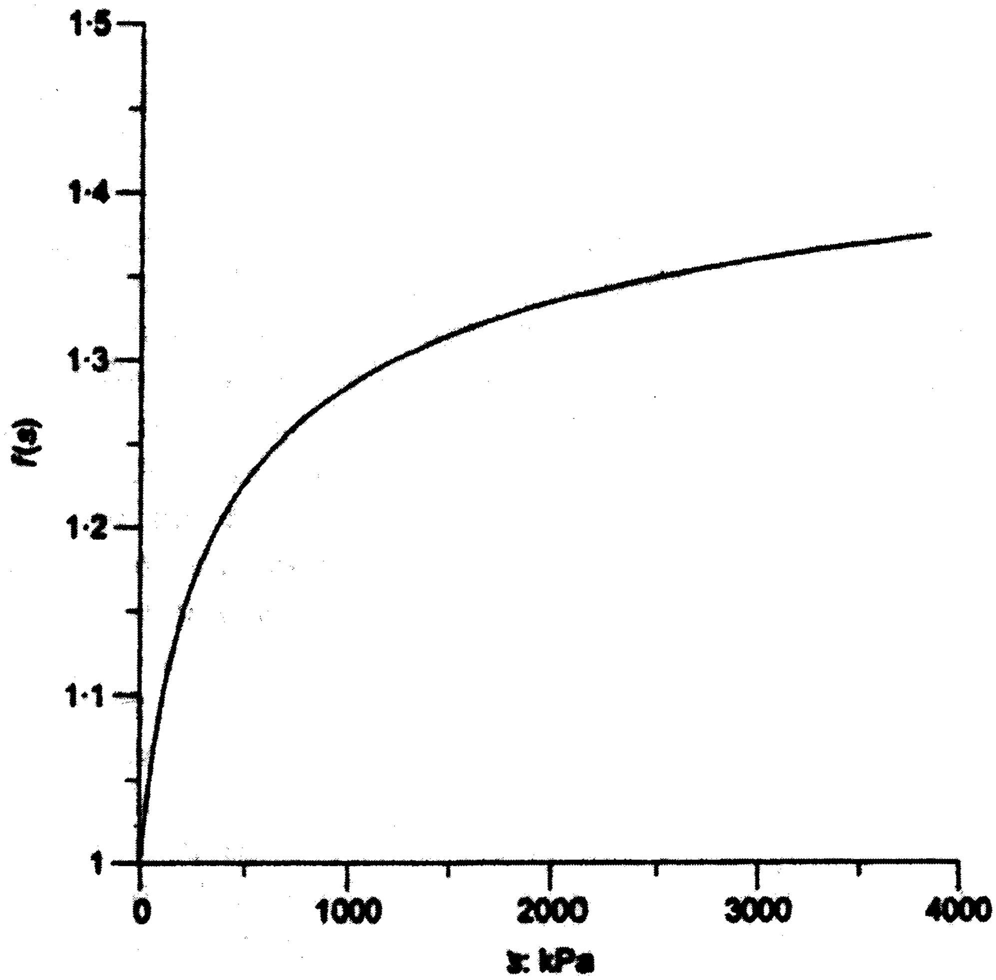

Figure 2.7 Ratio between inter-particle forces at suction s and at null suction due to a water meniscus located at the contact between two identical spheres [from Gallipoli et al. 2003].

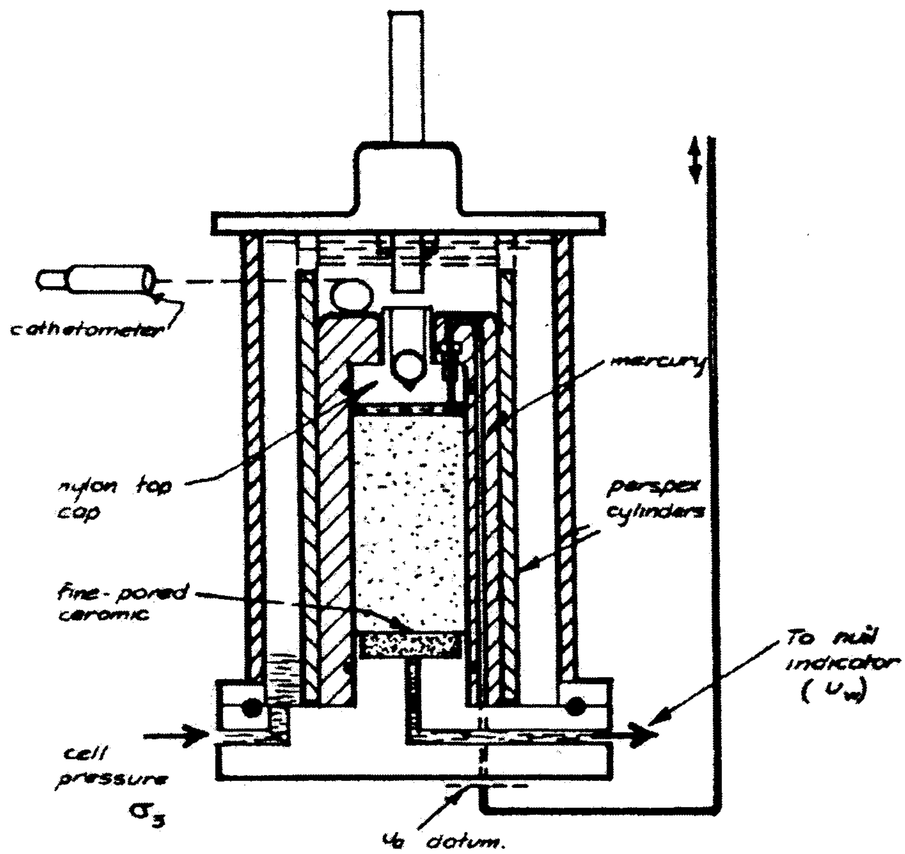

Figure 2.8 Schematic of the triaxial cell used by Bishop and Donald (1961).

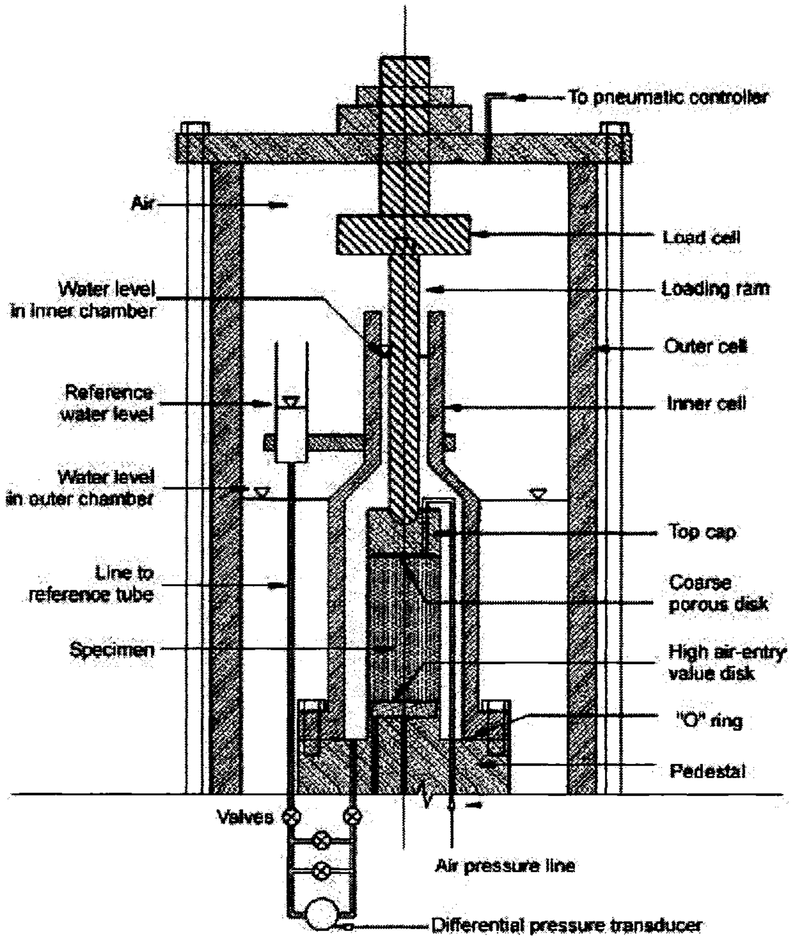

Figure 2.9 Triaxial cell used by Ng et al. (2002).

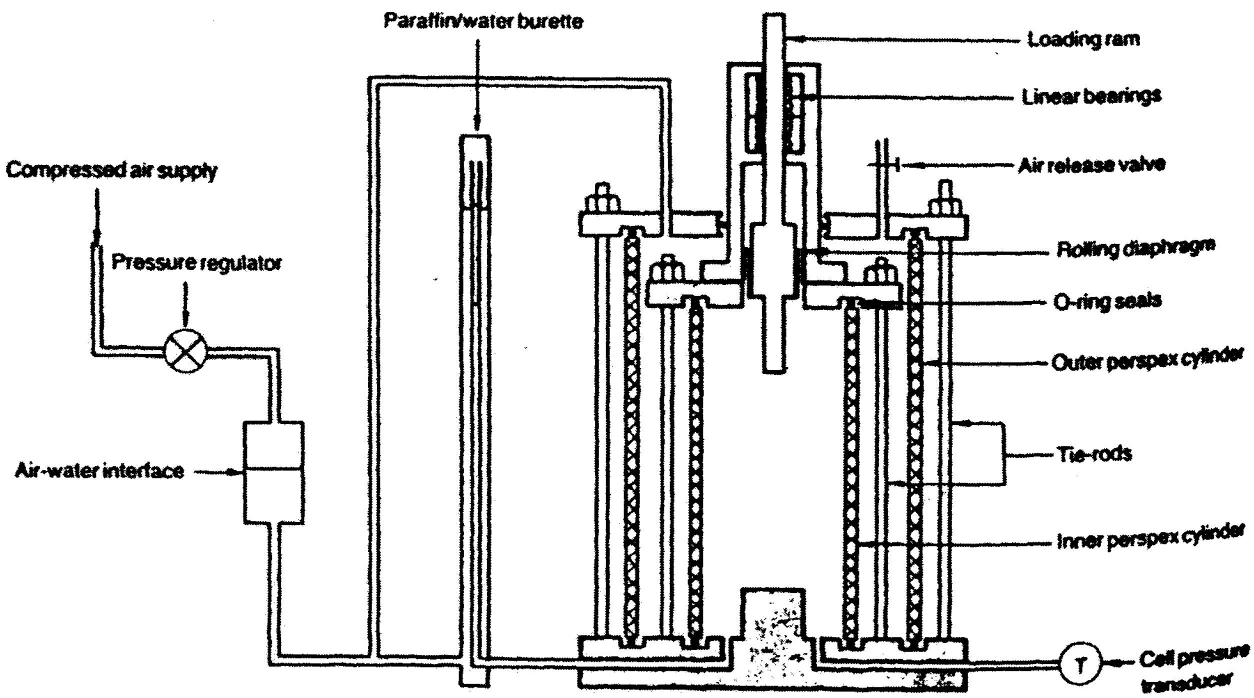

Figure 2.10 Triaxial cell used by Wheeler (1988).

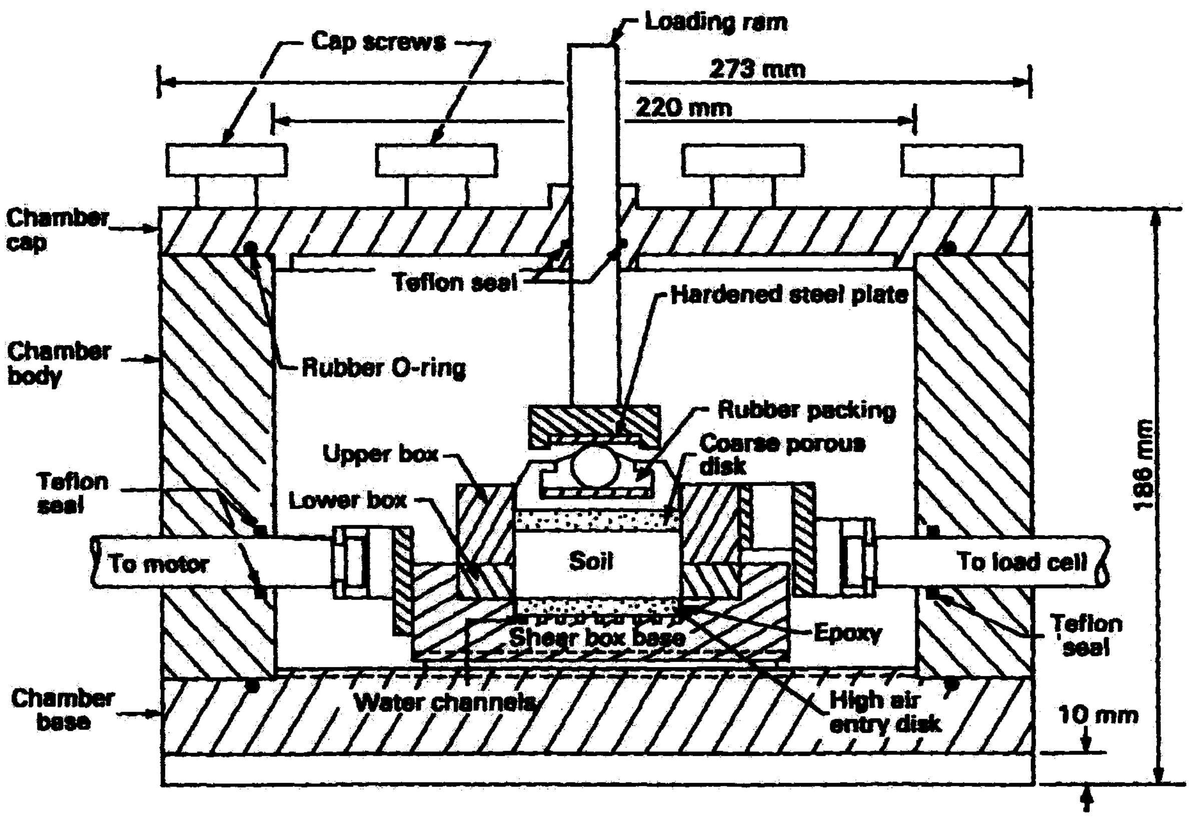

Figure 2.11 Modified direct shear device used by Gan et al. (1988).

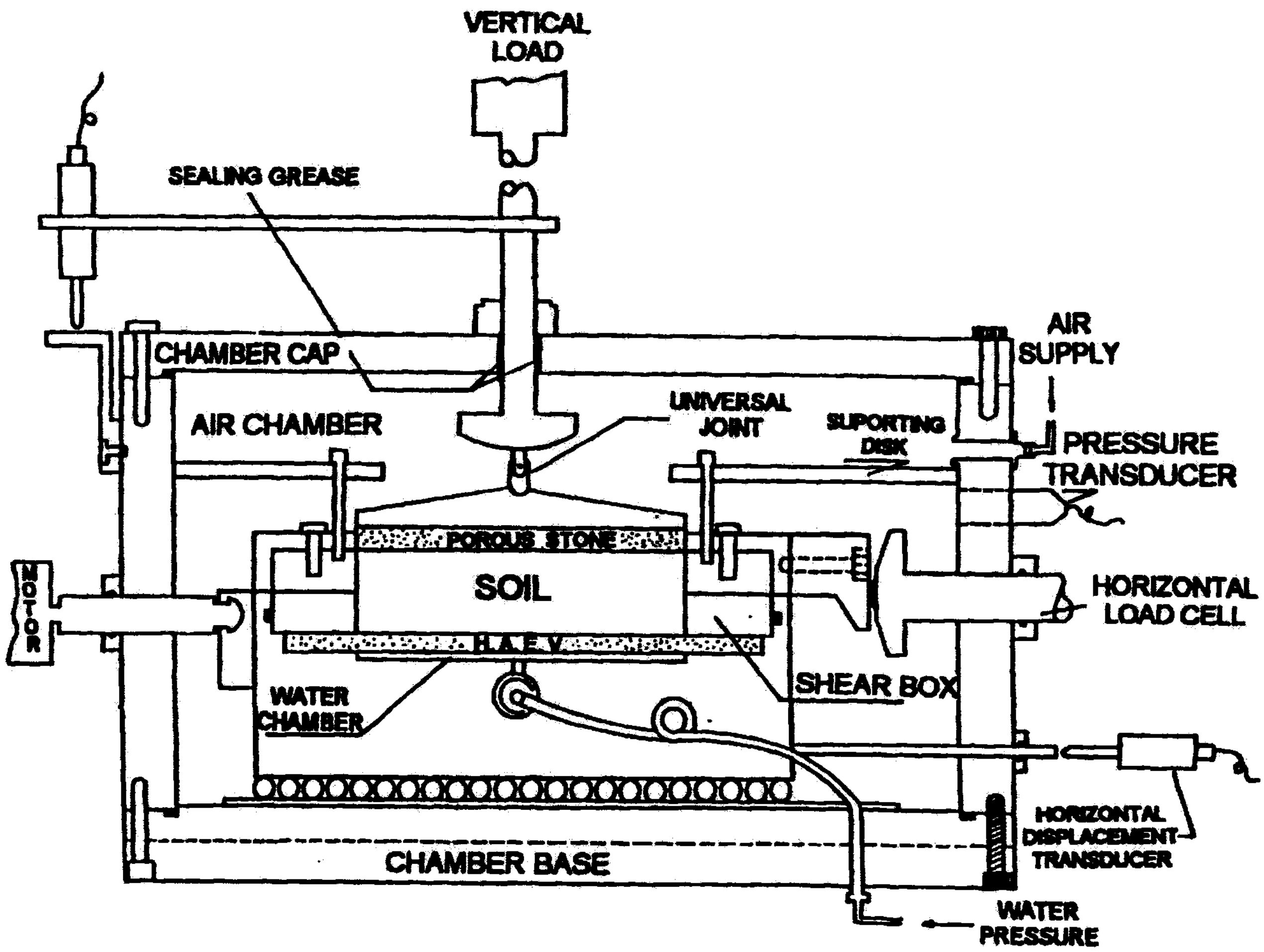

Figure 2.12 Direct shear test apparatus used by de Campos and Carrillo (1995).

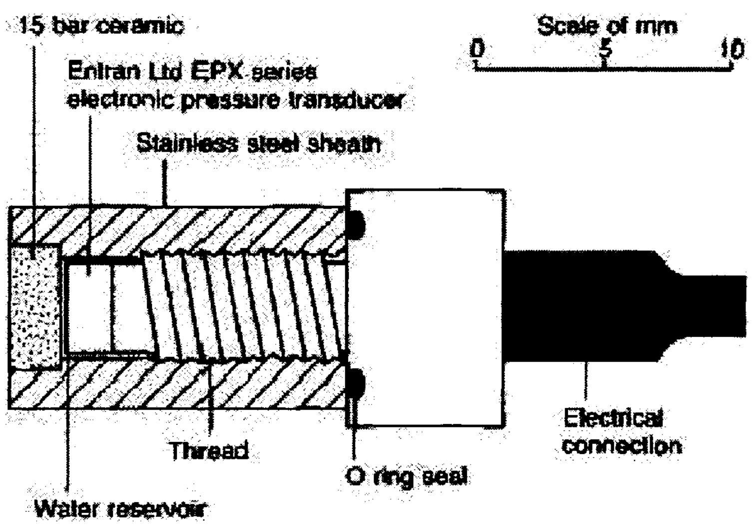

Figure 2.13 Transducer used by Ridley (1993).

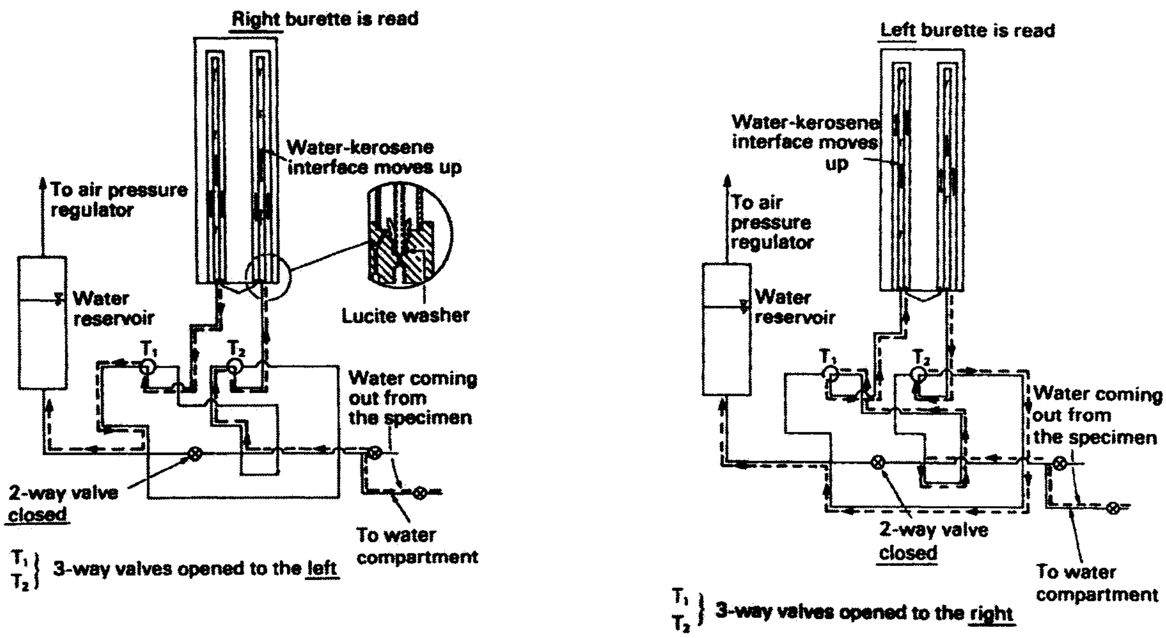

a) b)

Figure 2.14 Direction of water movement in a twin burette system with the three-way valves opened to the left, (a), and to the right, (b) [from Fredlund and Rahardjo (1993)].

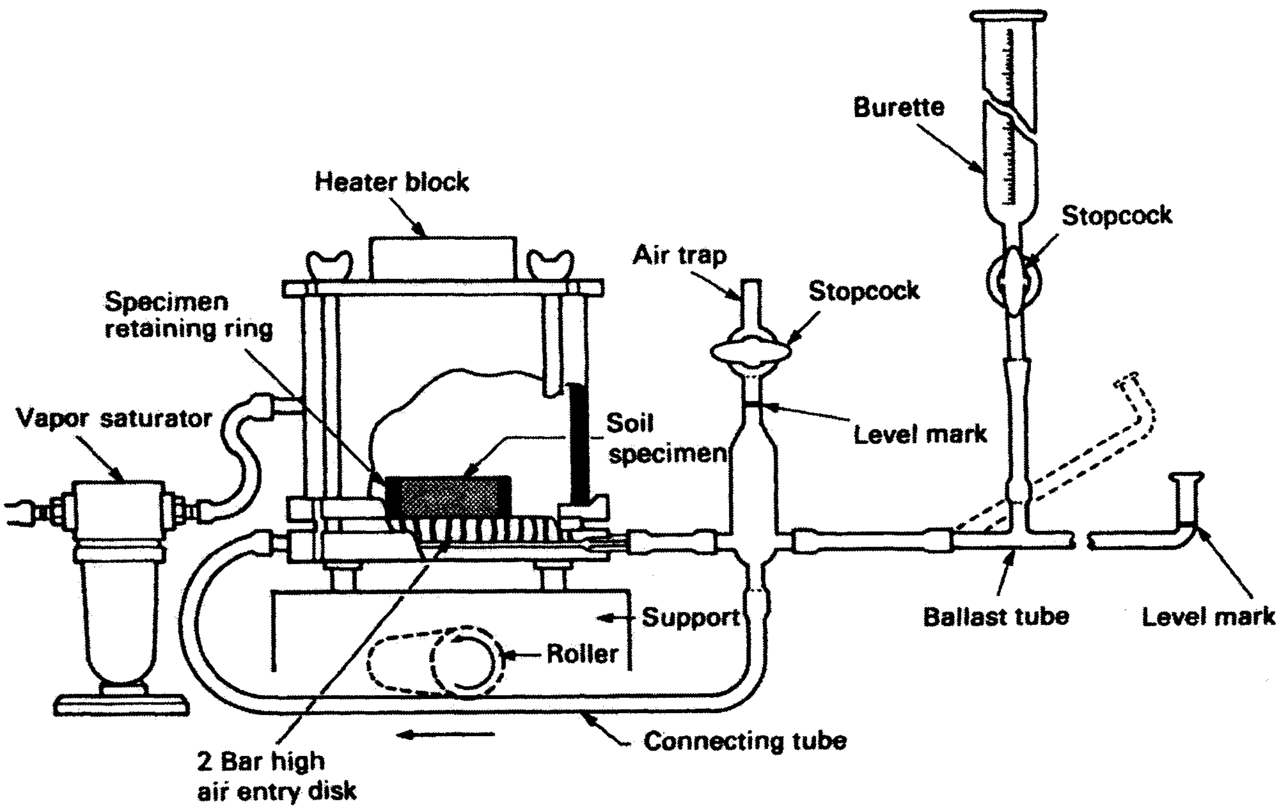

Figure 2.15 Volumetric pressure plate extractor with hysteresis attachments [Soilmoisture Equipment Corp. (1985)].

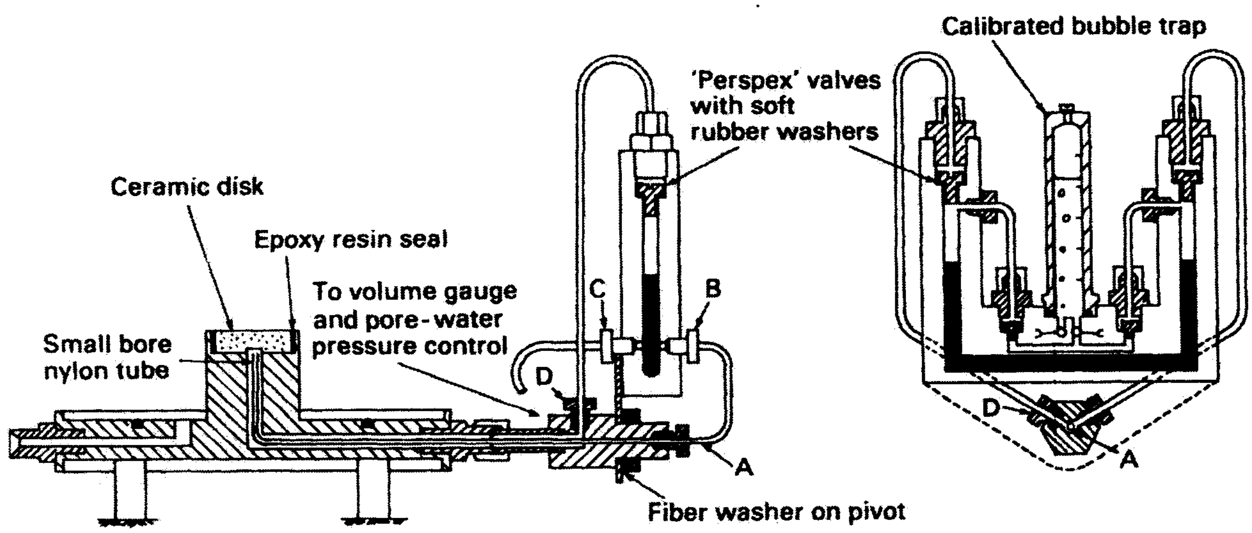

a)

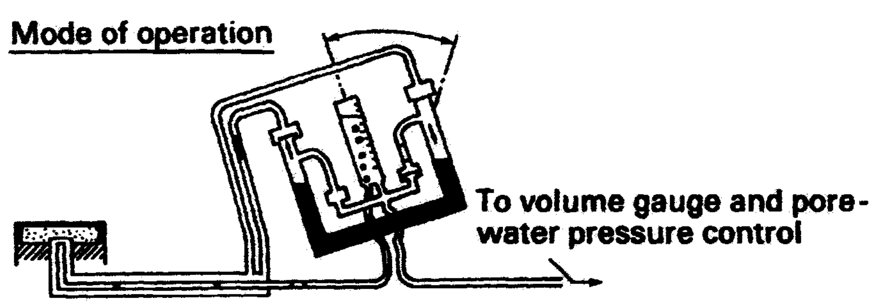

b)

Figure 2.16 Bubble pump an air trap [from Bishop and Donald (1961)].

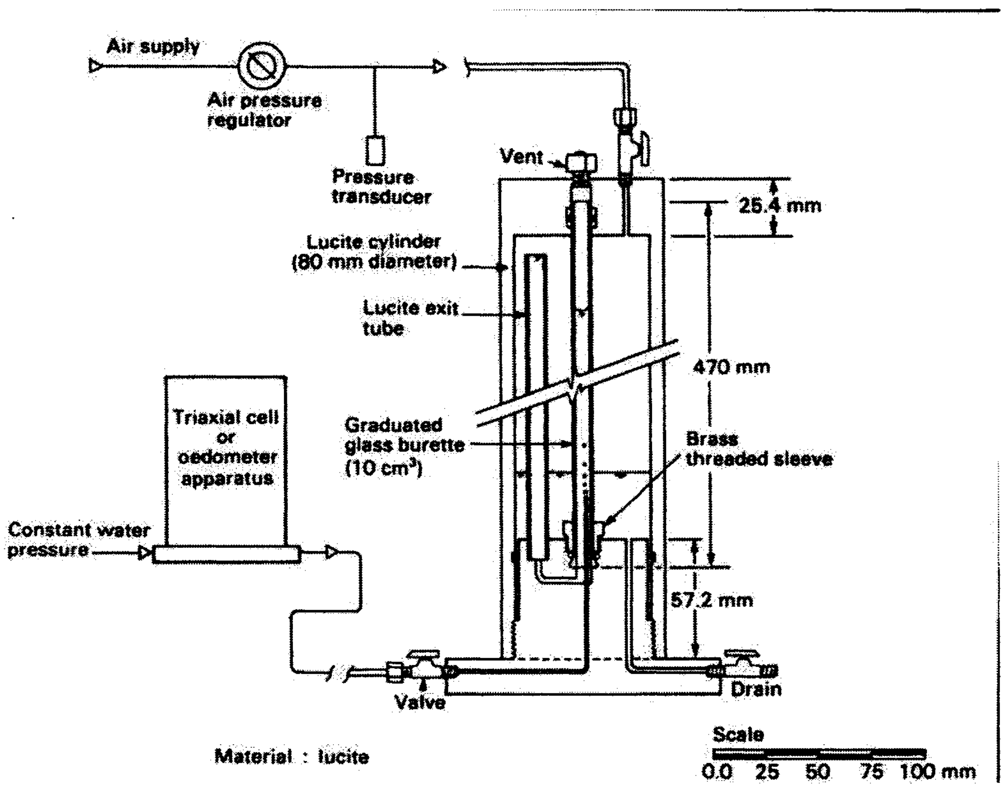

Figure 2.17 Diffused air volume indicator [from Fredlund (1975)].

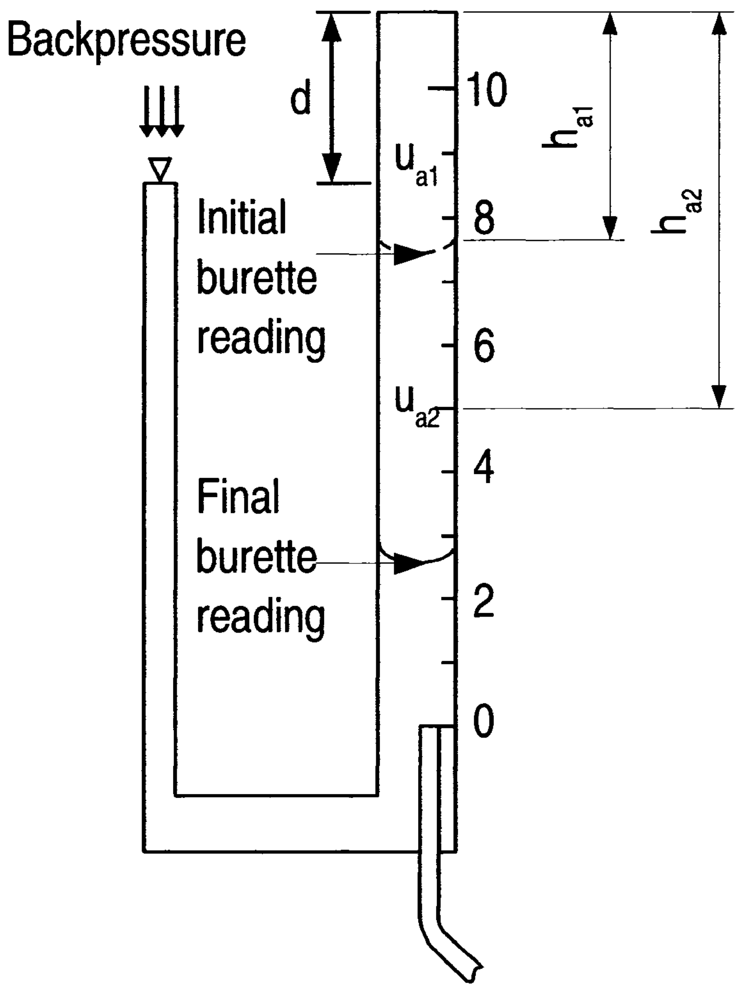

Figure 2.18 Measurement of the diffused air volume under isothermal conditions [from Fredlund and Rahardjo (1993)].

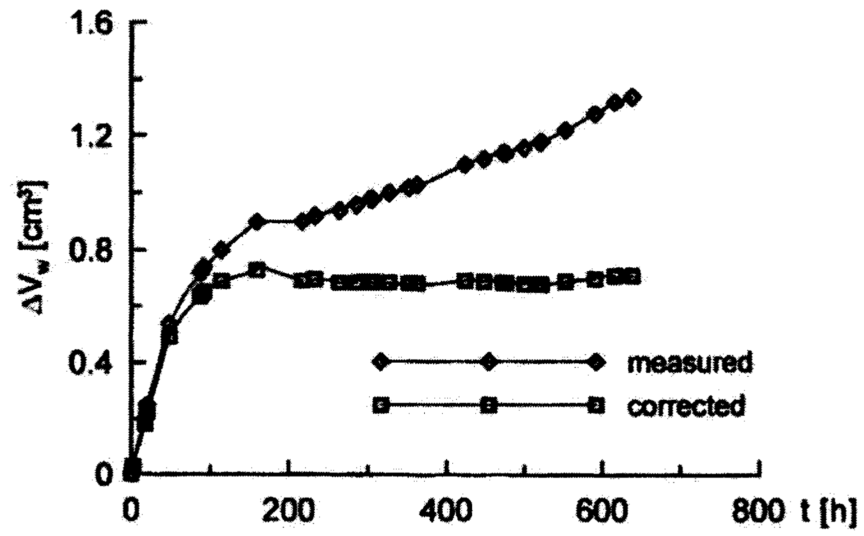

Figure 2.19 Settlement and water volume change versus time during equalization step [after Airò Farulla and Ferrari (2005)].

3 Axis Translation Equipment

3.1 Introduction

The laboratory testing of unsaturated soils requires specialized equipment. Several practical considerations typically limit the quality of the data generated. One such limitations is the direct application of negative water pressure beyond the range of about 90 kPa. As a negative water pressure of one atmosphere is approached, cavitation occurs, causing a discontinuity in the water column which prevents accurate measurement or control of the matric suction. To overcome this limitation, the axis translation technique (Hilf, 1956) was developed, whereby a positive air pressure is applied, while the pore water remains at a gauge pressure of 0 kPa. Since the matric suction is defined as the difference between pore air pressure, u_a, and pore water pressure, u_w, the matric suction, (u_a-u_w) is equivalent whether the pore air pressure is increased or the pore water pressure decreased.

The present chapter presents new laboratory devices that can be used in axis translation equipment to measure SWRC or conduct shear strength or consolidation tests under controlled suction conditions. These new devices have several advantages over the presently used equipment in testing unsaturated soils.

3.2 Compressible air Column Pressure Gauge.

This section presents a simple, economical, robust and accurate pressure gauge for the measurement of pressures in 0-700 kPa range. Its operational characteristics make it especially well-suited to testing unsaturated soils where greater precision is required in the low pressure range while maintaining the ability to measure pressures in the 0-700 kPa range. This gauge is therefore ideal for use in an axis translation technique for the determination of soil water retention curve or for testing shear strength of unsaturated soils. There are several pressure measurement devices that are commercially available;

however, most are expensive and many require auxiliary read out devices, or they do not have the required sensitivity to measure reliably the low pressures while simultaneously covering the range of pressures of interest.

It is important to measure or control suction with a high degree of precision for the reliable determination of the SWRCs. This is particularly true for coarse-grained soils such as sands which desaturate at a relatively faster rate over a small suction range (typically in the range of 0 to 20 kPa). In some cases, it may be necessary to measure the SWRC in a low suction range of only 0 to 5 kPa, with a sensitivity of measurements of 0.1 kPa, or better. Also, in several situations, the SWRC behaviour of fine-grained soils is sensitive in the low matric suction range and it may be difficult to reliably determine the air-entry value (AEV) of such soils. As air-entry value (AEV) is one of the key parameters of the SWRC, it should be reliably determined.

The working principle of this instrument is based on the principle of Boyle's law for gases.

3.2.1 Theoretical Concept

The pressure gauge consists of an air column trapped inside a closed tube, referred to as the gauge tube (Figure 3.1). A column of water in the open part of the tube separates the trapped air column from the atmosphere. An unknown pressure that has to be measured may be applied to the water column.

The pressure inside the air column before any external pressure is applied is indicated by P_0 and is equal to the atmospheric pressure. The initial gauge length of the trapped air column is L_0 (Figure 3.1) when the air inside the tube is at atmospheric pressure, P_o. On applying a pressure increment, ΔP to the column of water, the water level will rise in the gauge tube by a distance ΔH corresponding to the applied gauge pressure, ΔP. Equilibrium is reached when the sum of the air pressure in the gauge tube, P_n and the pressure of the water column ($\Delta H \cdot \gamma_w$, where γ_w is the density of water) is equal to the sum of the gauge pressure ΔP *and the atmospheric pressure,* P_o. This relationship can be represented using the equation below:

$$\Delta P + P_0 = P_n + \gamma_w \cdot \Delta H \qquad [3.1]$$

Using this equation, pressure increment in the gauge can be measured as

$$\Delta P = P_n + \gamma_w \cdot \Delta H - P_0 \qquad [3.2]$$

The difference in water head in is turn equal to:

$$\Delta H = L_0 - L_n \qquad [3.3]$$

where: L_0 = original length of air column at atmospheric conditions.

L_n = length of air column at gauge pressure ΔH.

Boyle's law states that at a constant temperature, the product of the pressure and the volume of a fixed amount of gas remains constant.

$$P_0 \cdot V_0 = P_n \cdot V_n \qquad [3.4]$$

In a tube of constant diameter of length L, the volume is expressed by:

$$V = L \cdot A \qquad [3.5]$$

where: A = cross-sectional area of the tube.

For the range of pressures considered, which is typically from 0 to 700 kPa, it may be assumed that the cross-sectional area of the tube remains constant. Equation [3.4] may therefore be rewritten as:

$$P_0 \cdot L_0 \cdot A = P_n \cdot L_n \cdot A \qquad [3.6]$$

which simplifies to:

$$P_0 \cdot L_0 = P_n \cdot L_n \qquad [3.7]$$

By substituting Equations [3.3] and [3.7] into Equation [3.2], the following relationship is obtained:

$$\Delta P=\frac{P_0 \cdot L_0}{L_0-\Delta H}+\gamma_w \cdot \Delta H-P_0 \qquad [3.8]$$

or

$$\Delta P=\frac{P_0 \cdot \Delta H}{L_0-\Delta H}+\gamma_w \cdot \Delta H \qquad [3.9]$$

Using Equation [3.8], it is possible to determine the pressure using a linear graduated scale attached to the tube. The scale can be used to read ΔH linearly. Alternatively, a customised scale can be developed that shows the gauge pressure directly. It should be noted that Equation [3.8] is to be used strictly with a vertical gauge tube. In a horizontal tube, the contribution of the water column to the pressure reading is eliminated and the equation below should be applied:

$$\Delta P=\frac{P_0 \cdot \Delta H}{L_0-\Delta H} \qquad [3.10]$$

A more general equation that can be used for any angle of inclination in the tube would be:

$$\Delta P=\frac{P_0 \cdot \Delta H}{L_0-\Delta H}+\gamma_w \cdot \Delta H \cdot \sin(\theta) \qquad [3.11]$$

where: θ is the angle from the horizontal of the gauge tube.

ΔH is then given by:

$$\Delta H=\frac{(\Delta P+P_0+\gamma_w L_0 \sin\theta)-\sqrt{(\Delta P+P_0+\gamma_w L_0 \sin\theta)^2-4\gamma_w \Delta P\, L_0 \sin\theta}}{2\gamma_w \sin\theta} \qquad [3.12]$$

This assumes that the rate of air dissolution in water and air diffusion through the water are negligible.

3.2.2 Application

Figure 3.1 shows one such gauge using a 435 mm long trapped air length. The core of the apparatus consists of two plastic bottles that are able to withstand the full range of pressures to be applied. The plastic bottles are generally rated for a pressure of 700 kPa (100 psi). These bottles are readily available and can be purchased as off-the-shelf items.

The first bottle contains air at the pressure to be measured. It is connected to the second bottle (the Mariotte bottle) into which air flows at a known reference level located below the surface of the water. This reference level provides the datum from which the head of water in the pressure gauge is measured.

The pressure in the first bottle is P, which is equal to the gauge pressure ΔP, (of interest) plus the atmospheric pressure. This pressure, P is transmitted to the air column. The "zero" of the gauge tube should be at the same level as the discharge point of the air in the Mariotte bottle. This ensures a common reference between the scale and the pressure to be measured, so that the reading on the scale accurately represents the gauge pressure, ΔP. Since there is some head of water above the discharge point tube in the Mariotte bottle, the air pressure in this bottle is P_m which is lower than P by $\gamma_w . h$ (Figure 3.3).

As the water level in the Mariotte bottle drops because of the movement of water into the gauge tube, the pressure differential between P and P_m is also reduced since the head of water, h is reduced. In addition, as the water level in the Mariotte bottle decreases as it flows into the gauge tube, the displaced volume is occupied by air from the first bottle.

A reflux tube also links both bottles. A check valve is placed in this tube to ensure that the air will only flow backward towards the first bottle if the applied air pressure in the first bottle is reduced. Without this provision, the water in the Mariotte bottle would flow towards the first bottle every time the pressure in the latter was reduced.

A simple check valve was fabricated with readily available 1 cc capacity syringe, without the needle (Figure 3.4). The plunger shaft of a standard 1 cc syringe (Figure 3.4 a) was cut leaving a third of its length (Figure 3.4 b), but leaving the syringes tube intact. Furthermore, the rims of the original rubber seal were shaved in order to permit air flow around it (Figure 3.4 c). This rubber "seal" will now function as a seal only when the plunger is pressed firmly against the end of the syringe. Next, a 5 mm outer diameter clear plastic tube is pressure fitted in the syringe shaft to maintain a seal. In order to ensure good contact between the plastic tube and the cut-off plunger shaft, a small spring is inserted between the two (Figure 3.4 d). The dimensions of the spring should be such that it does not enter the plastic tube. The type of spring commonly found in mechanical pencils has been found to be satisfactory for this purpose.

Figure 3.5 shows the operation of the syringe check valve. In the normal operation mode, P is greater than P_m, and the check valve will remain closed (Figure 3.5 a). When the pressure in the Mariotte bottle, P_m, is larger than that in the first bottle, the check valve will open, and the spring will compress (Figure 3.5 b). On equalising the pressures in the two bottles, the check valve will close since the spring will extend to activate the seal (Figure 3.5 c).

3.2.3 Graduated gauge scale

In practice, one could use a linear scale to calculate the air pressure from the measurement of the length of the air column in the gauge tube. However, a customised scale that would directly read the gauge pressure can also be provided. Such a scale uses Equation [3.12] which requires the length of the trapped air column, the barometric (atmospheric) pressure at the laboratory, and the angle of the air column with respect to the horizontal as input parameters. Figure 3.6 shows a plot of Equation [3.12] for two gauge length of air columns, namely 300 and 600 mm. Clearly, the scale generated is dependent on the length of tube used. The longer the value of L_o, the flatter is the resulting curve, which provides a greater spacing between the graduation lines. This feature demonstrates a key property of this apparatus, namely that the precision of measurements can be significantly increased, mainly in the low pressure range, by simply increasing the length of the gauge tube.

A macro program was written to generate such scales automatically in OpenOffice.org. The source code to the macro is provided in Appendix B. A screenshot of the macro interface is shown in Figure 3.7. A sample scale generated as mentioned above is shown in Figure 3.8. This output shows two scales: one for a horizontal gauge tube (Figure 3.8 a), and the other for a vertical tube (Figure 3.8 b), on which both a linear scale, in mm, for the length of the air column and a modified scale in kPa, for direct readout of the gauge pressure are shown. The sample scales shown in Figure 3.8 were generated for an atmospheric pressure of 101.3 kPa, and a trapped air length of 300 mm.

3.2.4 Calibration

In theory, it is possible to directly measure the length of the air column and to deduce the gauge pressure. However, this may introduce some inaccuracy because it can be difficult to measure accurately the length L_0 (Figure 3.1). This length may be influenced by the type of fitting used to provide the closed end of the gauge tube. In particular, the ferrule inserted into the plastic tube to provide a good bite to the outer ferrule assuring the seal, may cause an apparent shortening of the tube by reducing the diameter of the tube over its length. Therefore, it is advisable to calibrate the length of the trapped air column versus known gauge pressures, ΔP for both loading and unloading stages. With a non-linear fitting algorithm and using Equation [3.11], it is possible to fit for the trapped air length L_o. An actual calibration curve for a gauge with a trapped air column is shown in Figure 3.9. The calibration was conducted under an ambient pressure of 100.1 kPa, and yielded a trapped air length of 428.78 mm. The best measurement that could be obtained when measuring was 435 mm, which, as it is apparent in Figure 3.1, does not accurately match the measured data.

3.2.5 Effect of Atmospheric Pressure

Equation [3.12] shows that the gauge pressure is a function of the atmospheric (barometric) pressure. If a pre-generated scale for direct readout of gauge pressure is to be used, then it is necessary to evaluate the impact of the daily fluctuation of atmospheric pressure on the accuracy of the deduced gauge pressure. Figure 3.10 shows the fluctuations of the atmospheric pressure sampled randomly at Ottawa, Canada, during a period ranging from February to May, 2005. The solid line represents the average pressure, 101.34 kPa, during that period and the dotted lines represent one standard deviation boundaries, ±0.87 kPa.

Figure 3.11 shows the influence of the measured barometric pressures during the four month period on the deduced value of the gauge pressure. The effect of the daily variation of the barometric pressure is insignificant for the gauge length utilised.

The influence of the variation in atmospheric pressure as a function of the measured gauge pressure for different gauge tube lengths is shown in Figure 3.12. The results are expressed in terms of relative error which is defined as:

$$\epsilon = \frac{\Delta P_{average} - \Delta P_{std.\ dev.}}{\Delta P_{average}} \qquad [3.13]$$

where:

$\Delta P_{average}$ = the gauge pressure measured using a gauge scale generated using the average atmospheric pressure as P_o.

$\Delta P_{std.dev.}$ = the gauge pressure measured using a gauge scale generated using a standard deviation offset from the average for the atmospheric pressure Po.

Figure 3.12 shows that the relative error decreases as the gauge length increases. At lower gauge pressures, the relative error is even lower than at higher pressures, and confirms that the variation of barometric fluctuation is negligible.

3.2.6 Limitations of the air pressure gauge

The main limitation of this instrument is the slow solution of the air into the water. At a constant gauge pressure, the height of the water column in the closed tube, ΔH, will increase. The apparatus therefore cannot be used for *continuous* monitoring of a pressurized system. It can only be used for spot readings. Before taking any measurements, it is necessary that the system be reset by introducing atmospheric pressure in the gauge tube and in the first bottle. This can be conveniently carried out by modifying the arrangement of valves as shown in Figure 3.8. For the purpose of equalising atmospheric pressure, valves *A* and *B* are open to atmosphere while valve *C* is closed. For spot measurement of gauge pressure, valves *A* and *B* are closed and valve *C* is opened.

The effect of the diffusion can be minimized by reducing the contact area between the air and water phases. This can be accomplished by using a buoyant material, such as floating plastic ball in the gauge tube. In a vertical tube, it will float on the water at the interface, and thus minimize the contact area between the gas and liquid phases. This is only practical in large diameter tubes where the capillary effect between the plastic ball and the sidewall is negligible. For the apparatus used, with an internal diameter of 3.18 mm, the use of the plastic ball would be inappropriate. Investigation on minimising diffusion effect has not been undertaken. It is emphasised that diffusion effect is not a factor for spot measurements of the gauge pressure since the device is reset immediately before taking a reading. Similarly, while temperature variations would be a major concern during extended monitoring of the pressure, it is not a factor for spot measurements of the gauge pressure.

3.2.7 Typical Result

The nature of the instrument which shows a higher precision at lower pressures, suits it for use in geotechnical laboratories for the application of the axis translation technique to unsaturated soils. Coarse grained soils which are particularly sensitive to small changes at low suction values, and yet must be subjected to the full range of suctions for the generation of the SWRC are well served by this device. This is illustrated in Figure 3.7 which shows the SWRC generated for three different sands using this device. The tested sands are a silty sand, Barahona sand (a fine sand) and a washed concrete sand. The same device can also be used for fine grained soils such as silts and clay since the device can sustain the full range of air pressures up to 700 kPa. The air entry value for the sands lies in the range of 1 to 10 kPa. It would have been difficult to obtain precise measurements in this low pressure range without resorting to either a water column device or an expensive transducer.

3.3 Integrated Volume Gauge and Air Trap

The testing of unsaturated soils requires both precise measurement of the water movement to and from the specimen, as well as a means of removing the air bubbles that accumulate beneath the ceramic discs after having crossed the air-impervious barrier by diffusing through the water. It is also necessary to quantify the volume of air that diffuses through the stone if the measurements of the water volume are to be relevant.

It is common practice in the geotechnical laboratories to measure the volume of water with a twin burette system. For the testing of unsaturated soils, such devices should have a precision in the order of 0.01 ml. Such burettes generally have a capacity of 10 ml, yet this can be increased indefinitely by reversing the direction of the flow within the twin burette system.

In addition to the twin burette volume gauge, a flushing system and air trap, with diffused air volume indicator (DAVI) should be used. The air trap and DAVI may be included in a closed circuit with the tube and groove system collecting bubble under the discs, and the twin burette volume gauge, such as that proposed by Bishop and Donald (1961). Alternatively, it may be external to the system, such as the one proposed by Fredlund (1975). In the latter case, the volume gauge must be isolated during the flushing operations so that the volume readings remain unchanged. Because of the need for the air trap to have a diameter sufficiently large to allow for the free movement of the air bubbles, the precision of the readings of the air volume indicator will likely be lower than the precision of the readings of the water volume gauge.

The current section presents a device (Figure 3.6) integrating the volume gauge burette and the air trap into a single tube with a high precision of the readings and large capacity. This device eliminates the need to keep a separate volume gauge and a DAVI, thus significantly simplifying the layout of tests for unsaturated soils testing. Furthermore, the diffused air volume is inferred from the corrections applied to the volume measurement curve, allowing for air volume estimations with the same precision as the water volume measurements.

The main components of the gauge system are illustrated in Figure 3.5. It consists of an outer glass tube of a 14.61 mm (0.575") inner diameter inside of which is inserted a small bore glass tube of 5.72 mm (0.225") outer diameter, and 3.18 mm (0.125") inner diameter. These tubes form both the air trap and volume gauge. A mirror is placed behind the glass tubes to provide parallax correction when measuring the water level in the inner tube.

In addition, the system includes a pump, for the purpose of flushing the air bubbles from below the ceramic disk of the axis-translation cell, a water reservoir for filling the system with water, and two water chambers used to isolate the accumulated air and thus avoiding moisture exchange with the external environment. The system, however, allows air to exit and enter as the diffused air is collected or when the inner tube is inserted and retracted. A set of valves numbered 1 through 3 shown in Figure 3.5, are also used to isolate sections of the system, as required.

3.3.1 Operation of the Device

Before beginning the test, it is necessary to saturate the system. Valve number 3 is opened to supply the system with water. When enough water has entered the system, including the grooves below the ceramic disc of the pressurized cell, and some water in the outer tube of the integrated burette, valve number 3 is closed. A flushing operation is required to get rid of any air trapped in the lines.

The flushing operation is illustrated in Figure 3.4 (a), where the pump is used to circulate the water below the ceramic disc of the pressurized cell through the whole system. The air bubbles are collected into the outer tube, acting as an air trap, where the inner tube has been lifted to leave a space between the bottom of the inner tube and the water surface in the outer tube.

Once air bubbles are no longer collected in the outer tube, the inner tube is lowered until the end stopper contacts the spacers at the top of the outer tube (Figure 3.4 (b). The water level inside the inner tube can be read on the external graduated scale. One millimetre on the scale is equal to a 0.007 ml volumetric change. The difference in the reading taken before the flushing operation and after it corresponds to the volume of water removed during flushing.

At this precision, the entire range of the graduated scale (about 600 mm) could only read up to a total volumetric change of 4.2 ml. This may be insufficient to accommodate the water content changes occurring in the specimen, and therefore the number of spacers can be adjusted to accommodate a greater volume change. The level of water in the inner tube drops to a new reading by the addition of spacers. This is illustrated in Figure 3.3. The new reading is used as a new reference level, from which volume is calculated by adding the new volume increments to the cumulative volume accumulated before the addition of the spacer.

Calibration of the graduated scale is done by carefully measuring the mass of water that results in a given increase in the water column. A manual pump which consists of a syringe a *T* junction and a valve at each end of the *T* is used for this purpose (Figure 3.2). First, with the syringe in a fully closed state, valve (1) is closed while valve (2) is opened. The syringe plunger is then pulled back, drawing in water from a deaired water reservoir sitting on top of a precise electronic balance. Valve 2 is then closed and valve 1 is then opened and the plunger is fully pushed in, thus expelling the water from the syringe into the apparatus. The water level in the inner tube rises and can be read off the graduated scale. The operation is repeated to generate a calibration curve for the whole range of the scale. Proper conversion of the mass of water to volume requires a knowledge of the current room temperature.

3.3.2 Air Phase Isolators

The air phase isolators are two water filled containers used to separate the air phase inside the gauge system from the external air. Whenever the inner tube is lowered, or the water level is increasing because of water expelled from the tested specimen, air must be allowed to exit the system, or the air pressure could increase within it. At the same time, it is not desirable that the air phase be directly in contact with the external air since this could cause a loss of moisture from the air in the tube, which is close to saturation, and the outside air phase which is usually at a significantly lower moisture content. Similarly when the level of water goes down, or the inner tube is lifted, air must be allowed in.

The operation of the system is illustrated in . When air needs to be expelled from the system, it does so through the left isolator, where the outflow tube is situated below a small head of water. This head of water is smaller than the head that would be required in the right chamber to lift enough water up to the top air intake tube.

Similarly, when there is a need for air to enter the system, it will be easier for it to enter from the right isolator, where the air phase is directly connected to the air phase of the glass tube, while in the left chamber there is water barrier. The air enters the right isolator from atmosphere through a tube under some head of water. This allows some humidification of the air from the water in the chamber. Extended contact time in the isolator between the air and the free water further ensures that the air in the isolator is at the same degree of saturation as the air in the glass tubes.

3.4 Conclusion

This chapter has presented two simple devices that can be used in the laboratory testing of soils using the axis-translation technique. These provide high precision measurements that are required for testing of unsaturated soils.

The pressure gauge offers a variable precision that is well suited to the application of the axis-translation technique. It is simple and inexpensive to build, and is very robust. Furthermore, it is easy to upgrade to a greater precision if the need arises with the substitution of a longer gauge tube.

On the other hand, the integrated volume gauge and air trap offers the high volumetric precision required for testing unsaturated soils, while maintaining the capability of accommodating large volumes of water through the used of spacers and a large diameter outer tube. Because the volume of air is deduced from the volume of water, the precision of the measurement of the volume of air is of the same order as that of the volume of water. This device has the added advantage of simplifying the layout of testing unsaturated soils, by integrating two instruments into one.

3.5 Figures

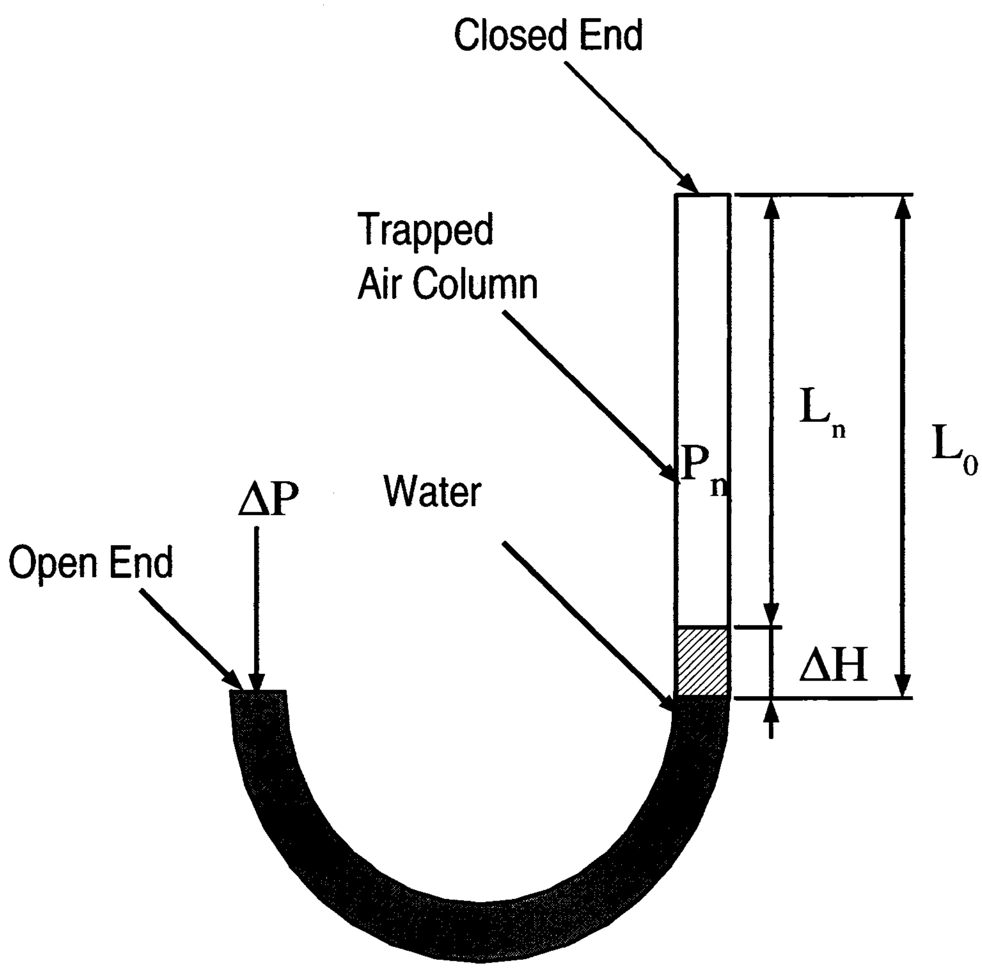

Figure 3.1 Conceptual model of the pressure gauge.

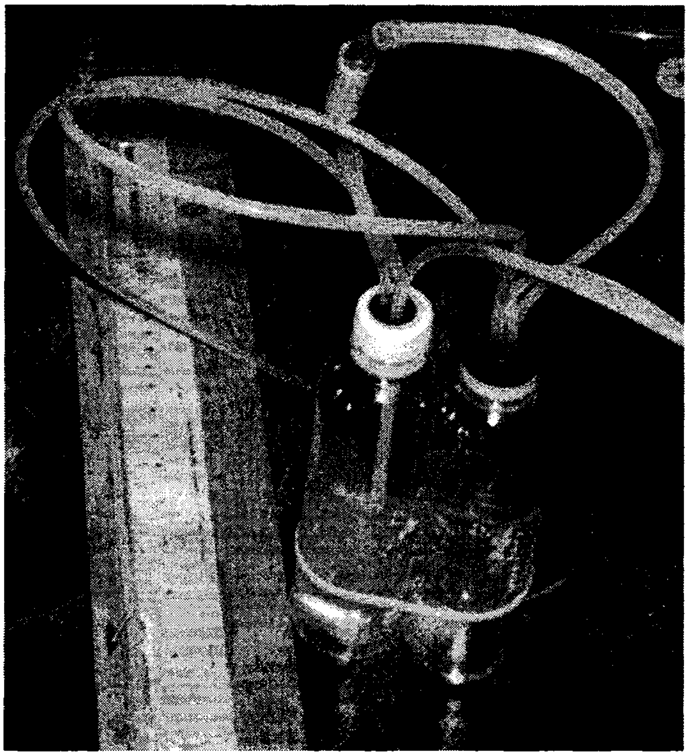

Figure 3.2 Pressure gauge designed with the aid of Mariotte bottle and a 343 mm long scale.

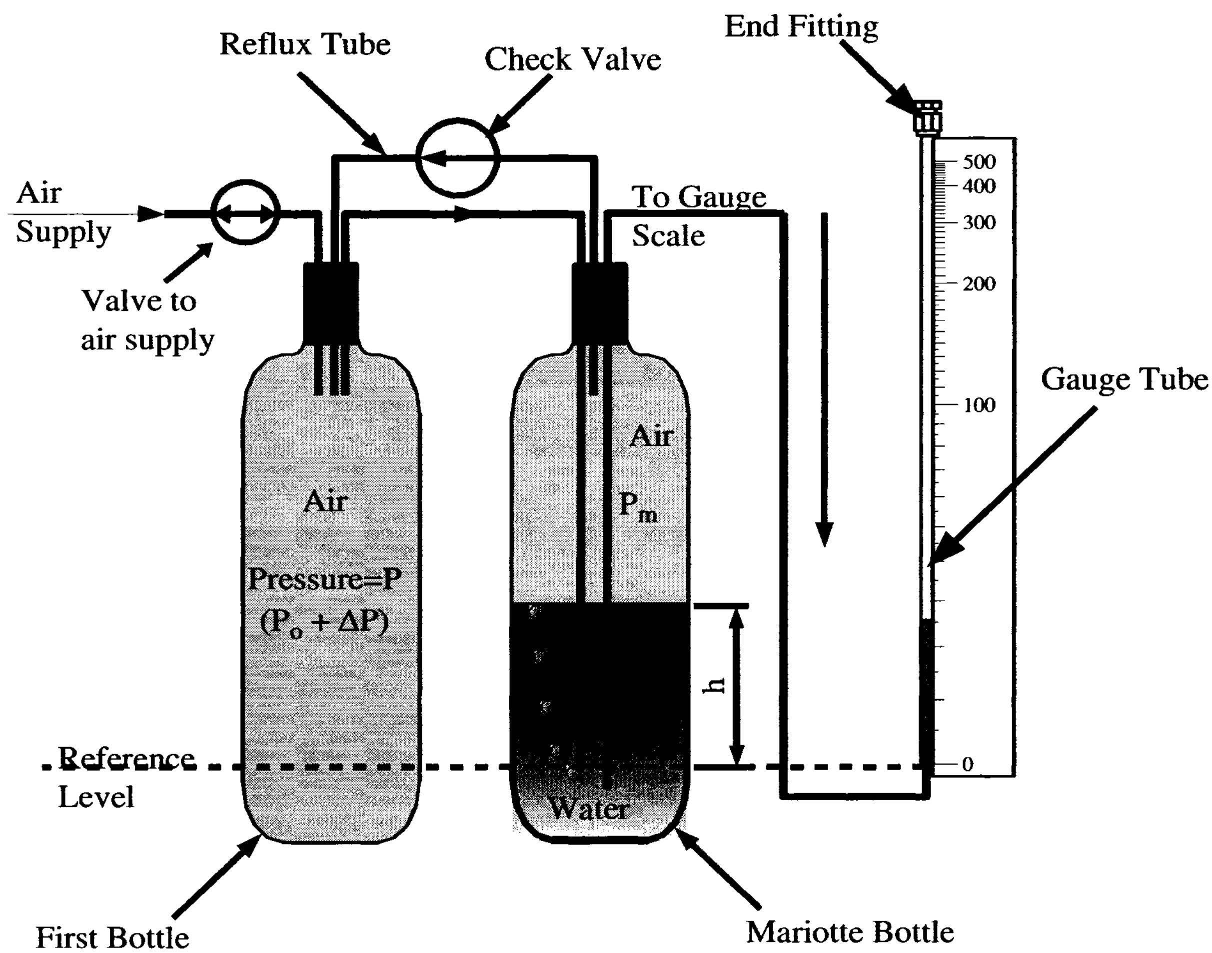

Figure 3.3 Schematic of pressure reading system

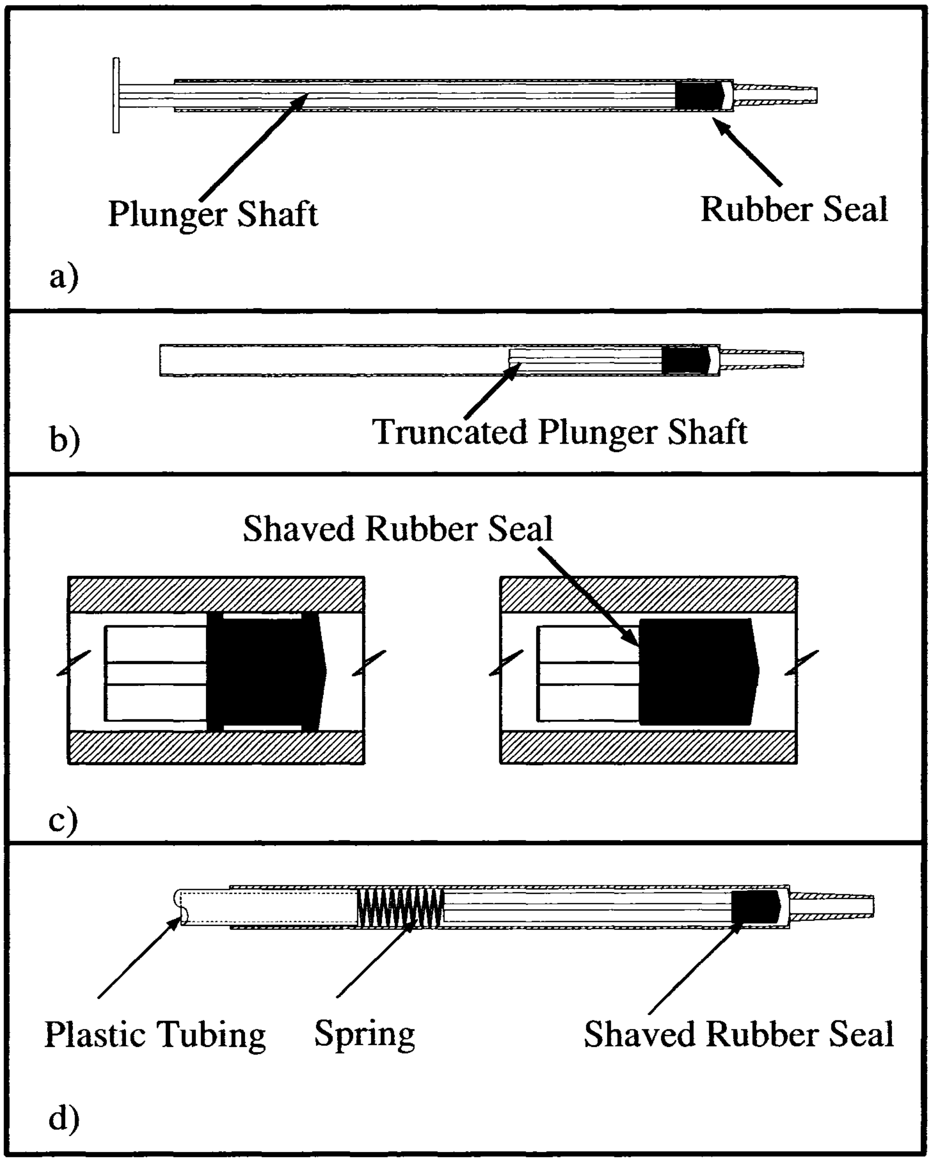

Figure 3.4. Design of a check valve using a 1 cc syringe and a small spring.

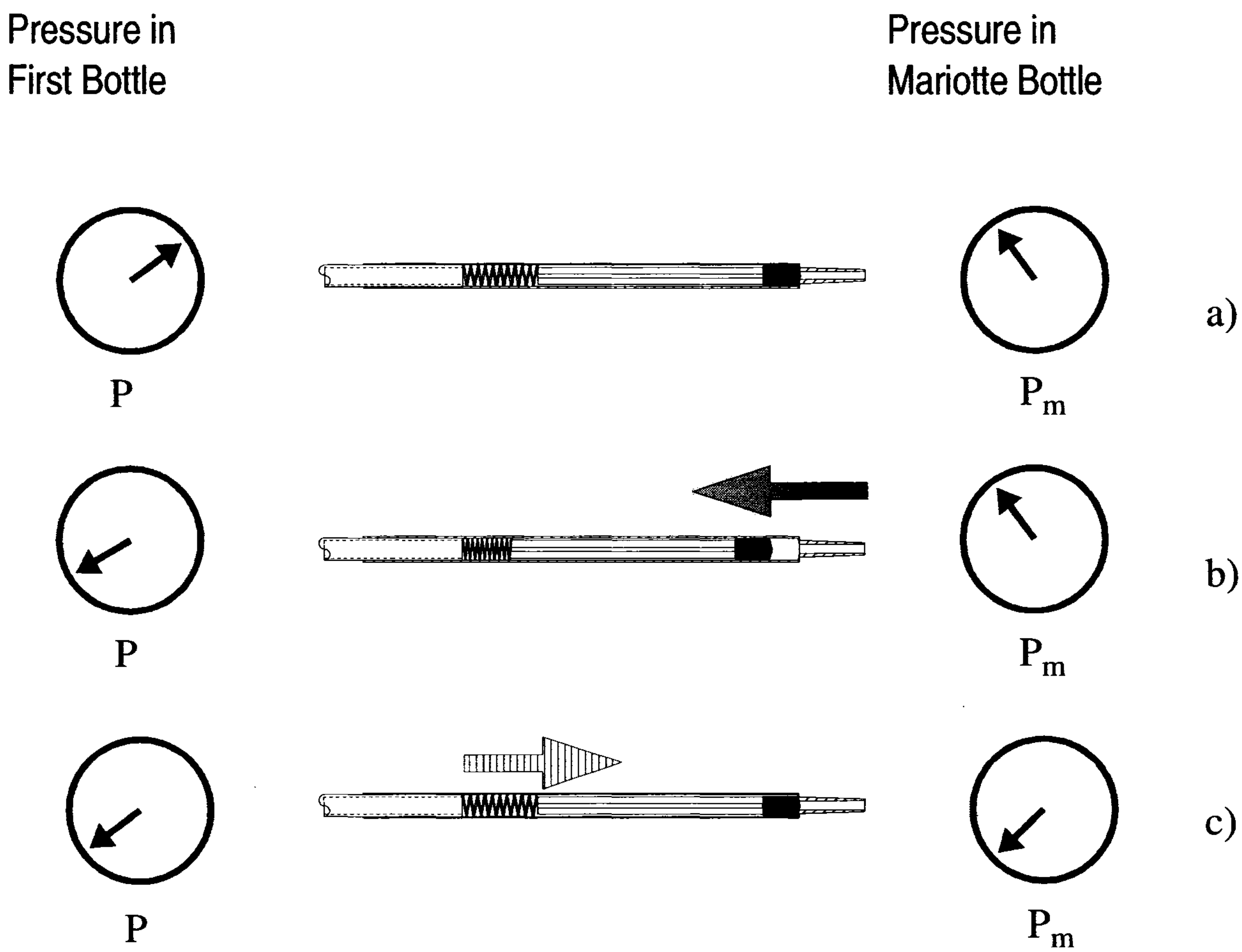

Figure 3.5 The operation of the syringe check valve.

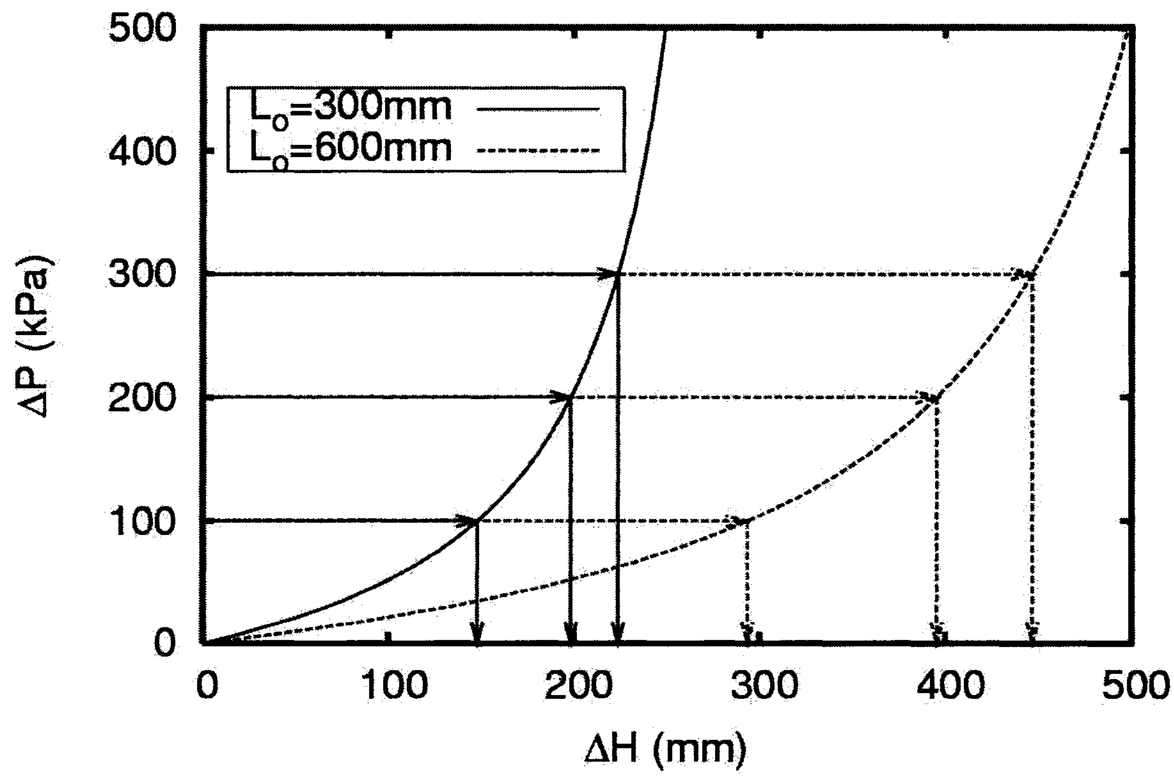

Figure 3.6 Illustration of the generation of a pressure scale for a number of predetermined gauge pressure values ΔP.

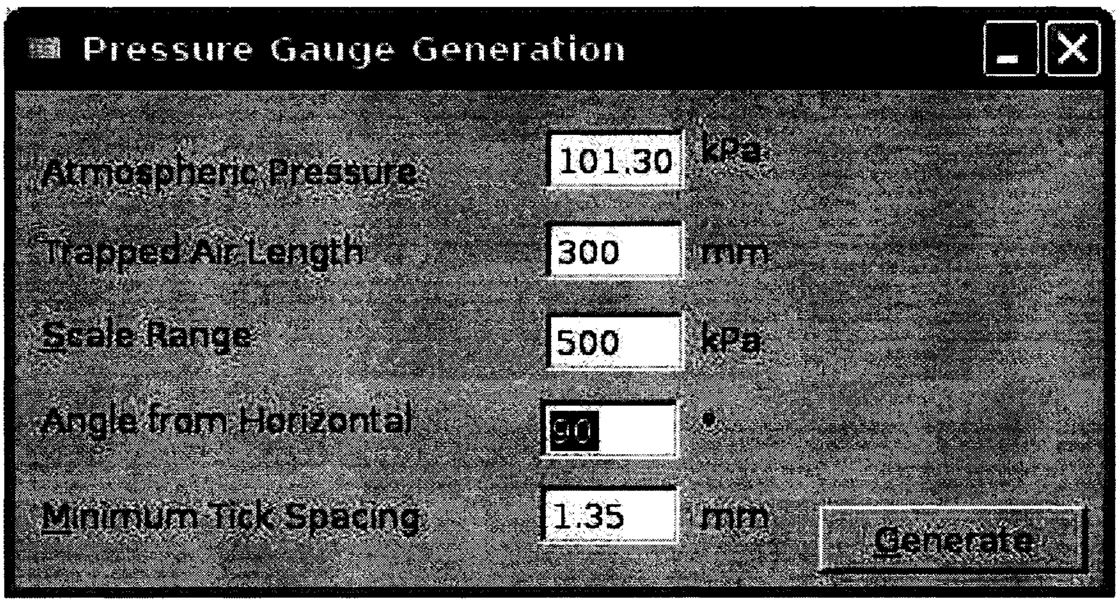

Figure 3.7 Interface to the macro program to generate a custom graduated pressure scale.

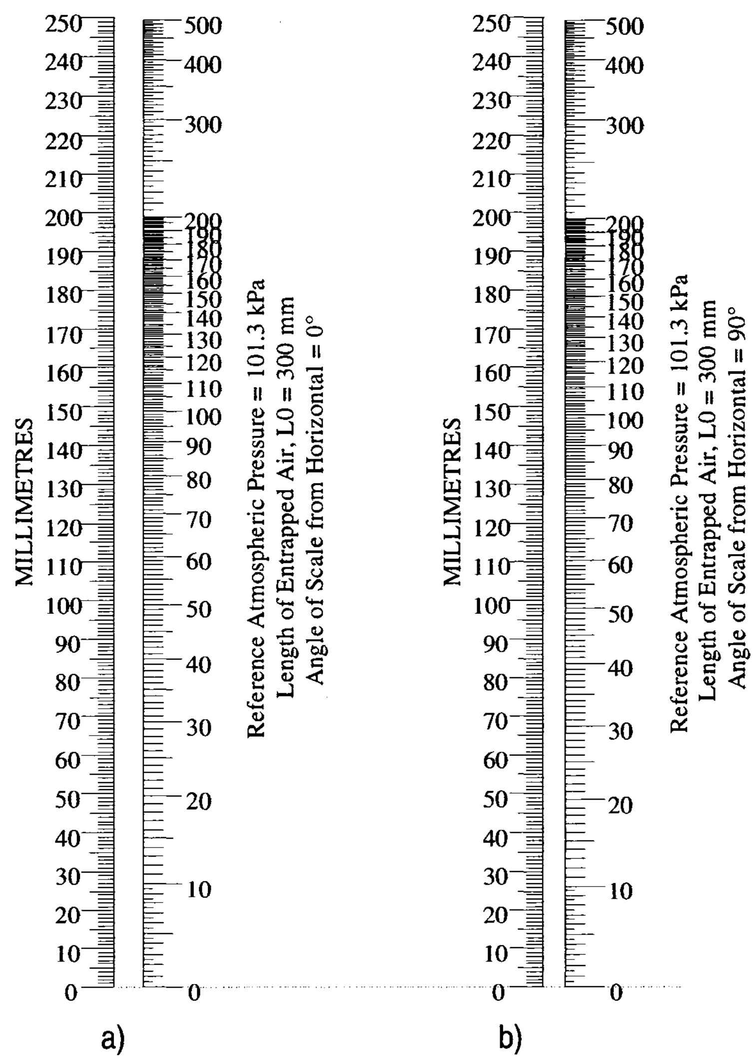

Figure 3.8 Custom horizontal and vertical scales generated for an atmospheric pressure of 101.3, and a trapped air length of 300 mm.

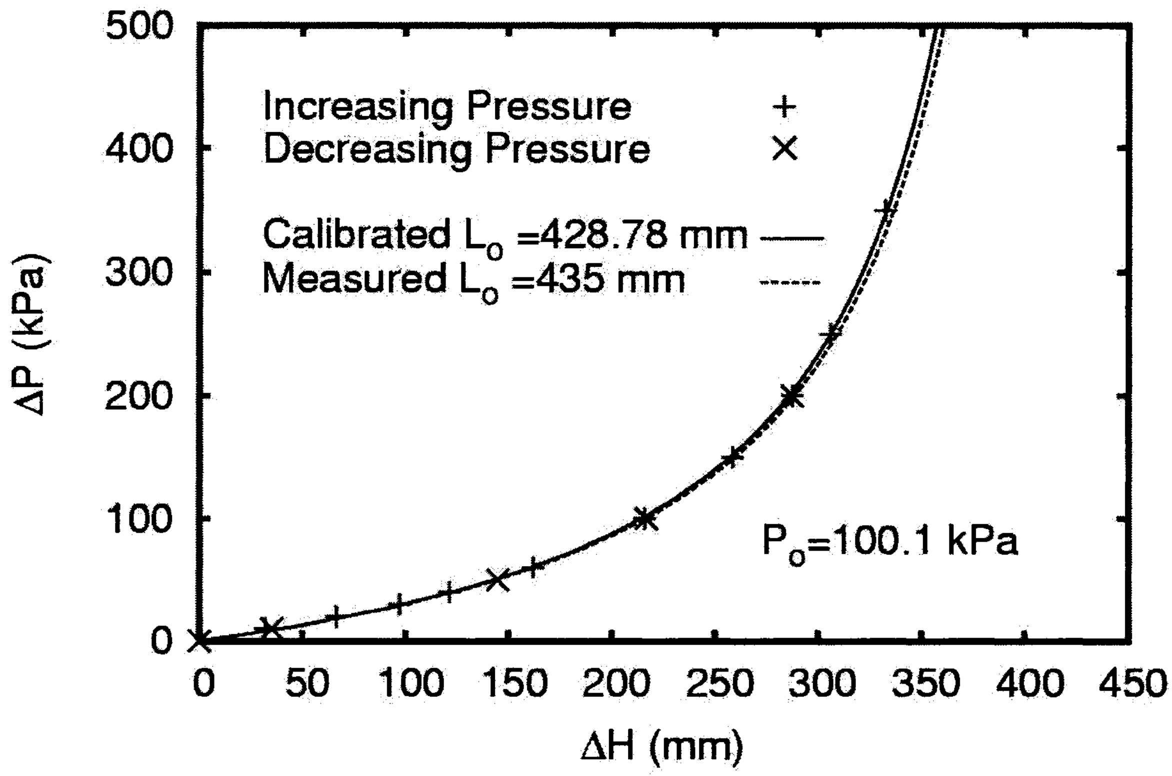

Figure 3.9 Calibration of a 430 mm long horizontal gauge tube, with both increasing and decreasing pressures.

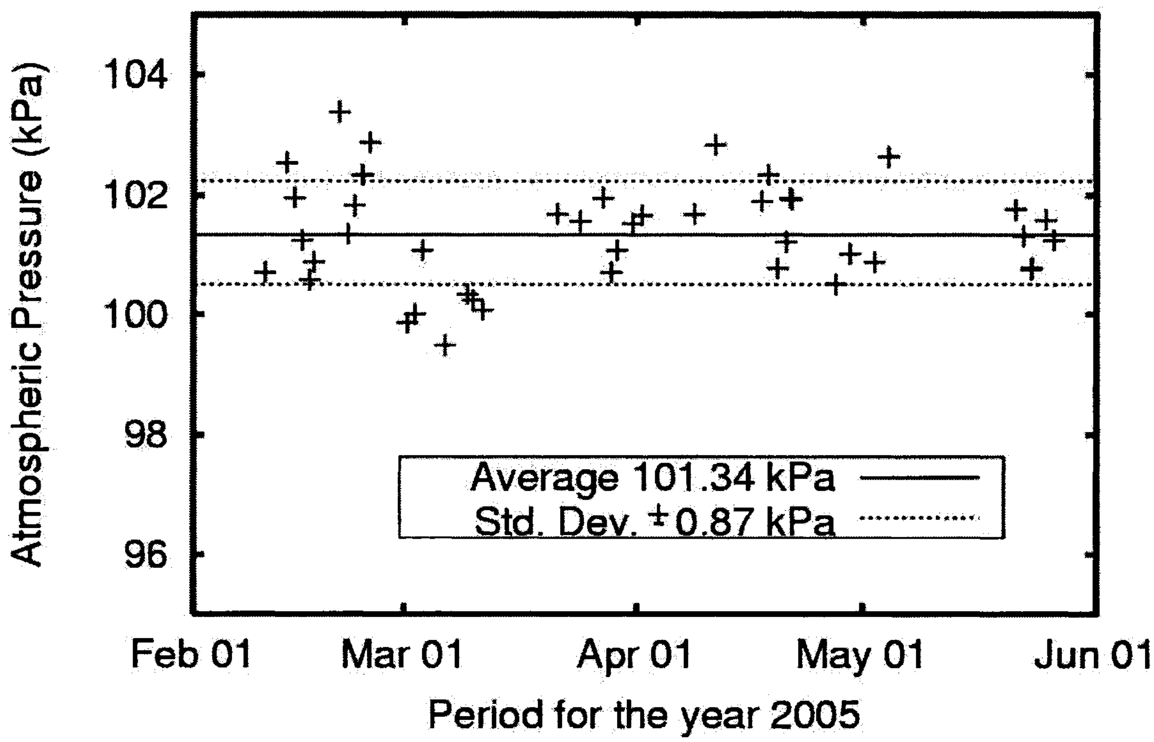

Figure 3.10 Random samples of the atmospheric pressure taken in Ottawa, Canada, during a period of almost 4 months. Data from Environment Canada.

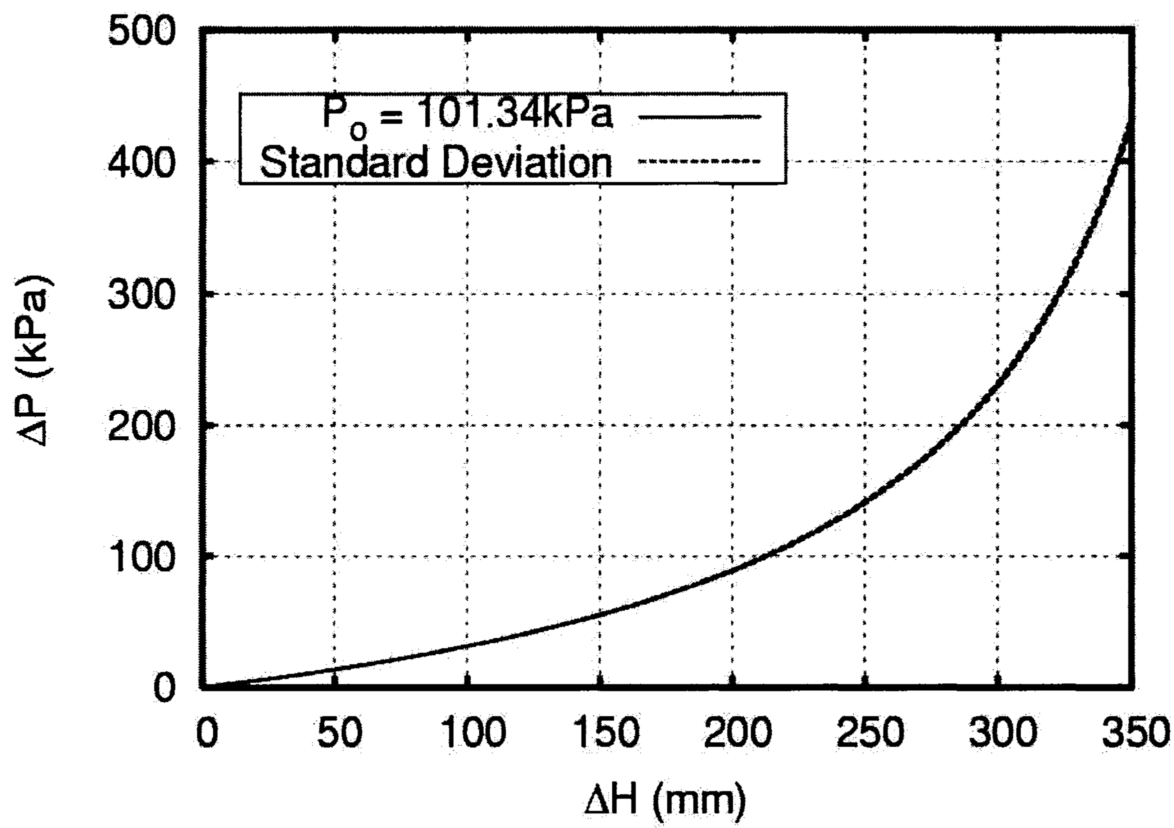

Figure 3.11 Variations of the pressure reading for a gauge of 430 mm trapped air length using either an average atmospheric pressure P_o of 101.3 kPa or ± 1 standard deviation (0.87 kPa).

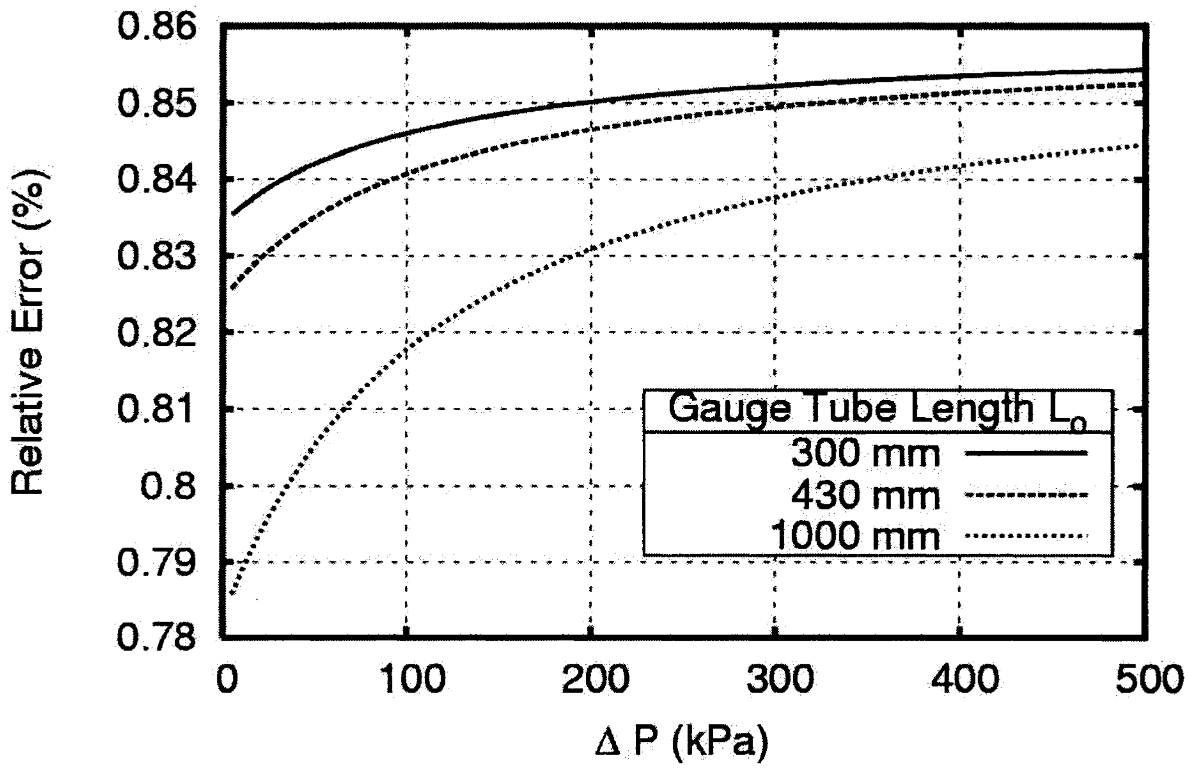

Figure 3.12 Relationship of the relative error in measurement at the standard deviation boundaries with respect to gauge pressure ΔP, for different lengths of gauge tube lengths L_o.

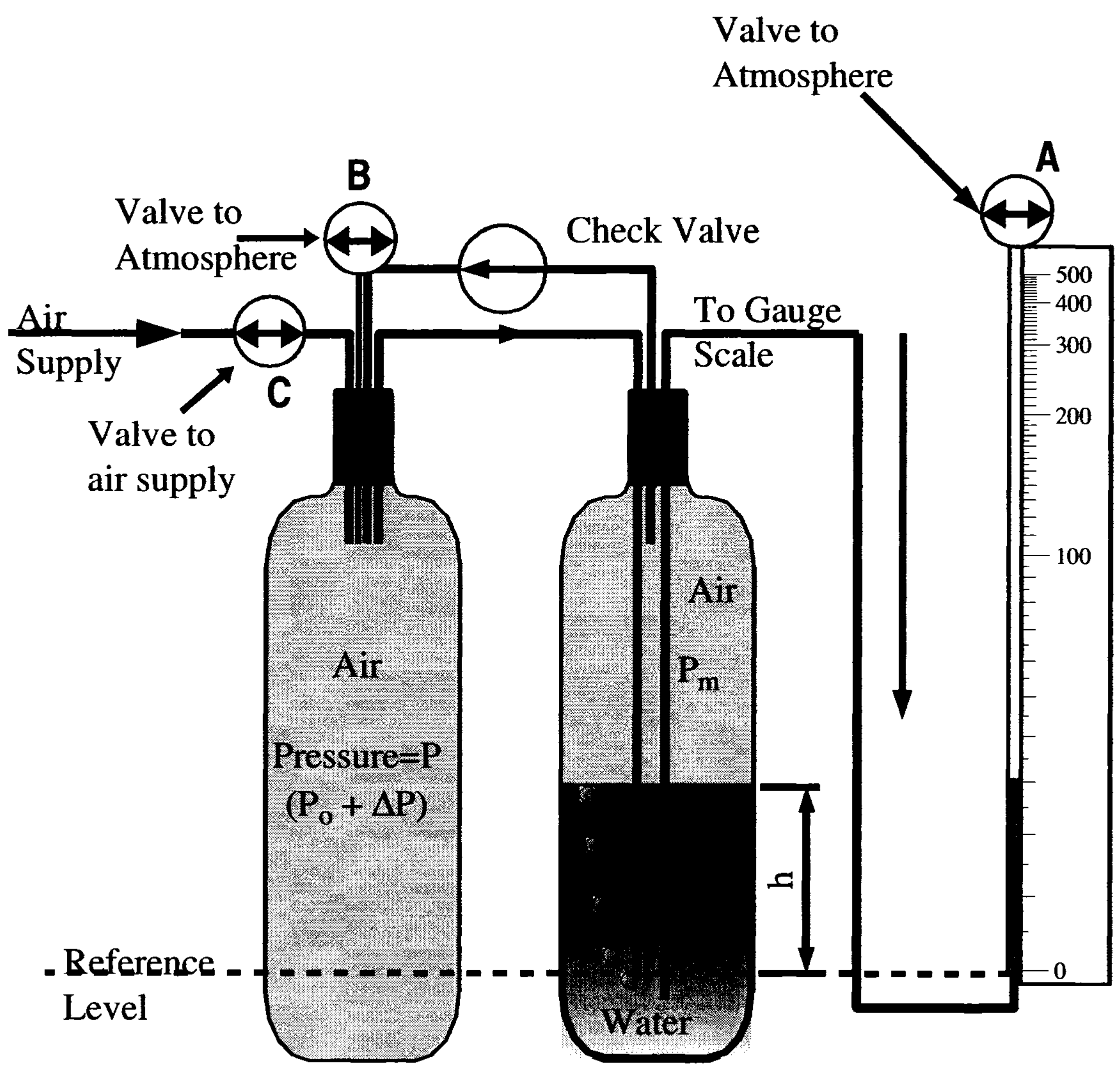

Figure 3.13 Two valves to atmosphere can be added to facilitate resetting of the pressure gauge.

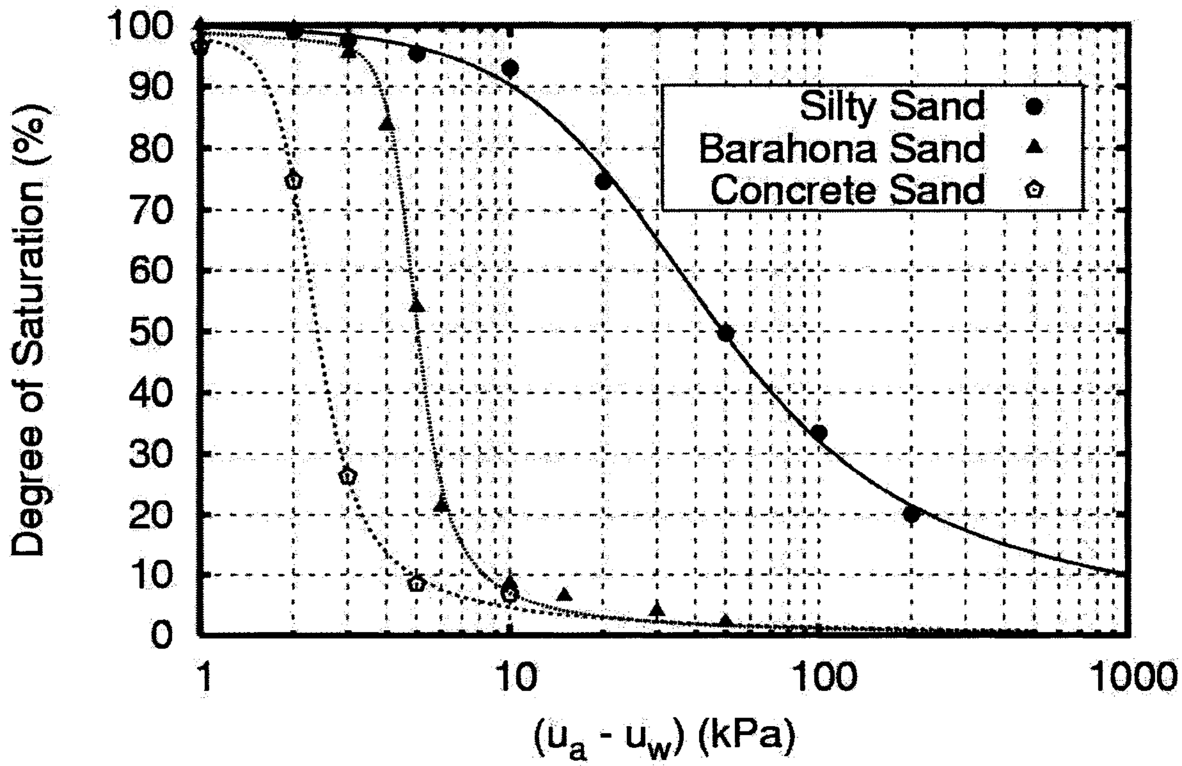

Figure 3.14 Soil water rentention curves for 3 different sands (silty sand, Barahona sand, washed concrete sand), generated using the trapped air column pressure gauge for a range from 1 to 500 kPa.

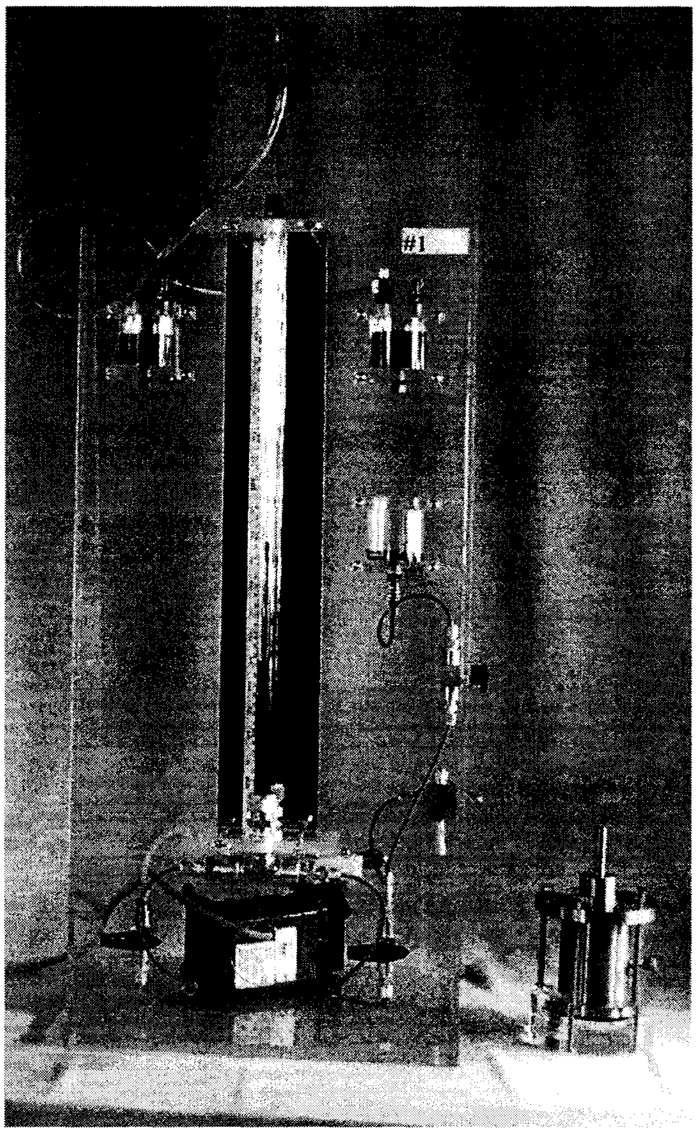

Figure 3.15 View of the flushing system/volumetric gauge apparatus connected to a tempe cell for axis translation technique.

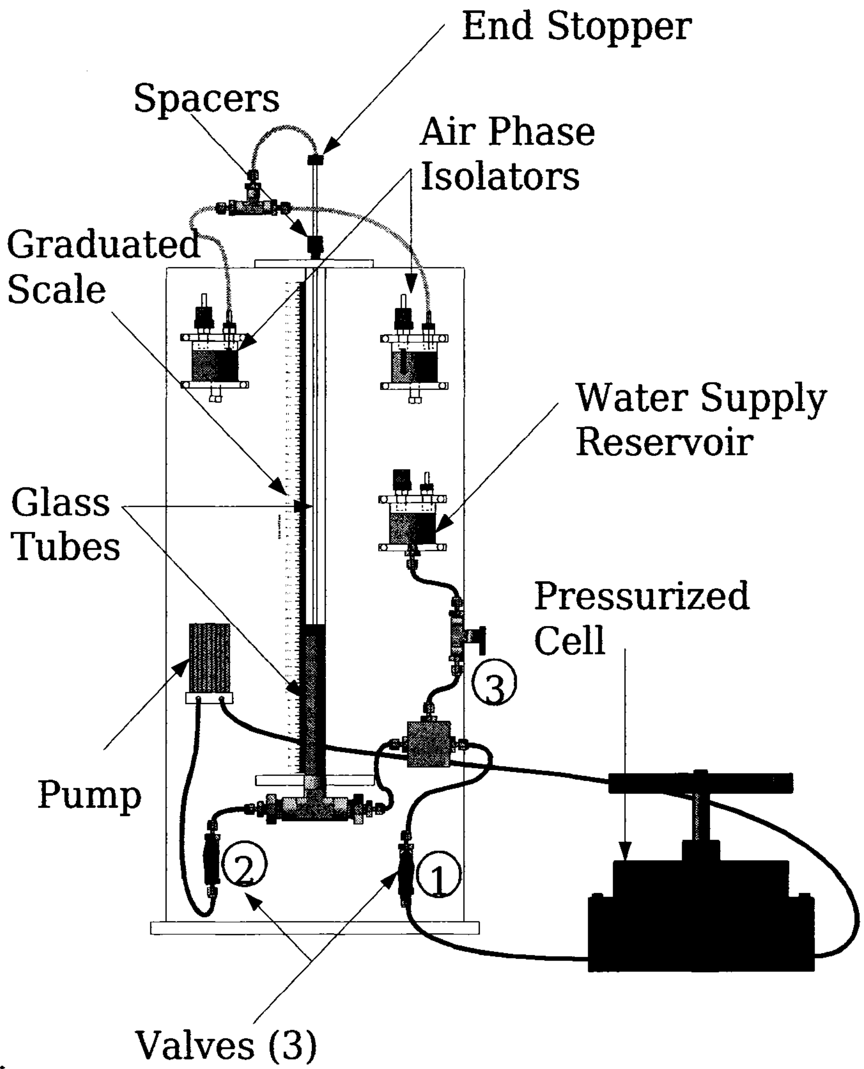

Figure 3.16 Schematic view of the flushing/gauge system.

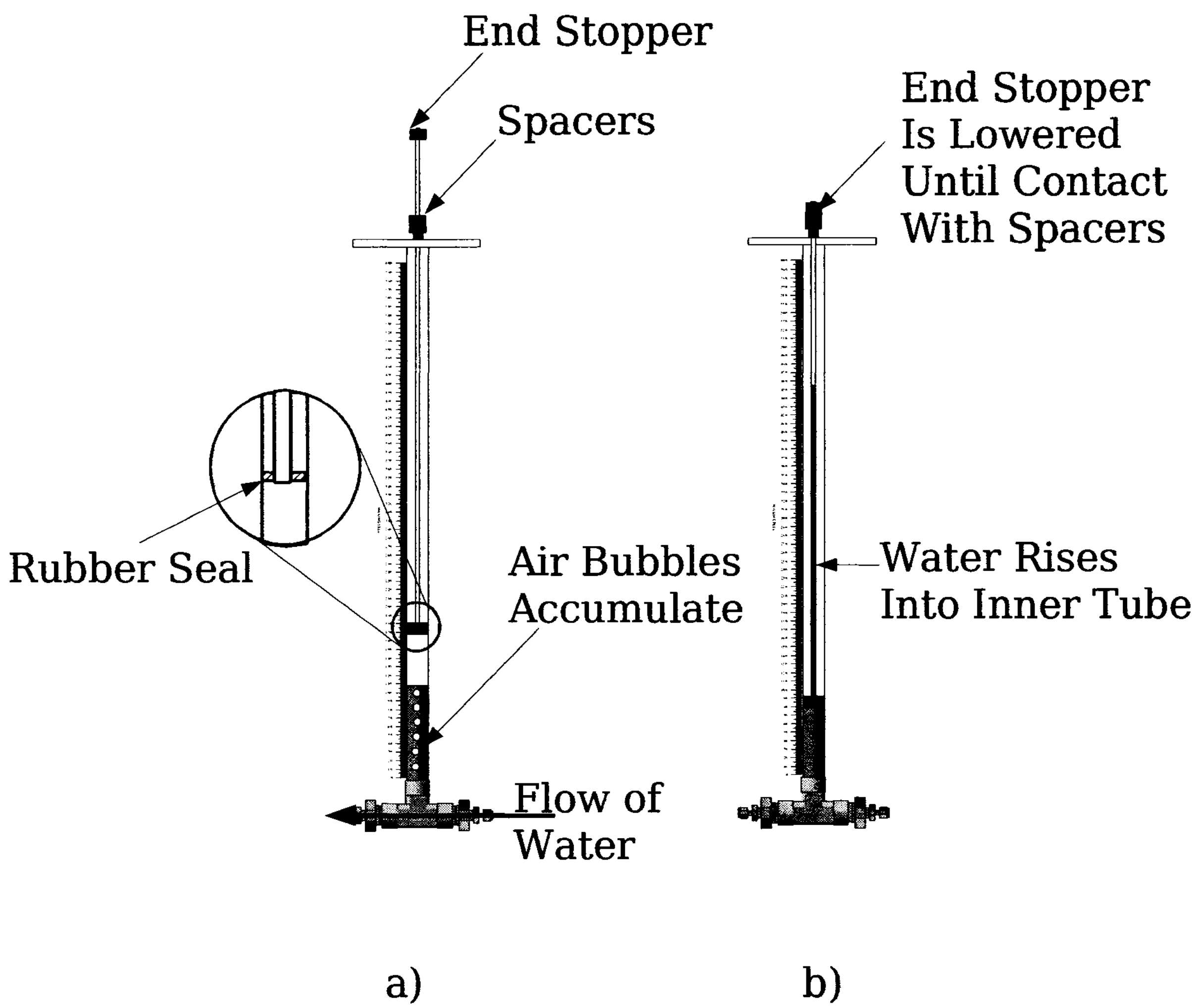

Figure 3.17 Inner tube is raised for flushing (a), and lowered for taking readings (b).

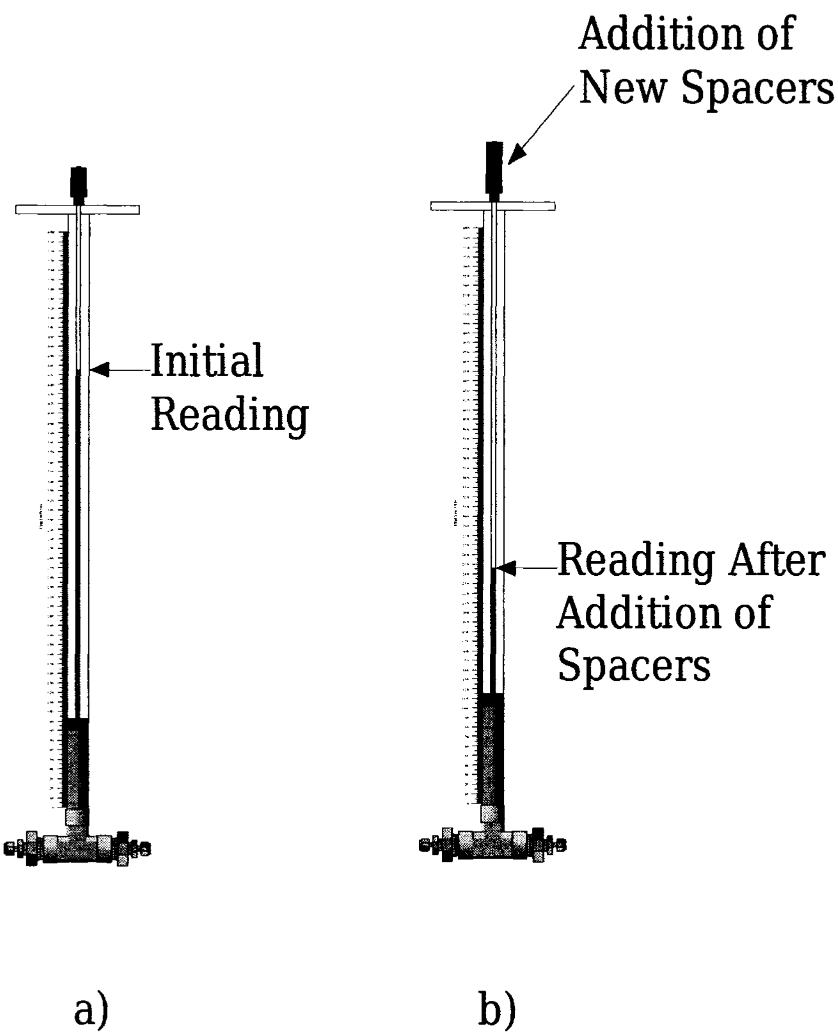

Figure 3.18 Adding spacers to increase range of readings.

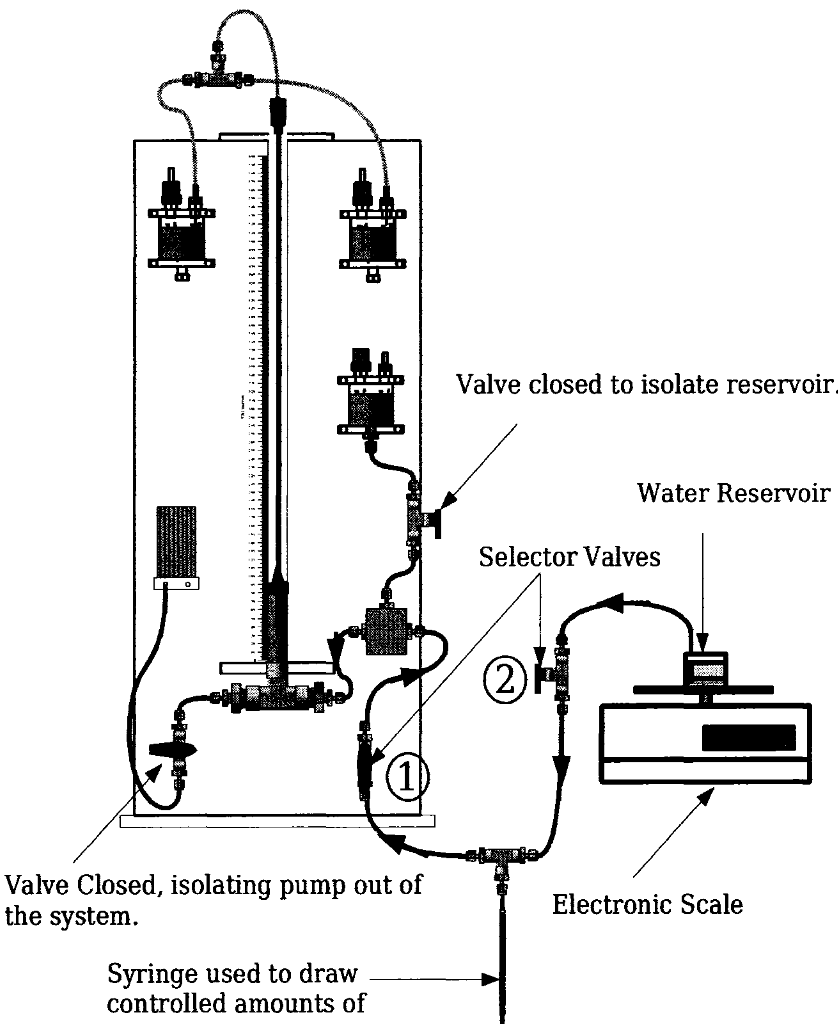

Figure 3.19 Calibration of the volume gauge.

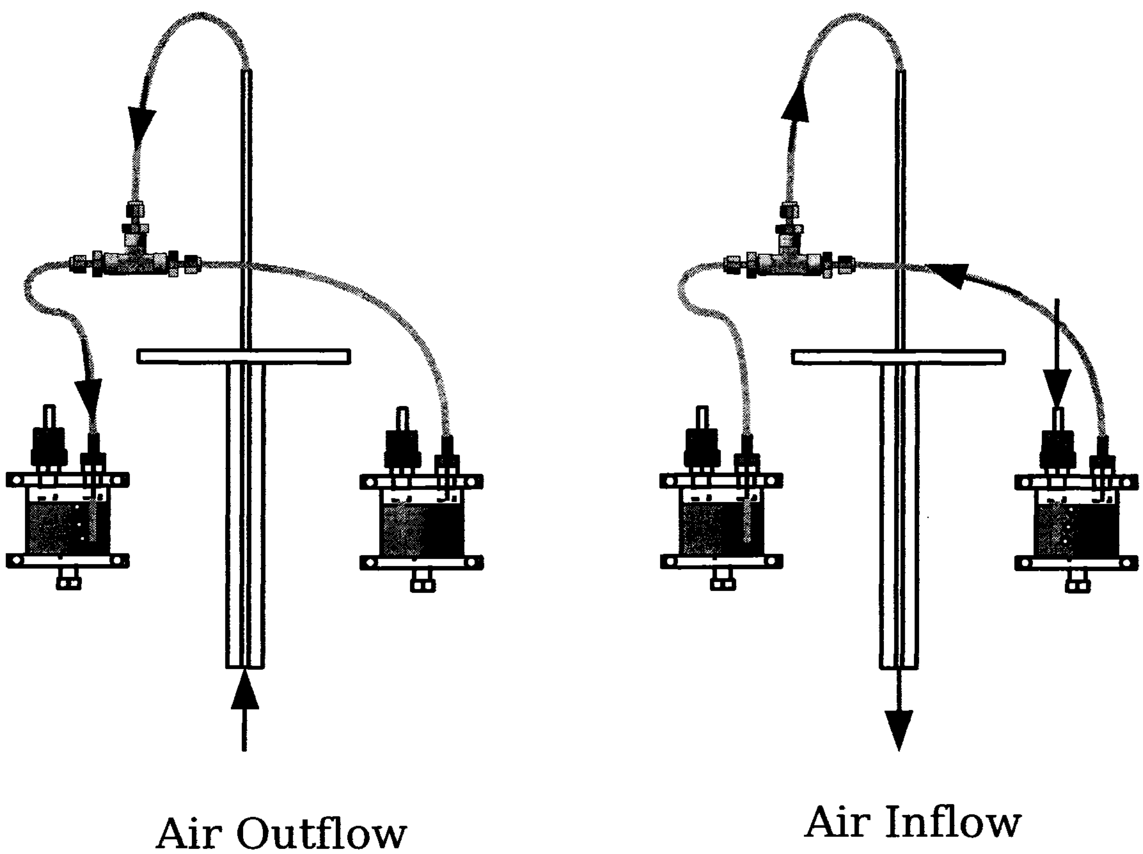

Figure 3.20 Air outflow (during lowering of inner tube or rise in water level), and inflow (during raising of the inner tube, or decrease of water level).

4 Modified Ring Shear Cell

4.1 Introduction

The axis translation technique introduced by Hilf (1956) has been used as a conventional tool in the determination of the shear strength of unsaturated soils. In this technique, a positive air pressure is applied to control suction in the soil specimen, thus avoiding the problem of cavitation in the apparatus for suction values greater than 101.3 kPa. During the last few decades, conventional testing equipment such as direct shear, triaxial and unconfined compression testing apparatus used for saturated soils testing have been modified and extensively used in the determination of the shear strength of unsaturated soils in the suction range of 0 to 500 kPa [Bishop and Donald (1961), Ho and Fredlund (1982), Gan and Fredlund (1988), Escario and Jucá (1989), Hettiaratchi et al. (1992), Ridley (1995) de Campos and Carrillo (1995), Vanapalli et al. (1996), Caruso and Tarantino (2004)]. The modified direct shear tests are particularly convenient for the determination of the shear strength of fine-grained soils [Fredlund and Rahardjo (1993)]. These tests offer an advantage over the triaxial tests because the drainage path in the soil specimens is relatively much shorter. The time required to reach equilibrium conditions under different values of applied matric suction is relatively much lower. However, shear strength and deformation behaviour of unsaturated soils can be studied only over a limited range of displacement. Due to this limitation, the critical state shear strength behaviour of some unsaturated soils cannot be determined using modified direct shear test

A conventional ring shear device used for determining the shear strength of saturated soils has been modified for the specific purpose of testing the shear strength and volume change behaviour of unsaturated soils using the axis translation technique. The modified ring shear equipment incorporates an automated data acquisition and control system which allows independent control of the pore-air pressure, u_a and the net normal stress, $(\sigma - u_a)$.

Both the peak and critical shear strength behaviour of unsaturated soils can be determined in single stage tests using the modified ring shear apparatus. This is possible because the shearing deformations follow the annular shape of the specimen, and as such the geometry of the shear surface is not affected by the shearing process. In addition, multistage tests can be carried out on the same specimen without any restriction of shear displacements. The current design of the modified ring shear test apparatus allows for the measurement and/or control of the specimen volume, water content and matric suction. In other words, this apparatus can also facilitate the measurement of soil-water retention characteristics of the specimen in the ring shear device.

In most ring shear test devices, the shear box is made of two halves with a gap separation introduced before shearing. This is similar to the direct shear box, and favours the formation of a horizontal plane of failure at the location of the separation. This method of testing is simple and provides a well defined shearing plane, but raises concerns with respect to the nature and magnitude of the stress concentration at the boundaries of the specimen.

The current cell design of the modified ring shear equipment is based on the apparatus previously developed by Garga and Infante Sedano (2002). In this apparatus, the confining cell walls of the annular specimen are made of stacks of 2 mm thick rings. These rings can easily slide over each other so that they can independently move with the soil at their respective depths. This technique reduces the stress concentrations which are typical of conventional ring shear tests. In addition, the introduction of a predetermined horizontal plane of failure is avoided using this apparatus. While the specimen is allowed to fail along its natural weaker plane, tests conducted on sand using the original unmodified prototype of the constant volume ring shear device have shown that there was still a localized zone of failure within the specimen and that the shearing was not uniform [Garga and Infante Sedano (2002)]. No systematic investigation on the nature of the failure zone has yet been conducted on the modified device while testing unsaturated soils.

4.2 The Cell

Figure 4.1 shows the modified ring shear cell with the different components. The modifications include the addition of a cell cover to allow the application of a positive air pressure, as well as the provision of a number of high air entry discs in the base, and a base groove for drainage. The principal modifications are described in later sections.

4.2.1 Cell base

The cell base is made from an aluminium cylinder, in which an annular space (Figure 4.1 and 4.2) has been machined. This ring cavity is 40 mm wide and 30 mm deep to accommodate two stacks of ten 2 mm thick lateral confining rings and the soil specimen (Figure 4.3). The cell must be deep enough to accommodate the specimen thickness of 18 mm to 20 mm as well as the 8.9 mm thickness of the bottom platen (Figure 4.1).

A meandering groove provision at the bottom of annular space facilitates de-airing of the specimen (Figure 4.4). This groove is connected at each end to an orifice leading to a connector at the base of the cell. This arrangement is useful to collect any diffused air bubbles that collect below the ceramic and to flush them intermittently with water. The meanders of the groove correspond to the position of the ceramic discs of the base platen such that 63% of the disc area is covered by the groove.

4.2.2 End platens

The lateral confinement of the tested specimen is achieved through the use of confining ring stacks. The vertical confinement is provided by the end platens. The top platen is a brass ring, with a roughened surface, placed under the top cap (Figure 4.1). The function of the top cap is to transmit the normal load and provide a shearing resistance at the interface with the specimen that is higher than the angle of internal friction, ϕ' of the soil.

The bottom platen was designed to incorporate high air entry ceramic discs such that the axis translation technique can be used. The role of these high air entry ceramic discs is to act as a barrier to air flow from the pressurized cell. These are required to be permeable such that the water in the specimen, ceramic discs, and external reservoir remain interconnected. In this manner, a differential pressure can be established between the pore-air, u_a, and the pore-water pressure, u_w. The difference between the pore-air and pore-water pressures is the matric suction, $(u_a - u_w)$.

The ceramic disc area covers about 80% of the specimen area. Handling and machining considerations steered the design towards the use of a number of small circular ceramic discs encased in a brass ring (Figure 4.5), rather than the use of a single annular disc.

The thickness of the ceramic discs is slightly smaller than the brass ring. The discs therefore are recessed, leaving a lip of 2 mm depth to the surface of the brass ring. The recesses significantly increase the friction between the soil and the bottom platen, which in turn favours the formation of a shearing plane within the specimen, rather than at the interface with the bottom platen.

An epoxy was used to provide both bonding of the ceramic to the brass ring and seal against the air pressure. The epoxy was applied in three layers to ensure a good bonding and minimize leaks. A trial and error investigation undertaken at the University of Ottawa has shown that the use of multiple layers improves the control of the application of the epoxy and avoids the formation of interconnecting bubbles which can result in air leaks. A time interval of 24 hours is necessary for the epoxy to harden between successive layers.

4.2.3 Cell Cover

An aluminium cell cover, with a wall thickness of 6.4 mm, (Figure 4.1) was designed to be fitted onto the base of the cell to provide a pressurized environment. The cover is secured into place using twelve 5 mm diameter screws. The pressurized cell was sealed from the external environment by inserting an O-ring in the cell base, at the interface between the cell base and the cell cover.

4.2.4 Torque Arm

The use of the cell cover to provide a pressurized environment for the specimen resulted in the need to extend the torque arm. The extension rod of the torque arm projects out of the cap through the cell cover and is fastened to the torque arm. A bushing (Figure 4.6) keeps the pressurized chamber sealed. The bushing also facilitates the vertical alignment of the torque arm which keeps the top platen sitting horizontally on top of the specimen. The free end of the rod was machined to provide four plane faces which allow four screws to lock the torque arm to it. Dismantling the torque arm is simple due to the addition of this feature.

4.3 Flushing System and Water Volume Measurement

Although free air cannot cross the high air entry discs placed between the soil and the measuring system, some air can cross this barrier through the water phase. Below the disc air can come out of solution and form air bubbles. It is therefore a recommended practice in unsaturated soil testing to provide a mechanism for removing the air bubbles that form under the ceramic disc when using the axis-translation technique. This procedure maintains the continuity of the water phase. It also provides the necessary data to apply the correction to the water content measurement, through the measurement of the volume of air that collects into an air trap. Without such a correction, the air bubbles forming under the ceramic discs would be interpreted as an increase of water coming out of the specimen, or a reduction of the water going into the specimen.

A flushing system has the additional advantage that it can correct any small air leaks which may occur due to cracks in the ceramic discs or to defective bonding of the epoxy. However, bubbles formed as a result of such small leaks cannot be distinguished from the diffused air coming out of solution. In some cases, air intrusion from small leaks may be the dominant cause for the presence of air bubbles below the ceramic discs. The exact source of the air bears no impact on the final results as long as the air can be removed and its volume determined.

Figure 4.7 shows an idealized schematic of the flushing system used in conjunction with the modified ring shear cell. It incorporates the de-airing groove in the cell base, an air trap for collection of air bubbles, and a displaced water measurement gauge. A gear pump is used to circulate water through the groove and flush out air bubbles. Gear pumps are displacement pumps which use the meshing of gears to circulate the water (Figure 4.8). The micro pump used for the current system provides a flow of 2100 to 2200 ml/min under an approximate head of 20 kPa using a 12 V power supply.

The pump draws water from the air trap and directs it into the de-airing groove of the ring shear cell. The water and any air bubbles thus collected flow back to the air trap, to complete the circuit (Figure 4.7). All air bubbles accumulate at the top of the air trap. The collected air can be removed using a syringe connected to the valve at the top of the air trap. A small diameter, 1 ml capacity syringe (Figure 4.9) with a precision of 0.01 ml, permits the volume measurement of the collected air, when resetting the water level in the air trap to a fixed reference level. All water volume measurements are taken using this reference level. This small diameter syringe can serve as a diffused air volume indicator since the volume of air in the syringe once the water level is at its reference mark can be measured directly. The main measurement system, however, is the indirect measurement by the sudden drop in the recorded volume of water after each flushing operation. Since the measurement of the water volume is done with an instrument of higher precision, the indirect method provides a more accurate air volume measurement.

Any water expelled from the specimen pushes water into the air trap, and the displaced water moves through the capillary overflow tube. The volume of water displaced can be measured through the use of an overflow tube which is attached either to a calibrated scale or a volume gauge. In this research, the overflow tube is connected to a closed jar (shown as overflow jar, in Figure 4.7) placed on a precise electronic balance. The mass of the jar is measured to a precision of 0.001 g (over a maximum range of 500 g). The use of an electronic balance permits the automation of the water content change measurements. It also permits readings over a much broader range than most electronic sensors of equivalent precision.

Special attention must be paid to the connection of the tubes and the overflow jar when using a precise balance and an overflow jar to measure the changes in water content. It should be noted that even a tiniest moment build-up at the junction between the overflow tube and the jar causes continuous changes in the measured readings. In such conditions, it is impossible to maintain a stable reading even in a closed system. This type of system can also be sensitive to any ambient changes and air movements that are transmitted to the jar through the overflow tube.

Ideally, a simple connection that ensures no transmission of moment from the tube to the jar is required to eliminate any instabilities associated with the readings. In practice it is difficult to completely remove these instabilities in the measurements. Several attempts were made to overcome this physical limitation and stabilize the system. These included replacing overflow tube by one made of a more flexible material in the hope that a less rigid system would reduce the transmission of moments to the overflow jar. This proved insufficient and the problem persisted.

In an attempt to minimize the contribution of external factors to the changes in readings, the overflow tube leading to the overflow jar was fixed at two points to the glass inside of the case enclosure of the balance. Once again, although some improvement was observed, it was insufficient to obtain reliable readings.

This problem was finally resolved when a mass of sealing gum was pasted to the flexible tube segment in the last segment of tube (Figure 4.10). This dampening mass was added to the lowest point of the tube, before it looped back up to the overflow jar. This allowed maximizing the inertia of the tube against rotation. On initial installation of the mass, several minutes were required for the system to reach a state of equilibrium.

The resulting system was so effective at reducing the influence of the external environmental effects that the readings remain stable even if the overflow tube is knuckled outside the balance enclosure. Intentionally lifting the balance caused only temporarily change in the readings by a few thousandths of a gram, before the readings reverted to the initial value in a few seconds. The electronic balance was used for measurements only after it was verified that this level of reading stabilization could be achieved.

4.4 Automation

The apparatus has been extensively automated to allow a greater flexibility in the types of tests that can be performed. Indeed, although strictly not necessary for constant load tests, where the data could easily be collected manually, automation proves to be helpful for constant volume or constant water content tests which require continuous monitoring of the volume and water content changes in order to adjust the applied load or air pressure. Automation results in a smoother operation and more reliable testing.

4.4.1 Instrumentation

The array of sensors used to monitor the state of the specimen during test consists of the following components (Figure 4.11):

1. One LVDT to measure the vertical deformations.

2. Two load cells for the measurement of the torque. The distance separating the point of application of the resisting forces measured by the two load cells is 152.4 mm (6"). The shear resistance of the specimen is calculated from the torque measured by these load cells, and the cross-sectional area of the specimen on the shear plane.

3. One pressure transducer to monitor the pressure of the air phase, and therefore the matric suction.

4. One rotational potentiometer to measure the angular displacement of the cell with respect to the top platen. This device combined with the data acquisition system has a resolution of 0.3 degree over the full range of 360 degrees.

5. One load cell connected to the loading arm of the ring shear device. The normal load acting on the specimen is increased by a lever factor of 10:1 due to the moment arm.

6. One precise electronic balance (resolution of 0.001 g) to measure the water over flow from the air trap, and thus facilitate the measurement of water content change of the specimen.

4.4.2 Pneumatic Control Systems

Two pneumatic systems are used to control both the applied air pressure corresponding to the matric suction and the vertical net normal load acting on the specimen. The main components of the system are two computer controlled pressure regulators (Figure 4.12). In the case of the matric suction, the pressure regulator directly controls the air pressure applied to the specimen. The air provided to the specimen is first bubbled through water, after having passed through the regulator, to increase its humidity such that it will not cause the desiccation of the specimen. A pressure transducer in the cell cover measures the pressure actually applied to the specimen.

The second pressure regulator controls the air pressure that is supplied to a pneumatic actuator (Figure 4.13) that provides the normal load during shear. This actuator, with an internal piston diameter of 35 mm pulls on a rod connected to a lever arm, with a ratio of 10:1. It should be noted that the load applied by the piston is measured by a load cell as it pulls on the lever arm. It is not calculated from the applied air pressure. Also, because the applied cell pressure causes a net upward force on the top cap, a correction to the applied normal force must be applied that corresponds to the cell pressure times the cross-sectional area of the torque rod (Figure 4.1).

4.5 Compaction

4.5.1 Compaction Equipment

The production of compacted specimen for the ring shear apparatus has required the development of specialized tools to ensure uniformity of the compaction over the entire span of the specimen. This section provides the key details of this equipment. The first component of the compaction equipment is the ring stack alignment ring (Figure 4.14). This thick aluminium ring is normally used to provide alignment for the confining rings when placing them in the ring so that they will be perfectly centred. It therefore has the same geometrical characteristics as a soil specimen, and can be used to compact the soil.

In order to apply the compaction stress on the specimen, a compactor block was built that would fit exactly on the alignment ring (Figure 4.15). The diameter of the block is 136.27 mm. The middle part of the block is raised by a few millimetres in a circular area of 95.25 mm diameter (Figure 4.16) that fits exactly inside the inner area of the compaction ring. This ensures that the compaction block is perfectly centred when applying the load to the compaction ring, and therefore the load will be uniformly distributed over the specimen.

A rod of a diameter of 31.75 mm is attached to the compaction block, and goes through two alignment beams tied to a triaxial loading frame, before connecting to a proving ring or a load cell at the other end (Figure 4.17). The setup allows for measurement of the applied stress as well as ensuring proper alignment of loading forces, so that a uniform compaction stress may be applied.

4.5.2 Specimen compaction procedure

The ring shear specimen is prepared in several layers by compacting each one to the desired compaction stress. Care is taken to weigh the specimen before and after each layer has been compacted so that any loss of water during the time interval of the compaction sequence can be taken into account. The compaction load is applied until a stable load reading can be achieved with few corrections.

In order to ensure the proper alignment of the cell and the loading rod, the centre of the wide foot is raised by a few millimetres with respect to the surface (Figure 4.16). This raised portion fits inside the alignment ring's central hole, and centres the cell and specimen with respect to the loading rod. This ensures that the load is applied on the specimen both vertically and without any eccentricity.

4.6 Types of Tests

The instrumentation and pneumatic control systems can be used in conjunction with a computer to run four basic types of shear tests. These tests involve the measurement of the applied normal load and the resulting volumetric changes and shear stresses as the specimen is sheared, as well as the applied air pressure and the resulting water content changes. Two servo motor activated air pressure regulators described above are used to automatically adjust the applied air phase pressure and net normal stress acting on the specimen.

4.6.1 Constant Load with Constant Suction (CLS) Tests.

In this type of test, both the net normal stress and the matric suction (i.e., the applied air pressure) are maintained constant. Computer control is not necessarily required in this case since both pressure regulators can be set at a constant predetermined value. This test corresponds to the conventional consolidated drained (CD) tests.

The specimen volume changes are monitored on a continuous basis so that the density and void ratio of the specimen can be determined accurately at any stage of the test. The water content of the specimen can change during the shearing process in this test. It is therefore necessary to provide for precise volume measurements to monitor the volume of water displaced to and from the specimen.

4.6.2 Constant Volume with Constant Suction (CVS) Tests.

In this test, the applied air pressure is maintained constant, but the normal load is modified on a continuous basis so that the volume of the specimen remains constant.

Since the matric suction is maintained constant, the volume of water entering or leaving the specimen must be continuously monitored to establish the relationship between matric suction and water content of the specimen. As the volume of the specimen remains constant, the degree of saturation will be a direct function of the water content.

4.6.3 Constant Load with Constant Water content (CLW) Tests.

In this test, both the applied normal stress and the water content of the specimen are maintained constant throughout the shearing process. There is no restriction on the drainage of the air phase. Since it is required to measure the applied matric suction, the drainage conduits remain open and the constant water content is maintained using the null point technique. In this technique, any tendency of the water to leave or enter the specimen is countered by changing the applied air pressure such that the water content remains the same. A volume gauge must be attached to the overflow tube of the flushing system to measure these volume change tendencies. The applied air pressure must be changed on a continuous basis to keep the specimen water content constant. The initial matric suction of the specimen is also determined in this way before the shear test begins.

The normal load applied on the specimen must also be modified so that the net normal stress remains unchanged. This is to accommodate the effect of unbalanced air pressure that acts as an upward force on the cross-sectional area of the torque arm extension. In other words, the applied load should be compensated to accommodate the change of air pressure in the specimen chamber.

During this type of test, the volume change of the specimen is monitored on a continuous basis. This information is useful to determine the density and void ratio of the specimen at any time during the test.

4.6.4 Constant Volume with Constant Water Content (CVW) Tests.

In this test, both the applied air pressure and normal load must be modified on a continuous basis so that neither the volume nor the water content of the specimen is allowed to change. In other words, the degree of saturation and the water content of the specimen will be constant throughout the test.

The continuous control of both the air pressure and the normal load requires the constant monitoring of the vertical deformation of the specimen to detect any tendency of the specimen to change volume. Again, the water content change is monitored through the use of a volume gauge while an LVDT is used to monitor the vertical deformations so that the volume may be measured and maintained at a constant value.

4.6.5 Soil-Water Retention Curve (SWRC)

The ring shear test device can be used to determine the soil-water retention curve (SWRC) of a soil specimen. An unsaturated soil specimen in the ring shear apparatus can be saturated by applying a back pressure to the water phase. Once saturation of the specimen has been verified, the top platen and cell cover are placed on top of the specimen. The matric suction is then increased at chosen intervals and the water content is allowed to reach equilibrium before the next increment of matric suction is applied. The amount of water leaving the specimen is carefully monitored at different values of matric suction at equilibrium conditions. The volume gauge connected to the flushing system can then be used to monitor water content changes.

It is also possible to determine the SWRC while maintaining a normal load applied on the specimen to investigate the effect of the applied stress on the SWRC. The ring shear device can also be used as an instrument to determine the soil-water retention characteristics at any stage of the shearing process.

4.7 Summary

The modified ring simple shear device presented in this chapter is a useful and versatile one for the study of the shear strength behaviour of unsaturated soils. It permits the determination of both the peak and critical state shear strength envelopes, with respect to both the net normal stress and the matric suction.

The constant volume tests for their part are also useful to study the changes in the SWRC that occur during the shearing process. Indeed, since the SWRC is a function of the void ratio and fabric, the ability to maintain a constant volume allows an understanding of the influence of the shearing process on the relationship between water content and matric suction when the void ratio remains unchanged.

Shear tests have successfully been conducted under CLS and CVS conditions, and the device is also capable of subjecting specimens to CLW and CVW conditions. The SWRC can also be obtained for a single specimen under various conditions. Such conditions include subjecting the specimen to a constant volume, or a constant net normal load. This can be done for specimens whether or not they have been subjected to shear. Furthermore, a single specimen can be subjected to a multistage shearing sequence and the SWRC obtained represents the end condition of each shearing stage. By using a single specimen, the relationship between the degree of saturation and the matric suction represents the SWRC of that single specimen after undergoing shear. The uniqueness of the specimen used to generate a SWRC does not need to be assumed from test results on several specimens.

In the following chapter, a procedure is described to correct the water content readings from the acquired data by observing the breaks in the curve, to quantify the rate of air infiltration by the combined effect of air diffusion and leakage. The corrections discussed, also include the identification of the rate of moisture exchange between the specimen and the air in the cell through evaporation or condensation.

4.8 Figures

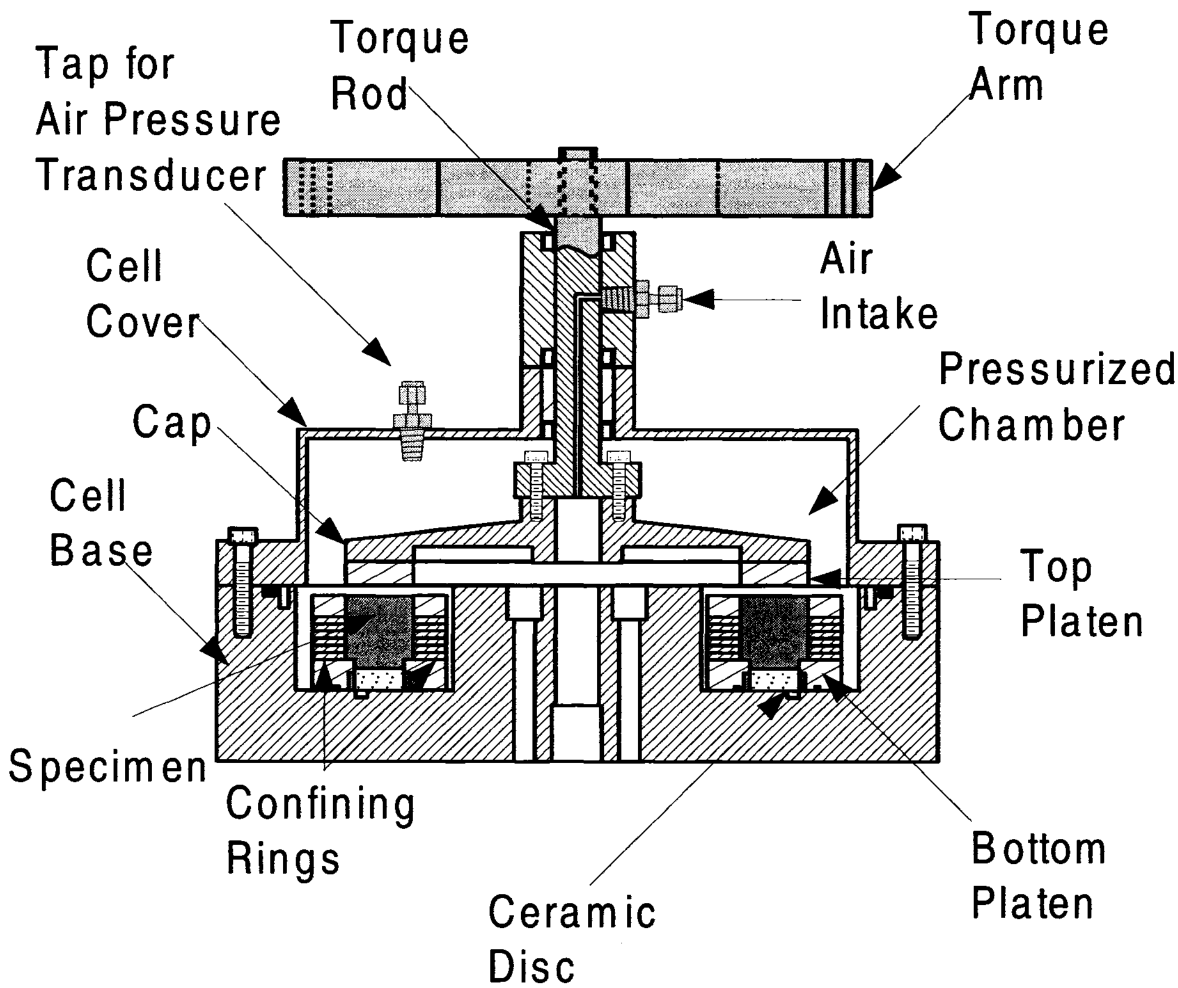

Figure 4.1 Cross-section of the modified ring shear cell.

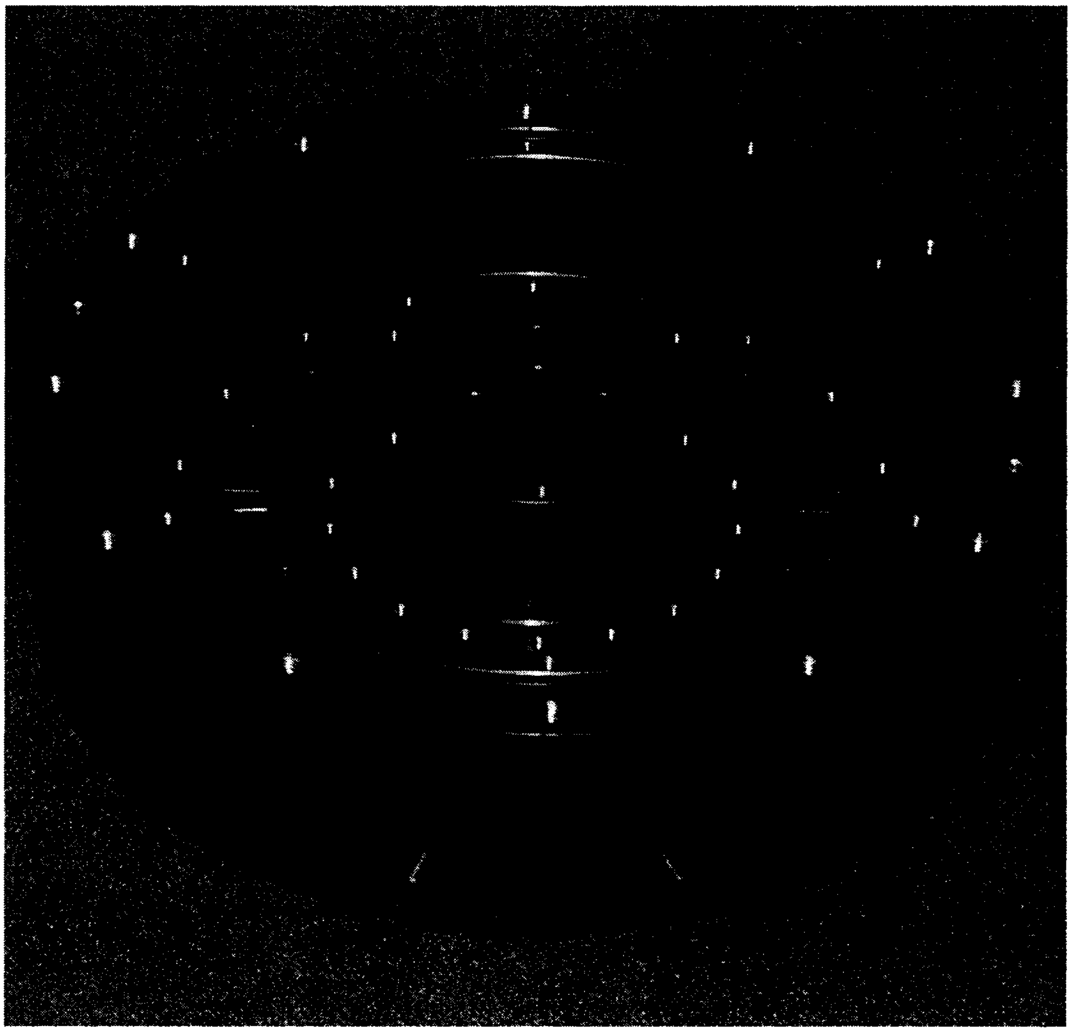

Figure 4.2 Base of the ring shear cell showing details of the flushing system.

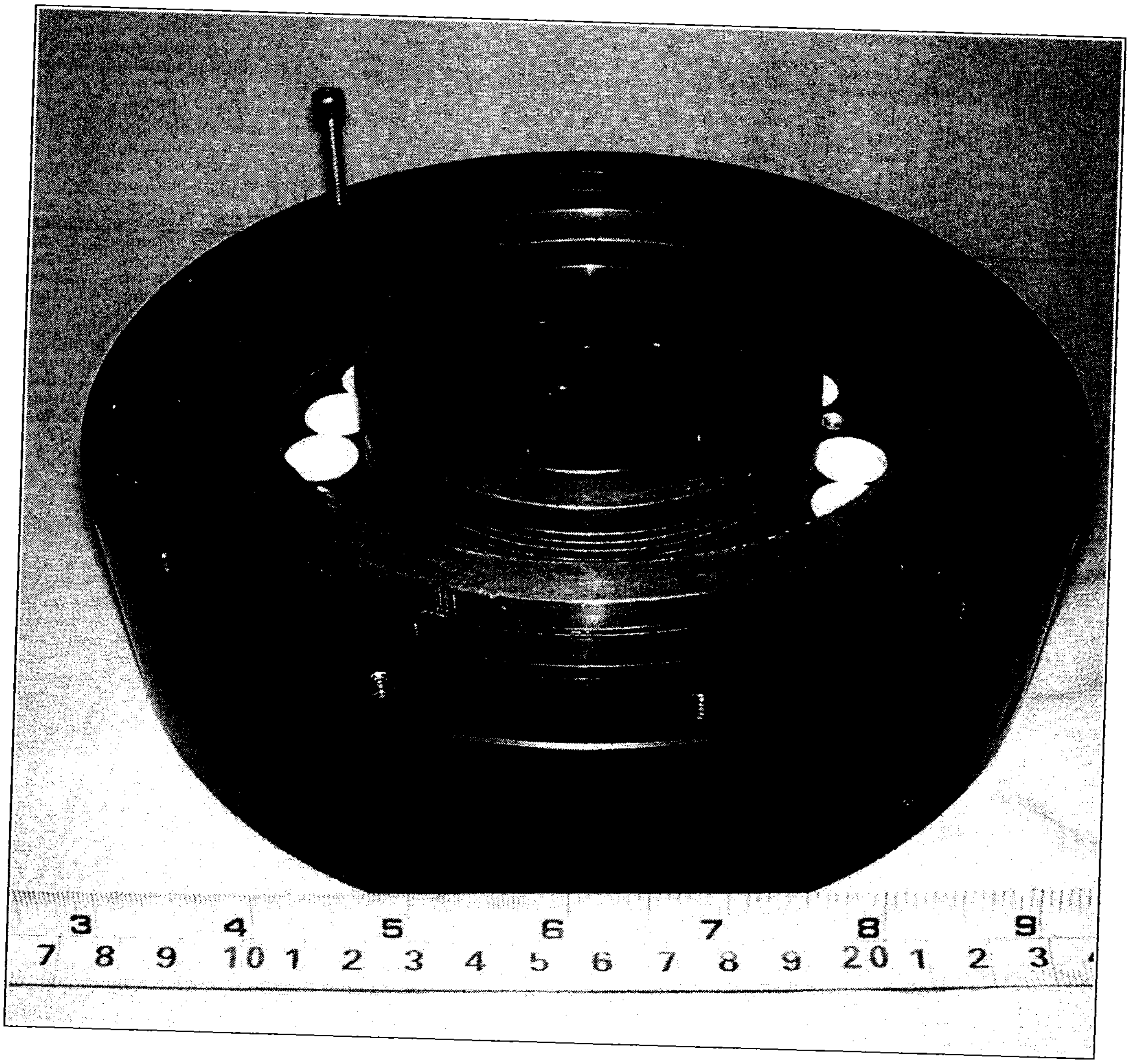

Figure 4.3 Base of the unsaturated ring shear cell with ceramic discs and inner confining ring stacks in place.

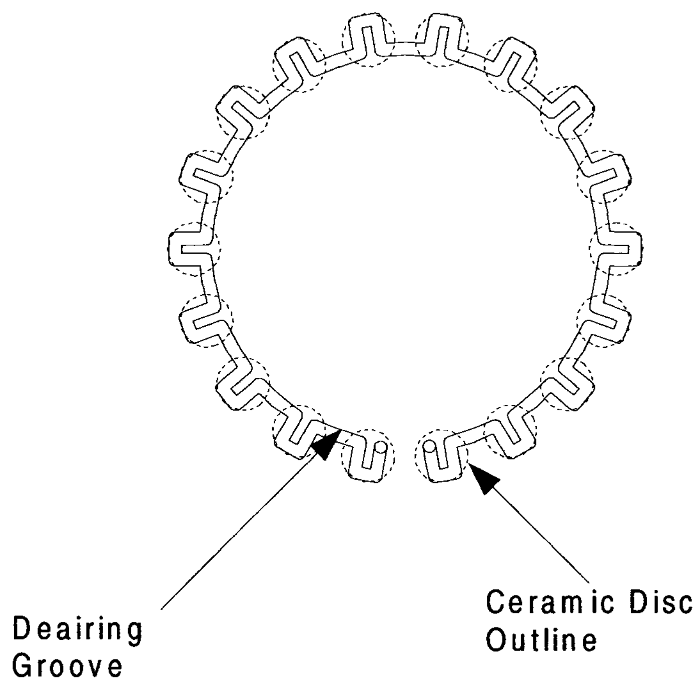

Figure 4.4 Dearing groove disposition under the ceramic discs.

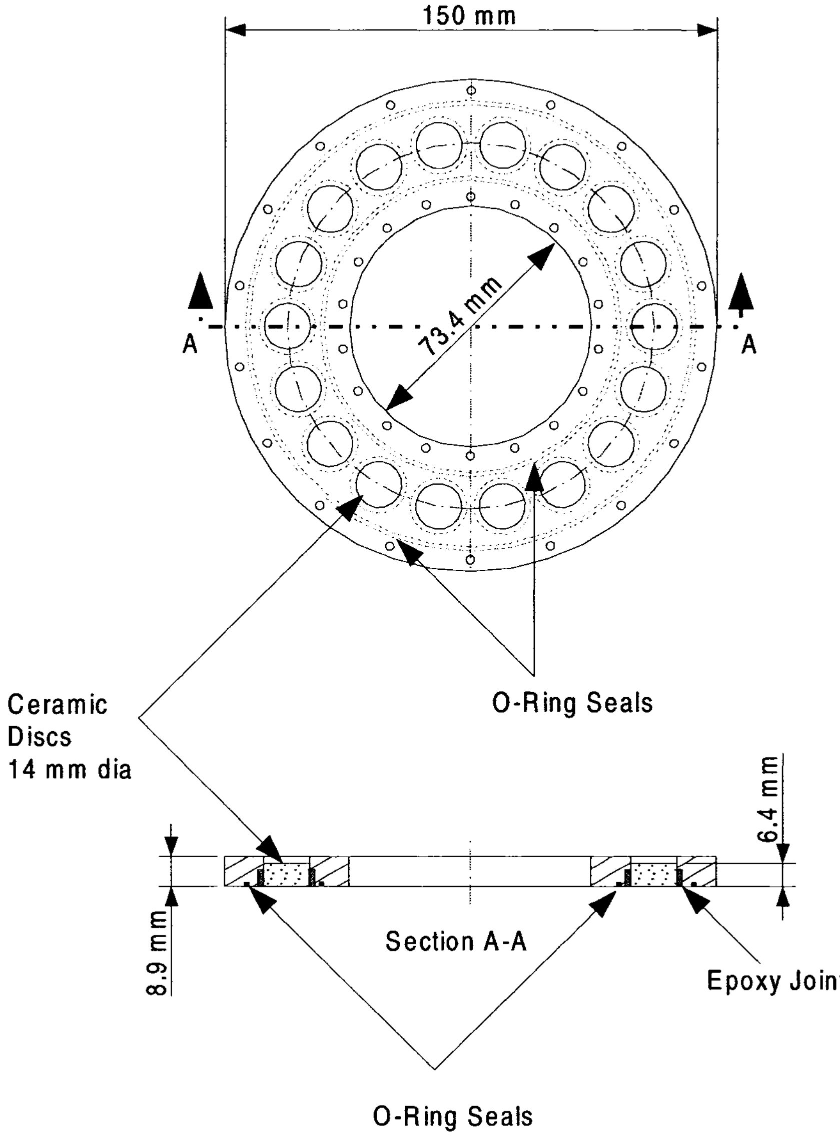

Figure 4.5 Bottom platen of the modified ring shear test apparatus.

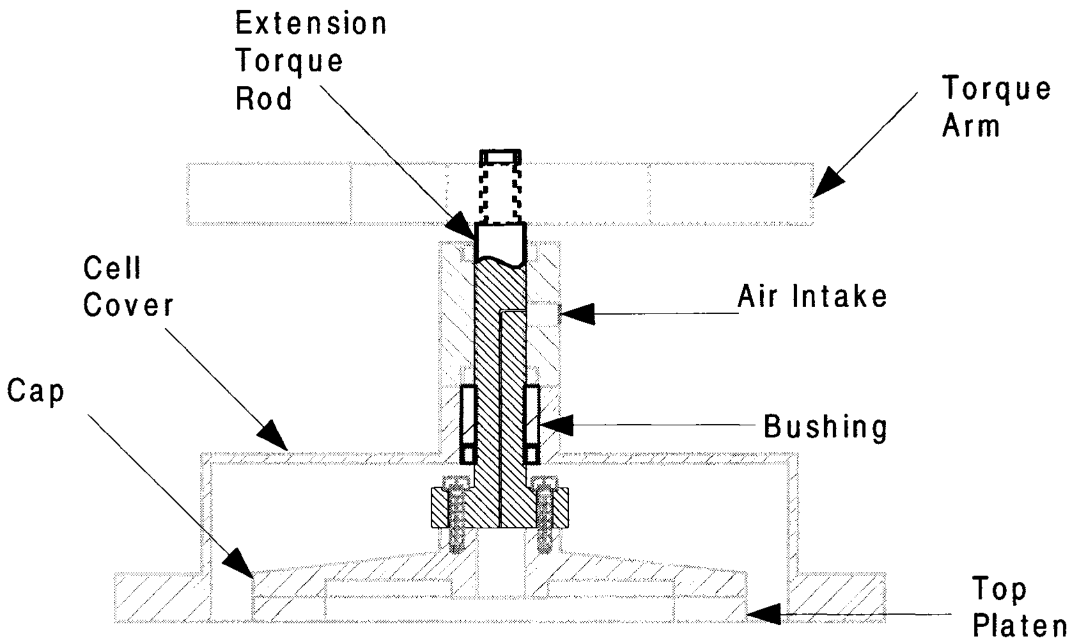

Figure 4.6 Torque arm extension.

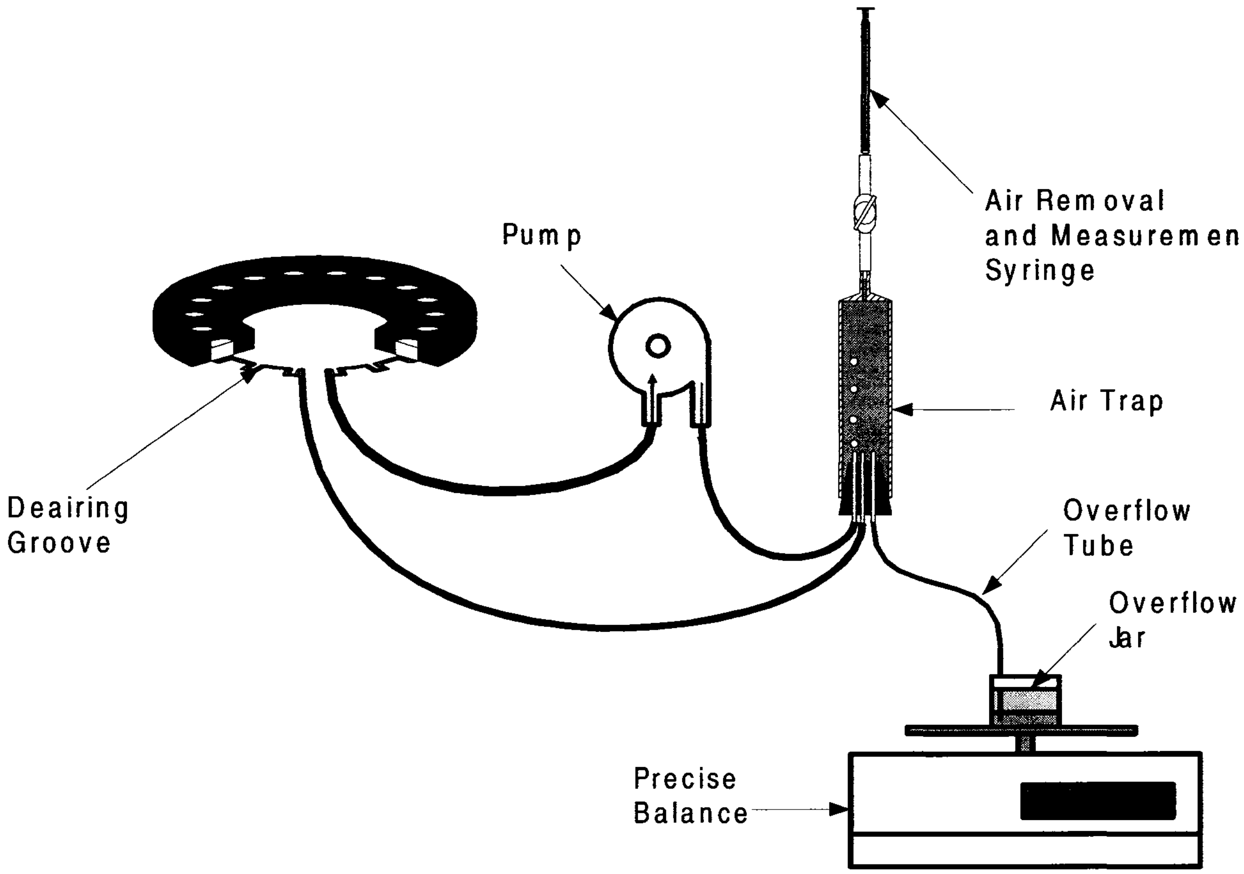

Figure 4.7 Idealized schematic of the de-airing system, including the groove found below the ceramic discs, and the tubes leading to the pump, and the air trap.

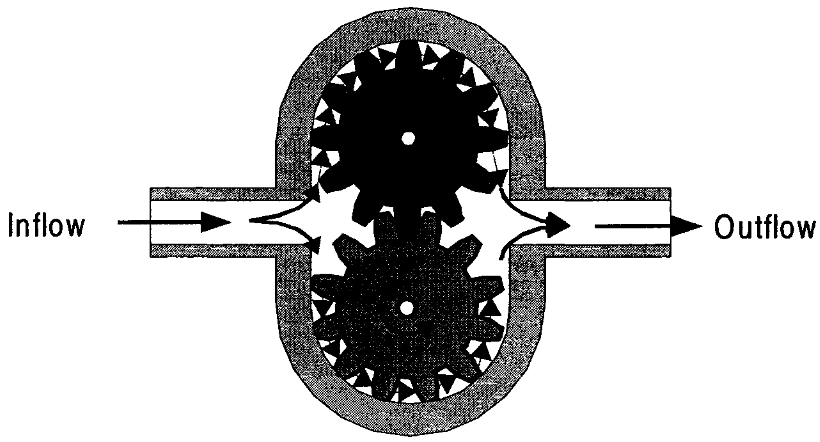

Figure 4.8 Schematic view of a simple gear pump.

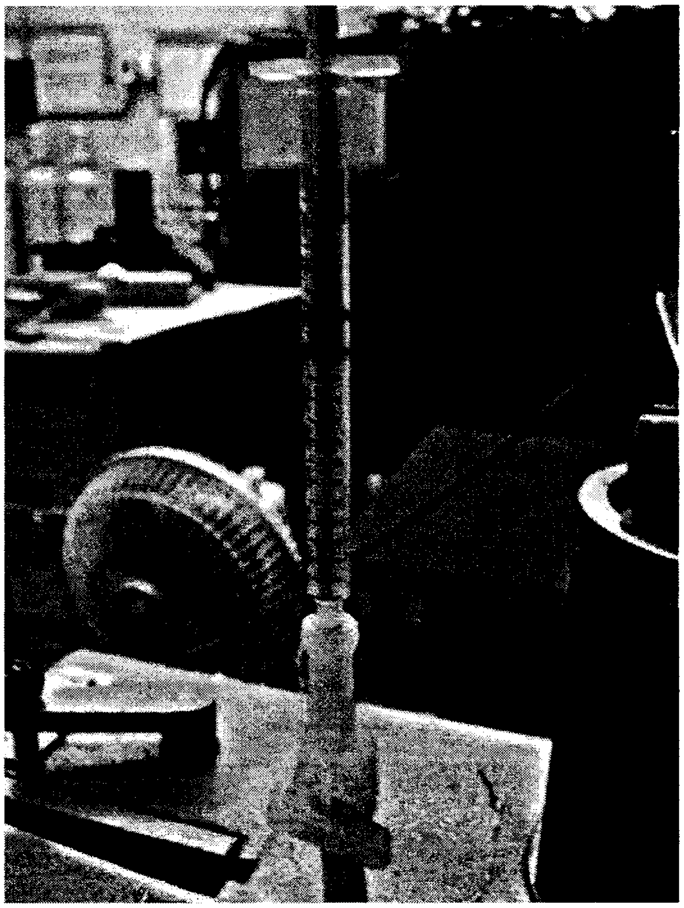

Figure 4.9 1 ml syringe used to reset the water level in the air trap, and provide confirmation reading on the volume of removed air.

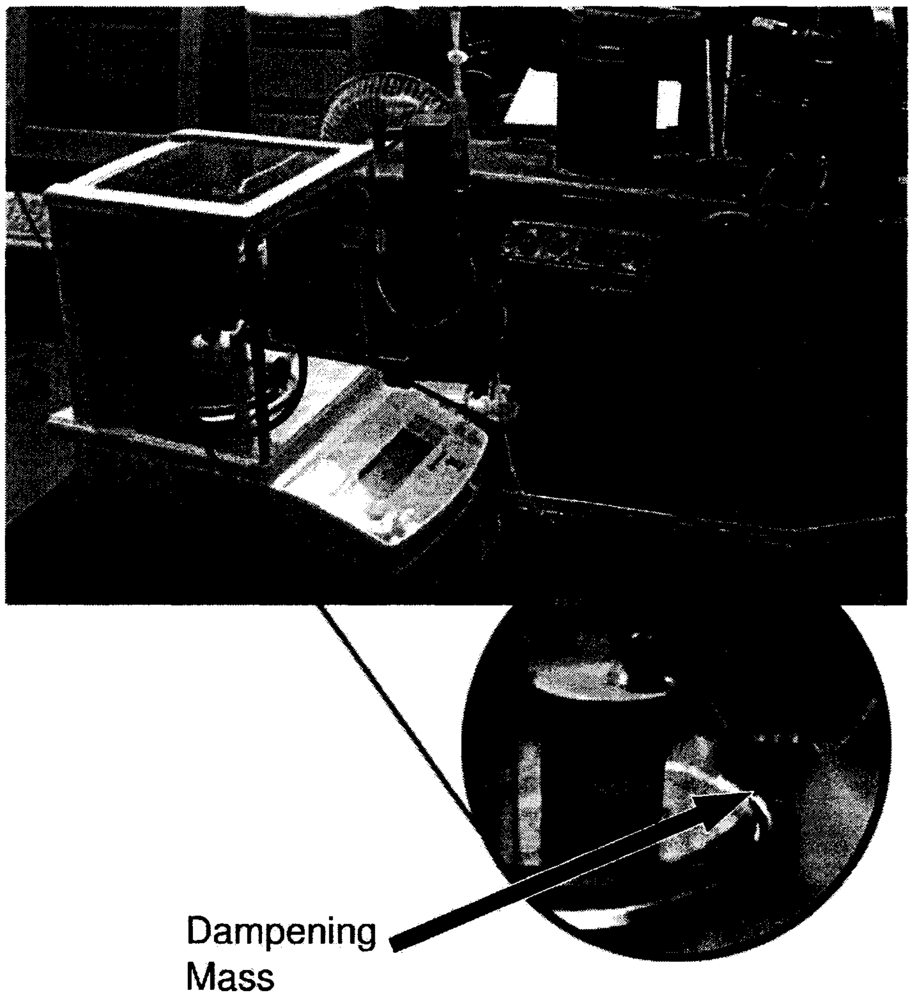

Figure 4.10 Close up view showing the dampening mass added to the lower part of the last segment of the overflow tube.

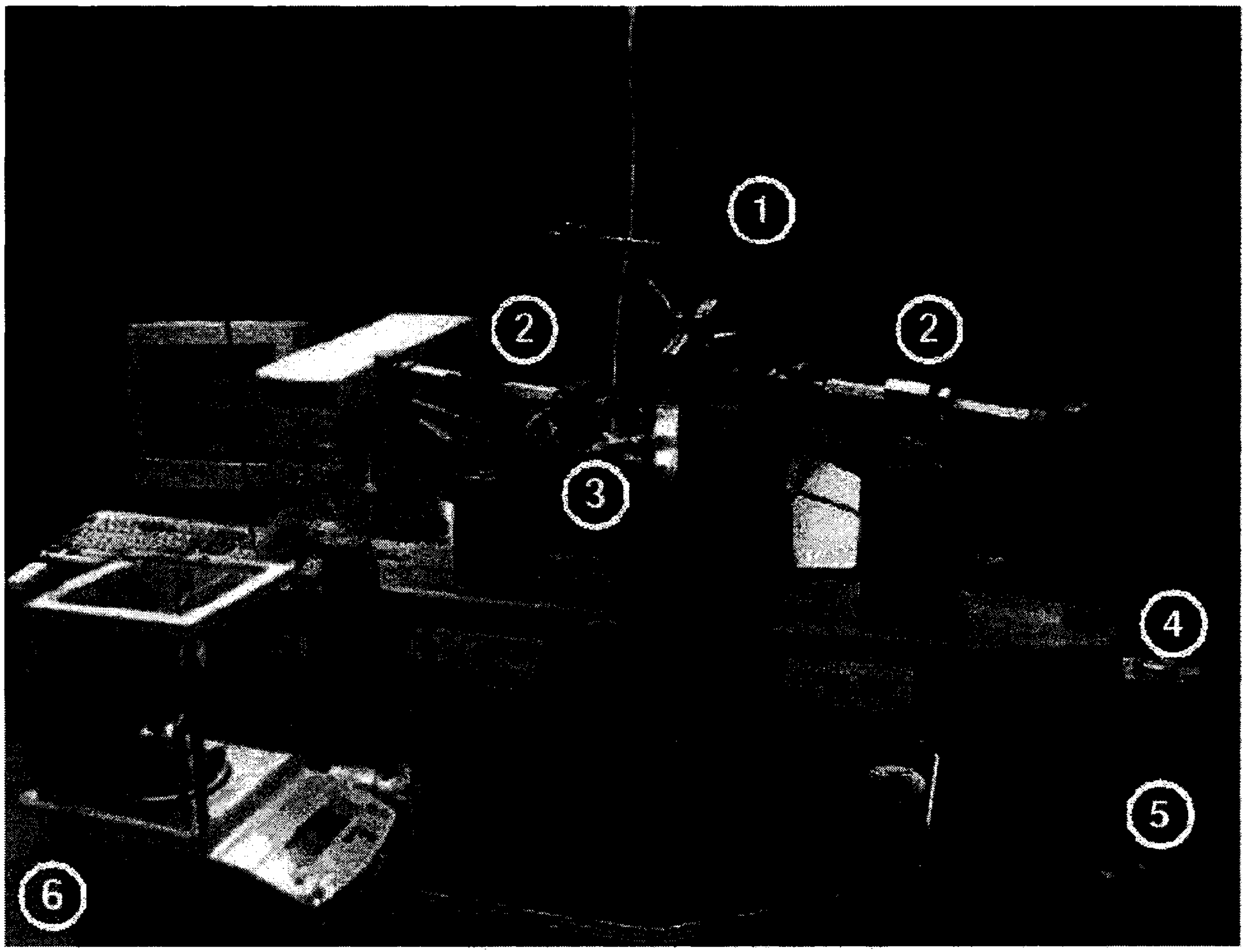

Figure 4.11 Instrumentation of the modified Ring Shear Test apparatus.

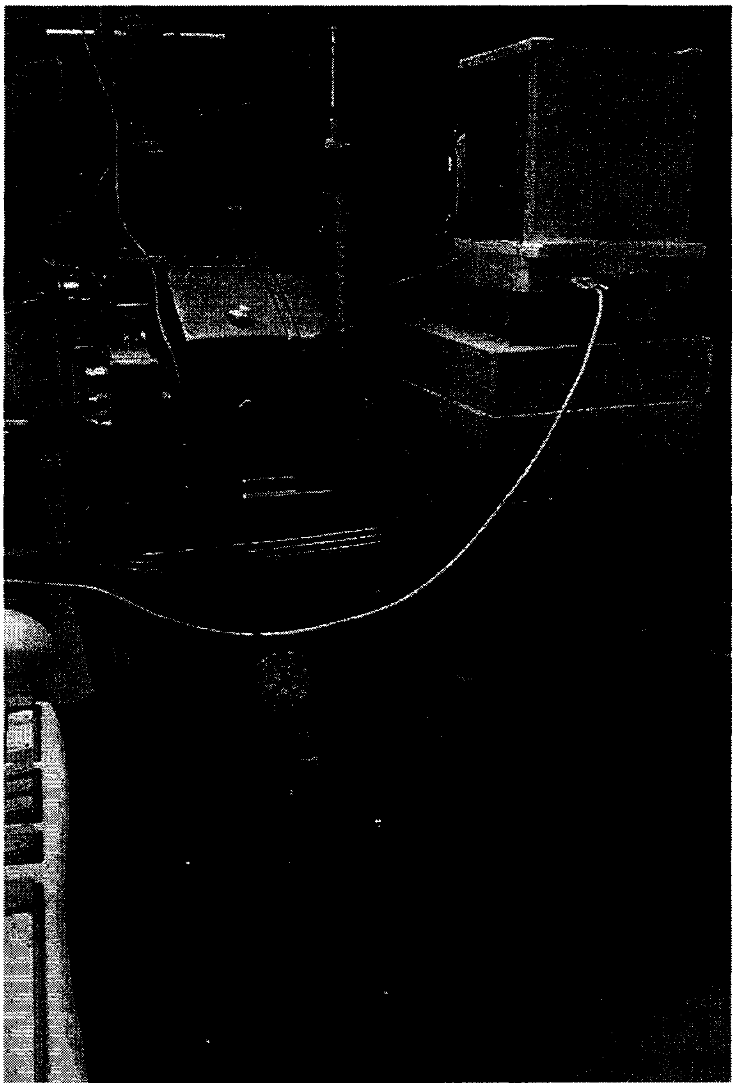

Figure 4.12 Pressure regulators used to control the normal stress and applied air pressure.

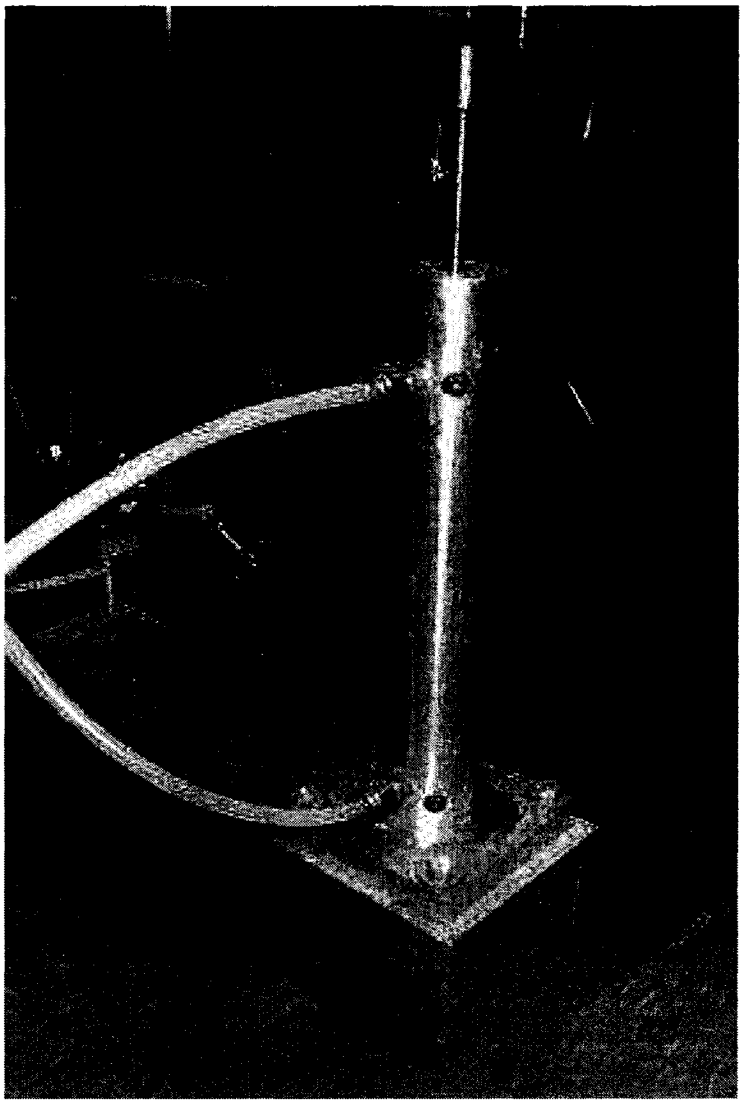

Figure 4.13 Actuator converting the air pressure into a normal force.

Figure 4.14 Alignment ring.

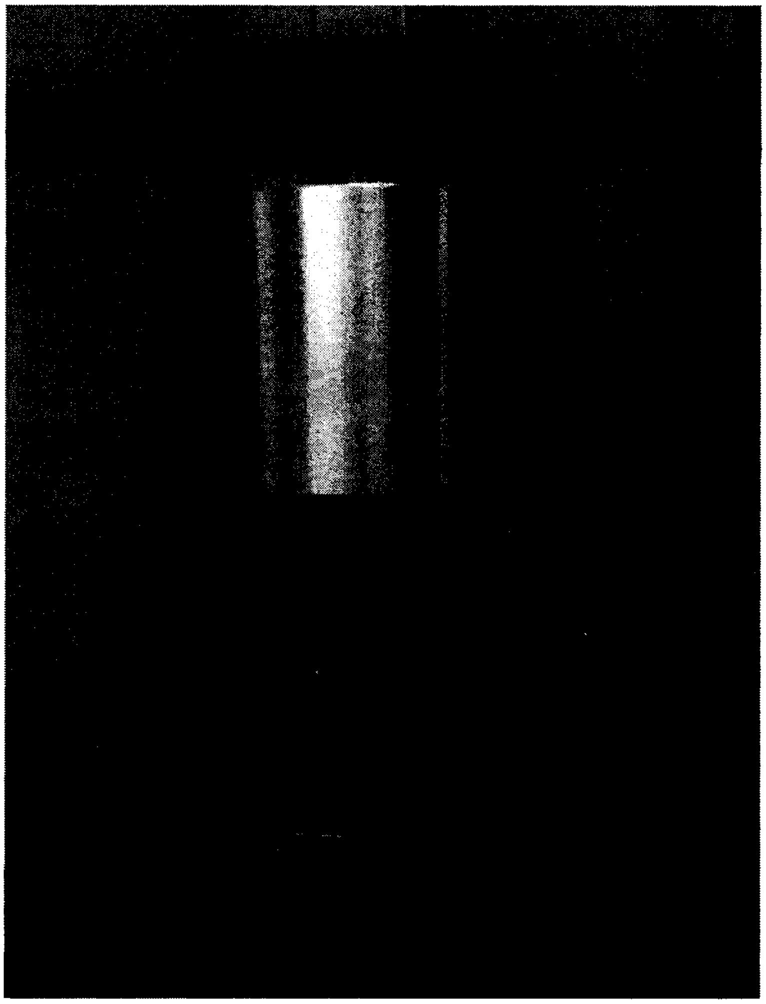

Figure 4.15 Compactor loading block and ring shear cell.

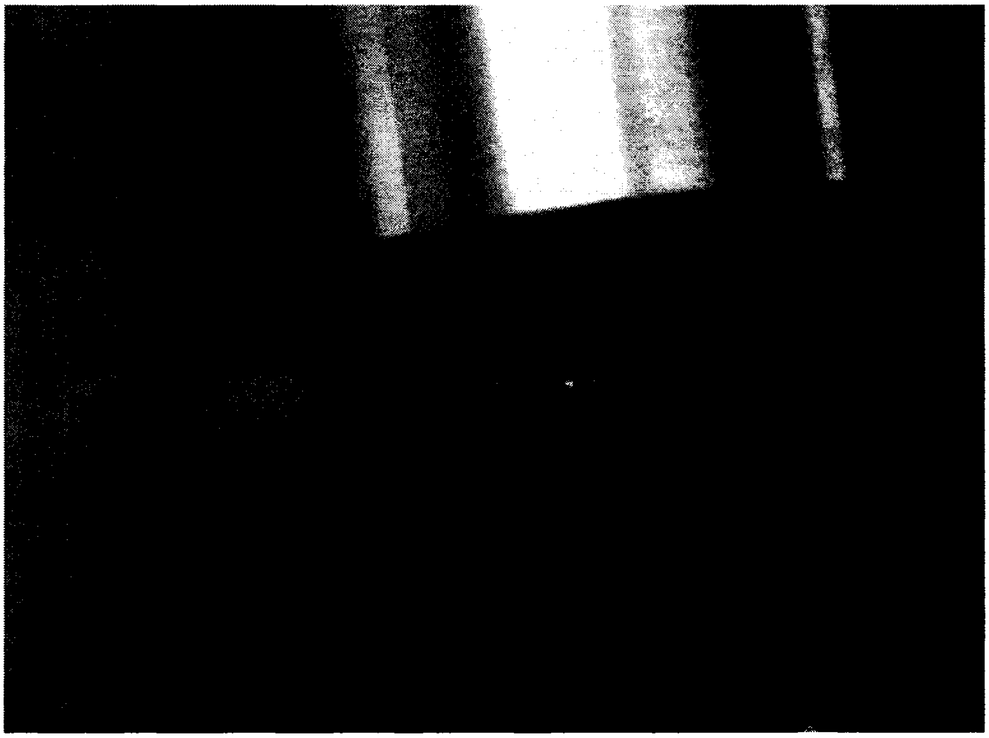

Figure 4.16 View showing the uplifted central portion of the loading foot used to align the specimen with the loading rod.

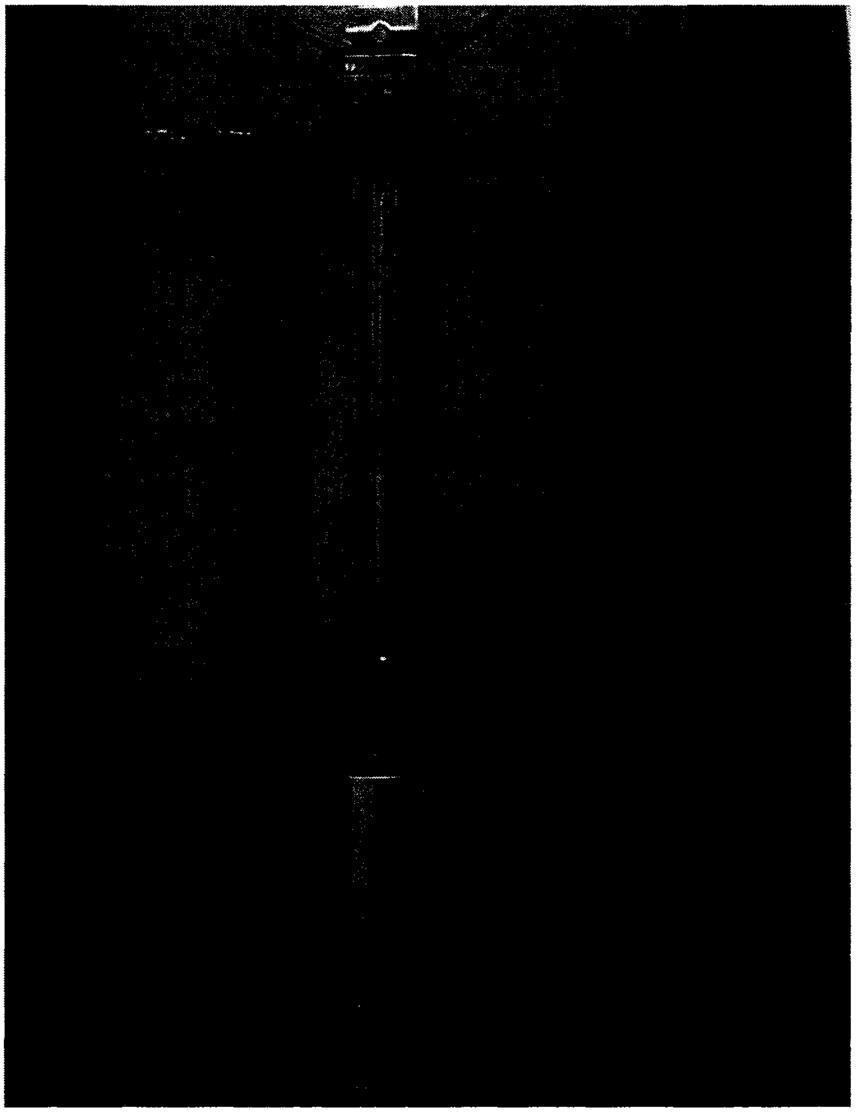

Figure 4.17 Static compaction loading frame of a specimen.

5 Experimental Results

5.1 Introduction

Several studies are reported in the literature for predicting the shear strength of unsaturated soils using soil-water retention curve (SWRC) as a tool. However, recent studies have shown that water content versus suction relationship during shearing stage can be significantly different from the SWRC behaviour determined from conventional testing procedures [Vanapalli et al. (2003)]. This has an effect on the equations that depend on the SWRC for the prediction of the shear strength of unsaturated soils for these make no provisions for the changes to which the SWRC may be subjected during the loading and shearing stages. This hydro-mechanical coupling also has an impact on the elasto-plastic models that are developed to model the behaviour of unsaturated soils. In recent years models have been proposed that include provisions for hydro-mechanical coupling [Vaunat et al. (2000), Gallipoli et al. (2003), Wheeler et al. (2003), Chiu and Ng (2003)].

The experimental program presented in this thesis focussed on investigating the influence of the hydro-mechanical coupling behaviour of unsaturated soils. There are only a few experimental studies that are reported in the literature that provide evidence about the effect of hydro-mechanical coupling on the shear strength behaviour of unsaturated soils [Tarantino and Tombolato (2005)]. In the present program, a modified ring shear test apparatus equipped with accessories to precisely measure the changes associated with the water content as well as the volumetric changes was used. The data of water content and volume change along with stress state variables are required in providing the necessary information towards better understanding the hydro-mechanical behaviour of unsaturated soils. The modified ring shear apparatus also permits to subject the specimens to large deformations and hence suitable to determine the peak and ultimate shear strength of unsaturated soils. The information collected using the modified ring shear apparatus in the present study should be useful in providing new insights into the relationship between hydro-mechanical behaviour of unsaturated soils.

5.2 Soil Characterization

The soil used during the current investigation is Indian Head till. This is a glacial till obtained from the province of Saskatchewan.

5.2.1 Conventional soil properties

The physical characteristics of the till as measured in the laboratory are as follows:

Liquid limit, w_L:	32.5%
Plastic limit, w_p:	17.%
Plasticity index, I_P:	15.5%
Specific Gravity, G_s:	2.71
Angle of Internal Friction, ϕ':	26.3°
Effective cohesion, c':	10.61 kPa
Max unit weight (from Proctor's curve):	18.0 kN/m^3
Optimum moisture content:	14.40%

Figure 5.1 shows the grain size distribution of the soil studied in this research program (ASTM D422-63). The particle size distribution above 0.075 mm (standard sieve #200) were determined using the mass collected on a series of sieves. The particle distribution below 0.075 mm was determined using the hydrometer test which uses the time required for the particles to settle at the bottom of a sedimentation tube and a hydrometer (measuring the density of the water) to determine the particle size distribution. The liquid limit and plastic limit values were obtained using the standard methods described in ASTM D4318-05. Figure 5.2 shows the standard Proctor compaction curve developed using the conventional procedure (ASTM D698). Also shown in the figure are the static compaction curves obtained on the same soils specimens using static compaction stresses of 750 kPa and 375 kPa respectively.

5.2.2 Static Compaction

Static compaction tests were conducted on specimens at various water contents. The soil was prepared by thoroughly mixing soil with an appropriate amount of water. The prepared soil was then placed into sealed double bags and stored inside a humid chamber, to allow moisture to reach equilibrium conditions over a period of no less than 24 hours. Twenty four hours before any specimen preparation, the uniformity of the moisture content within the bag was verified by taking samples from different location

Statically compacted specimens were prepared by placing the soil loosely in a compaction cylinder. This compaction cylinder is a brass block with a cylindrical hole of 50 mm diameter. The bottom segment of the compaction cylinder is made of the stainless steel oedometer ring, also of 50 mm diameter, which contains the compacted specimen. The brass block is split vertically and the two halves have a provision to be split open to release the oedometer ring. A set of four screws keeps the two halves together during the process of compaction.

The soil is placed loosely into the compaction cylinder, filling it well over the height of the oedometer ring. Then, a compaction ram is inserted into the cylinder, and a drill press is used to compact the specimen (Figure 5.3). After completion of the compaction process, the compaction cylinder is opened and the oedometer ring containing the specimen is retrieved. A straight edge is used to remove the small amount of soil that may protrude from the oedometer ring. Using the mass of the specimen and ring, the density can be computed by volume mass relationships.

Figure 5.4 shows the relationship between the applied load and vertical deformation. This relationship was determined by using a load cell to measure the force transmitted to the soil specimen using the drill press and a linear potentiometer to measure the vertical displacement of the ram. The area below the force/deformation curve is equal to the work accomplished due to the process of static compaction on the specimen. The applied stress of 375 kPa on the soil specimen at a water content of 15% corresponds to a compaction energy of approximately 60 kJ/m^3. This value was determined by integrating the area under the curve. The maximum unit weight of the soil specimen was found to be approximately equal to 17 kN/m^3 under the applied static force (Figure 5.5). This is the peak unit weight attained due the application of this compaction force. Some amount of rebound would be observed on releasing the load. Typical compacted specimen unit weight was in the order of 16.2 kN/m^3. The compaction stress of 375 kPa was maintained for 1 minute for all the specimens (i.e., in the preparation of testing the shear strength parameters both under saturated and unsaturated shear conditions and the SWRC) in this research program.

5.2.3 Saturated shear strength

The modified ring shear apparatus has been used for determining both the saturated shear strength parameters as well as for testing the soil under unsaturated conditions. The saturated shear strength parameters were determined on specimens that have been compacted at a water content, w_c, of 19% under a static compaction stress of 375 kPa. Vanapalli et al. (1996), had observed when conducting direct shear tests on the same soil that the saturated shear strength parameters showed essentially no variation based on the compaction water contents.

After compaction, the specimen was allowed to imbibe water for a period of 24 hrs. Once saturated, as verified by volume and mass relationships, the specimen was consolidated under a normal load of 150 kPa. Figure 5.6 shows a plot of the shear strength versus normal effective stress for a saturated Indian Head till specimen tested under consolidated drained conditions in the modified ring shear cell, at a deformation rate of 0.048 mm/min. For the tests results where a peak shear strength could be expected under saturated conditions (initial stage of saturated tests or multistage unsaturated CLS tests), the specimen shows no notable difference between the peak and residual shear strengths. It does show, however a c' parameter consistent with overconsolidation. The specimen should therefore be considered slightly overconsolidated. Extensive testing of the contribution to the measured shear resistance by friction from the confining ring systems have shown that their contribution is negligible [Infante Sedano (1998)].

5.2.4 SWRC

The SWRC of statically compacted specimens were determined at two different initial compaction water contents, namely 15% and 19% as shown on Figure 5.2. The 50 mm diameter specimens were compacted using the same method detailed in section 5.2.2. Figure 5.7 shows the SWRCs determined on statically compacted specimens at two different initial water contents using a pressure plate extractor. Each point shown on this curve is an average of three specimens. The SWRC curves have been generated using two sets of specimen compacted at a water content of 15%, and one set of specimens compacted at a water content of 19%. All specimens were then saturated by placing them on filter paper and soaking in a water bath which allowed imbibation of water. A load of approximately 2 kg was placed on top of the oedometer ring. This was to prevent the specimen from swelling out of the oedometer ring during saturation. Full saturation conditions were ensured from volume and mass relationships. Studies have show a time period of 48 hours sufficient for saturating the specimens.

In total three sets of three specimens were prepared. One set was compacted with a water content of 19%, and the other two at a water content of 15%. The SWRC was determined immediately after saturation for the specimens compacted at 19% water content, and for one set of specimens compacted at a water content of 15%. The remainder set of specimens compacted with a water content of 15% was subjected to a consolidation stress of 150 kPa after the saturation phase and prior to the initiation of the SWRC test. This consolidation, which lasted 24 hrs and is similar to the stress history of the specimens used in the modified ring shear apparatus prior to the shearing operation.

Figure 5.7 compares the three SWRC obtained from these tests. Each point on the graph represents the average of the three specimens. Comparing the two SWRC curves obtained by conventional means, without consolidation after compaction, it is apparent that the specimen compacted at a water content of 15% (dry of optimum) has a lower air entry value than the specimen compacted at a water content of 19% (wet of optimum). This is consistent with a flocculated structure that is to be expected of a specimen compacted dry of optimum and the lower densities achieved for those specimens. After subjecting the specimens compacted at 15% to a consolidation stress equal to 150 kPa (while saturated), the SWRC changes significantly. The resultant SWRC curve has a significantly higher air entry value, and the curve lies higher than the curve from the specimens compacted wet of optimum.

5.3 Testing Program

The modified ring shear apparatus can be used for conducting four different types of shear strength tests on unsaturated soils as discussed in the chapter 4. The different shear strength tests conducted and are summarized below:

1) Constant Load and constant Suction (CLS)

2) Constant Volume and constant Suction (CVS)

3) Constant Load and constant Water content (CLW)

4) Constant Volume and constant Water content (CVW)

Air leakage is a significant parameter that must be taken into account when designing a device for testing unsaturated soils behaviour [Wang and Benson (2003)]. Several trial studies were undertaken to arrive at an optimal technique to reduce both the air and as well as water leakage in the design modified ring shear apparatus. Much time was required to design, test and modify the equipment after conducting several preliminary testing runs. A more ambitious research program that was originally planned had to be shortened due to the loss of a significant amount of time in the development of the equipment. For this reason, the testing program was limited to the tests summarized in Table 1. A shear deformation of 20 mm was chosen as representative of the large deformations. This shear deformation range is comparable to the large deformation ranges obtained in other devices such as the triaxial device or the direct shear box with multiple reversals. A single stage CVS test was also completed to verify the validity of using such shear rates.

Table 1 Testing program

Test Id	*Test Conditions*	*Shear Rate (mm/min)*	w_c	$(u_a - u_w)$ *(kPa)*
CLS-19-150-E3	Const. Load & Const. Suction	0.048	19%	0,25,50,100,200,350
CVS-19-150-E3	Const. Volume & Const. Suction	0.048	19%	0,25,50,100,200,250
CLS-15-150-E3	Const. Load & Const. Suction	0.048	15%	0,25,50,100,150,250,400
CVS-15-150-E3	Const. Volume & Const. Suction	0.048	15%	0,25,50,100,150,250,400
CVS-15-150-150-E5	Const. Volume & Const. Suction	0.022	15%	150
				$(\sigma - u_a)$ *(kPa)*
CD-19-000-E3	Consolidated Drained (saturated)	0.048	19%	25,50,150,200

All constant load and constant suction, CLS, tests were conducted at a net normal stress, $(\sigma_n - u_a)$ of 150 kPa. The constant volume and constant suction, CVS, tests were consolidated in saturated conditions under an applied normal stress of 150 kPa. The consolidated drained, CD, tests were consolidated under an applied normal stress of 150 kPa, and conducted in saturated conditions. Table 1 provides a list of the test series conducted, the shear rate, the compaction water content, as well as the various matric suction stages at which the specimen were tested. Conducting all CLS tests under the same net normal stress, and consolidating all specimens to the same value of net normal stress allowed to limit the number of independent factors affecting the measured shear strength, as well as volume and water content changes.

5.4 Specimen Preparation

All ring shear specimens were compacted in six layers. The thickness of each layer after compaction was approximately equal to 3 mm. The soil was deposited in the annular chamber of the ring shear device with a spoon, taking great care to make it as evenly distributed as possible. After initial placement of each layer, the compaction ring was placed on top of the loose soil. This compactor ring has similar dimensions to those of the specimen. It is used to transmit the load from the compactor ram to the soil. The cell was then placed in the compactor frame which was used to apply a normal stress of 375 kPa. The stress of 375 kPa was maintained for a duration of 1 minute for each layer.

After the compaction of each layer, the compaction stress was released, and the modified ring shear cell removed from the compactor frame. The compactor ring, which rested on the specimen, was lifted, and the surface of the specimen layer was thoroughly scarified. The next layer was deposited on top of the scarified material and the compaction process repeated until the last layer was in place. The surface of the final layer was not scarified.

Following the specimen preparation, the top platen was placed on the specimen, which was allowed to draw water permeating through the ceramic discs of the bottom platen. For this purpose, a pressure of about 20 kPa was applied to the water below the ceramic discs to accelerate the saturation process. From preliminary studies it was observed that the surface of the specimen was thoroughly wet after an interval of approximately 24 hours assuring the specimen was fully saturated. Volume/mass relationships showed that the degree of saturation was unity after the saturation phase. The same procedure had been used on the specimens used for conventional SWRC tests confirming that indeed saturation was achieved. The dry unit weight of the soil specimen after saturation was approximately equal to 16.2 kN/m^3.

5.5 Consolidation Phase

Once the specimen was saturated, the ring shear cell was placed onto the ring shear frame for the consolidation stage. The soil specimens were then consolidated under a net normal stress of 150 kPa in both the CLS and CVS test series. Typically, the specimen was consolidated for a period no shorter than 24 hrs. The unit weight of the specimens after the consolidation stage was approximately equal to 17.3 kN/m^3.

5.6 Suction Increment Stage

Most of the tests conducted in the current experimental study are multi-stage tests conducted at various matric suction values, $(u_a - u_w)$, on the same specimen. The procedures detailed in Fredlund and Rahardjo (1993) were followed for conducting these tests. The multistage tests were conducted by first increasing the matric suction to a pre-determined value, then allowing the specimen to reach equilibrium conditions under the applied suction value for a period of 24 hrs. The shearing of the specimen was conducted at a rate of 0.048 mm/min for all specimens. After completion of the shearing phase, the matric suction was increased once more and allowed to reach equilibrium conditions. Several trial runs showed that a period of 24 hours was sufficient to reach equilibrium conditions after an increase in matric suction value. Similar multistage testing had previously been conducted on glacial till by researchers using the modified direct shear apparatus [Gan and Fredlund (1988), Vanapalli et al. (1996)].

The CLS tests were conducted at a net normal stress, $(\sigma - u_a)$, of 150 kPa. The CVS tests were initially consolidated under a normal stress of 150 kPa. An additional set of CD tests was conducted under saturated conditions and sheared at various net normal stresses ranging from 25 kPa to 250 kPa (see Table 1.1). This stress range encompassed the net normal stress used as the consolidation stress for all unsaturated CVS and CLS tests.

5.6.1 Correcting for air infiltration.

In conventional testing of unsaturated soils, an instrument such as the diffused air indicator (DAVI) presented by Fredlund (1975), is commonly used if the volume of diffused air is to be monitored. This device allows the removal of air, but requires the prior isolation of the volume gauge from the measurement system. The volume readings are therefore not affected by the flushing operation. The current experimental study also used a flushing system to remove diffused air bubbles from beneath the ceramic discs. However, unlike conventional layouts, the current setup does not require a DAVI since the volume of diffused air is determined from the changes in the readings of the water volume.

Typical water mass readings of such a suction increment phase are shown in Figure 5.8. These readings were recorded automatically by a precise electronic balance with, a resolution of 0.001 g, connected to the computer controlling the experiment. The characteristic features of the curve are the sharp breaks at different time intervals. These breaks in the curve are caused by the removal of the air bubbles.

During normal operation of the device, water expelled from the specimen flows through an overflow tube into an overflow jar which rests on the balance as described in the chapter 4, on the Modified Ring Shear Apparatus. A gear pump is used to periodically flush water beneath the ceramic stones on the base platen of the cell. The flushing operation causes the air that was trapped beneath the ceramic discs of the modified ring shear to collect at the apex of the air trap. The valve at the upper extremity of the air trap is then opened, and the syringe connected to it is then used to remove the infiltrated air, and re-establish the water level in the air trap to a fixed reference mark.

The removal of the accumulated air in this way results in a drop in the mass of water in the overflow jar, and causes the drop in the water mass readings. The change in the reading of the water mass (and corresponding volume) is equal to the volume of air removed from the system since water was drawn to fill in the volume previously occupied by air. The rate of air infiltration in terms of mass of water (in grams) displaced per unit time increment is obtained from the drop of the mass reading, ΔW (i.e., for the time interval between two consecutive flushings) (Figure 5.9). The conversion of mass of water into volume is based on a density of water of 0.9994 g/cm^3 at the controlled laboratory temperature of 21°C. For the calculation of the gravimetric water content of the specimen, however, the volume conversion is not necessary.

An independent verification of the measured air volume is also obtained manually using the 1 ml syringe that is used to draw the air from the air trap. Although the main purpose of this syringe is to permit the readjustment of the water level in the air trap to a fixed reference level, the position of the plunger can be used as a simple DAVI to obtain a volumetric reading from the syringe graduations themselves. Although these volume readings are in the order of 0.01 ml (as compared to the 0.001 g precision of the balance) they provide a direct measurement to verify the volume of infiltrated air that was removed during the flushing operation. It should be noted, however, that a precision of 0.01 ml is commonly used in conventional DAVI systems. All syringe and balance readings were compared and found to be compatible within the accuracy of the syringe readings (0.01 ml).

Once the air infiltration rate is known, it is possible to correct the water content measurements. The infiltration rate can be assumed to be constant during the time interval between successive flushings. This assumption seems valid from the observation that once steady state has been reached, the calculated rate of air infiltration tends to remain constant between successive flushing stages. The assumption may not be valid shortly after the application of the higher air pressure (i.e. at the beginning of the suction equilibrium stage) when relatively larger amounts of water flow across the ceramic discs of the modified ring shear apparatus. This error is mitigated by the fact that larger volumes of water are involved earlier in the suction increment stage, and therefore the relative magnitude of air infiltration will be smaller.

Before applying any correction for air infiltration, the various broken segments caused by the flushing operation are adjusted to produce a single continuous (i.e., unbroken) curve. This *continuous readings curve* (Figure 5.10), represents the readings that would have been possible if no flushing were performed, or if a diffused air indicator arrangement similar to the ones used by Bishop and Donald (1961) or Fredlund (1975) had been used.

The generation of the *continuous readings curve* may be automated on a spreadsheet (Table 2) by computing the rate of volume change between successive readings. The rate of water flow into the overflow jar tends decrease to a low positive value when approaching equilibrium conditions after increasing the matric suction applied to a specimen. When flushing is performed, however, there is a sudden drop in the water mass readings. This mechanism translates into a sudden drop in the rate of water mass change, which becomes highly negative for the space of one reading and returns to earlier values on subsequent readings. The rate of water mass change is compared to a threshold value using a simple logical comparison formula. If the measured rate is more negative than this value, then the last known "valid" rate is used as a substitute. This is equivalent to performing a linear extrapolation from the last known mass reading value to the time of the reading following the flushing operation.

Table 2 Spreadsheet table for automated generation of the Continuous Readings Curve.

Time Since Beginning of Suction Stage (hr)	Rate of Water Mass Change (g/day)	Adjusted Rate of Water Mass Change (g/day)
14:44	0.830	0.830
15:24	0.790	0.790
16:06	0.780	0.780
16:41	-22.950	0.780
17:13	0.660	0.660
17:50	0.620	0.620
18:30	0.660	0.660
19:10	0.600	0.600
19:51	0.620	0.620
20:32	0.200	0.200
21:07	0.620	0.620
21:41	-5.270	0.620
22:17	0.570	0.570
22:48	0.640	0.640

Figure 5.11 shows the rate of water mass changes as a function of time. The flushing phases are clearly visible as two sharp downward spikes. These spikes correspond to the rows highlighted in grey in

(Table 2). The corrected values are shown as data points which are more in agreement with the neighbouring values.

The rate of mass of water change was computed by dividing the difference of two consecutive mass readings by the difference of the corresponding time values (*Δmass/Δtime*). Another spreadsheet column multiplies the corrected rate by the time interval to obtain the mass increment for a time interval. The summation of the mass increments is equivalent to integrating the corrected rate column and generates the *continuous readings curve* automatically. Visual inspection of the resulting continuous readings curve confirms that the automatic corrections are satisfactory. From the continuous readings curve, the air infiltration rate may be subtracted, as a linear function of time between successive flushing stages (Figure 5.12). The specific rate computed at each flushing should be used to correct the continuous readings curve for the time interval between two flushing's since the rate of air infiltration may vary between successive flushings.

5.6.2 Correcting for evaporation/condensation.

A non-horizontal slope may still be expected even after the correction for air diffusion. The slope may present a downward trend as in Figure 5.13(a) or an upward trend as in Figure 5.13(a). The expected outcome, however, is that the water mass readings would converge to a horizontal asymptote corresponding to the readings after equilibrium has been reached at a new applied matric suction value. A downward slope indicates that water is being removed from the closed system. Alternatively, the curve can show an upward slope if water is added to the system. Water removal from the system is attributed to evaporation. There are two potential sources of evaporation: the water loss to the air in the pressurized chamber, and water lost to the air phase in the overflow jar. Romero (1999, 2001), and Airò Farulla and Ferrari (2005), used a similar technique to correct for both the air diffusion and the evaporation simultaneously. Since the air diffusion occurs at a constant rate then both effects combine linearly.

In early tests, evaporation in the pressurized cell was a predominant factor. This behaviour can be attributed to limitations in the plugs used to close three holes left in the cell from earlier design requirements. This is supported by the observation of very slow continuous bubbling in the humidity chamber during the tests. The humidity chamber is a sealed bottle partially filled with water through which air is made to flow before entering the ring shear cell. The purpose of this chamber is to humidify the incoming air and reduce the losses associated with evaporation. In later tests, attempts were made to improve the quality of the plugs by sealing the three holes of the ring shear cell. Initially plugs each using 2 O-rings were used to close the holes, but had proven inadequate to properly seal them. When they were replaced with soft rubber conical plugs, evaporation rates dropped from 0.8 g/day to values below 0.1 g/day and bubbling was no longer observed in the humidity chamber. On such instances, where a net condensation was observed, it was in the order of 0.05 g/day.

5.7 CLS Test Results

Figures 5.14 and 5.15 show the failure envelopes obtained for CLS tests conducted on specimens compacted at water contents, w_c, of 15% and 19% respectively, and under a net normal stress of 150 kPa. These results were obtained using multistage testing procedures. As such, the results of shear strength for matric suctions, greater than zero had already been previously sheared. Nonetheless, a peak failure envelope diverging from the ultimate state envelope was formed (Figure 5.16). The peak strength failure envelope shown in this figure is not the true peak since it was a multistage test. As such the difference between peak and residual strength cannot be attributed to the destruction of the fabric resulting from the compaction process. Such a destruction would have occurred in any of the previous shearing stages, and indeed, under saturated conditions, when a true peak could be achieved, the difference between peak strength and residual strength was negligible.

Figure 5.17 shows a typical stress versus deformation curve for a CLS test on Indian Head till under a net normal stress of 150 kPa. Both the applied air pressure, u_a, equal to the matric suction, $(u_a - u_w)$, when the water is maintained at atmospheric pressure, and the net normal stress, $(\sigma_n - u_a)$, are controlled and maintained constant throughout the test. The plots show that the system adequately maintained these two stress state variables at their intended values with minimal fluctuations throughout the testing period.

Figures 5.18 and 5.19 show two stress versus deformation curve relationships for specimens compacted at water contents of 15% and 19% respectively. In all cases, the shear strength curves show that an ultimate shear strength value has been reached and sustained for an extended range of shear deformations. The maximum shear deformation for these tests was approximately equal to 20 mm for each stage.

Critical state is defined as the state of a specimen which under continued shearing exhibits no further change both with respect to shear strength and volume change behaviour. Figure 5.20 indicates that this has largely been achieved in most cases after a shear deformation approaching 20 mm. A larger shear deformation was required to reach critical state for the same specimen when sheared under lower matric suctions. The specimen showed dilatant behaviour in the early stages of all shear tests for matric suctions in excess of 50 kPa (Figure 5.20).

The soil behaviour was similar to that of normally consolidated clay at low suction values. However, the soil behaviour is typical to that of an overconsolidated clay at higher suction values. This behaviour suggests that contribution of matric suction to shear strength decreases during the shearing stage. This suggests that a change in the SWRC relationship occurs during shearing stage.

Figure 5.21 shows a plot of the water mass readings as a function of time. The time range covered includes the matric suction increment stage (from 25 to 50 kPa) and the shear stage. The two vertical lines indicate the shearing period. The onset of shearing is clearly visible from this plot. This also indicates that the shearing deformations have a distinct influence on the relationship between the water content of the specimen and the matric suction. The plot of the rate of water mass readings rate change as shown in Figure 5.22 provides a clear indication of the onset of the shearing process. This confirms the influence of the shearing process on the SWRC, and can serve as an explanation of the overconsolidated behaviour of the unsaturated soil specimen. If the matric suction contribution to the average particle stress is transmitted through the water, then the degree of saturation of the specimen will have an effect on the magnitude of this contribution. If the degree of saturation decreases at a given suction, then the contribution of matric suction would correspondingly be reduced. As the water content is reduced during shearing stage, the degree of saturation would decrease unless the specimen compresses sufficiently to cancel the influence of the change in water content, or even cause an increase in the degree of saturation.

Figures 5.23 and 5.24 show plots of the water content, w, as a function of shear deformation, δ, for specimens tested at various matric suctions. Figures 5.25 and 5.26 show the same data in terms of water ratio, $e_w = w \cdot G_s = e \cdot S$. Within the shear deformation range of the test, most specimens exhibit an apparent linear relationship between the deformation and the changes in water content. Such a behaviour was however not noticed in the specimen tested at a matric suction of 25 kPa (Figure 5.23). In this case, the initial slope is similar to that obtained at other matric suctions. However, after a shear deformation of 3 mm, the slope becomes steeper. This is attributed to the combined effect of the relatively low matric suction (and correspondingly higher initial degree of saturation) and the large volumetric strains involved when shearing the specimen at that suction value. This combined effect causes the specimen to approach saturation conditions. This increases the amount of water that must be expelled and also causes volumetric strains resulting in water expulsion. Tarantino and Tombolato (2005), also observed that Speswhite kaolin sheared at lower matric suction tended to approach saturation during shearing.

It must be noted that the rate of water movement from the specimen remained apparently linear in all other cases. This indicates that the critical state condition was not reached at the shear deformations that were imposed.

This also implies that it is not sufficient to observe the shear strength and volumetric changes to determine critical state in an unsaturated soil. Since the rate of water movement was apparently still linear for different matric suction values tested, it can be assumed that still there is a significant amount of water to be expelled at the end of the test. For this reason, to obtain a full understanding of the conditions of the specimen at critical state, it must be ensured that all parameters that have an influence on the critical state conditions such as the net normal stress, void ratio, matric suction and degree of saturation should attain constant conditions. All these parameters are interdependent. The fraction of the matric suction that is transmitted to the soil particles depends on the degree of saturation which in turn is a function of the water content and the void ratio. The void ratio at critical state itself depends on the normal stresses acting on the soil particles, which is composed of the net normal stress and the fraction of the matric suction transmitted to the particles, and therefore the degree of saturation. Therefore, a complete expression of the critical state in unsaturated soils must be the state for which under continued shear deformations, further increments in shear distortions will not result in any change of void ratio, degree of saturation, net normal stress or matric suction.

Figure 5.27 provides a closer look in the phenomenon by plotting the change in water content from the water content at the beginning of each shear test, $\Delta w = w - w_{initial}$. This helps to normalize the data by having all curves have the same origin point, which allows the scale to be magnified so that the smaller changes are more readily visible. While not entirely parallel, the curves at matric suctions greater than 25 kPa, do show slopes that vary within a relatively narrow band of values. Other than the curve at a matric suction of 25 kPa there is no apparent dependence of the slope of the curve (i.e., rate) on the matric suction. As it has already been observed, the dewatering rate was much greater at 25 kPa after a shear deformation of 3 mm. This closely corresponds to the volumetric deformations shown in Figure 5.20 It confirms that the volumetric strain are the primary cause of the water movement at this low matric suction value.

Figure 5.28 shows the relationship of the degree of saturation, S, with respect to shear deformation, δ. These curves do not appear as linear as the plots of the gravimetric water content or water ratio. This is to be expected however, since the degree of saturation, S, is a function of the void ratio, e, which changes during the constant load shearing process, as illustrated in Figure 5.29.

The total water content change during the shearing stage is approximately in the range of 0.15% to 0.30% for CLS tests over a shear deformation range of 20 mm. These numbers are comparable in magnitude to the absolute change in water content due to a matric suction increment which is typically in the range from 0.3% to 1.3% for the suction increment stages reported in Table 1.

5.8 CVS Test Results

Figures 5.30 and 5.31 show the failure envelopes obtained from CVS test results. Since these are constant volume tests, the net normal stress is not constant. In other words, the net normal stress will be continuously changing throughout the shearing process. Therefore, it is not possible to analyze the data considering the full shear strength, since it does not represent a projection on a plane perpendicular to the τ vs. (σ_v-u_a) plane. For this reason, only the contribution of matric suction to the shear strength has therefore been shown in these figures.

The principal objective of the constant volume tests is to examine the changes that occur during the shearing process on the SWRC. If both the volume and the matric suction are maintained constant, any change of the water content reflects a change of the SWRC for the relationship between the degree of saturation and the matric suction is changing while the void ratio is not. If only the change in void ratio affect the SWRC, then shearing at a constant void ratio would not be expected to cause changes in the water content of the specimen. This would not be the case if the shearing process affects the SWRC other than by global volumetric changes. In that case, even constant volume change would cause distinctive changes in the relationship of water content and matric suction. The changes during CVS tests, however, would be expected to be of a lower magnitude than those of the CLS tests since the volume change would also contribute to the changes in SWRC. A series of constant volume ring shear tests were therefore conducted to examine the effect of shearing on the SWRC when volumetric strains are limited, therefore eliminating the effect of the volumetric changes.

Figure 5.32 shows the stress versus deformation relationship for specimens compacted at a water content, w_c, of 15% and consolidated under a net normal stress of 150 kPa under saturated conditions. Unlike the curves generated for CLS tests, these are not generated under a constant net normal stress. Figure 5.33 illustrates how the applied net normal stress is modified in order to maintain the volume constant. Because the net normal stress is adjusted to maintain constant volume conditions, the shear strength shown in these figures does not correspond directly to the shear strength shown in Figure 5.31.

Figure 5.34 shows the vertical deformation as a function of shear deformation for CVS tests. The vast majority of the data points fall within a narrow band of 0.001 mm in either direction of the initial specimen height. This is shown as horizontal lines when the void ratio is plotted against the shear deformation (Figure 5.35). These results suggest that the designed system was capable of maintaining a constant volume during the tests.

Figure 5.36 shows a typical water mass reading as a function of time curve generated during a CVS test. The onset of shear is marked by a sudden increase in the rate of water expelled from the specimen. The onset of shear is equally well defined for CVS tests as it is for CLS tests. However, the rate of water movement is not as large as it is in the case of the CLS tests. The initial void ratio of the CLS test varied from 0.540 to 0.485, decreasing with increased matric suction, while the initial void ratio of the CVS tests fluctuated between 0.505 and 0.495. When CLS and CVS test results are compared (Figure 5.37) it can be seen that the CVS curves form a band with a slope roughly a third of the slope from by the curves from the CLS tests. However, as in the case of CLS tests, all the curves remain fairly linear throughout the shearing stage up to the maximum shear deformation value of 20 mm. These results support the hypothesis that there is still a substantial amount of water to be expelled from the specimen even once a shear deformation of 20 mm has been achieved, even without any change in matric suction.

Given the larger volumetric deformations taking place in CLS tests, it was expected that the water content changes should typically have higher values. This is indeed the case; however, the rates observed in the CVS tests are still in the same order of magnitudes as those obtained in CLS tests. Although the total amount of water expelled for any given deformation is smaller than in CLS tests, it can still represent a significant fraction of the water expelled from the specimen due to the matric suction increment alone. The dewatering curves of neither the CLS or the CVS test results show any tendency towards horizontal asymptote. This behaviour suggests that a comparatively significant amount of water could still be expected to be expelled from the specimen under shear, even without any change in the matric suction.

Although the dewatering rates appear generally linear, it is clear that they must eventually tend towards a horizontal asymptote as the specimen contains only a finite amount of water. An additional CVS was conducted at a deformation rate of 0.022 mm/sec and a shear deformation of 95 mm to verify the range of shear deformations that would be required to achieve true critical state for an unsaturated Indian Head till. Figure 5.38 shows how this test compares to another CVS tests conducted at the same matric suction of 150 kPa. The time rate of water movement is lower in the case of the specimen tested at a shear deformation rate of 0.022 mm/min. This is in accordance with previous observations that the amount of water expelled from the specimen was linearly related to the shear deformation. When comparing the same data in terms of water mass readings changes as a function of the shear deformation (Figure 5.39), the results from this test are in good agreement with the other CVS test results. The difference in shear rate did not cause measurable differences in the rate of dewatering.

The results from this CVS test also appear quasi linear within the range of shear deformations to which previous CVS test had been subjected. This suggests that critical state has not been reached and that a comparatively substantial amount of water must still be expelled from the specimen. Figure 5.40 shows that the curve does begin to curve visibly at larger deformations. Despite this, after approximately 95 mm of shear deformations, still more water can be expected to be expelled from the specimen. The amount of water expelled from the specimen due to the shearing process is comparable to the water expelled between matric suction increments beyond a matric suction of 100 kPa. Since shearing causes water movements comparable to the matric suction increments, potentially large errors in the evaluation of the degree of saturation can be expected if the shear deformations imposed are not sufficient to reach critical state.

5.9 Critical State

The critical state is used to uniquely relate the void ratio, and shear strength to the normal effective stress for soils in saturated conditions. The critical state line can then be used as a tool for the prediction of the ultimate strength and void ratio of a soil at critical state if the normal effective stress is known.

In unsaturated soils, however, two stress state variables must be taken into account: the net normal stress, $(\sigma_n - u_a)$, and the matric suction, $(u_a - u_w)$. Each of these stresses contributes towards the shear strength of unsaturated soils. Figures 5.41 and 5.42 show that there is no unique relationship that relates the ultimate shear strength to either the net normal stress or the matric suction alone.

Upon examination, the vertical alignment of points in Figure 5.41 is a result of the CLS test series. Since the net normal stress is 150 kPa for all CLS tests, then all points are aligned vertically. In other words, the contribution of the net normal stress is the same for all CLS data points. The matric suction is different for each test stage, however, and since it does contribute to the shear strength of the soil, a vertical line is formed. For these tests, the vertical distance of the shear strength from the shear strength under saturated conditions (i.e. the lowest points on the vertical line) represents the contribution of the matric suction to the shear strength. This contribution from matric suction can be seen in Figure 5.42 where the shear strength of the CLS tests increases with an increase of matric suction.

The relationship between the void ratio and the net normal stress is shown in Figures 5.43 and 5.44. While there is no apparent relationship between the void ratio and the net normal stress, the plot of the void ratio and the matric suction seems to provide a well defined linear relationship. This, however, may be attributed in part to the limitations of testing program. Indeed, closer inspection reveals that the CLS tests (the solid shapes) are responsible for the trend observed, while the open shapes representing the CVS tests are scattered. Since the CLS tests were performed at a constant net normal stress, it is reasonable to expect that for both series of tests, the matric suction would independently control the void ratio. Interestingly, the two CLS series of tests overlap, suggesting that the initial compaction water content had no significant influence on the ultimate global void ratio during the shearing stage. This is in agreement with the results presented by Wheeler and Sivakumar (2000).

Studies by various researchers [Ridley (1995), Tarantino and Tombolato (2005)] have shown that the gravimetric water content, or its associated value, the water ratio e_w, are well correlated to the critical state of unsaturated soils. Both of these variables are plotted against matric suction in Figures 5.45 and 5.46. There is a clear linear trend in these plots on a logarithmic scale. These are well in agreement with the previously reported behaviour of unsaturated soils [Ridley (1995), Tarantino and Tombolato (2005)]. The test results indicate that both CVS and CLS tests follow the same trend line, and since no constraint was placed on the movement of water during the experiment this relationship is not the result of the testing procedure, but a real characteristic of the soil. When conducting tests under controlled suction, this line is the critical state line (CSL) and is expressed in the water content, or water ratio, versus matric suction space. If conducted under constant water content, the ultimate relationship between water content and matric suction is called the continuously disturbed line (CDL). Ridley (1995), observed that the CDL lied beneath the CSL but that they were both parallel.

The results obtained for both CLS and CVS tests from this study on Indian Head till suggest that very large deformations are required during such tests in order to reach the true critical state conditions. Due to time restrictions, only limited number of tests results were undertaken in this research program. However, these results provide evidence suggesting that the CSL and the CDL might in fact be one and the same, if sufficiently large deformations were applied to constant matric suction tests to truly reach critical state. Furthermore, the specimen tested under both CLS and CVS conditions showed a similar rate of water content change with respect to shear deformation. Since the rate of water movement with respect to shear deformation was not dependent on matric suction, specimens sheared to the same amount would be expected to lie equally far from the true CSL, thus resulting in an apparent CSL line parallel to the real CSL line. From this terminology, the real CSL line would be the ultimate condition to which the specimen would tend once equilibrium of shear strength, volume, degree of saturation would have been achieved under sustained uniform shearing. To verify the hypothesis, that the CSL and the CDL may in fact be one and the same, however, new series of shear tests would have to be conducted under both CLS and CLW conditions at shear deformations well in excess of 100 mm for a few different soils. Until then it remains a simple hypothesis.

5.10 Average Skeleton Stress

The results from this study confirm observations from the earliest days of testing of unsaturated soils that the shear strength is not a function of either the matric suction or the net normal stress alone. Various relationships between those stress state variables are available from the literature in the prediction models relating shear strength to both net normal stress and matric suction. Many of them [Bishop (1959), Vanapalli et al. (1996), Öberg & Sällfors (1997), Gallipoli et al. (2003)] use of the degree of saturation to relate matric suction to the shear strength. As noted by Vanapalli et al. (1996) the matric suction can only be transferred through the area of the water phase in contact with the soil particles. This mechanism dictates that the degree of saturation be used as a factor to reduce the contribution of the matric suction to the shear strength. While the degree of saturation can be used directly as a multiplication factor on the matric suction for granular soils, it is often inadequate to predict the shear strength contribution of fine grained soils. Different approaches have been proposed to accommodate this contribution through the use of empirical fitting parameters.

Romero et al. (1999) and Romero and Vaunat (2000) observed that there is a particular water ratio, e_{wm}, called the microstructural water ratio which separates the regions of inter-aggregate porosity and that of intra-aggregate porosity. Only the water in the inter-aggregate macropores contributes to the mechanical behaviour of the soil, while the aggregates act as large individual soil particles. Romero and Vaunat (2000) introduced a term called degree of saturation of the macro voids, S_{rM}. This value was defined for deformable clays. Indian Head till contains a significant fraction of clay, and it was decided to see how this value would fit the experimental data. The variable S_{rM} is defined as:

$$S_{rM}=\frac{e_w-e_{wm}}{e-e_{wm}} \qquad [5.1]$$

Tarantino and Tombolato (2005) used this parameter to define mean skeleton stress, σ_v'' as:

$$\sigma_v''=(\sigma_v-u_a)+(u_a-u_w)\frac{e_w-e_{wm}}{e-e_{wm}} \qquad [5.2]$$

Figure 5.47 show the relationship between the shear strength and an average skeletal normal stress defined strictly in terms of the degree of saturation:

$$\sigma_v'' = (\sigma_v - u_a) + (u_a - u_w) S \qquad [5.3]$$

The data points present a general trend despite some scatter. A relationship that would reduce this scatter would be of value, however. Such a relationship is possible with the aid of macro voids degree of saturation, S_{rM} It is necessary to evaluate the parameter microstructural water, e_{wm} in order to use the macro voids degree of saturation, S_{rM}. This value can be fitted to the shear strength data collected from the tested specimen. For the Indian Head till tested in this study, the fitted value was found to be equal to 0.275.

Figure 5.48 shows the variation of shear strength with respect to average skeleton stress, σ_v generated using the microstructural water value of e_{wm}=0.275. The data points show a better defined trend in comparison to using simply the parameter degree of saturation, *S*. This supports the notion that the water in the macro-voids plays a dominant role in the determination of the mechanical characteristics of unsaturated soils [Romero and Vaunat (2000), Tarantino and Tombolato (2005)].

Figure 5.49 was generated using an average skeleton stress developed from the degree of saturation raised to the power, κ, using the model presented by Vanapalli et al. (1996). A qualitative observation reveals that the scatter is very similar to the one observed in Figure 5.48. Both methods therefore seem equally adequate at predicting the shear ultimate strength of this unsaturated glacial till. However, the value of κ was obtained from the chart relating κ to the plasticity index [Vanapalli and Fredlund (2000)]. This relationship was generated by associating a SWRC developed by conventional means to the peak strength of a number of soils. Therefore, it would be more appropriate to back calculate a value of κ, in a procedure similar to the one followed for determining, e_{wm}. The fitting parameter, κ was found to be equal to 5.01 when using critical state data. Figure 5.50 shows the relationship between the shear strength and the average skeleton stress determined using the prediction equation proposed by Vanapalli et al. (1996). This relationship shows well defined trend for the experimental results presented in this study.

$$\tau = c' + (\sigma_w - u_a)\tan\phi' + \Theta^{\kappa}(u_a - u_w)\tan\phi' \qquad 5.4$$

5.11 Summary

The experimental program presented in this study has served to highlight the fact that the shearing process influences the water content of a specimen beyond the effect of the imposed matric suction. From Figure 5.37, it can be seen that a volume of water of similar magnitude is expelled from the specimen sheared under constant volume as well as constant load conditions. Furthermore, Figure 5.39 shows that upon continued shearing a substantial amount of water can still be removed under constant volume conditions. Given that both volume and matric suction remain constant under these conditions, the relationship of the water content to the matric suction is being modified by the shearing process at the same void ratio. From the detailed analysis of CLS and CVS tests it can be summarized that:

1) Volumetric strains have an important effect on changes in the SWRC of sheared specimens

2) The shearing process influence on the SWRC includes a component that is independent of the volumetric strain. This is attributed to the changes in the distribution of void ratios occurring within the specimen during shear.

The experimental program has also shown that although approximately 20 mm shear deformation is large considering the available range in conventional testing devices, it is insufficient to reach true critical state in some unsaturated soils, such as the tested Indian Head till. Shear deformations well in excess of 100 mm may be required to reach critical state for fine-grained soils. Based on this observation, it may be hypothesised that the CSL and CDL curves described by Ridley (1995), may in fact be the same if the tests were conducted to large deformations. More experimental data is required to substantiate or invalidate this hypothesis.

5.12 Figures

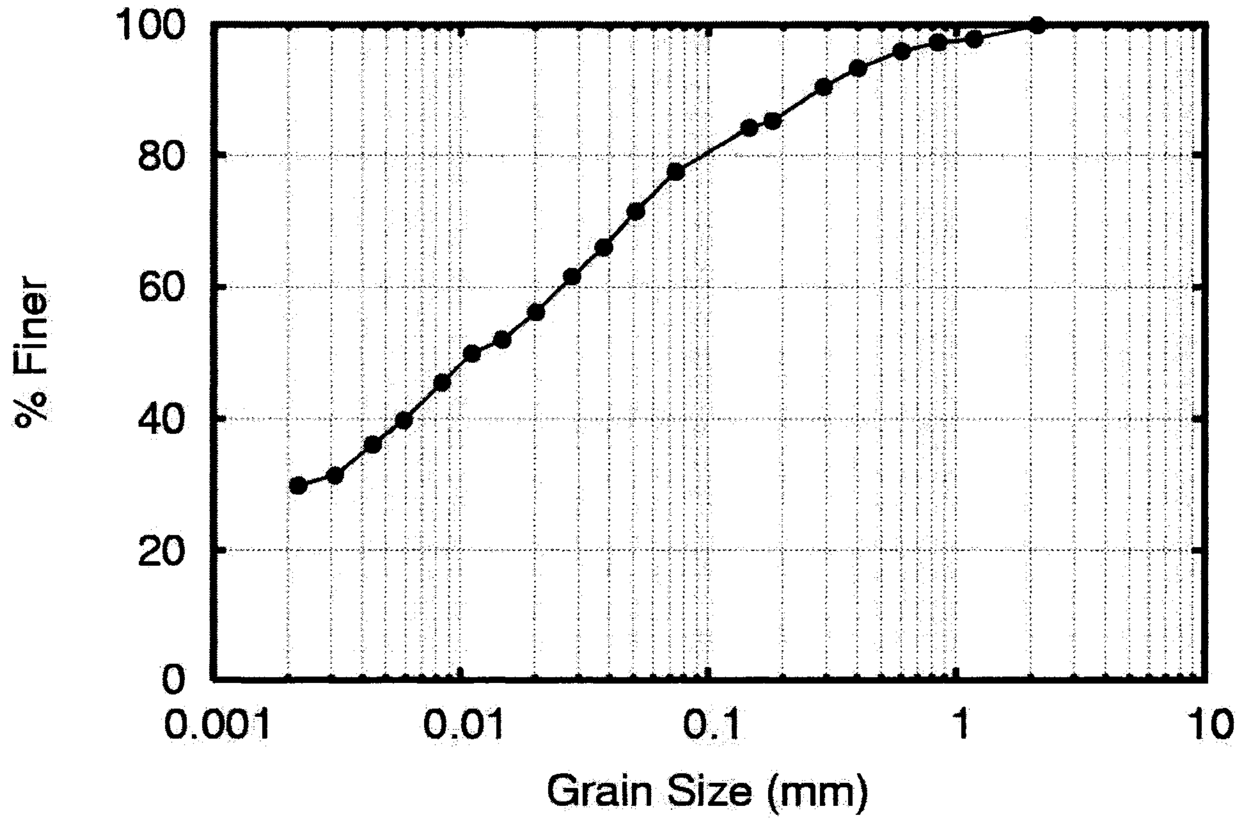

Figure 5.1 Grain size distribution of the Indian Head glacial till.

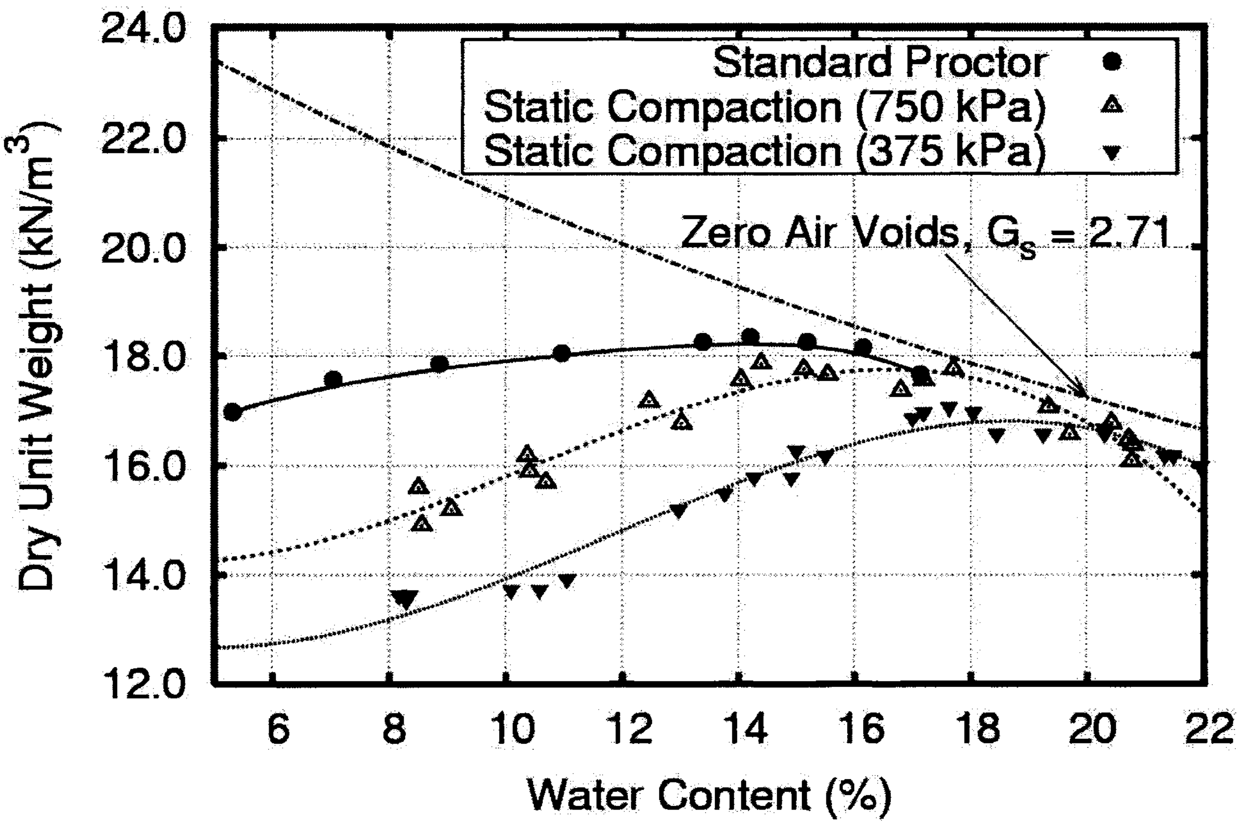

Figure 5.2 Compaction curves of Indian Head glacial till. Proctor density is compared to static compaction at compaction loads of 750 kPa, and 375 kPa respectively.

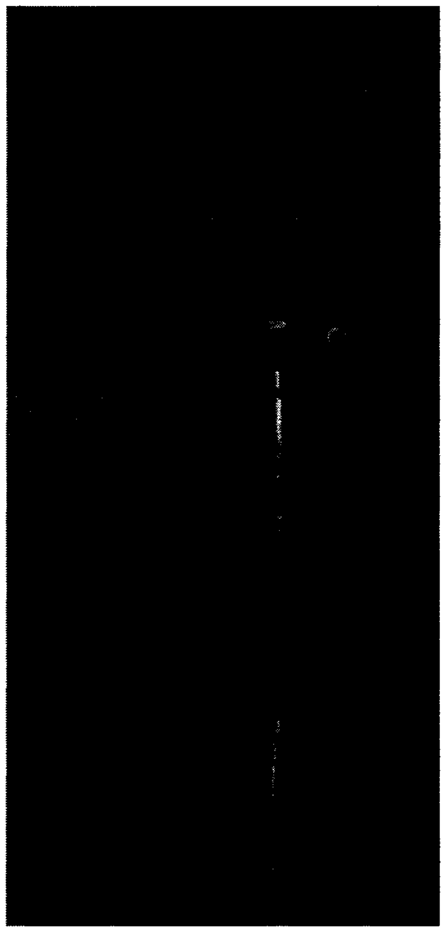

Figure 5.3 Drill press used to statically compact an oedometer specimen.

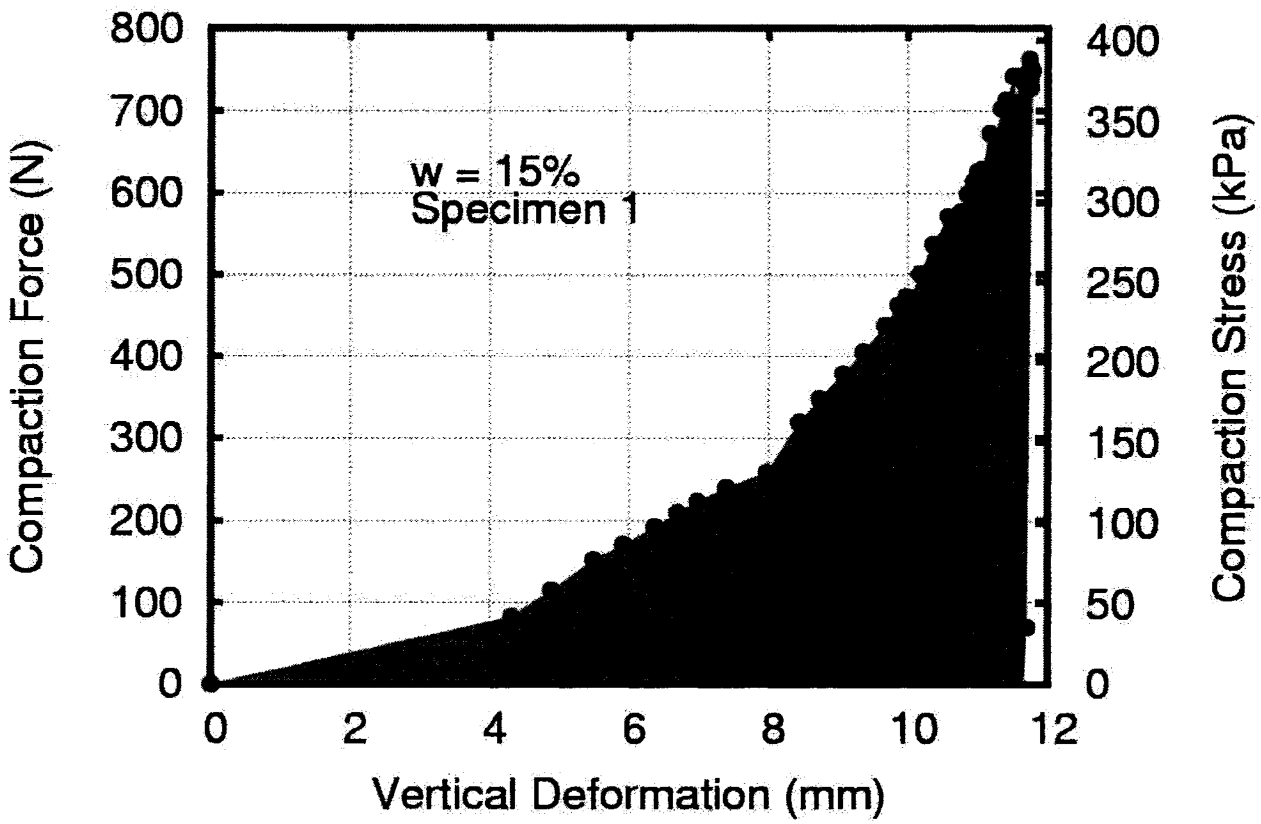

Figure 5.4 Compaction force applied to a 50 mm diameter oedometer specimen.

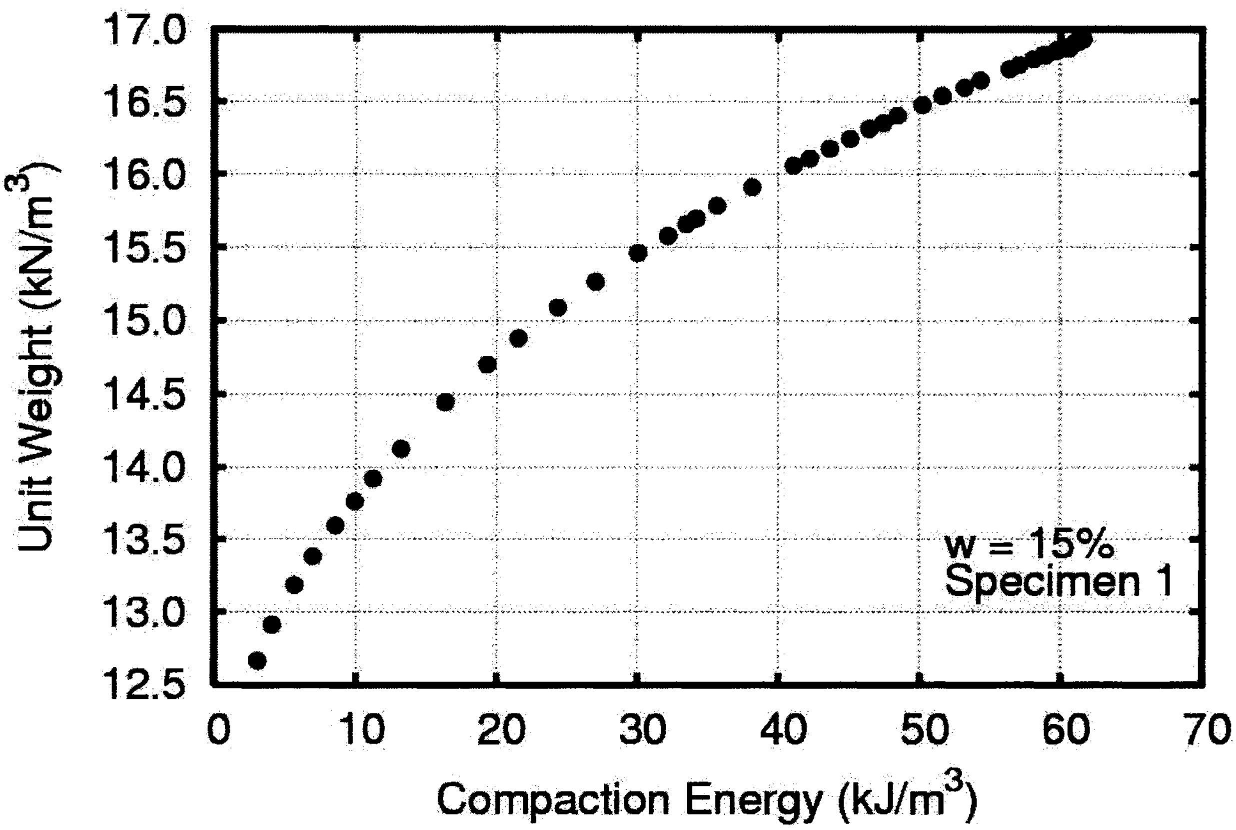

Figure 5.5 Compaction energy curve for an Indian Head Till specimen compacted at a water content of 15% under a vertical compaction stress of 375 kPa.

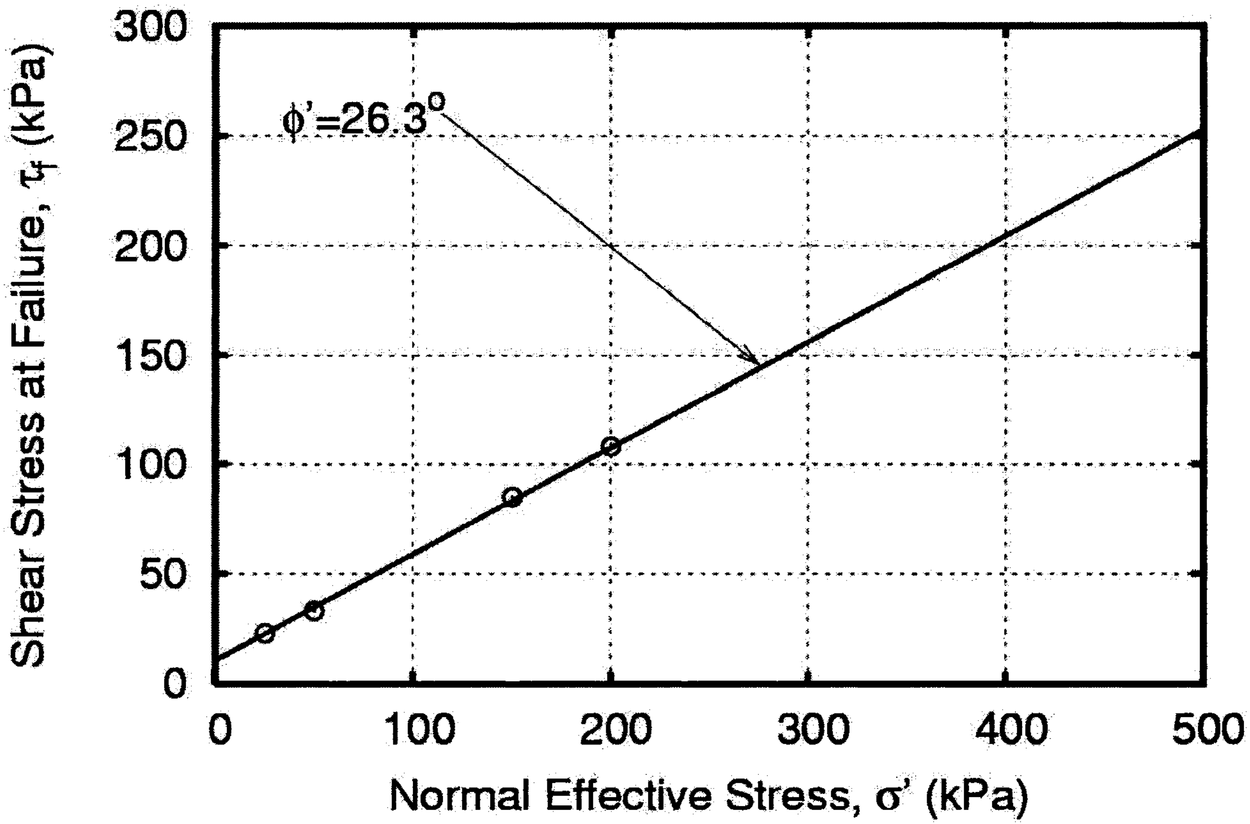

Figure 5.6 Shear strength envelopes at large deformations of Indian Head glacial till compacted at a water content of 19%.

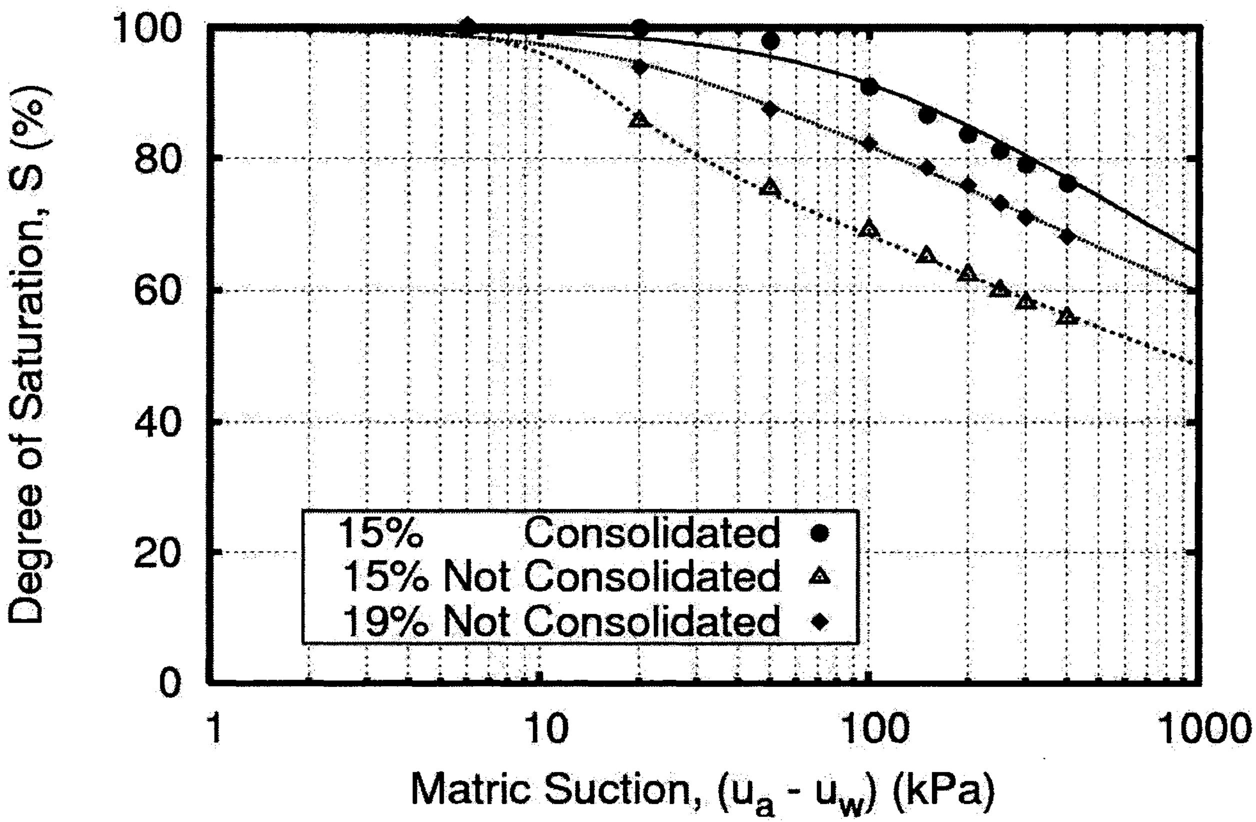

Figure 5.7 SWRC obtained from specimens compacted at two different water contents . Some specimens were consolidated in saturated conditions under a net normal stress of 150 kPa. Each point represents the average of 3 samples.

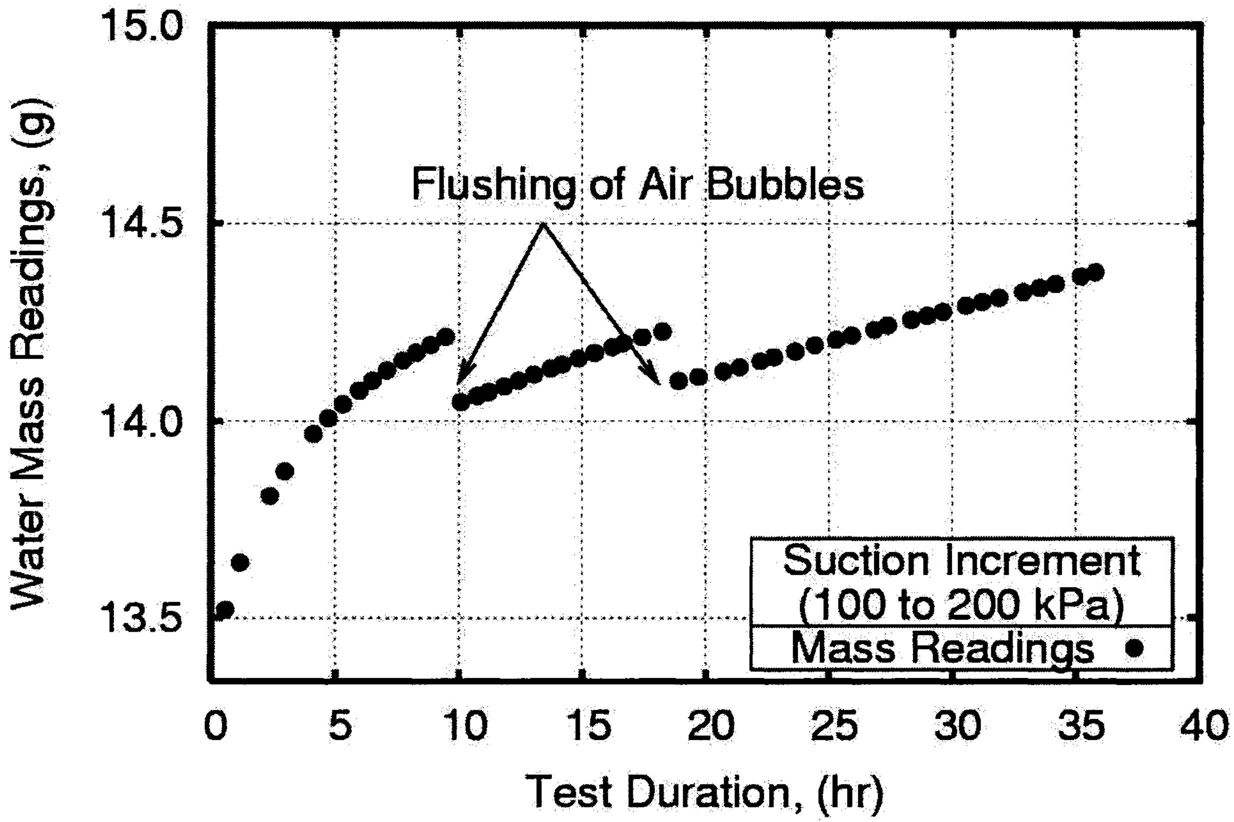

Figure 5.8 Typical overflow readings during a matric suction increment phase.

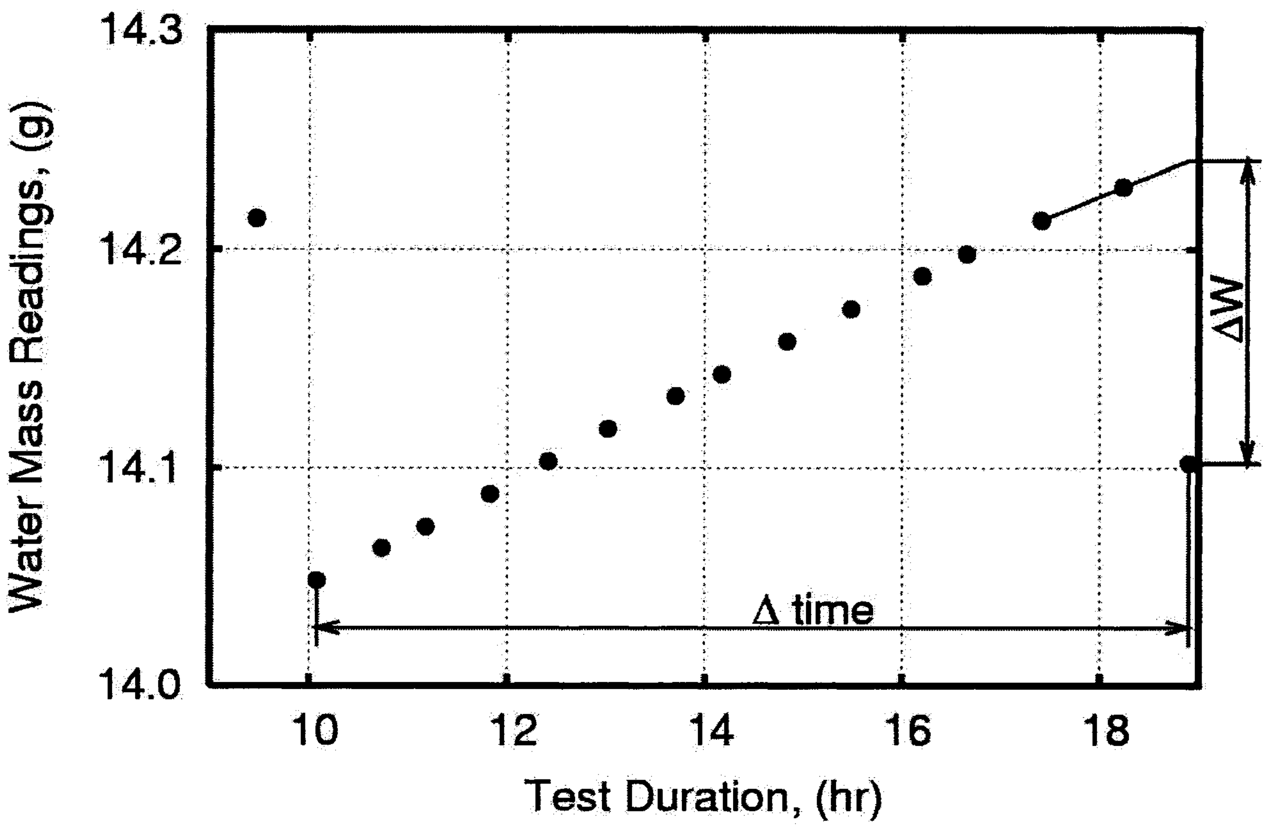

Figure 5.9 Extracting diffusion rate from recorded water movement data between flushing stages.

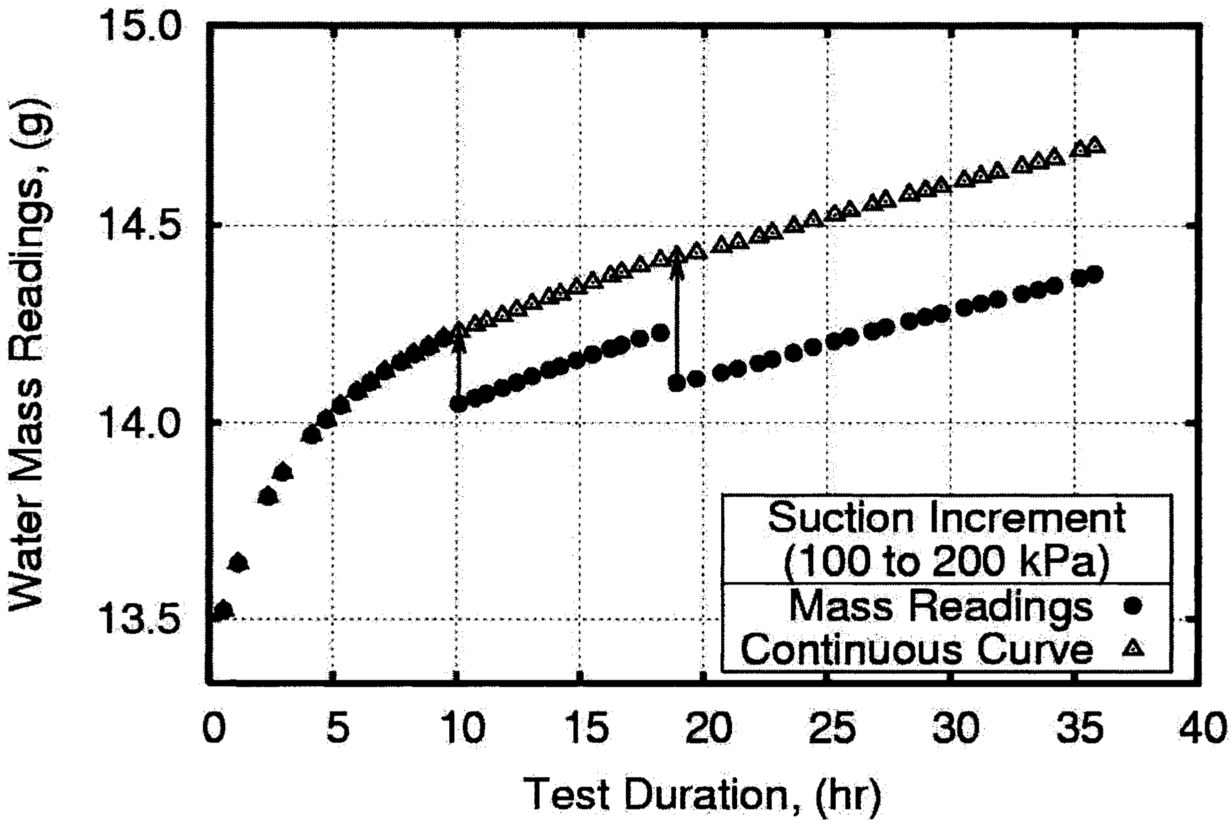

Figure 5.10 Readings realigned into a continuous curve, as if deairing cycles had not been conducted.

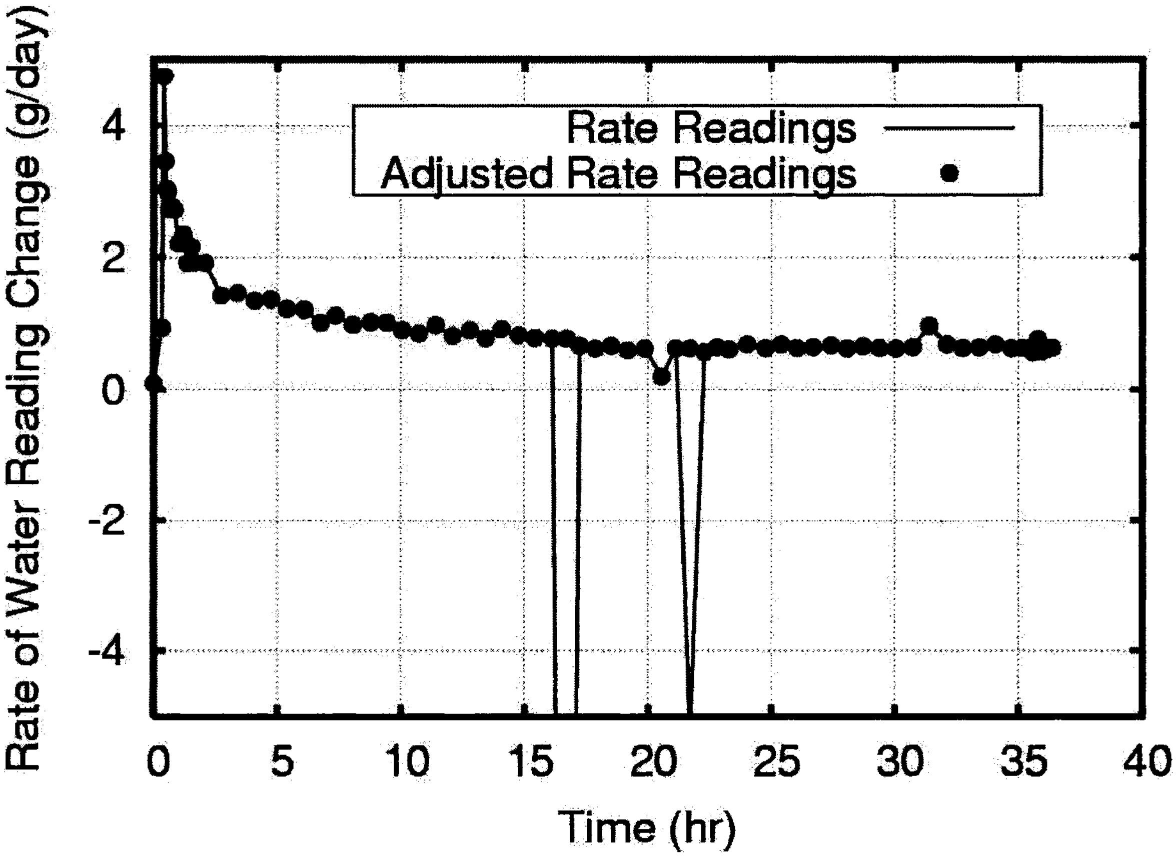

Figure 5.11 Illustration of the correction of rate anomalies due to flushing operations.

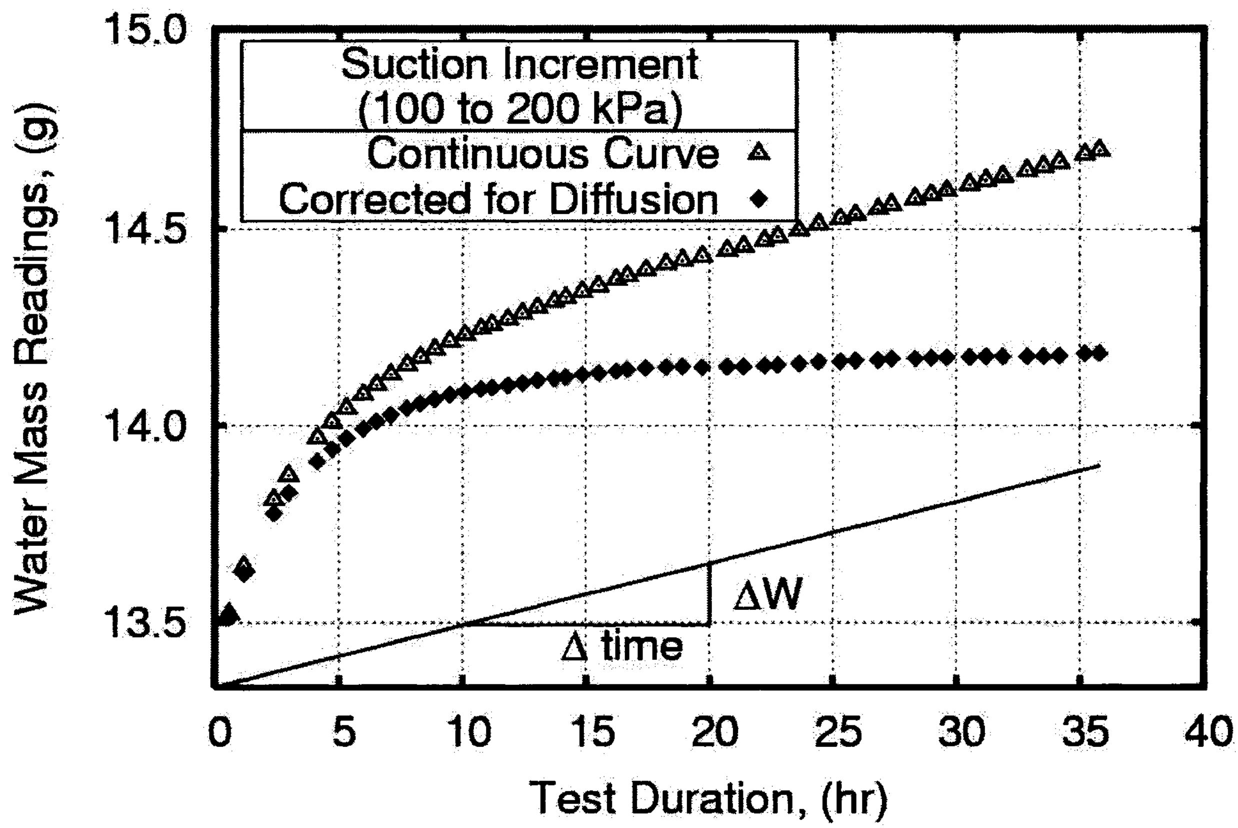

Figure 5.12 The calculated diffusion rate is used to remove the cumulative air diffusion from the continuous readings curve.

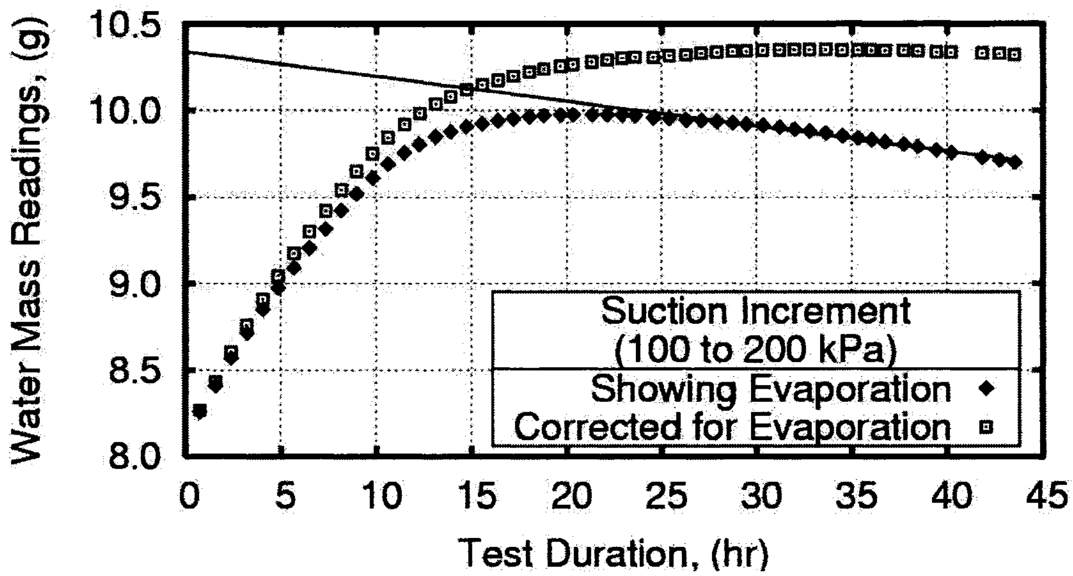

a)

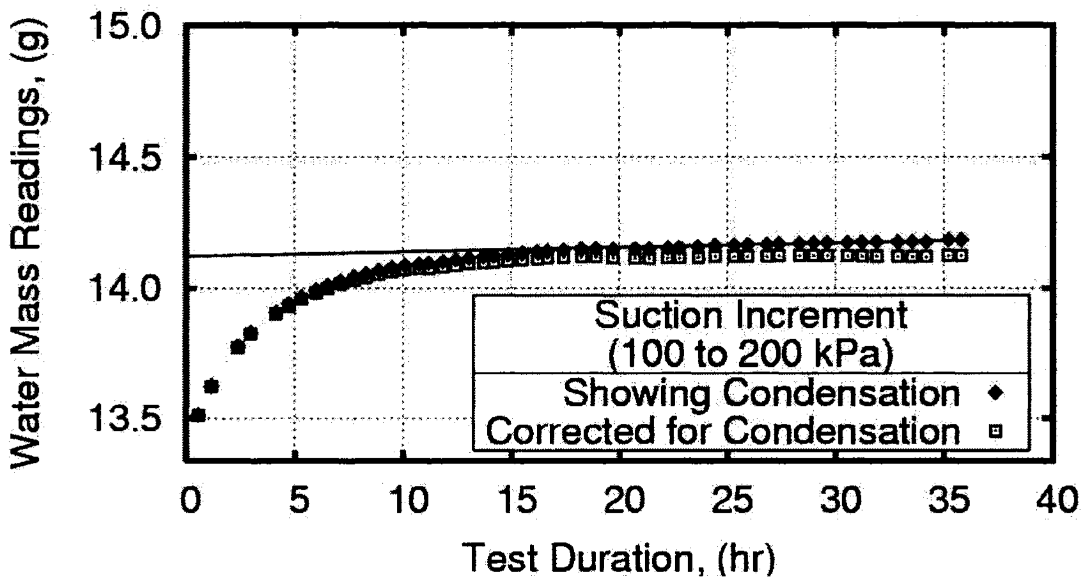

b)

Figure 5.13 Water mass readings corrected for evaporation/condensation.

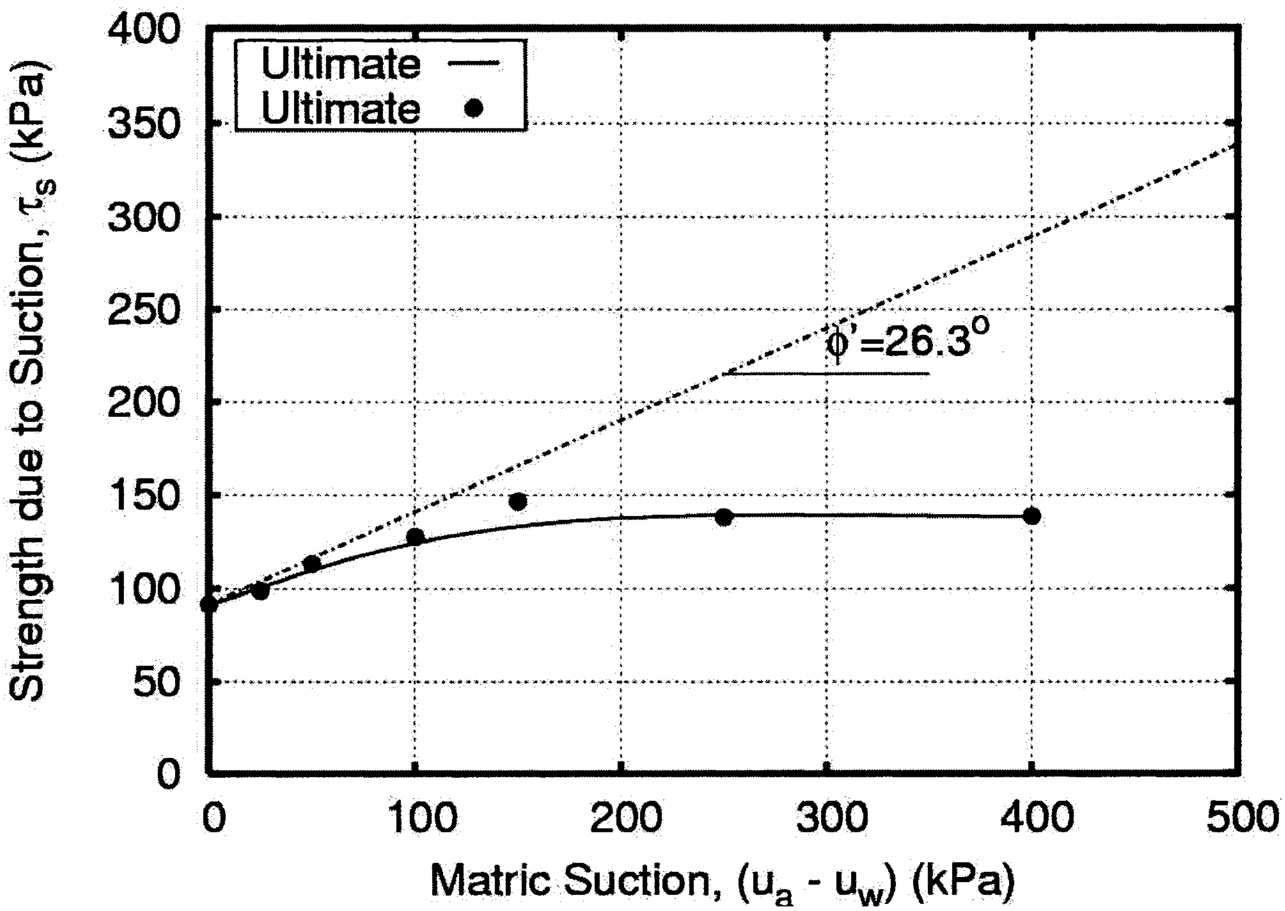

Figure 5.14 Failure envelope of an Indian Head till specimen sheared under CLS conditions. The compaction water content, w_c, was 15% and the applied net normal stress was 150 kPa.

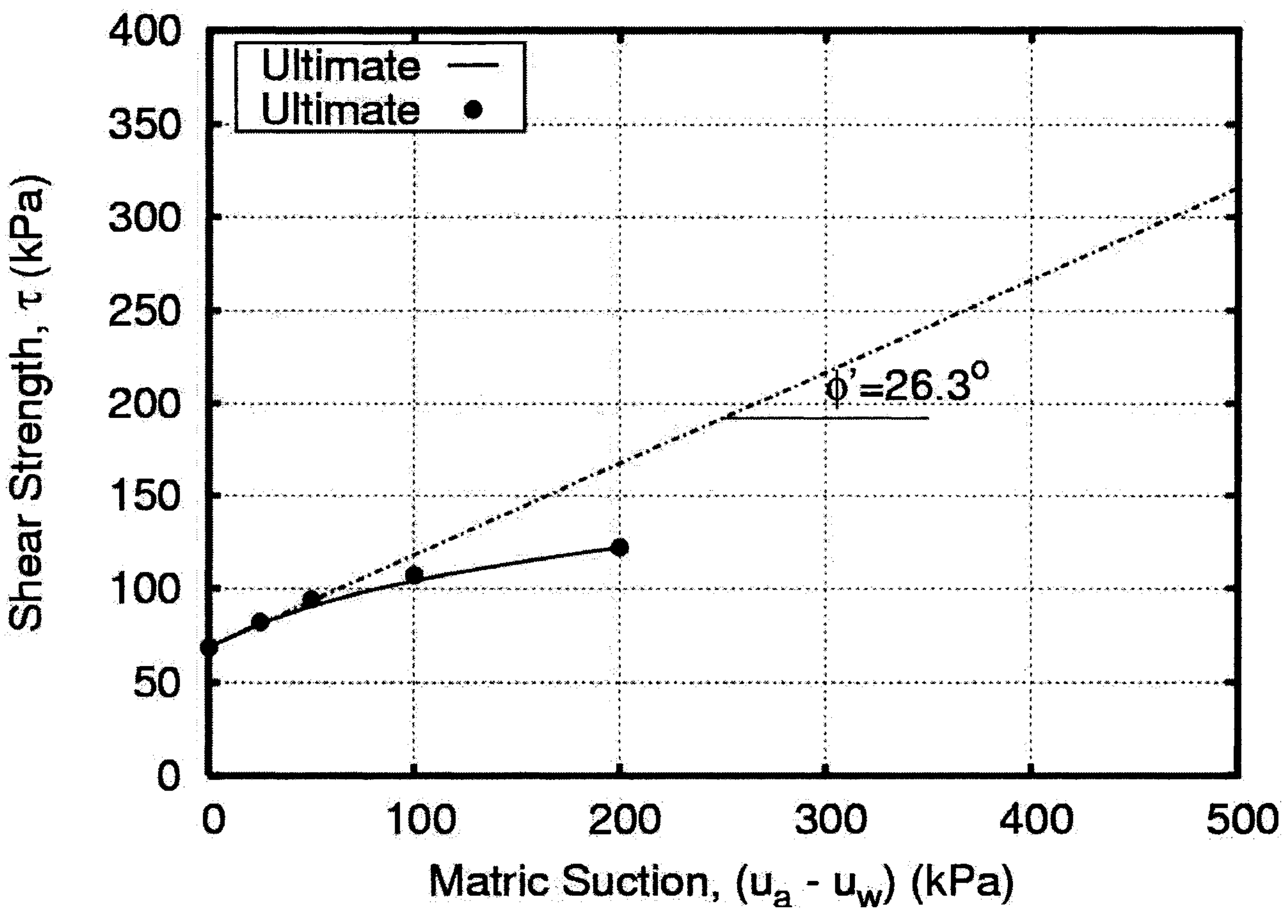

Figure 5.15 Failure envelope of an Indian Head till specimen sheared under CLS conditions. The compaction water content, w_c, was 19% and the applied net normal stress was 150 kPa.

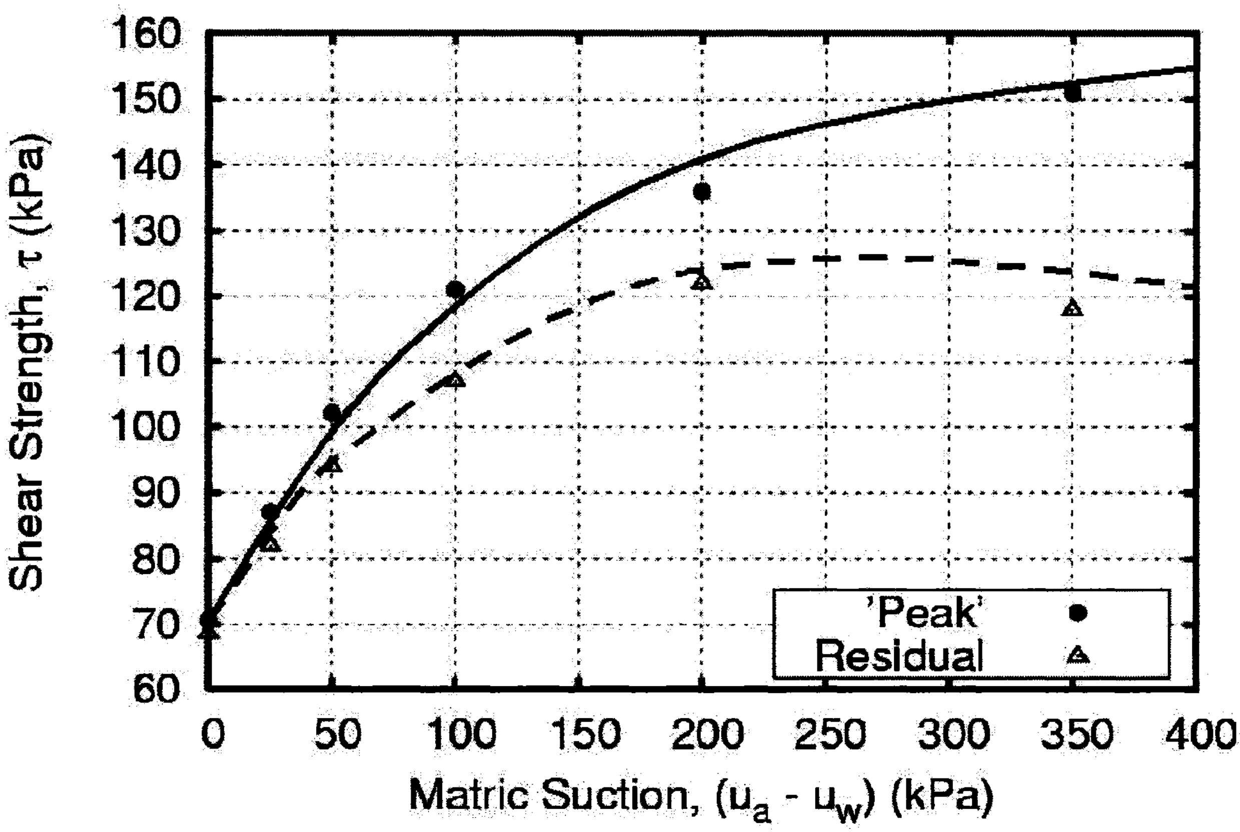

Figure 5.16 Difference between the pseudo peak and the residual failure envelopes with respect to matric suction for a specimen compacted at at water content, w_c, of 19%, tested under CLS conditions under a net normal stress of 150 kPa.

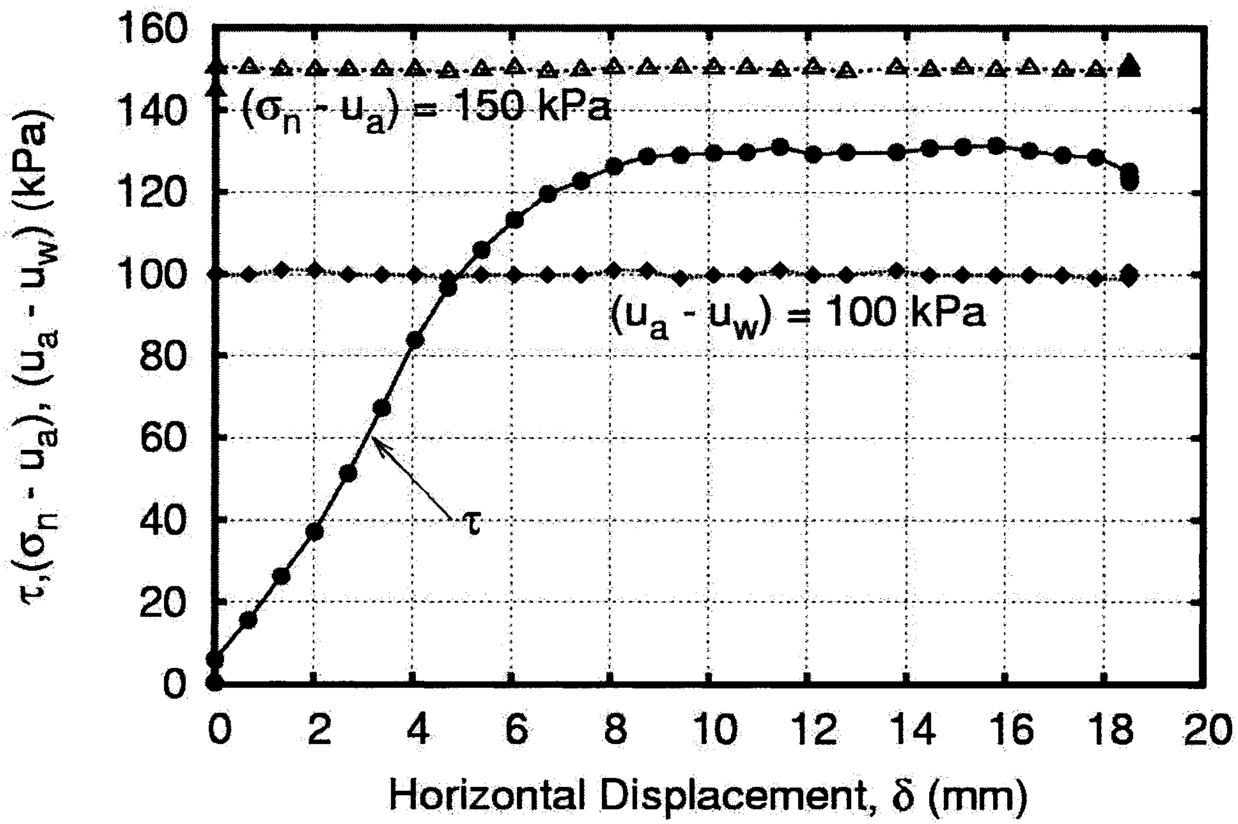

Figure 5.17 Typical stress/deformation relationship for a CLS test on a ring shear specimen compacted at 15% and consolidated under saturated conditions under 150 kPa normal load.

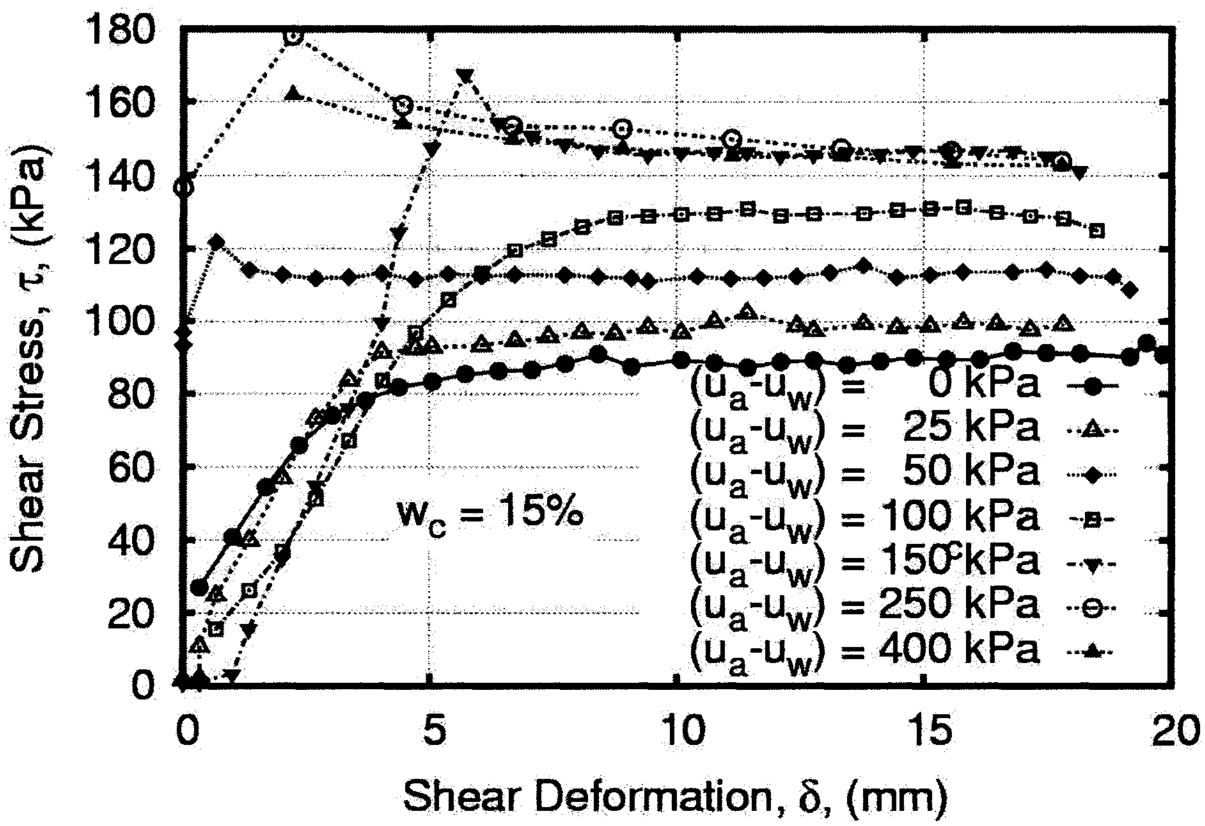

Figure 5.18 Stress-deformation curves for specimens compacted at a water content of 15% and sheared under a constant net normal stress of 150 kPa.

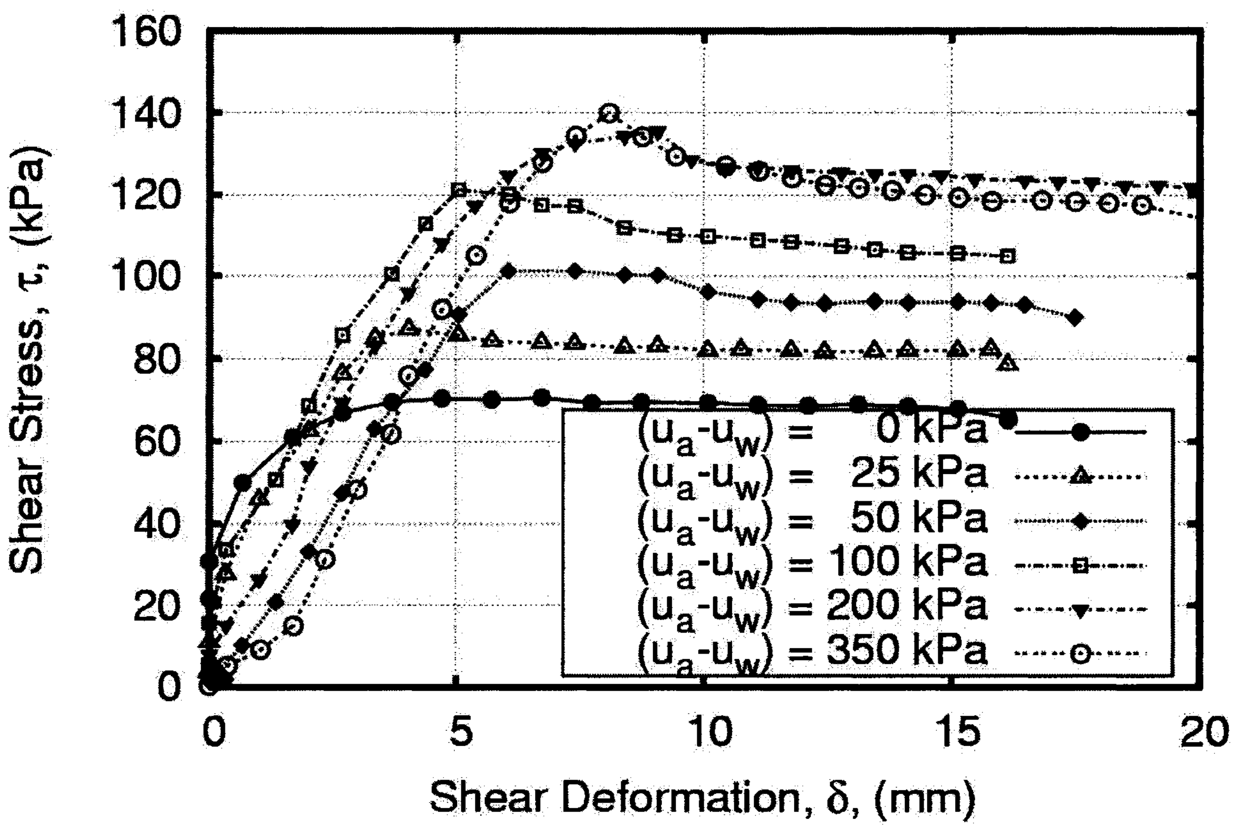

Figure 5.19 Stress-deformation curves for specimens compacted at a water content of 19% and sheared under a constant net normal stress of 150 kPa.

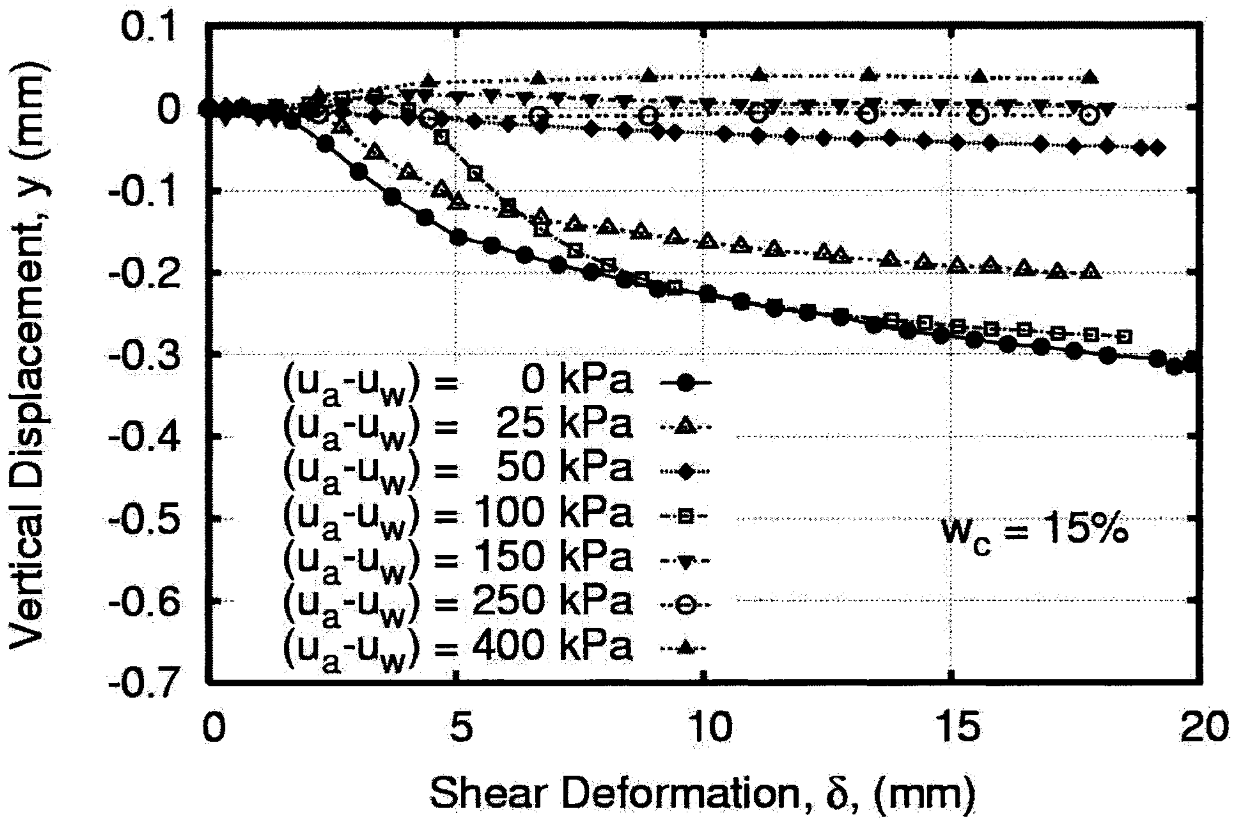

Figure 5.20 Vertical deformation plots for soils compacted at a water content of 15%, and sheared at a constant normal stress of 150 kPa.

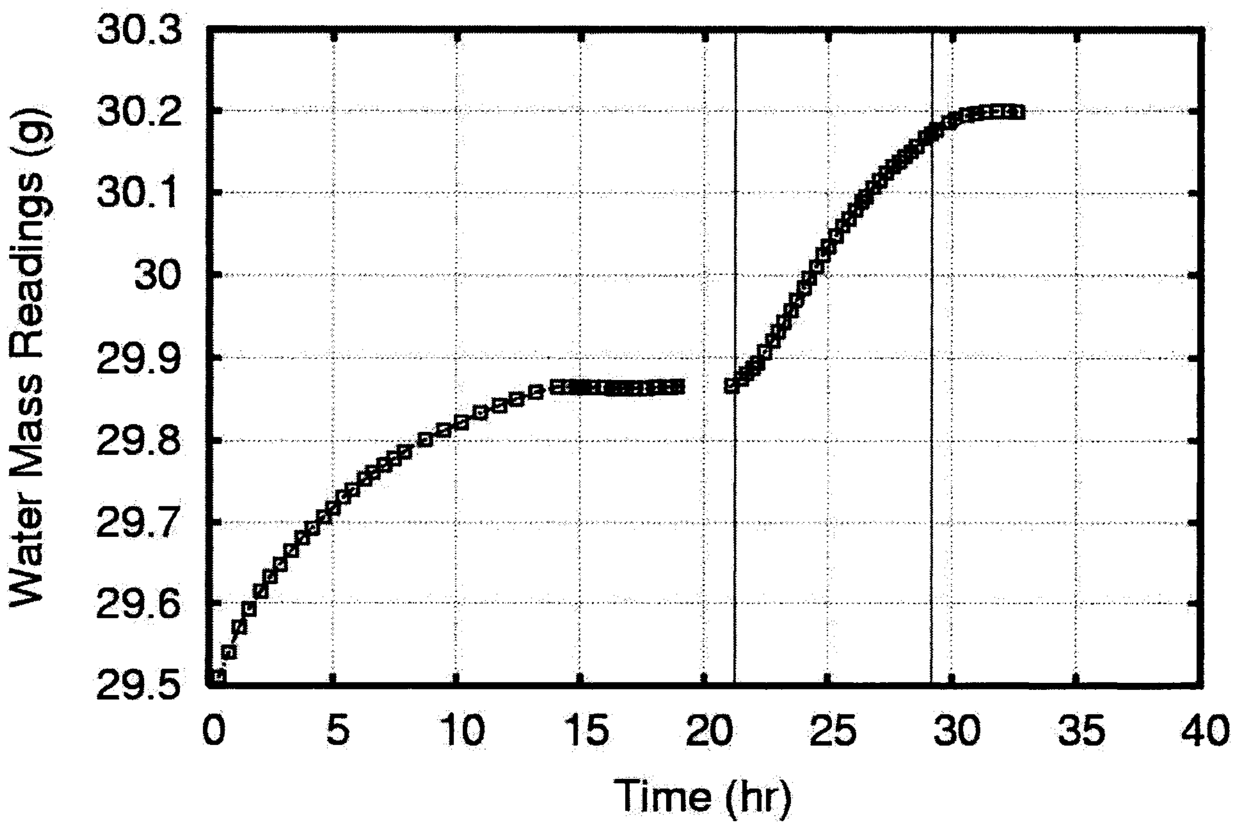

Figure 5.21 Typical plot of the change of water mass reading as a function of time. (CLS, w_c = 15%, $(u_a - u_w)$ from 25 kPa to 50 kPa). The two vertical lines indicate the shear period.

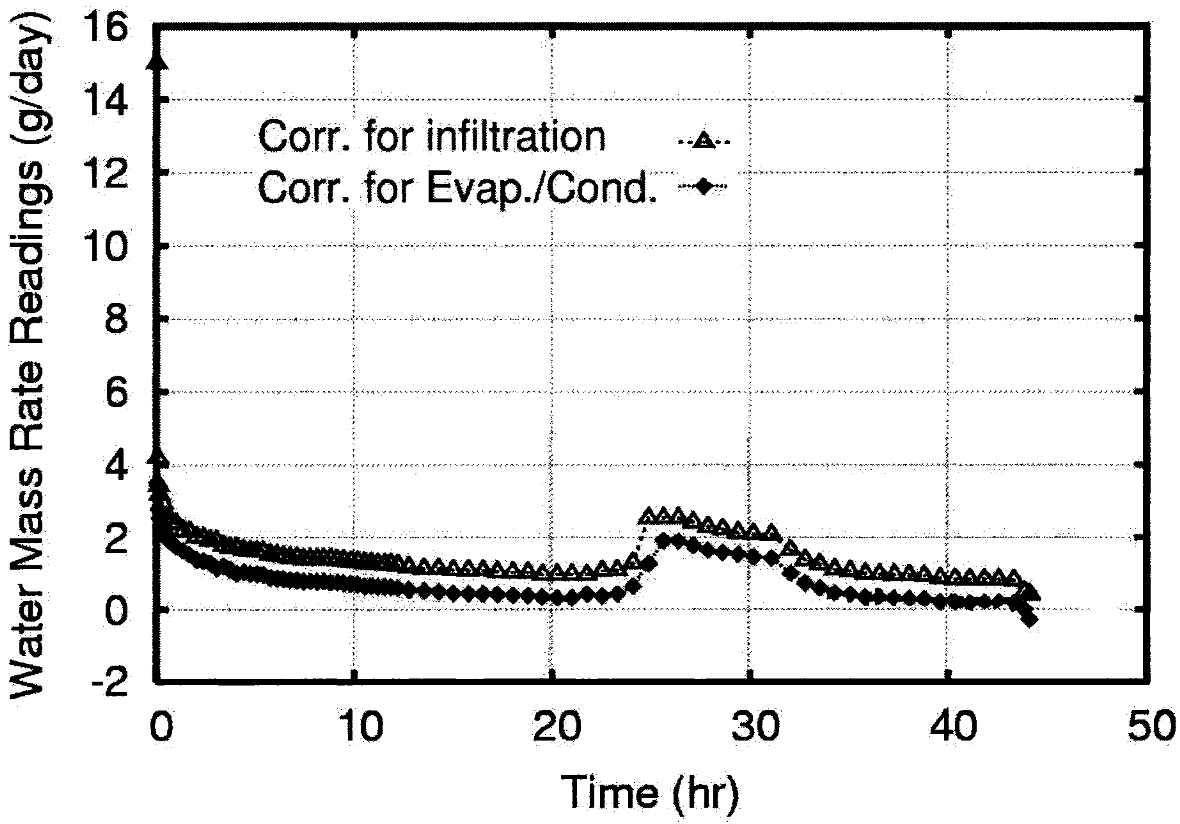

Figure 5.22 Rate of water overflow in grams per day. The onset of shear is clearly visible as a sudden increase in the water mass rate readings.

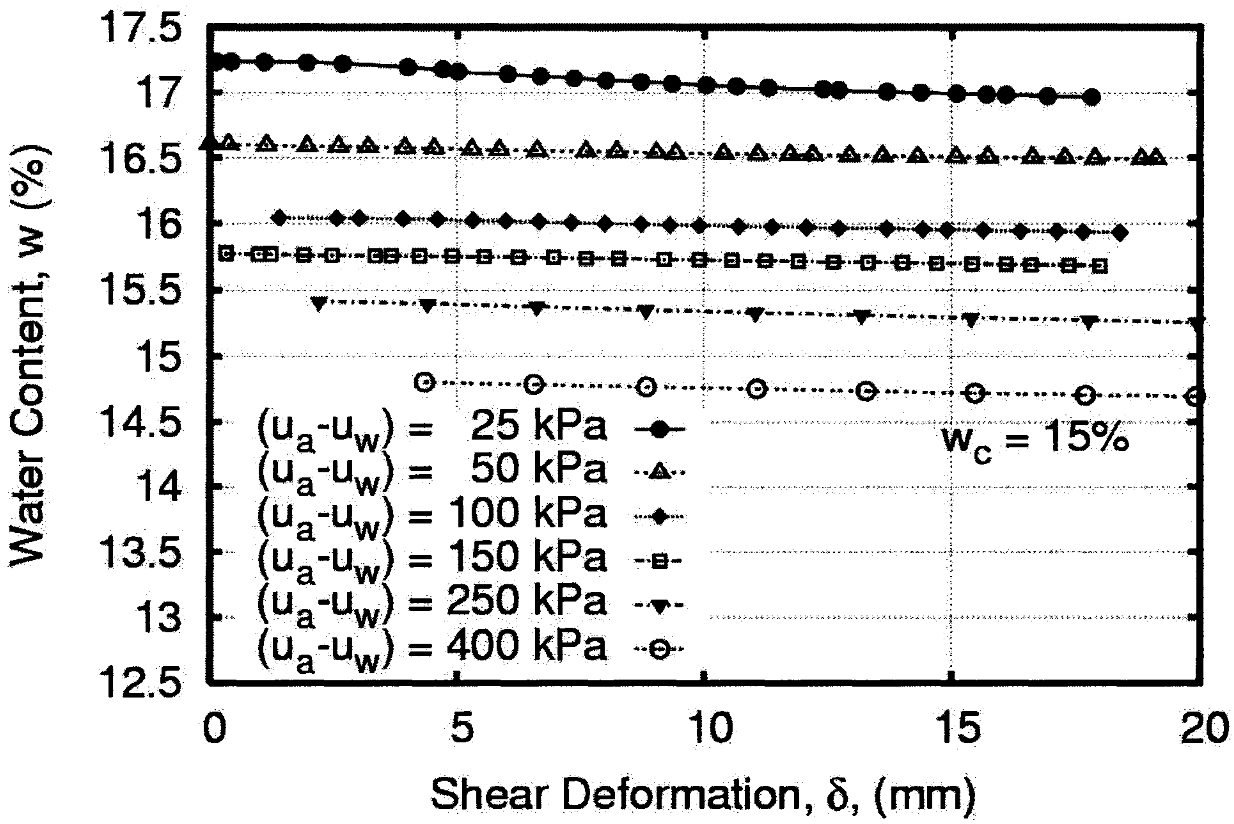

Figure 5.23 Variation of the water content of a specimen, compacted at a water content, w_c, of 15%, during CLS shear at various matric suctions (CLS).

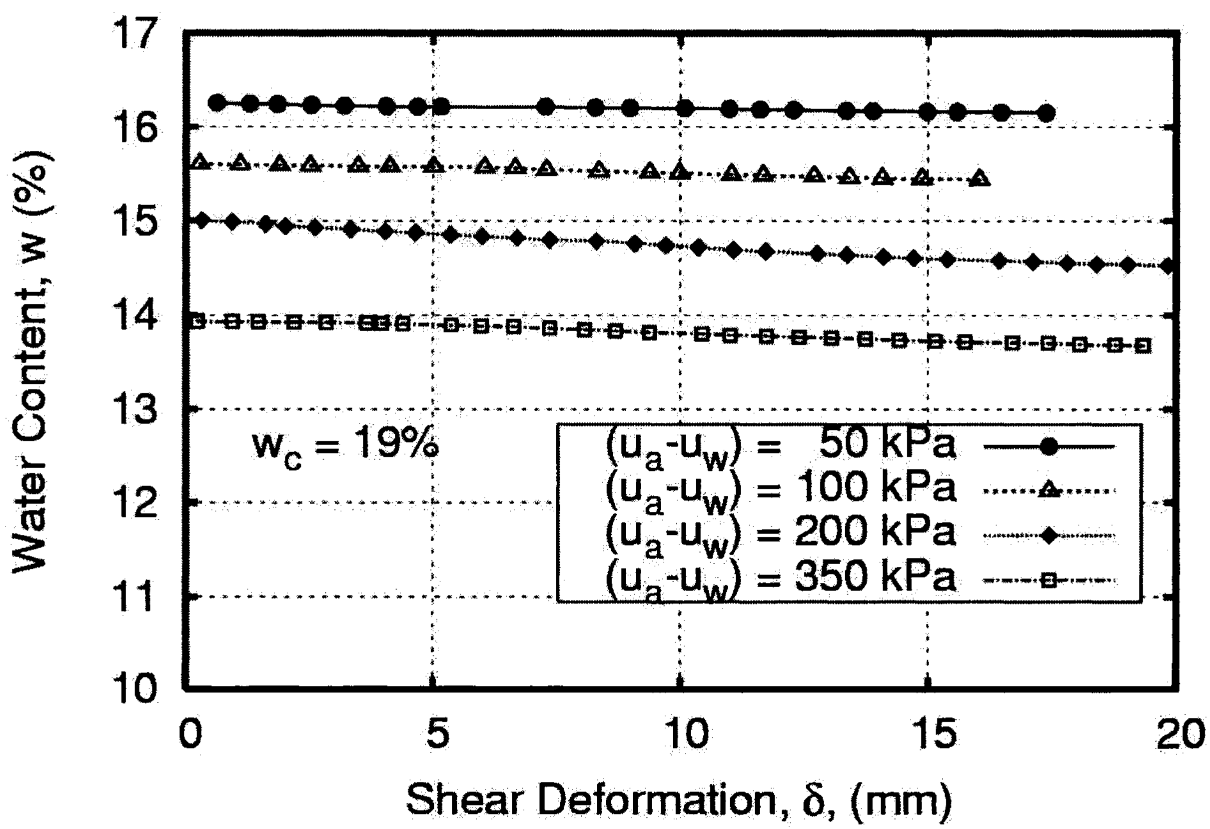

Figure 5.24 Variation of the water content of a specimen, compacted at a water content, w_c, of 19%, during CLS shear at various matric suctions.

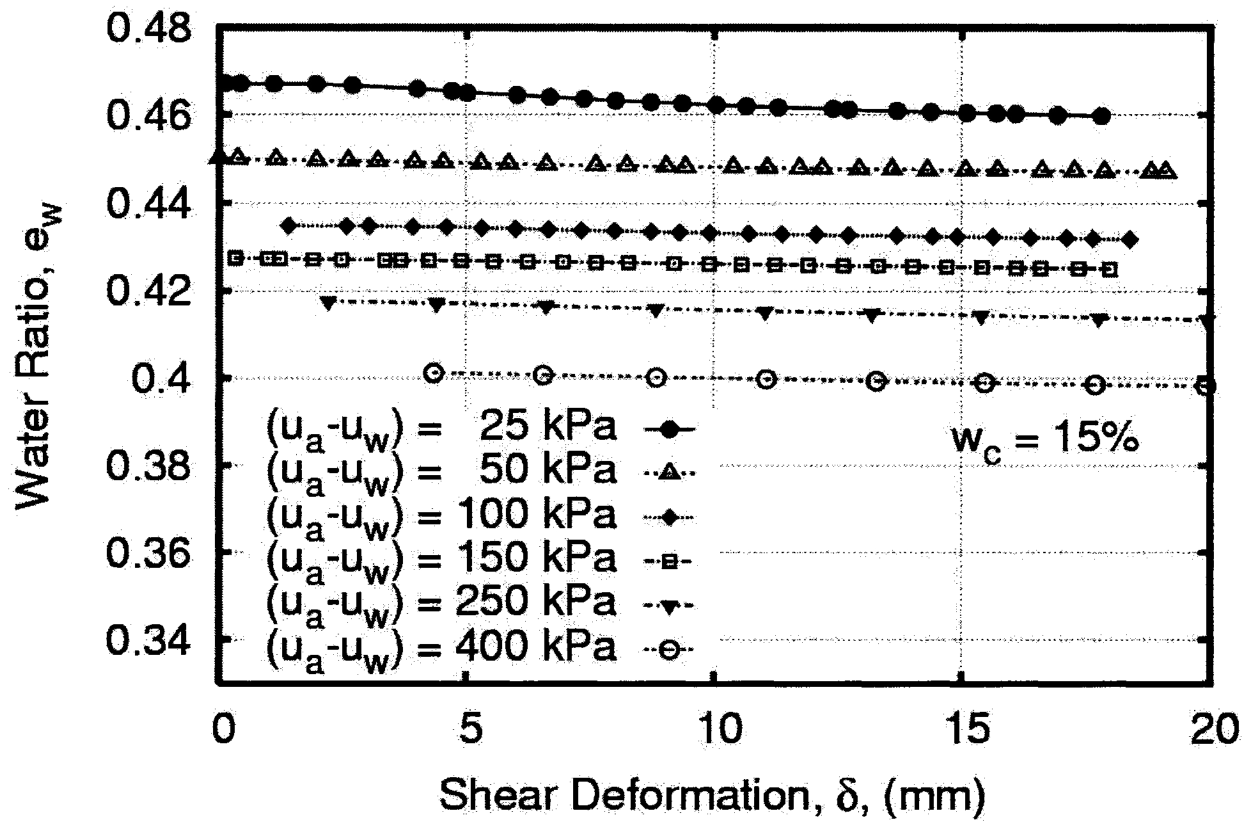

Figure 5.25 Variation of the water ratio, e_w, of a specimen, compacted at a water content, w_c, of 15%, during CLS shear at various matric suctions.

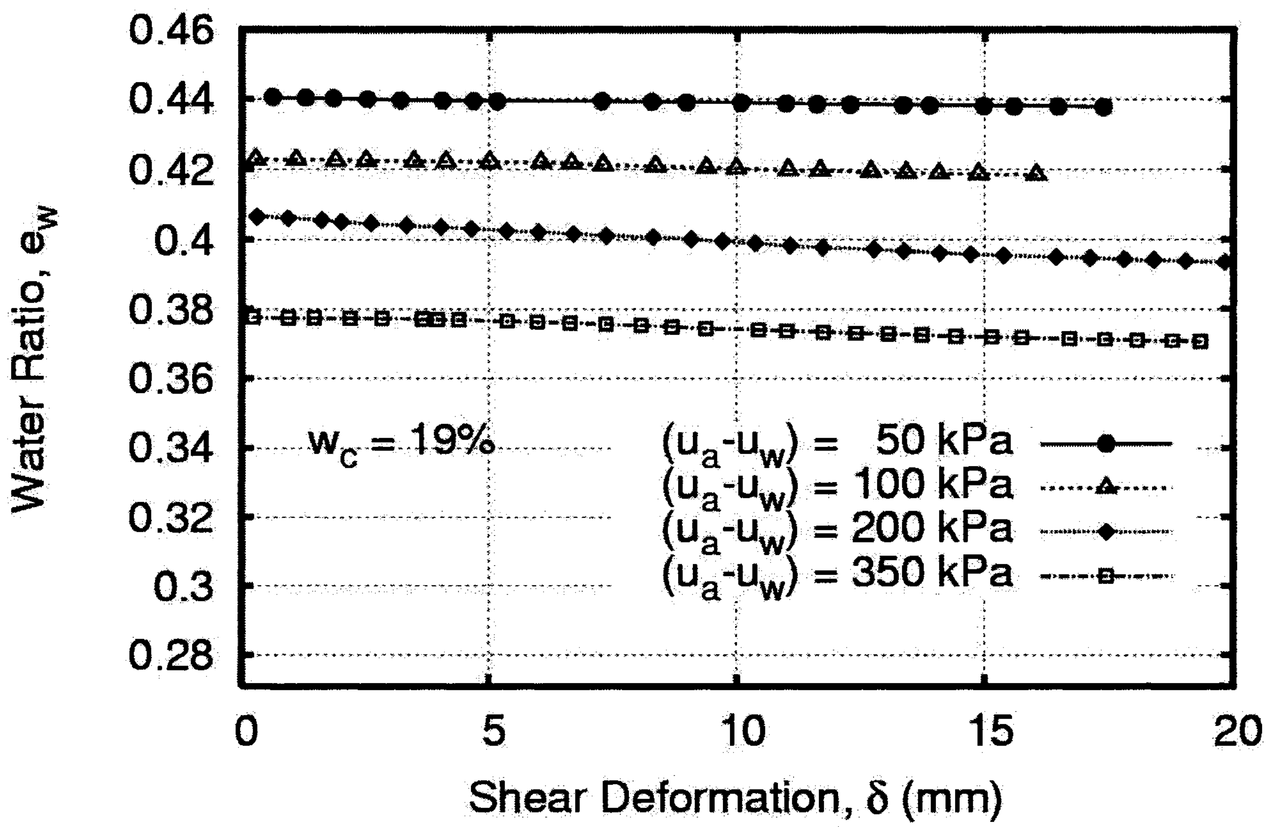

Figure 5.26 Variation of the water ratio, e_w, of a specimen, compacted at a water content, w_c, of 19%, during CLS shear at various matric suctions.

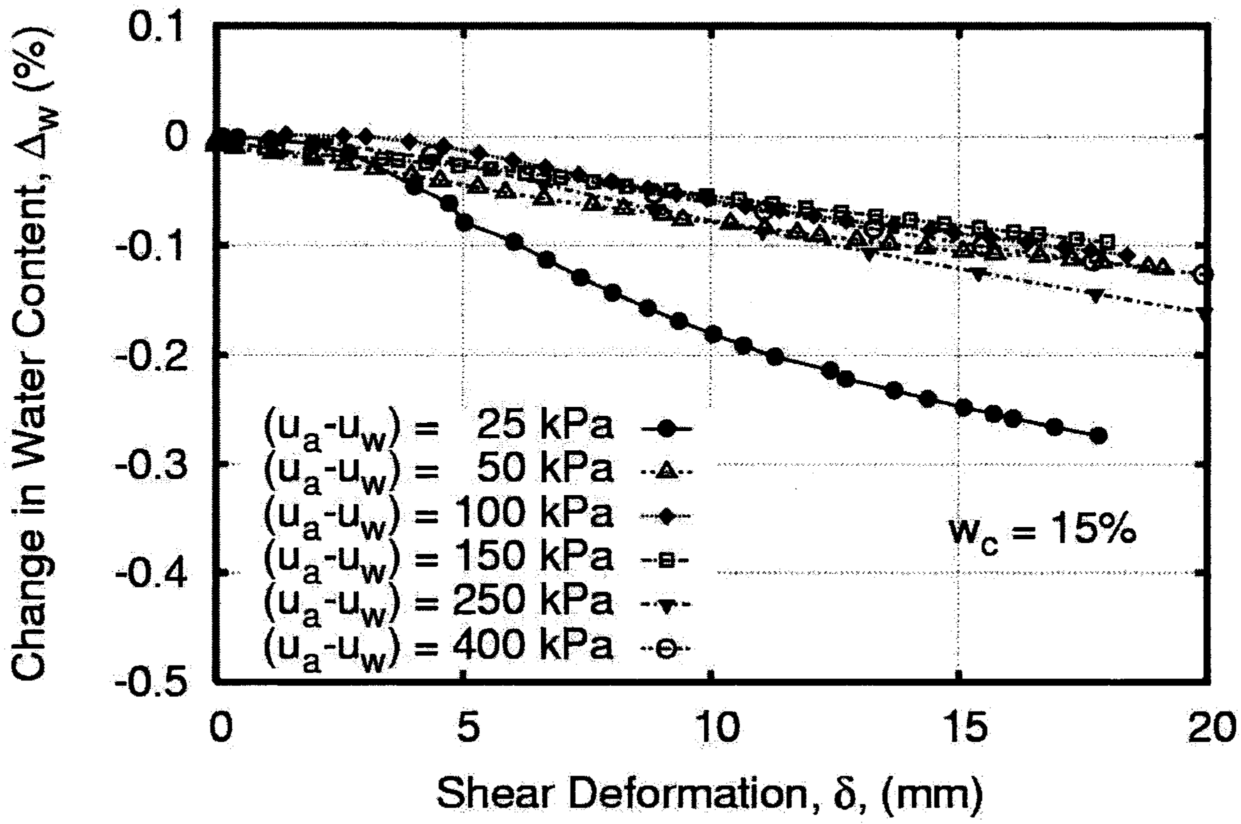

Figure 5.27 Water content changes from water content at beginning of shear, Δw, for a specimen, compacted at a water content, w_c, of 15%, and sheared in CLS conditions at various matric suctions.

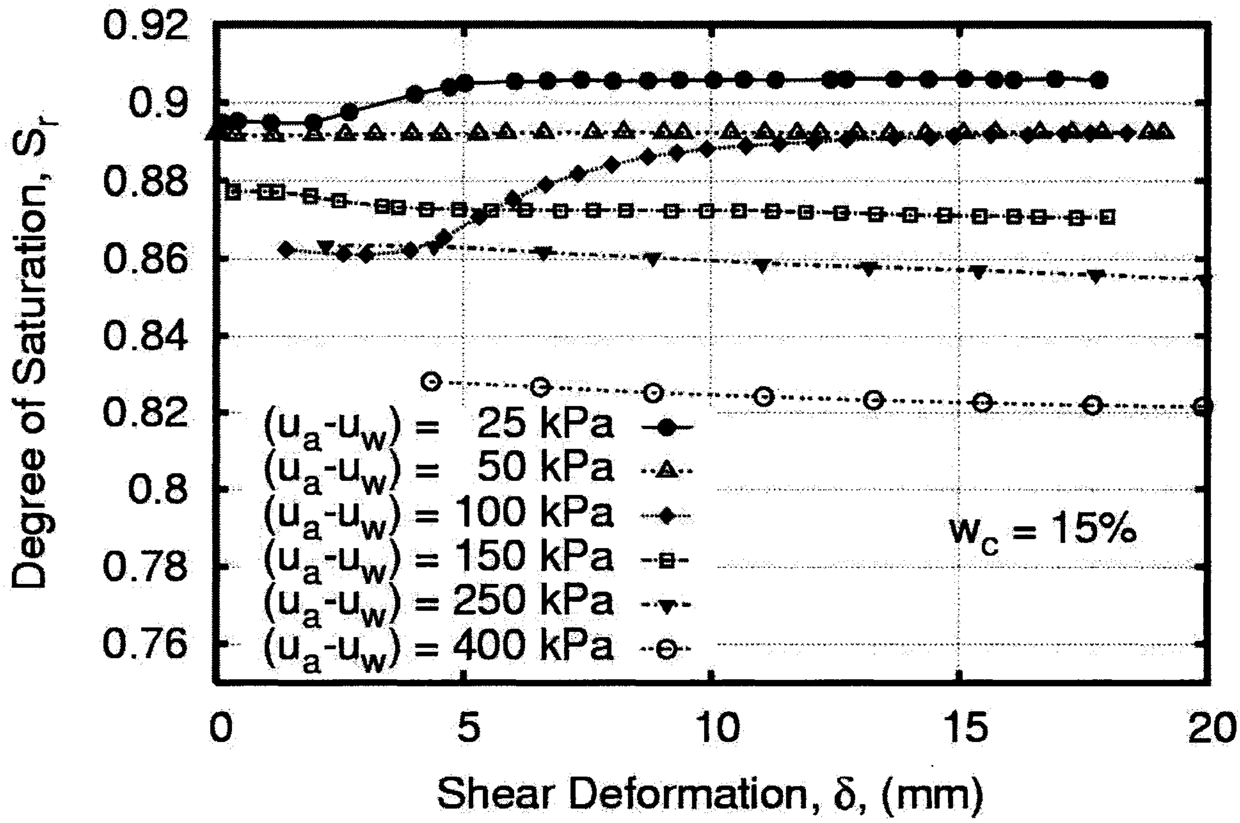

Figure 5.28 Variation of the degree of saturation, S, of a specimen, compacted at a water content, w_c, of 15%, during CLS shear at various matric suctions.

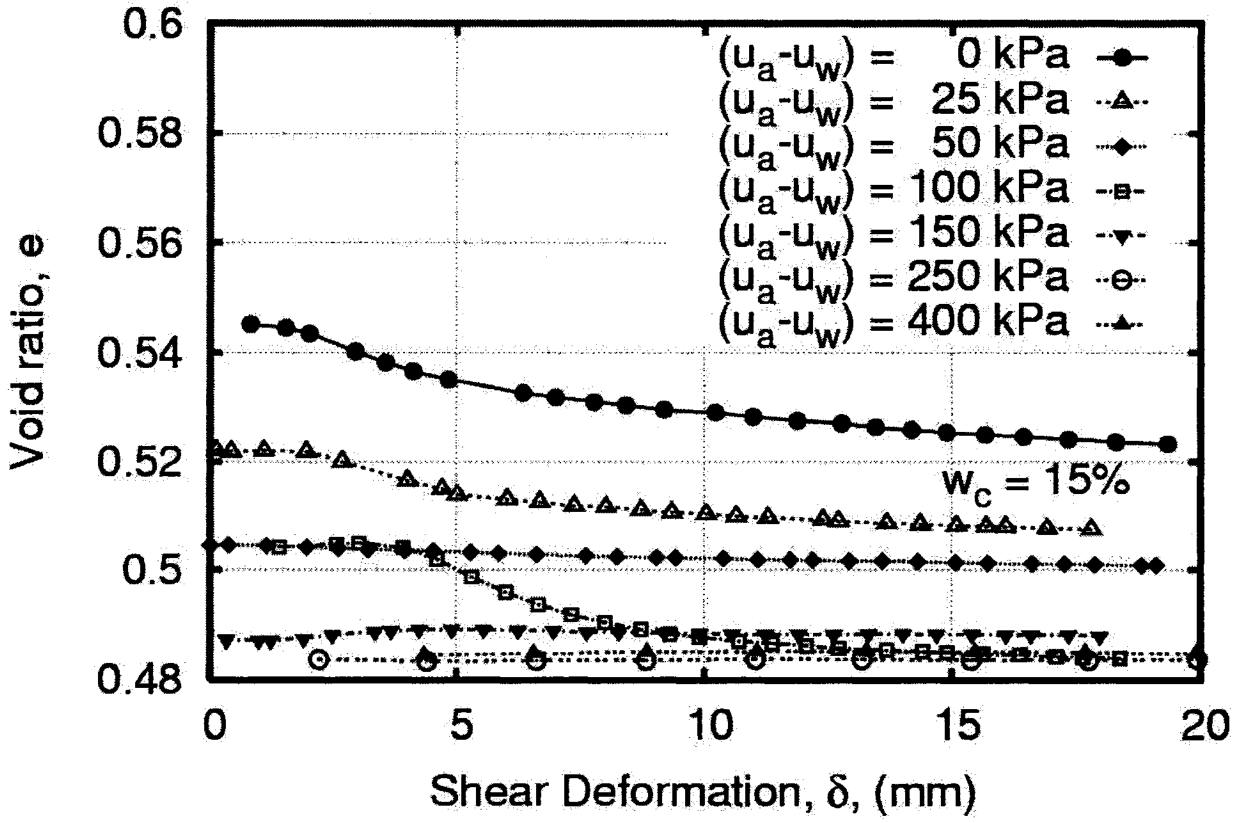

Figure 5.29 Variation of the void ratio for a specimen, compacted at a water content of 15%, and sheared under CLS conditions at a net normal stress of 150 kPa.

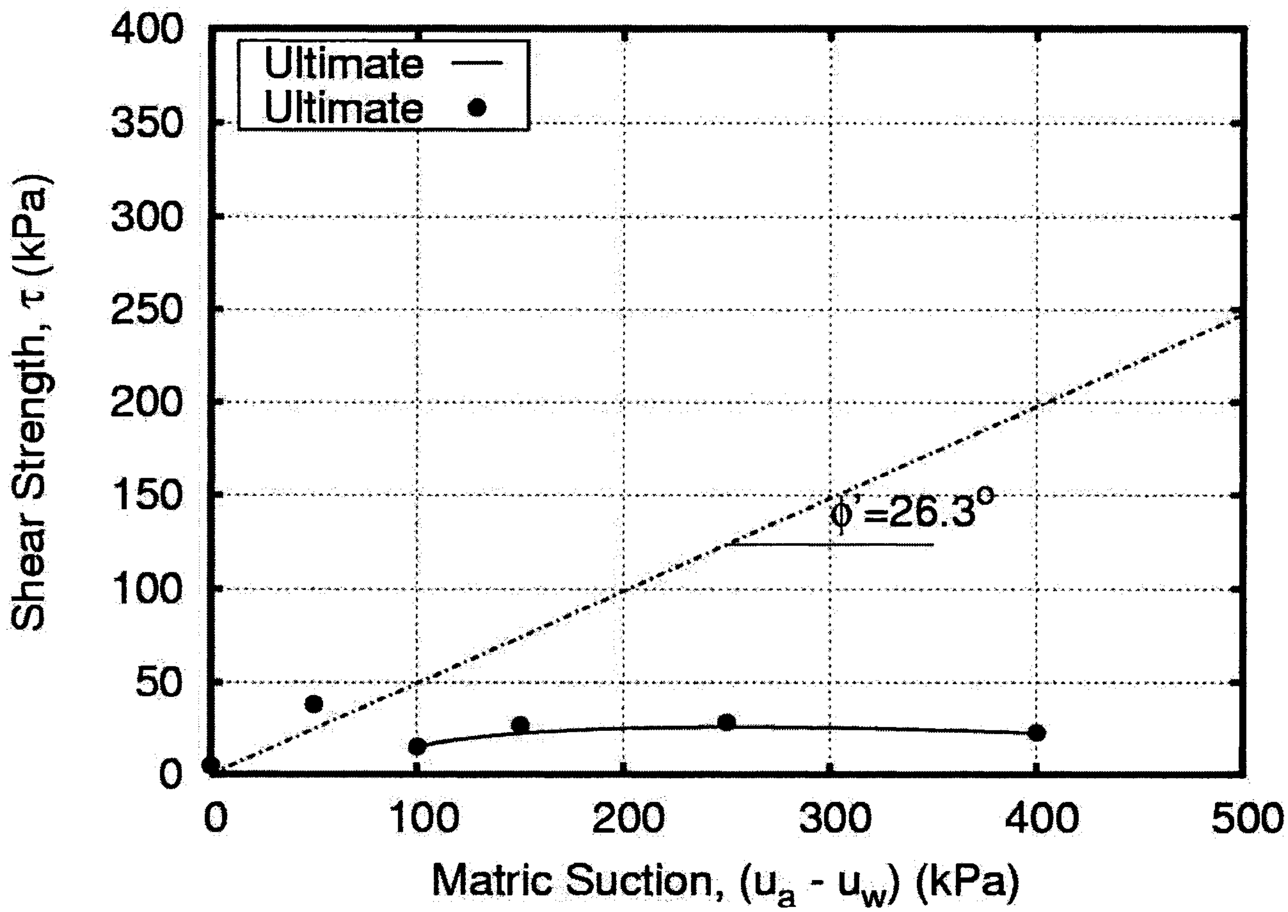

Figure 5.30 Failure envelope with respect to matric suction for specimens tested under CVS conditions. The compaction water content ,w_c,was 15%.

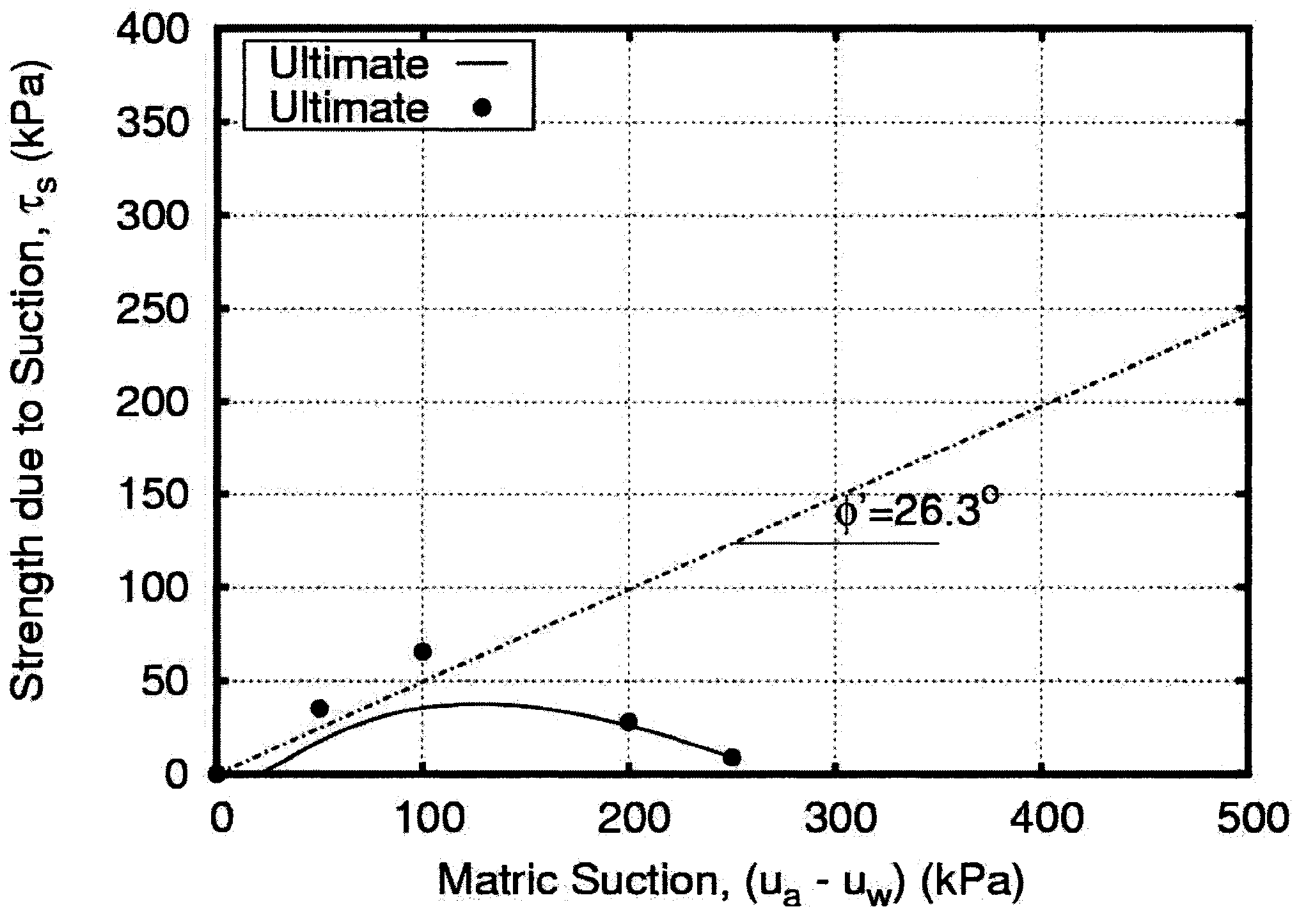

Figure 5.31 Failure envelopes for a specimen of Indian Head till tested under CVS conditions. The compaction water content, w_c, was 19%.

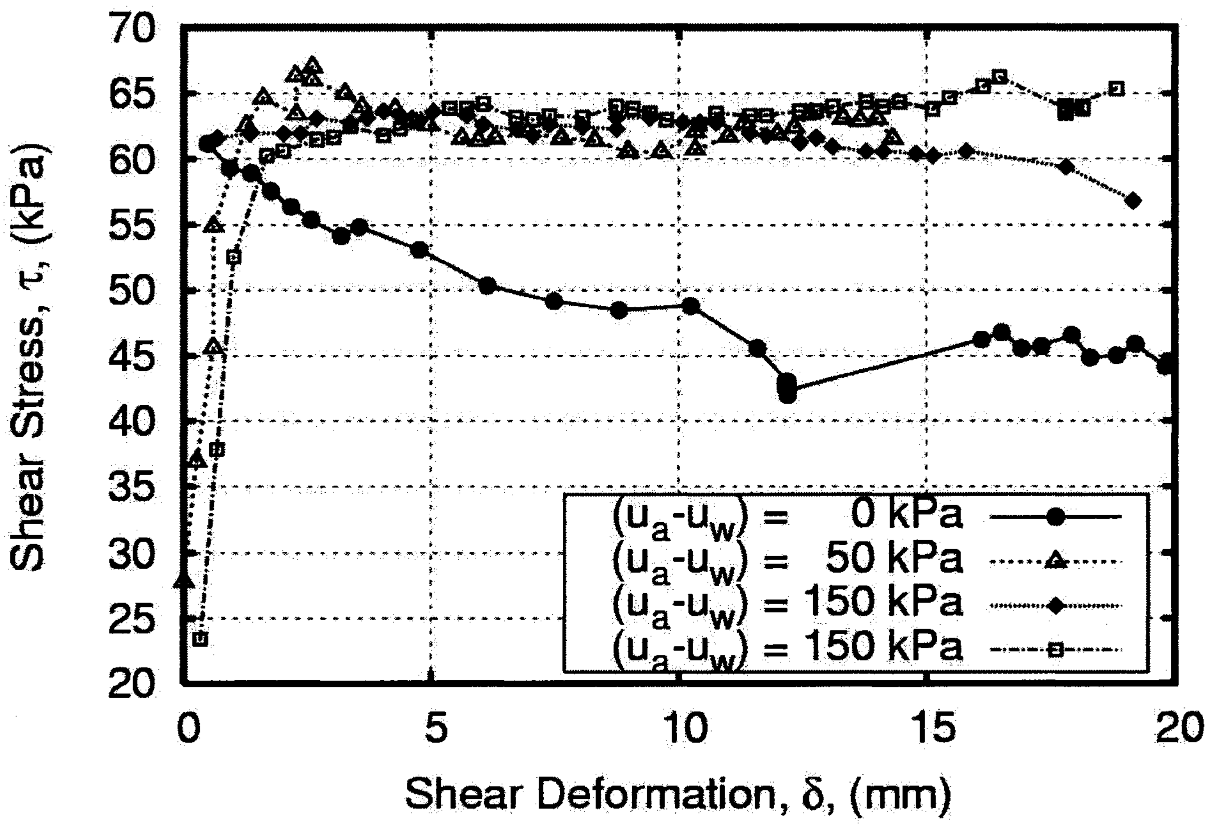

Figure 5.32 Stress-deformation curves for CVS shear tests on soils compacted at a water content, w_c, of 15%.

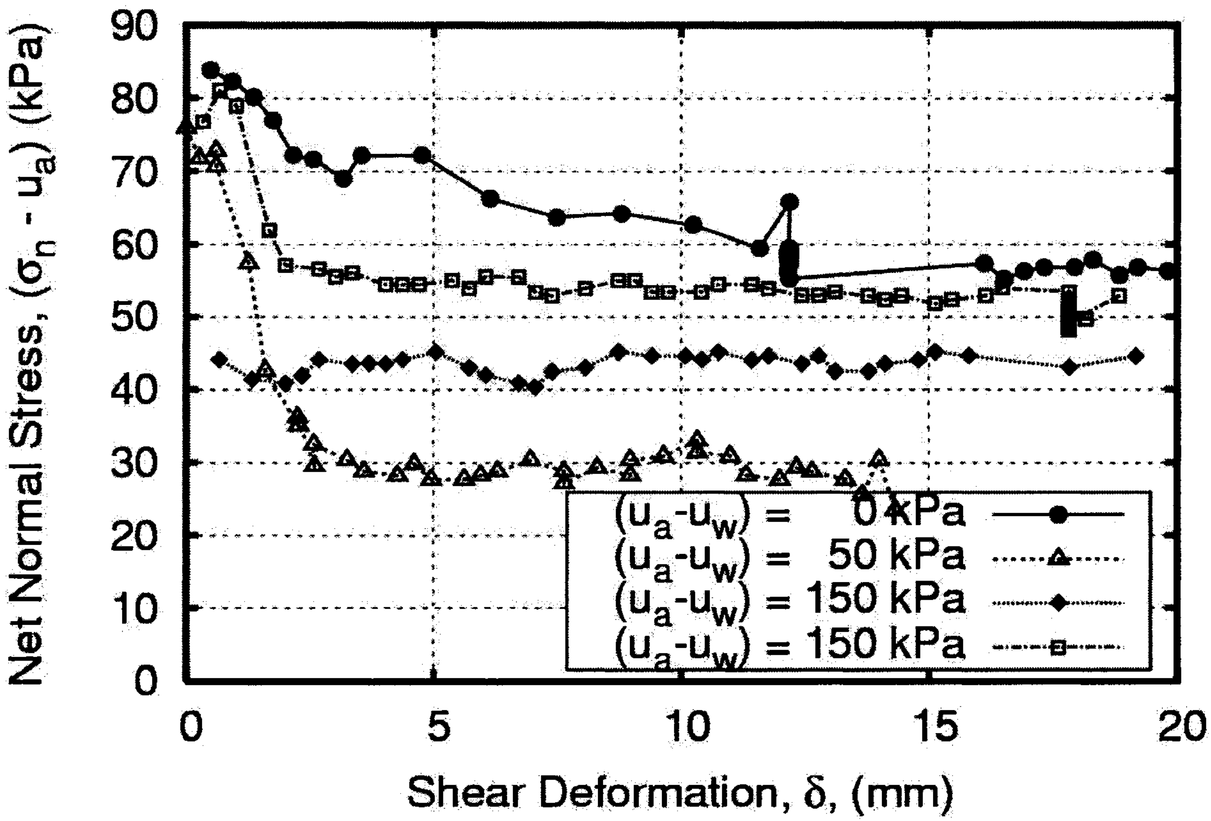

Figure 5.33 Variation of the normal stress during CVS tests.

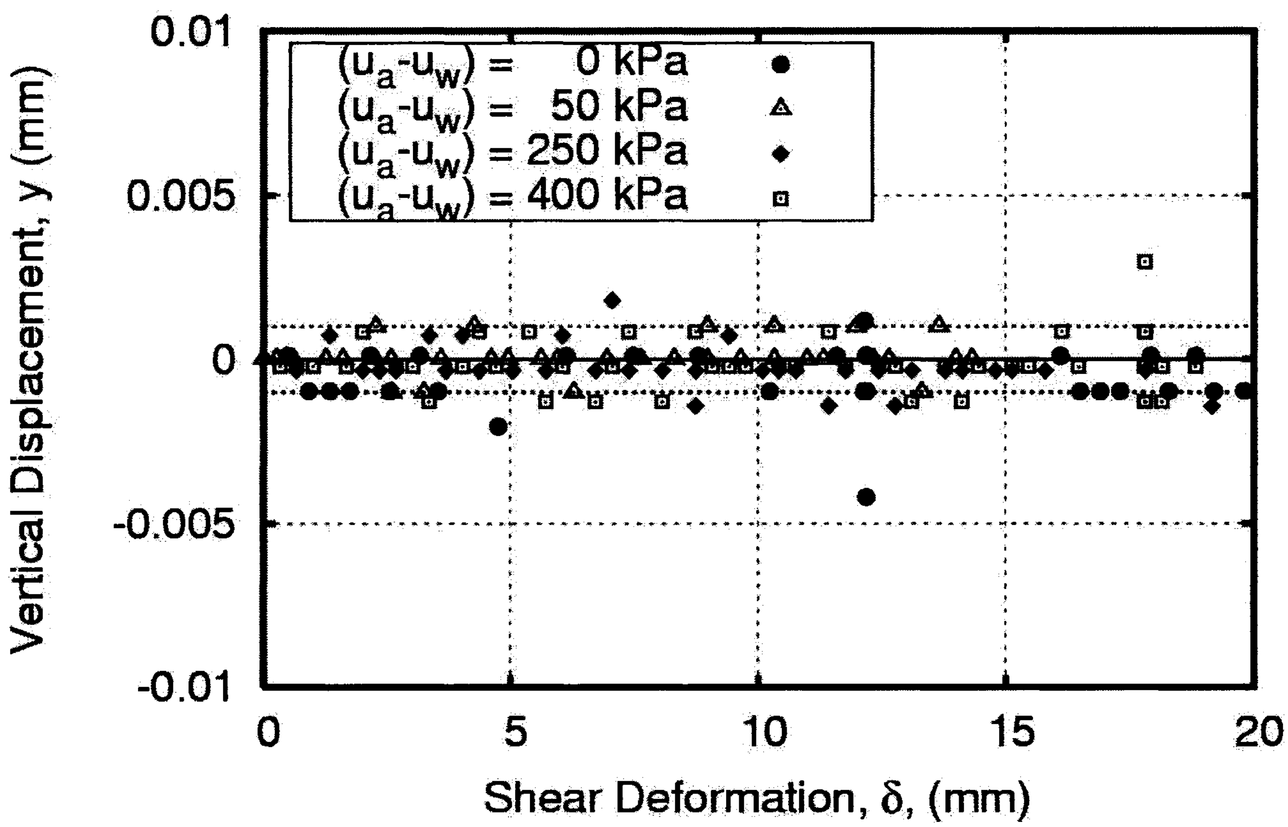

Figure 5.34 Vertical deformation plots for till compacted at a water content of 15%, and sheared at a constant normal stress of 150 kPa.

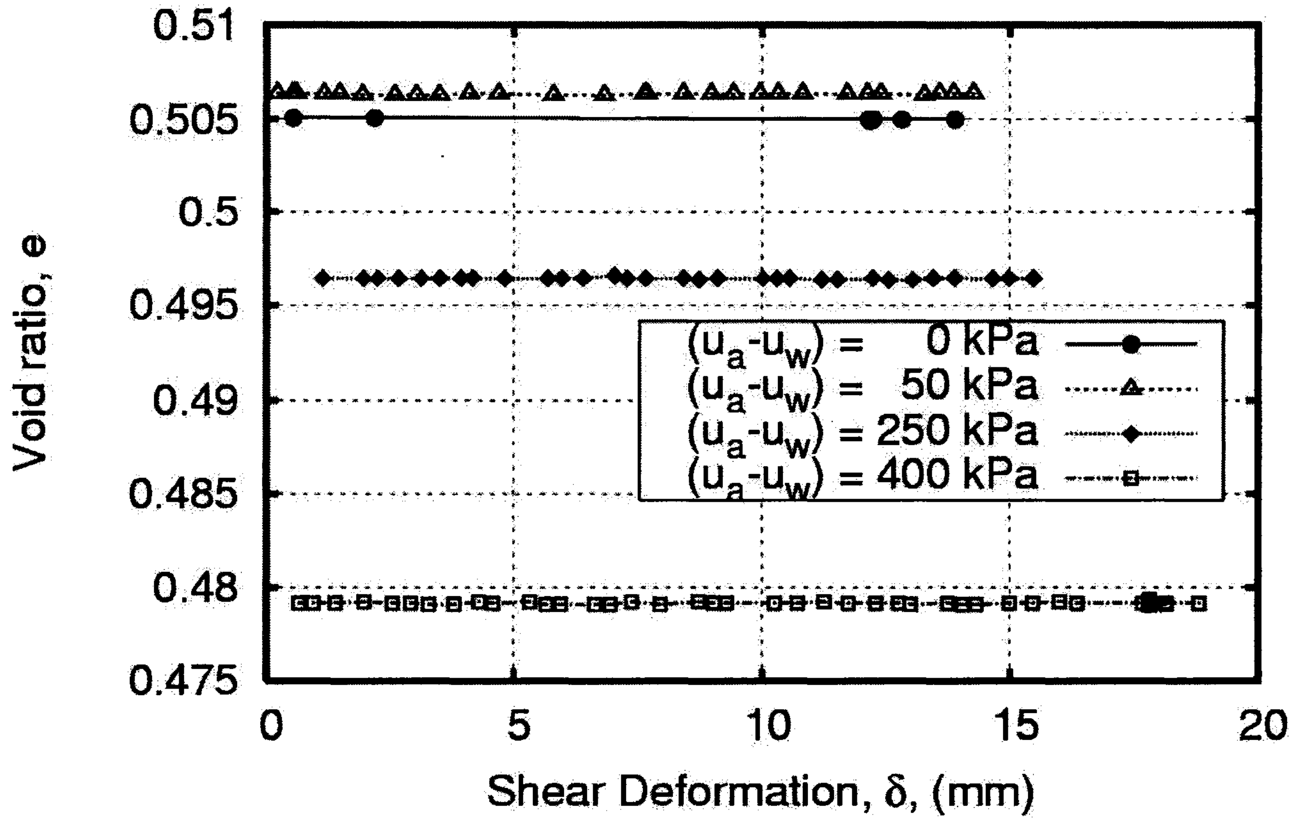

Figure 5.35 Void ratio during CVS shear for a specimen compacted at a water content, w_c, of 15%.

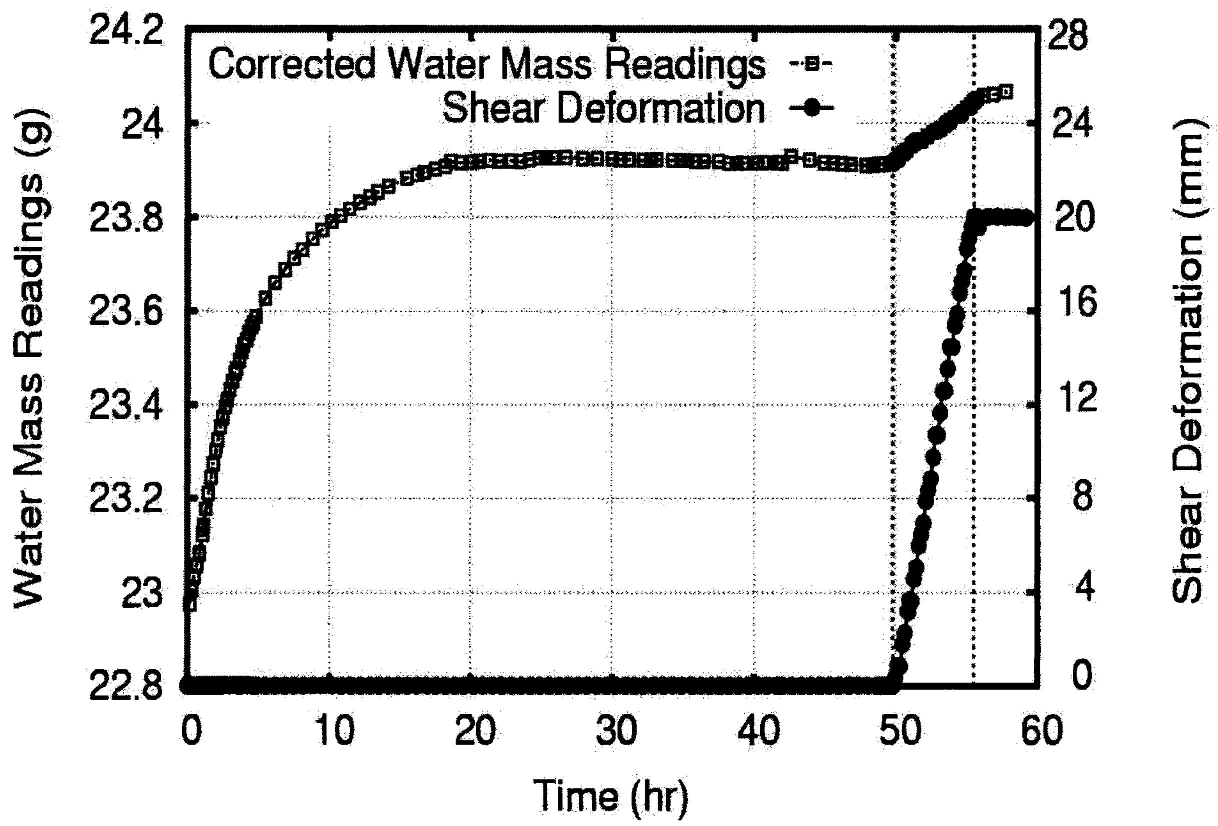

Figure 5.36 Water mass readings as a function of time for a CVS specimen compacted at a water content, w_c, of 15%, under a net normal load (σ-u_a) of 150 kPa, and a matric suction (u_a – u_w) of 50 kPa.

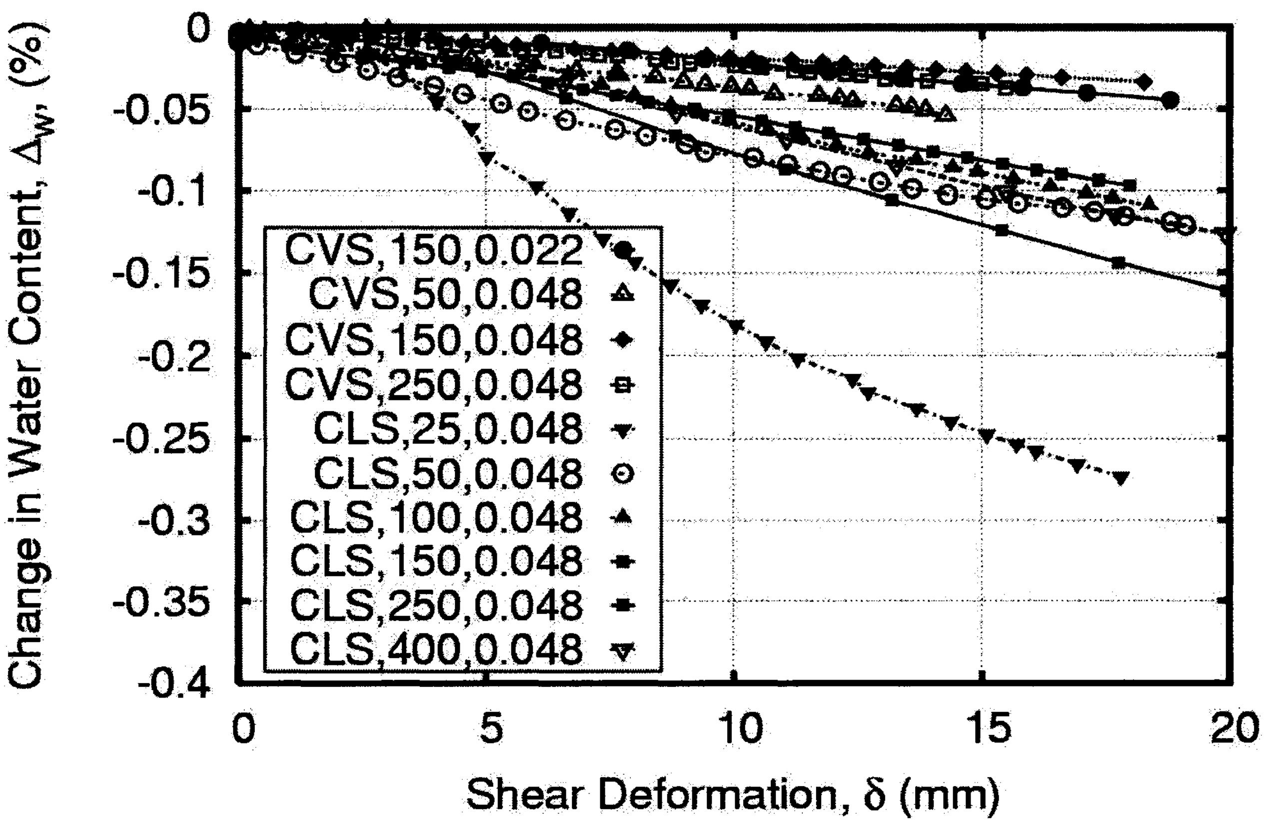

Figure 5.37 The change of water content for specimen compacted at a water content, wc, of 15%, including CVS (multi-stage and single stage)and CLS tests. The suction values range from 25 to 400 kPa, and the shear rate is either 0.022 mm/min or 0.048 mm/min.

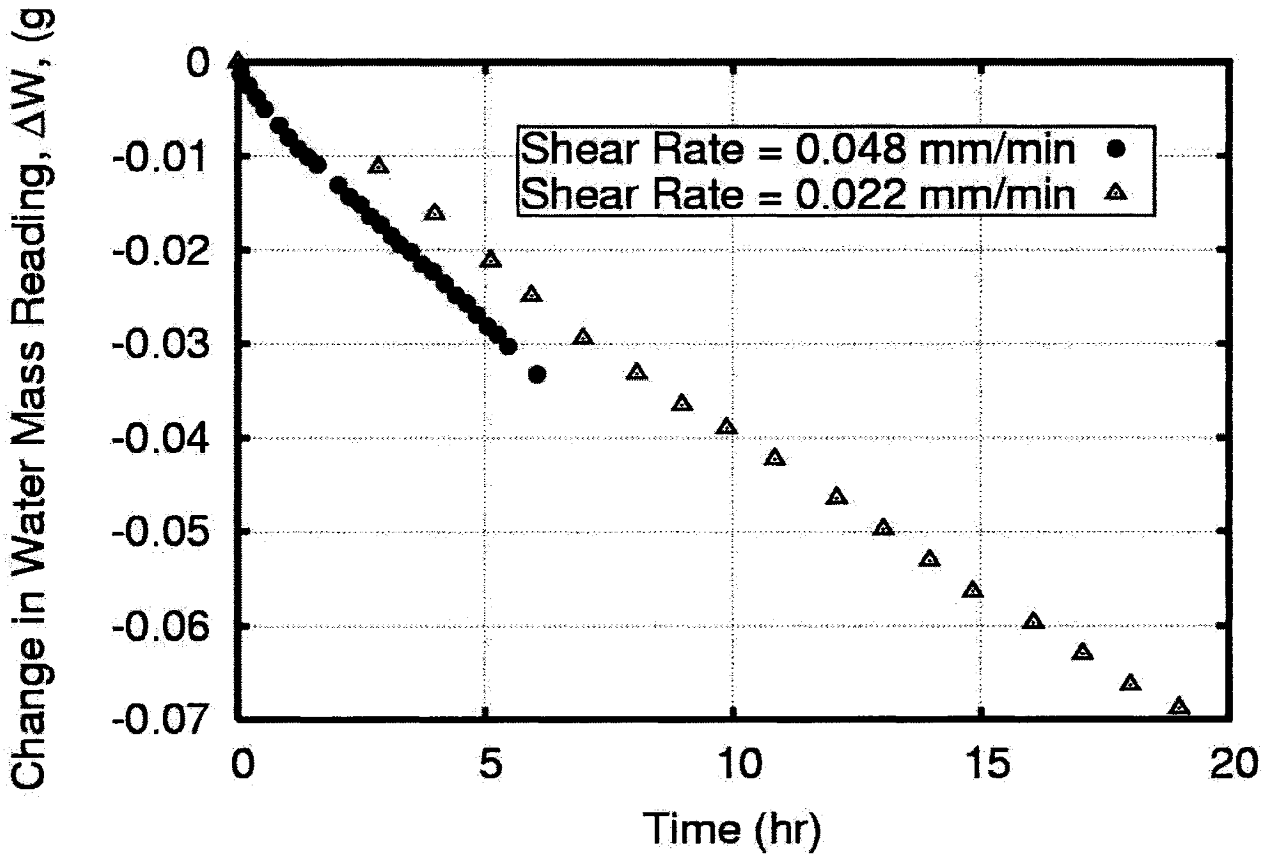

Figure 5.38 CVS tests on specimens tested at a matric suction, $(u_a - u_w)$, of 150 kPa.

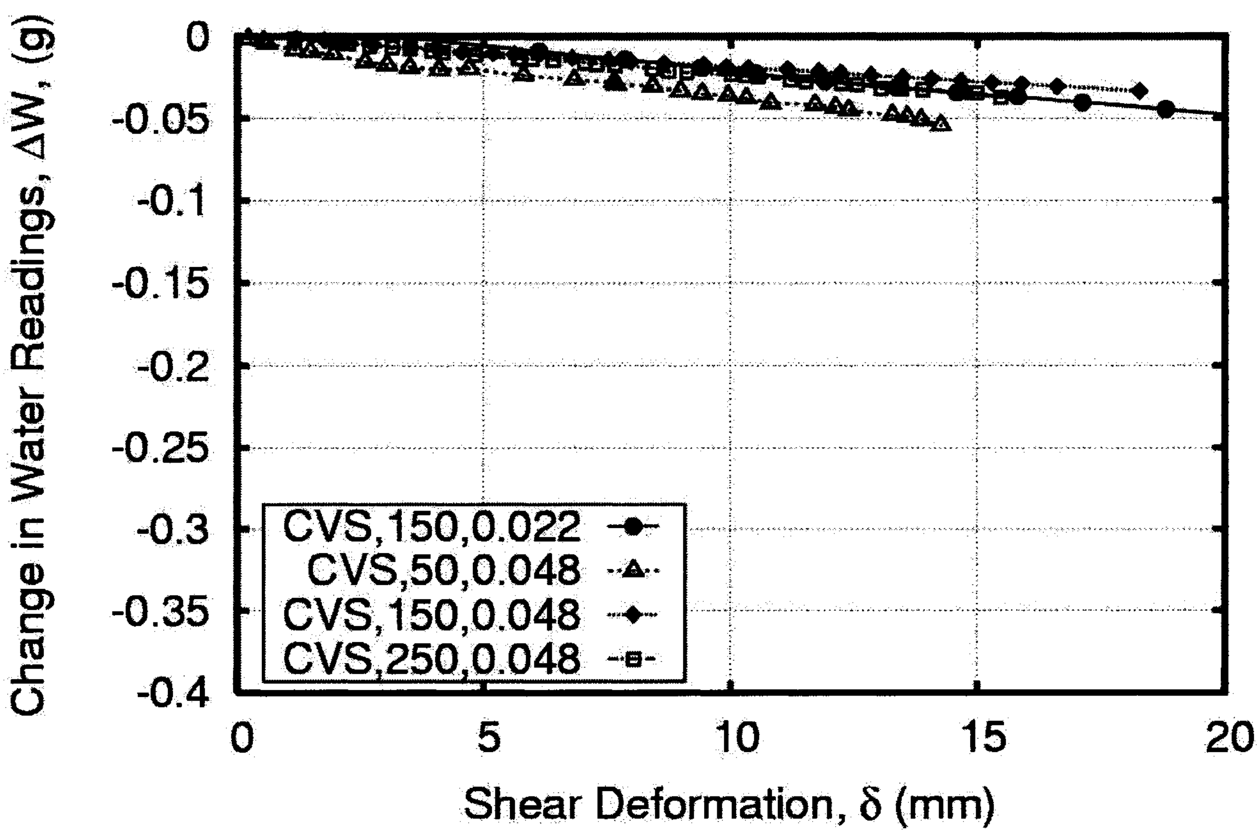

Figure 5.39 The change of water content for specimen compacted at a water content, wc, of 15%, during CVS tests. The suction values range from 25 to 400 kPa, and the shear rate is either 0.022 mm/min or 0.048 mm/min.

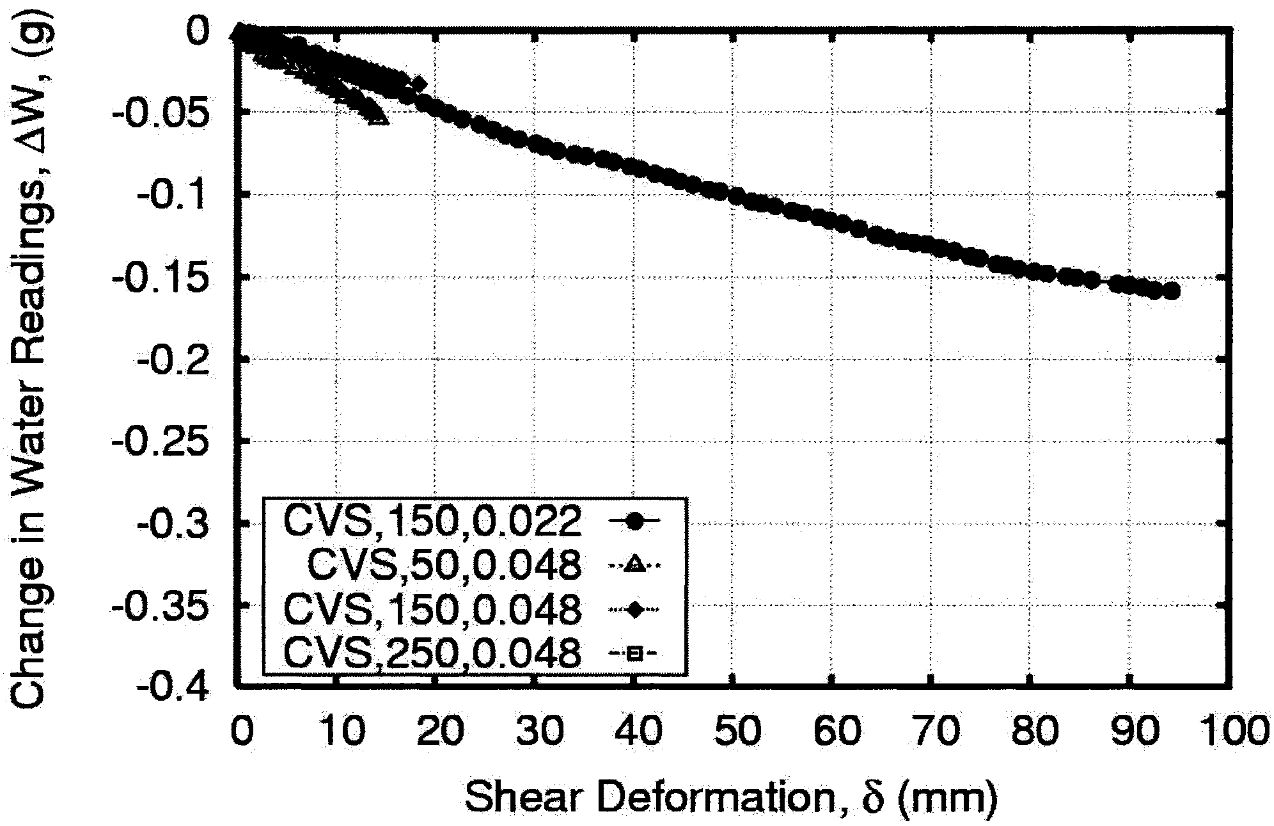

Figure 5.40 Comparison of the change in water content in CVS shear test for specimens compacted at a water content, w_c, of 15% and sheared to 20 mm, or 95 mm displacements.

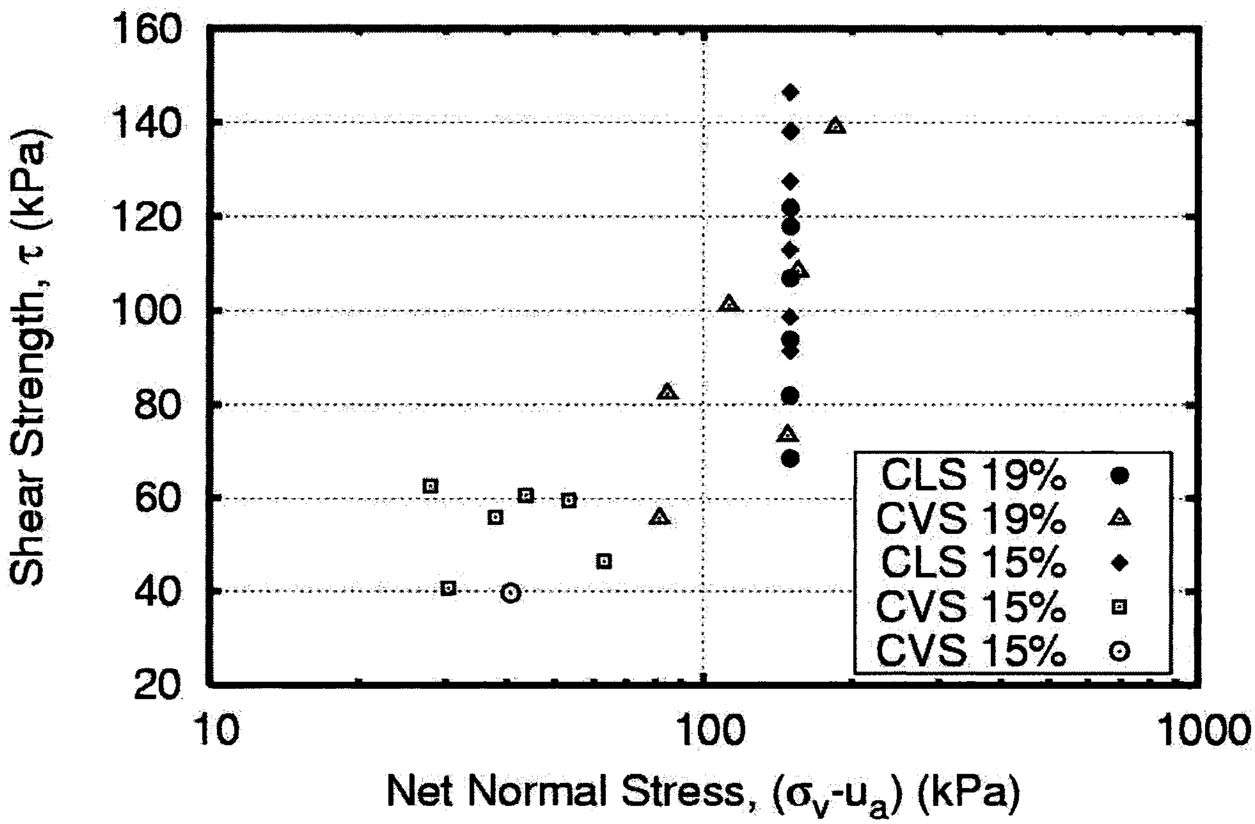

Figure 5.41 Shear strength versus net normal stress for ring shear tests on unsaturated Indian Head till.

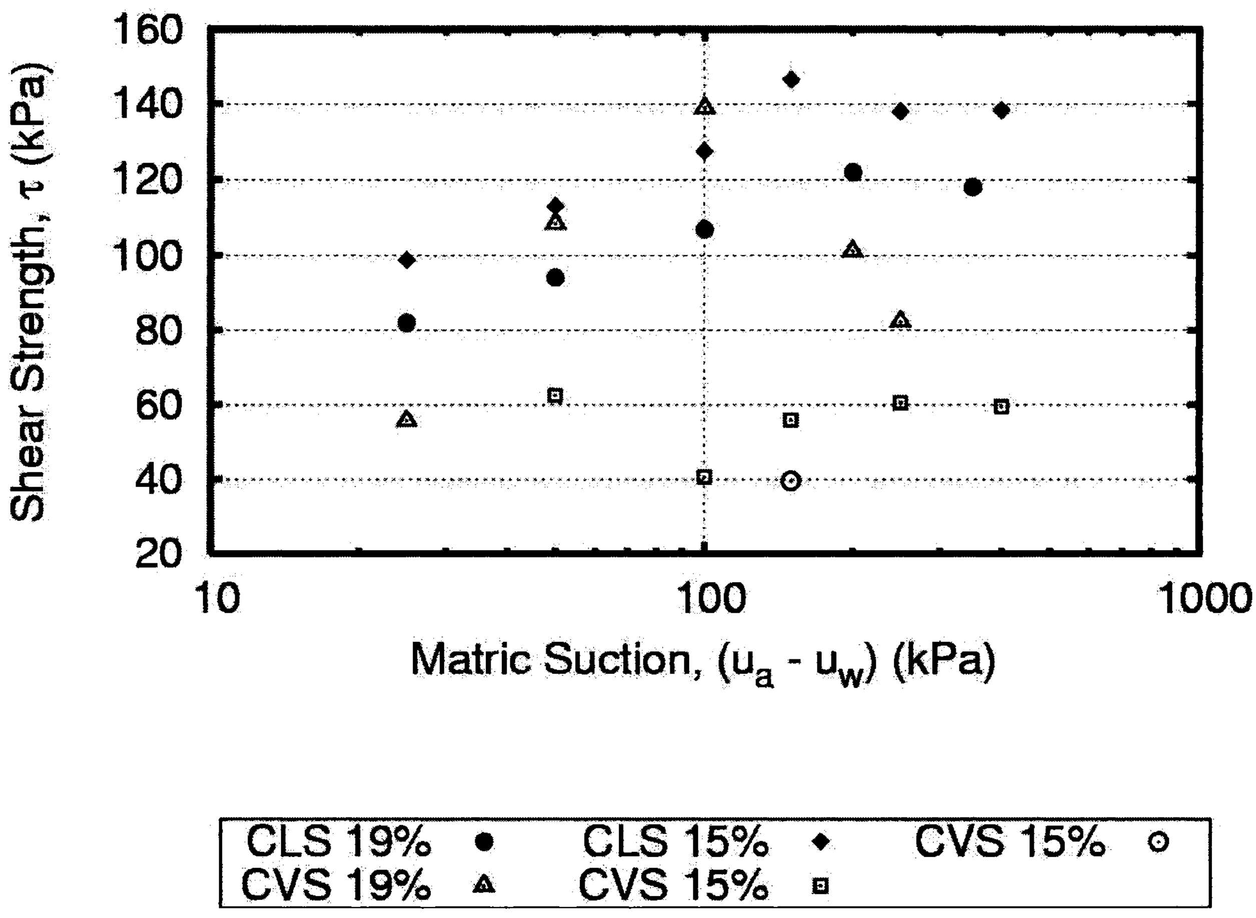

Figure 5.42 Shear strength versus matric suction for ring shear tests on unsaturated Indian Head till.

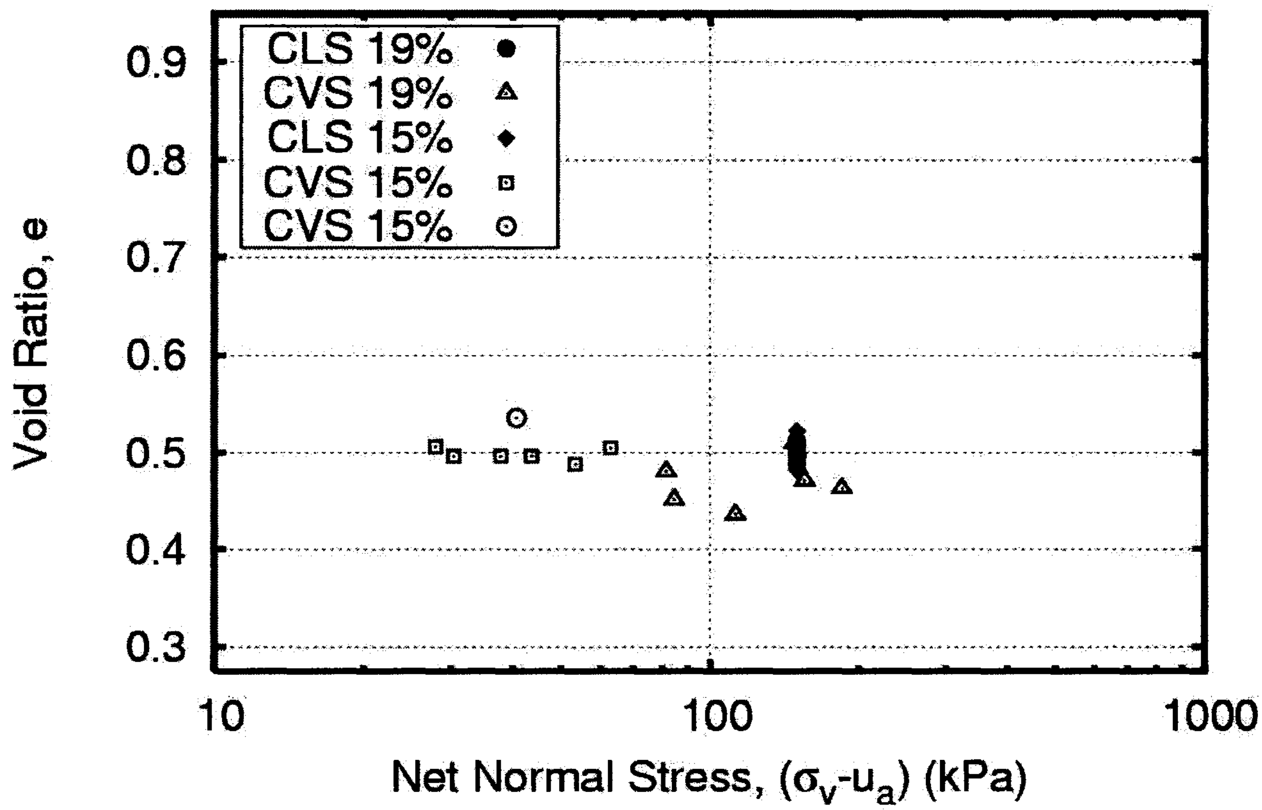

Figure 5.43 Relationship between the void ratio and the net normal stress at ultimate conditions from ring shear tests on unsaturated Indian Head till.

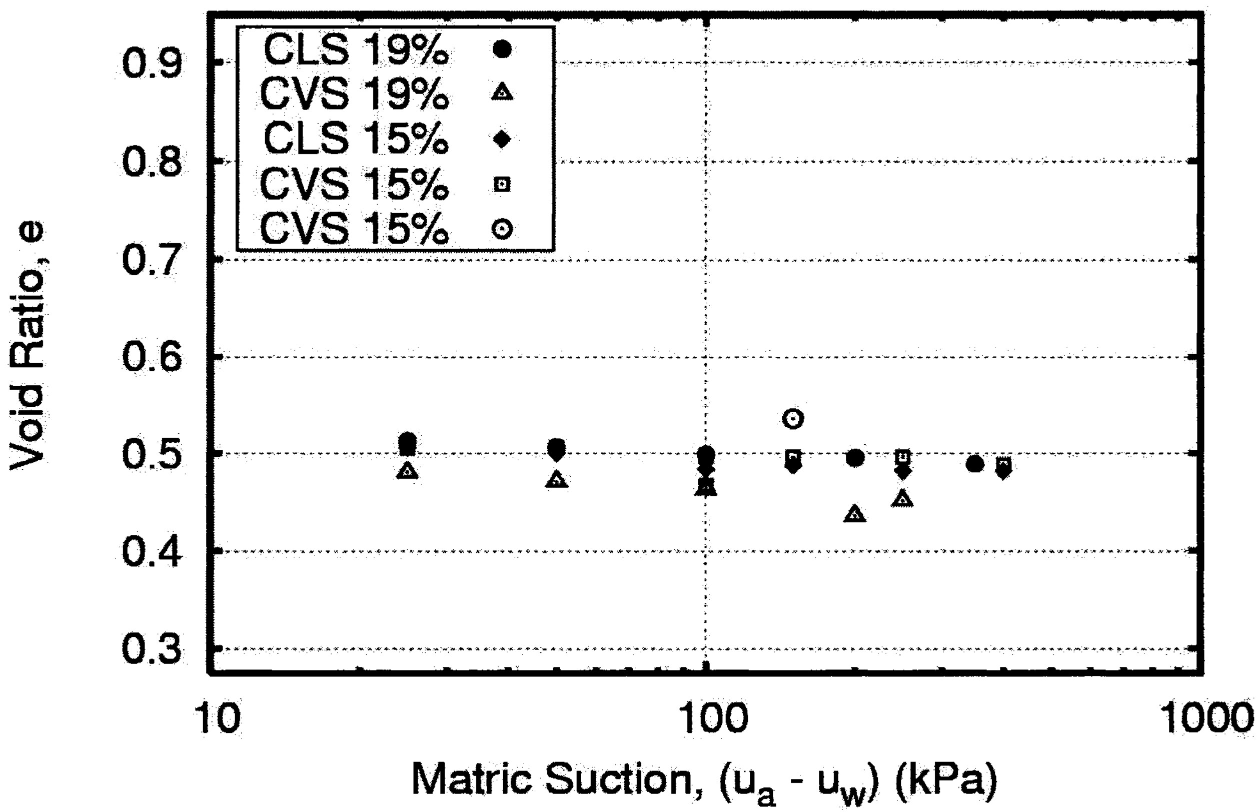

Figure 5.44 Relationship of the void ratio to the matric suction at ultimate state conditions for ring shear tests on unsaturated Indian Head till.

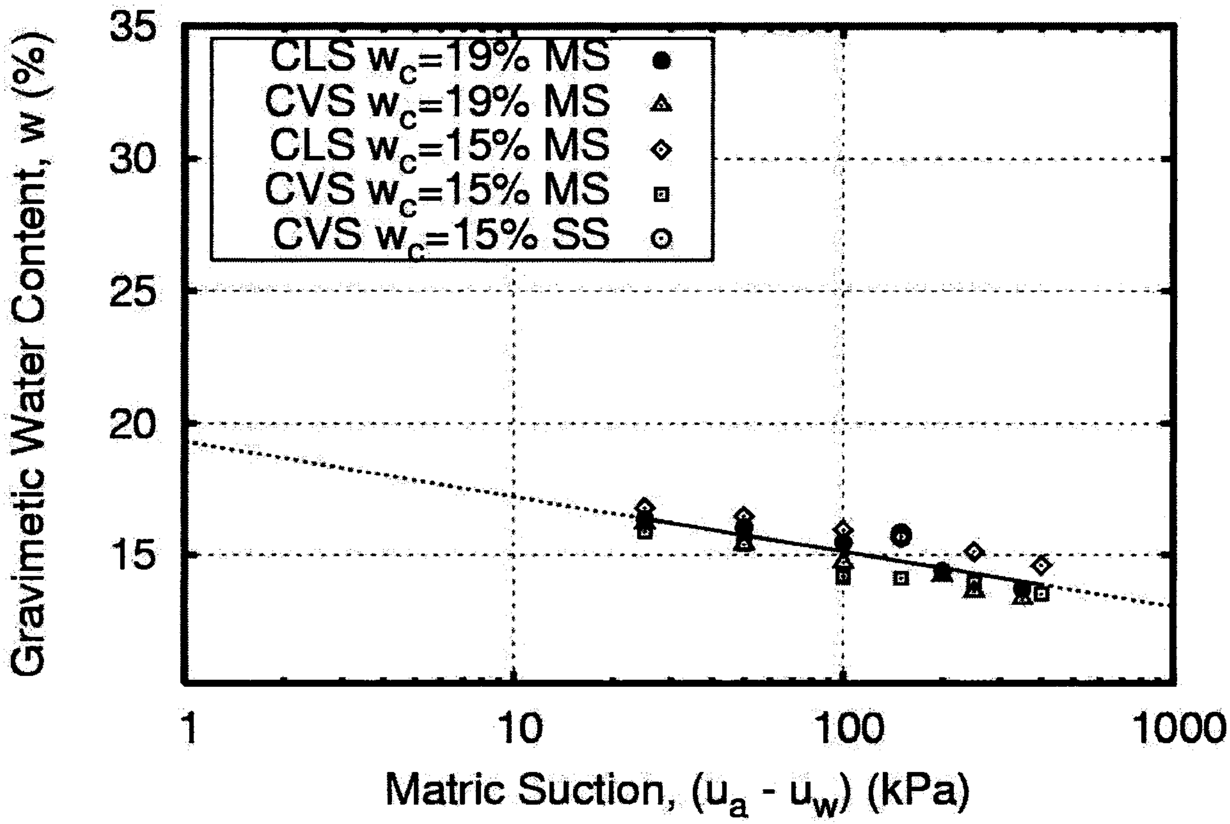

Figure 5.45 Critical state line (CSL) relating gravimetric water content, w, to matric suction, $(u_a\text{-}u_w)$, for Indian Head Till for single stage (SS) and multi-stage (MS) ring shear tests.

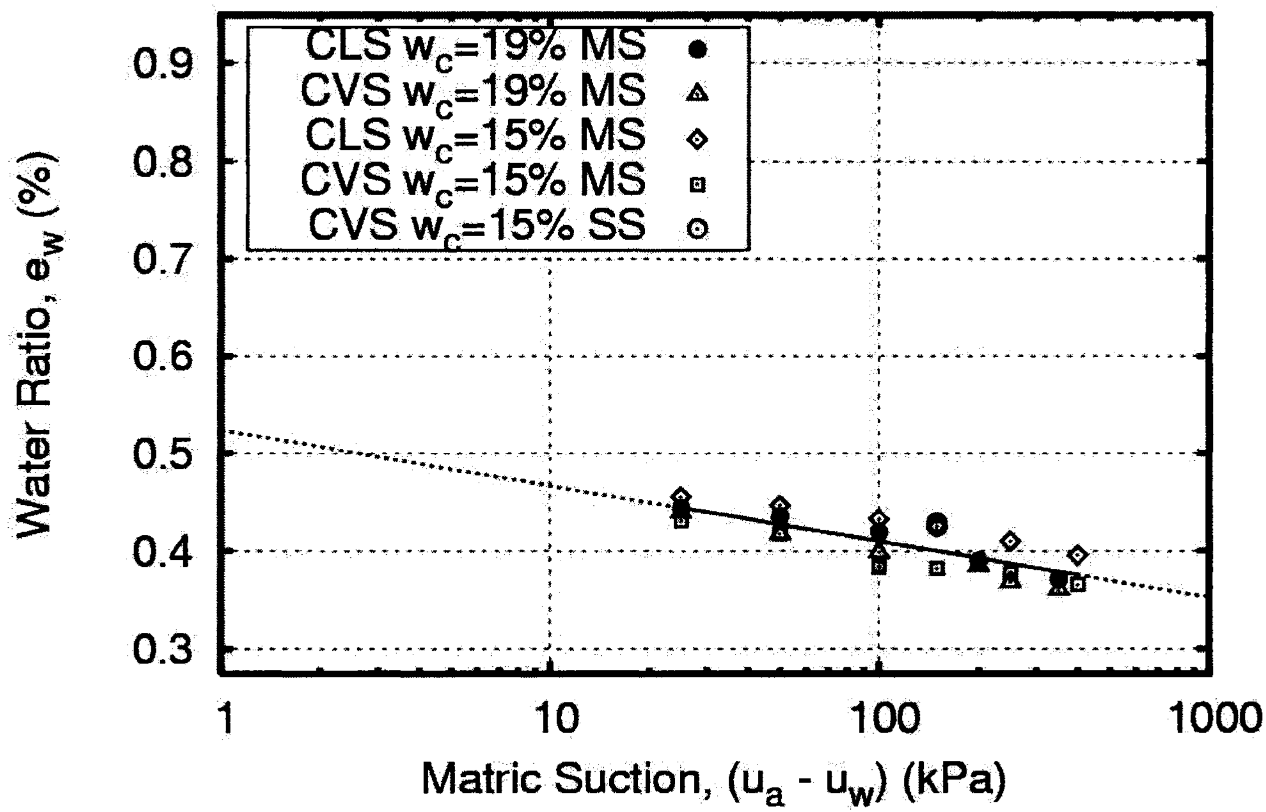

Figure 5.46 Critical state line (CSL) relating water ratio, e_w, to matric suction, $(u_a - u_w)$, for Indian Head Till for single stage (SS) and multi-stage (MS) ring shear tests.

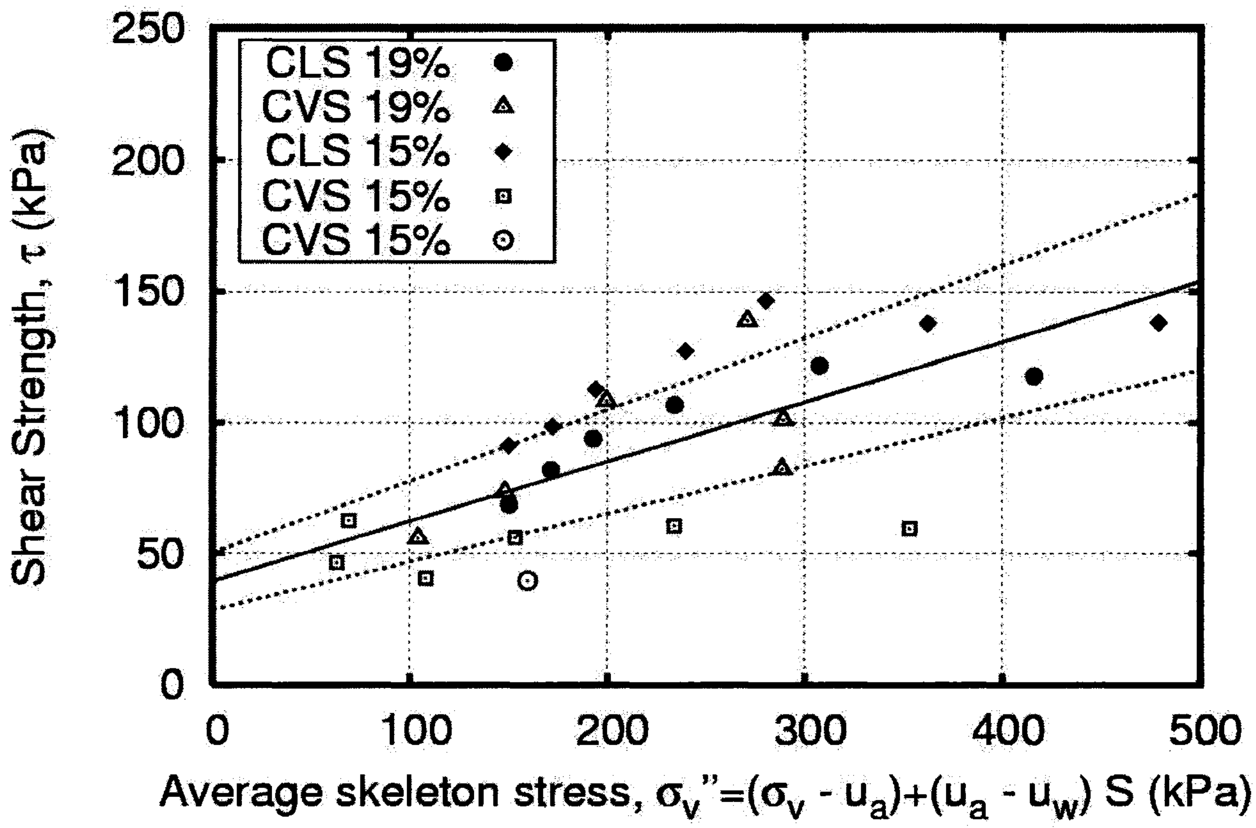

Figure 5.47 Shear strength of unsaturated Indian Head till plotted against an average skeleton stress defined in terms of the degree of saturation, S.

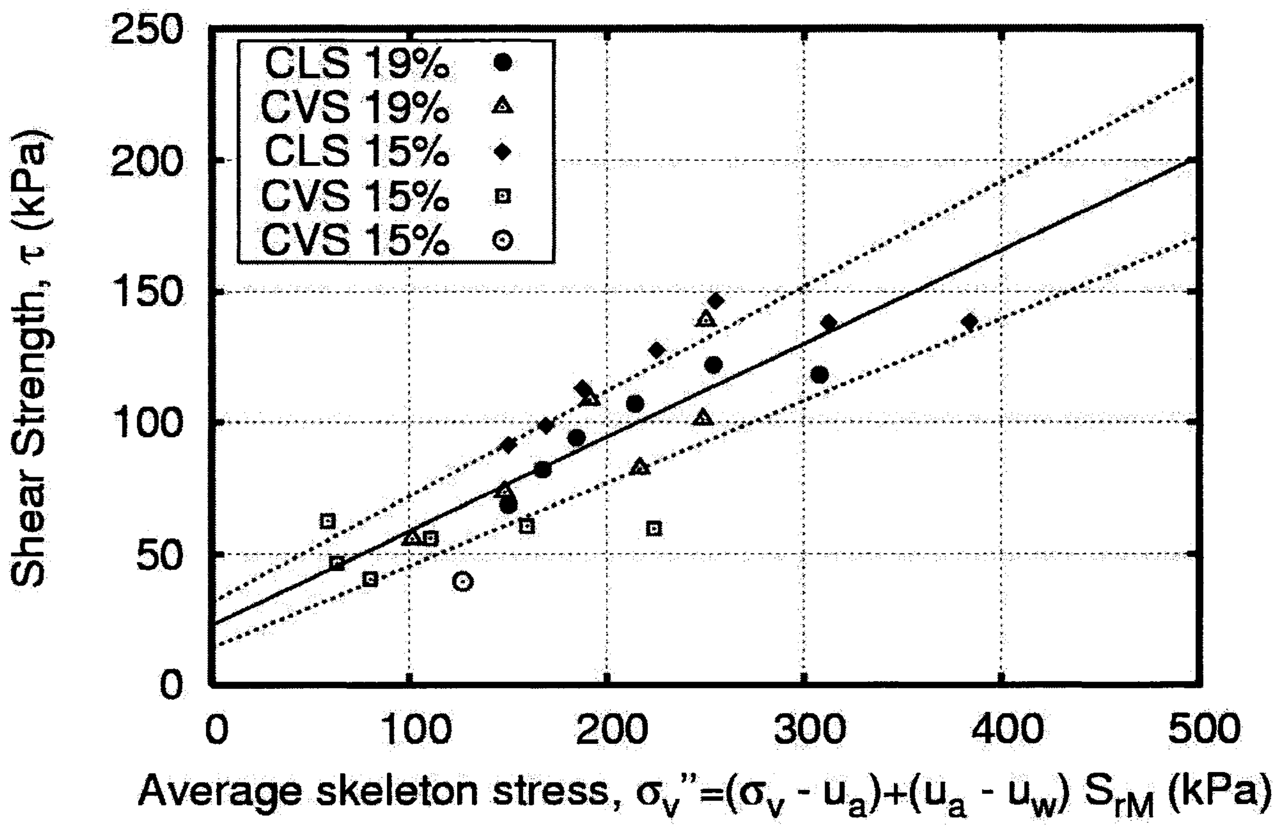

Figure 5.48 Shear strength of unsaturated Indian Head till plotted against an average skeleton stress defined in terms of the degree of saturation of the macro-voids, S_{rM}.

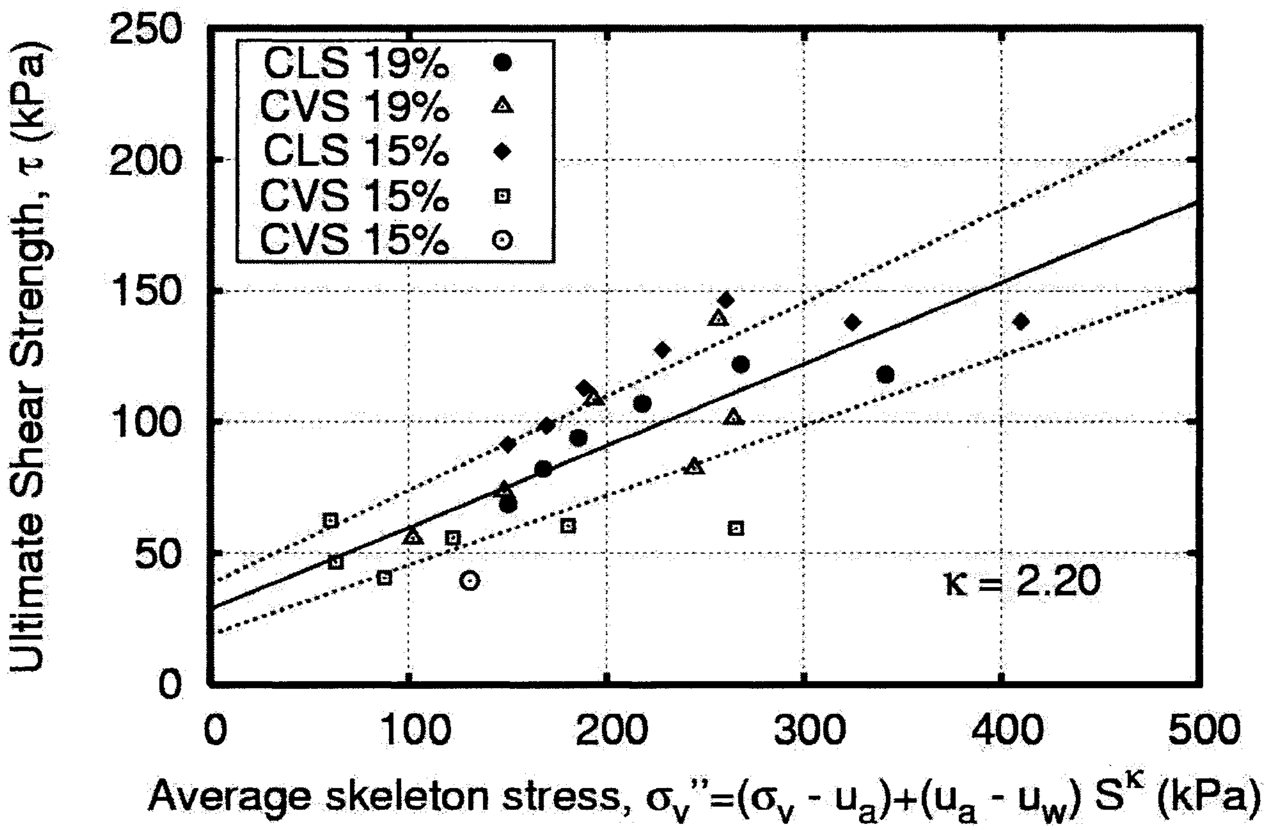

Figure 5.49 Ultimate shear strength of unsaturated Indian Head till plotted against an average skeleton stress defined in terms of the exponential degree of saturation, S^{k}. Fitting parameter, κ, is obtained from plasticity chart.

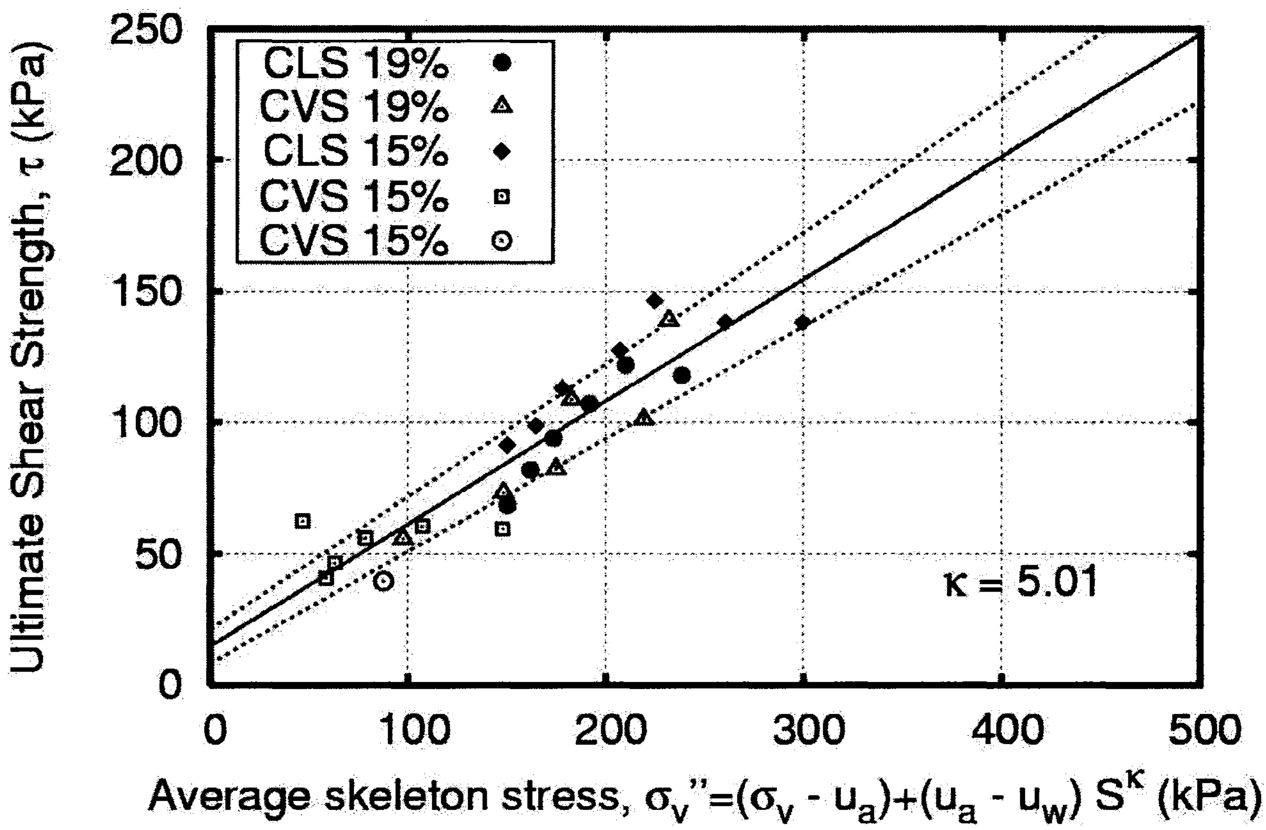

Figure 5.50 Ultimate shear strength of unsaturated Indian Head till plotted against an average skeleton stress defined in terms of the exponential degree of saturation, S^{κ}. Fitting parameter, κ, is back-calculated from ring shear test results.

6 SWRC and Shear Strength

6.1 Introduction

Shear strength and volume change form important engineering properties in the design of geotechnical and geo-environmental structures such as earth dams, retaining walls, pavements, soil liners, and soil covers. Many of these soil structures are typically in an unsaturated condition and often do not attain fully saturated conditions during their design life period. Thus, the mechanical behaviour (i.e., shear strength and volume change) of unsaturated soils is relevant in the design of several geotechnical and geo-environmental structures.

The shear strength of an unsaturated soil can be determined using modified direct shear or triaxial shear equipment. Experimental studies related to determination of the shear strength of unsaturated soils are time consuming and require extensive laboratory facilities [Escario (1980), Escario and Jucá (1989), Gan et al. (1988)]. In recent years, several semi-empirical procedures were proposed to predict the shear strength of unsaturated soils [Vanapalli et al. (1996), Fredlund et al. (1996), Khalili and Khabbaz (1998), Öberg and Sällfors (1997), Bao et al. (1998), Tekinsoy et al. (2004)]. The proposed prediction procedures use the effective shear strength parameters (c', ϕ') along with the SWRC data to predict the shear strength of unsaturated soils.

The SWRCs are conventionally measured using Tempe cell or the pressure plate apparatus on specimen sizes that are typically 50 mm in diameter and 20 mm in height. The volume change of the soil specimen is not commonly measured while determining the SWRCs. In several cases, the shear strength of an unsaturated soil is predicted using the SWRC measured without the application of any loading. In other words, the SWRC is measured without taking into account the influence of loading and the resulting volume change. The volume change with respect to soil suction is also ignored assuming it to be relatively small. From a practical perspective, the soil will be subjected to some loading and there will be volume change both during the loading and as well as the shearing stage. None of the procedures available in the literature have addressed the influence of volume change behaviour on the prediction of the shear strength of unsaturated soils.

In this chapter, the influence of the shearing process on the shear strength will be investigated using test data on two soils; soil test results obtained from the current study, as well as the data from test results on Dhanauri clay presented by Satija (1978). The analysis presented in this chapter provides new insight into the effect of shearing on the coupling of the hydro-mechanical properties of a soil.

6.2 Dhanauri Clay

Dhanauri clay is a naturally occurring transported soil from the banks of the Dhanauri River situated about 7 km from Roorkee (U.P.), in India. The soil contains 5% sand, 70% silt and 25% clay size particles. The plasticity index, I_p, of the soil is 23.5%. The soil can be classified as silty clay with medium to high plasticity. The effective shear strength parameters of statically compacted soil at an initial density of 15.9 kN/m³ are: c' =37.3 kPa and ϕ' = 28.5°.

The experimental program was undertaken using a standard triaxial shear strength testing equipment in which a high air-entry disk was used to allow water, but not air, to circulate at the base of the specimen. The air pressure was applied at the top of the specimen through a coarse porous stone. Two fabric discs, with excellent water repellent properties, but highly pervious to air were used to ensure that no upwards migration of water from the specimen would take place [Satija (1978)]. A desired value of matric suction was achieved in the initially saturated soil specimens of the triaxial shear equipment using the axis translation technique.

The triaxial cell was pre-calibrated in order to determine the magnitude of the cell expansion and creep characteristics when subjected to different levels of loading. Preliminary tests showed the necessity to reinforce the cell circumferentially by pressure-wrapping a permanent glue coated wick cloth at three locations along the height of the cell [Satija (1978)]. Volume measuring devices were used to monitor the volume of water entering and leaving the specimen from the triaxial cell with a precision of 0.05 cc. This information was useful in the calculation of the water content, w and the degree of saturation, S of the specimen both prior to determining the shear strength and at failure conditions of the test.

In the *first approach* the shear strength prediction is based on the information of the effective shear strength parameters (c', ϕ') and the SWRC. The information related to the soil-water retention (i.e., water content versus matric suction) data comes from different triaxial tests that were tested under a common confining stress condition but subjected to desaturation by applying different values of suction to the soil specimens. All the specimens satisfy the criteria of "identical" specimens (i.e., the initial density and compaction water content are the same for all the specimens). The SWRC derived as detailed in this *first approach* is referred as the pre-shear SWRC in the remainder of the chapter. This procedure is different from the conventional technique of the measurement of SWRC using a single specimen in Tempe cell or pressure plate apparatus, and is thus more uncertain.

In the *second approach*, the SWRC information is derived from shear strength data of triaxial tests at failure conditions. In other words, in this approach, the derived SWRC information from the shear strength test data takes account influence of volume change of the soil due to loading and shearing. The SWRC derived as explained in this *second approach* in this section is referred as the post-shear SWRC in the remainder of the chapter.

Comparisons are provided between the above two described approaches using the semi-empirical prediction equation proposed by Vanapalli et al. (1996).

$$\tau = c' + (\sigma_n - u_a)\cdot\tan\phi' + (u_a - u_w)\cdot\left(\Theta^{\kappa}\right)(\tan\phi') \qquad [6.1]$$

where:

c' = effective cohesion

ϕ' = internal effective friction angle

σ_n = total normal stress

u_a = pore air pressure

u_w = pore water pressure

Θ = normalized water content (i.e. degree of saturation)

κ = a fitting parameter

For the purpose of analysis, comparisons will be provided between the measured and predicted values of the component of shear strength contribution due to matric suction. Only the second part of the equation, shown in Equation [6.2] is required for predicting the shear strength contribution due to matric suction:

$$\tau_{suctin}=(u_a-u_w)\cdot(\Theta^{\kappa})(\tan\phi') \qquad [6.2]$$

Since the data presented by Satija was generated from triaxial tests with controlled confining pressure, σ_3, only the suction contribution to matric suction could be used to produce a failure envelope due to matric suction. This is because in such tests the stress path is not orthogonal to the plane defined by the shear stress, τ, and net normal stress, $(\sigma_v - u_a)$ variables. Such a stress path would therefore intersect several net normal stress values. The suction contribution from matric suction must therefore be isolated in such cases for appropriate comparisons. See Appendix C for a detailed explanation.

The experimental setup facilitated to control matric suction, $(u_a - u_w)$ in the soil specimen at all stages of testing. Since the information of both matric suction, $(u_a - u_w)$ and degree of saturation, S both at pre-shear and at failure conditions (i.e., post-shear) was available, the SWRC information related to pre-shear and post-shear conditions were derived as detailed earlier. This information was useful to study the influence of volume change behaviour on the prediction of the shear strength of the tested Dhanauri clay.

The plasticity index, I_p of the tested soil, Dhanauri clay was equal to 23.5% and therefore, a κ parameter of 2.48 was used from the κ versus plasticity index, I_p relationship [Vanapalli and Fredlund, (2000)] (Figure 6.1) for predicting the shear strength contribution with respect to matric suction using Equation [6.2]. The same value of κ was used for predicting the shear strength using both pre-shear and post-shear SWRCs.

The properties of Dhanauri clay are summarized as follows:

Plasticity index, I_p	23.5%
Fitting parameter, κ	2.48
Effective friction angle, ϕ'	28.5°
Cohesion , c'	37.3 kPa

Figure 6.2 shows the derived SWRCs for the pre-shear and post-shear (i.e., at failure) conditions. Figure 6.3 shows the variation of the predicted shear strength with respect to matric suction using Equation [6.2]. The measured shear strength values are shown as symbols in Figure 6.3, while the predicted values are shown as continuous curves. There is a reasonable agreement between the measured and predicted values of shear strength for the low matric suction range using both the pre-shear and post-shear SWRCs. However, the predicted values begin to diverge at higher values of matric suction. The curvature of the predicted shear strength function using the post-shear SWRC appears to follow more closely the apparent curvature of the measured shear strength values. This behaviour suggests that the influence of volume change characteristics on the prediction of shear strength may be negligible in the range of suction values tested (i.e., 0 to 400 kPa). Significant differences can be observed in predicted shear strength values when a large suction range (i.e., 0 to 1,500 kPa) is considered using both the approaches (Figure 6.4).

Figure 6.5 shows the derived pre-shear and post-shear SWRC data for Dhanauri clay tested under a net confining pressure of 386 kPa. The predicted and measured values of shear strengths are shown in Figure 6.6 (in the range of 0 to 500 kPa) and in Figure 6.7 (in the range of 0 to 1,500 kPa). Similar to the observations made for Figure 6.3, there is, globally, a reasonably good comparison in the lower suction range, although one point at a matric suction of 50 kPa lies markedly away from both prediction curves. In the absence of more data in the viccinity of a matric suction of 50 kPa, the nature of the outlying point cannot be determined. However, significant differences can be observed between the predicted shear strength values using the pre-shear and post-shear SWRC. As the experimental results are not available for the high suction range (i.e., greater than 400 kPa), it is difficult to comment on the relative accuracy of the predicted shear strength behaviour in the high suction range. The extrapolation of the variation of the shear strength with respect to matric suction was done to illustrate how the variations between the pre-shear and post shear SWRC ultimately affect the prediction results.

The analysis of shear strength undertaken on Dhanauri compacted clay suggests that the SWRC determined at a density and compaction water content consistent with the soil's original pre-shear condition may not be representative of the soil-water retentions once it is subjected to loading and shearing.

The degree of saturation of post-shear SWRC is higher in the suction range of 0 to 200 kPa. This behaviour suggests that the specimens consolidated (i.e., volume decrease) during the shearing stage. However, when the specimens were subjected to shearing at higher suction values, the soil specimens exhibit relatively higher desaturation characteristics. This behaviour can be attributed to dilation (i.e., volume increase) of the specimen during the shearing stage which suggests that at higher matric suctions the specimen behave as an over consolidated soil. This is consistent with the observations of Chapter 5 on the results from Indian Head till. Due to this reason, the shear strength prediction using the post-shear SWRC is slightly higher in comparison to shear strength prediction using the pre-shear SWRC the low suction range. However, in the high suction range, typically pre-shear SWRC predict higher shear strength values.

6.3 Indian Head Till

Shear strength results obtained from modified ring shear tests on an unsaturated glacial till are presented and analysed using Equation 6.2 in this section. The SWRC measured using conventional testing procedures are used in the analysis. The pre-stage shear and post-stage shear degree of saturation and suction obtained from the test data correspond more closely to a true SWRC since the tests were conducted as multi-stage tests. Since a single specimen was used for each SWRC, there is no need to assume that different specimens are identical. The terms *pre-stage shear*, and *post-stage shear* are used instead of pre-shear and post-shear because the analysis is based on multi-stage tests. In these tests once a shear plane has formed true pre-shear conditions are not known. For this reason, there will be a distinction between the pre-stage shear and post-stage shear conditions. In addition, as discussed in Chapter 5, a clear change in water regime occurs at the onset of shearing at each stage of multi-stage testing.

Figure 6.8 shows three SWRC determined on specimens compacted under a static stress of 150 kPa, at a compaction water contents, w_c, of either 15% or 19%. Each curve is an average value of test results undertaken on three specimens. After compaction, all specimens were saturated by placing them on a filter paper resting on a porous stone that was soaked with water. The water level was slightly below the surface of the stone to avoid washing away soil particles when handling the specimen. A flat board loaded with weights was placed on top of the oedometer ring containing the specimen to prevent swelling. After a period of 48 hours, the specimens mass was determined to calculate the degree of saturation. After assuring full saturation conditions of the specimen, one set of specimen compacted at w_c 15%, was then consolidated under a normal load of 150 kPa for a duration of twenty four hours. This procedure was followed to simulate the stress history, prior to shearing of the specimens used in the modified ring shear apparatus. Each SWRC data point presented is an average value obtained from three specimens prepared and tested under "identical" conditions. More details of the testing procedure are presented in section 5.2.4.

Figure 6.9 shows the SWRCs generated from the suction and degree of saturation data obtained experimentally from the modified ring shear apparatus on Indian Head till compacted at a compaction water content, w_c, of 15% and 19%. These curves are also compared to the SWRC obtained by conventional means on the same soil on specimens prepared at compaction water contents of 15% and 19%. Each of the ring shear curves was generated from a single specimen sheared at different matric suctions during multistage tests. The best-fit line was computed through a non-linear least squares analysis using the equation presented by Fredlund and Xing (1994). Since a single specimen was used, this line is representative of the SWRC of that particular specimen. In order to properly fit the data through that range, it was necessary to use a maximum degree of saturation lower than 100% (i.e., for degree of saturation values in the range of 85% to 94%). This corresponds to a SWRC with entraped air.

When modelling the SWRC, it is common practice to use the apparent SWRC. The apparent SWRC is a curve which always shows a degree of saturation of 100% when the matric suction value is 0 kPa. It is representative of the SWRC as it exists in the soil outside the pockets of entrapped air, where the degree of saturation is higher, reaching 100% when the suction drops to 0. To achieve this, the degree of saturation at any point on the curve is linearly stretched by dividing it by the maximum degree of saturation so that the curve effectively reaches saturation at 0 kPa. The apparent SWRC curves are shown in Figure 6.10. The most notable feature is that all data of the sheared specimen lie along an approximately unique SWRC, whether they were compacted dry or wet of optimum, and sheared under constant load or constant volume conditions. Furthermore, this curve shows a higher degree of saturation for any given matric suction than even the SWRC measured by conventional means on a consolidated specimen.

Figure 6.11 Shows the pre-shear and post-shear SWRC of each stage. Both curves are almost identical. Such similar curves can be expected given the multi-stage nature of the experimental program. If the SWRC shown in Figure 6.10 has already been reached in earlier stages of shear, little variations are to be expected. There is no longer any significant fabric left to be disturbed at that stage.

Figures 6.12 and 6.13 show the variation of the shear strength with respect to matric suction obtained by using the SWRC shown in Figure 6.8 for a κ of 2.2 (obtained from Figure 6.1) and κ of 5.01 (fitted from data at large deformations), respectively. Equation 6.1 was used in the fitting of the κ value. The average κ value from the experimental data was found to be equal to 5.01. The value of 2.2 is expected to fit the peak shear strength values with the conventional SWRC. The value of 5.01 is expected to provide a better fit to the ultimate state data using the SWRC generated from the shear strength test results since these were used in calculating the κ parameter value. In the analysis of the results only the ultimate shear strength data from the multi-stage shear strength has been used.

Figures 6.14 and 6.15 show the failure envelopes generated with κ=2.2 and κ=5.01, respectively, plotted against the failure envelopes of specimens tested under CLS conditions. The specimens were compacted at a water content, w_c, equal to 15%. The SWRC derived from the consolidated specimens matches closely the SWRC from the shear strength test data. Both SWRC closely match the experimental data at the lower suction levels but diverge at higher matric suctions when using κ=2.2. The curve generated using the SWRC that had been generated from the specimen generated in a standard manner, with the same compaction and saturation procedure as the modified ring shear specimens but without the consolidation, shows the most pronounced divergence with the experimental data.

When using κ=5.01, there is a much closer agreement between the predicted values of shear strength from the SWRC obtained from consolidated specimens. The non-consolidated SWRC is even more divergent when using a value of κ=5.01 than using a value of κ=2.20. The shape of the curve generated from the 15% consolidated conventional SWRC test specimens is the one that most closely matches the general trend of the data. The fact that the water content of the sheared specimens had not been stabilized by the end of the shearing phase, could account for a low accuracy of the lower SWRC generated from the sheared specimens. Figures 6.16 and 6.17 show similar trends for the specimen compacted at w_c=19% using κ=2.2 and κ=5.01, respectively, as those observed for the specimen compacted at w_c=15%. Only the SWRC obtained from conventional methods was available in this case. The divergence from the low suction values is even greater in this case, however when using κ =5.01.

Figures 6.18 and 6.19 show the shear strength contribution of matric suction as a function of the matric suction, as predicted using the conventional SWRC from specimen compacted at w_c=15%, as well as from the specimen sheared in CVS conditions. Comparisons are provided only for the shear strength contribution due to the matric suction component since the net normal stress on the plane of failure changed in order to maintain constant volume conditions. Using a value of κ=2.2 did not provide a good fit to the measured data. However, even with a value of 5.01, the predictions using the conventional SWRC with consolidation as well as those generated from shearing data tend to overestimate the shear strength. They provide a better correlation to the data at the lower suction values, within the range where the data still plots closely to the *tan* ϕ' line (the failure envelope of the saturated soil). The air entry values appears to be at 50 kPa for the CVS tests as opposed to 100 kPa for the CLS tests.

Figure 6.20 and Figure 6.21 show the predicted and measured shear strength of a specimen compacted at a water content w_c=19% and sheared under CVS conditions. It should be noted that while the volume was controlled during the shearing stages, the net normal stress was reset to 150 kPa between the suction stages. As such, volume changes did occur between the shearing stages while in the case of CVS specimen compacted at a water content of 15% the volume was controlled even between the suction changes. As such the CVS tests of the specimen compacted at w_c =15% represent a true constant volume envelope, while the CVS tests of the specimen compacted at wc=19% presents CVS shear test results, but within a consolidated inter-stage condition. The failure envelope therefore more closely resembles the CLS envelope.

For all test series analysed, using the κ of 5.01 proved to be a much better fit than using a κ of 2.20. This is to be expected since κ=5.01 was fitted tothe current data set, and κ=2.20 was obtained from the peak strength of tested specimens. It can be observed, however that the predictions using κ=5.01 produce curves that quickly diverge from the saturated ϕ' envelope (which represents the upper boundary shear strength for unsaturated soils, attained only while the specimen is still tension-saturated). This can be attributed to a low estimation of the degree of saturation from the experimental data. As previously noted, the SWRC obtained from the shear strength test data tended towards maximum values in the range of degree of saturation from 85% to 94%. The apparent degree of saturation may therefore be more representative of the degree of saturation in the shear zone.

Using the apparent SWRC, a fitting parameter $\kappa = 7.25$ was obtained that could fit reasonably well the CLS envelopes for specimens compacted both at wet and dry of optimum (Figures 6.22 and 6.23) as well as for the CVS at w_c = 19% (Figure 6.24) for which, as it has been commented before, the net normal stress was maintained at 150 kPa for each suction increment and constant volume control was only provided during the shearing phases. In all these cases, volume changes due to consolidation were observed during each suction increment. It can also be noted from Figure 6.22 that using the SWRC with a value of $\kappa = 5.01$ yields a prediction curve that also closely matches the prediction using the apparent SWRC curve from sheared specimens. The difference in the magnitude of the κ parameter between the curves using the apparent degree of saturation of the sheared specimens and the SWRC from the pressure plate apparatus on consolidated specimens reflects the fact that the apparent SWRC from sheared specimens retains a degree of saturation close to unity for higher matric suction than the consolidated conventional SWRC. Therefore, despite a higher exponent, the degree of saturation can remain close to unity (and the computed failure envelope remains close to ϕ') for higher values of κ. The high values of κ, however, allows the curve the reapidly diverge from ϕ' as soon as the degree of saturation decreases a little, thus matching the relatively horizontal failure envelope obtained from the measured shear strength after a matric suction of about 100 to 150 kPa has been reached.

The same value of the fitting parameter, however cannot be used to succesfully predict the shear strength of the CVS test on the specimen tested at w_c=15% (Figure 6.25). In the case of this specimen, the void ratio was maintained constant even between suction increment stages. This failure envelope therefore corresponds to a single void ratio. Although no discernible difference can be seen between the apparent sheared SWRC from this specimen and he others (Figure 6.10), a significant difference exists between the predicted and the measured shear strength using κ=7.25. In order to obtain a better fit, a value of κ=12.3 must be used. It should be noted that using a κ=8.2 with the SWRC obtained by conventional means but having been subjected to a consolidation equal to the initial consolidation pressure of the sheared specimen (150 kPa) also provides a reasonable fit to the observed shear strength. No value of κ could be found that would allow a good fit of the observed data using the SWRC obtained by conventional means using the same compaction procedure as the sheared specimen but without undergoing an equivalent saturated consolidation stage under a normal stress of 150 kPa. Similarly, no value of κ could be found to adequately fit the data using the observed degree of saturation of the specimens without correction for entrapped air (by using the apparent SWRC).

This confirms that the selection of a proper SWRC is of critical importance when deciding on a model to predict the shear strength of unsaturated soils. A more extensive experimental program is required to provide more general observations on the validity of the use of the conventional SWRC obtained by conventional means but having subjected the specimens to consolidation as well as the use of the apparent SWRC obtained from the sheared specimens. The markedly different value of κ obtained from the specimen tested under a controlled void ratio for all matric suctions suggests that κ may not only be dependent on the soil type but also on the void ratio of any given soil. More data is required to explore this hypothesis.

6.4 Summary

From the observation of this chapter it can be concluded that:

1) The choice of SWRC will have a marked influence on the prediction of the shear strength of unsaturated soils.

2) The SWRC obtained by conventional means can be substantially different from the SWRC obtained from the characteristics of a sheared specimen. In particular, the maximum degree of saturation of the SWRC generated from shear data is lower than 100%, suggesting that entrapment of air occurs during the shearing process.

3) Subjecting the SWRC specimens to a stress history comparable to the stress history of the test specimens before the shearing process can markedly improve the quality of the prediction.

4) The apparent SWRC obtained from sheared specimens provide a better fit to the shear strength of Indian Head till at large deformations, both at low and at high matric suctions.

6.5 Figures

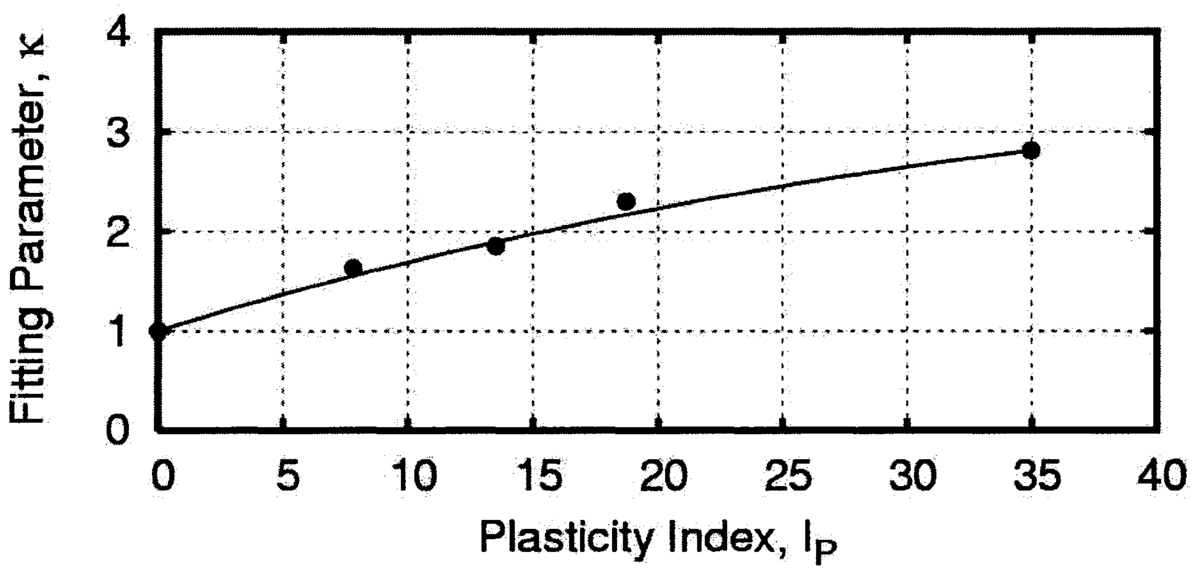

Figure 6.1 Fitting parameter κ versus plasticity index, I_p [from Vanapalli and Fredlund, (2000)].

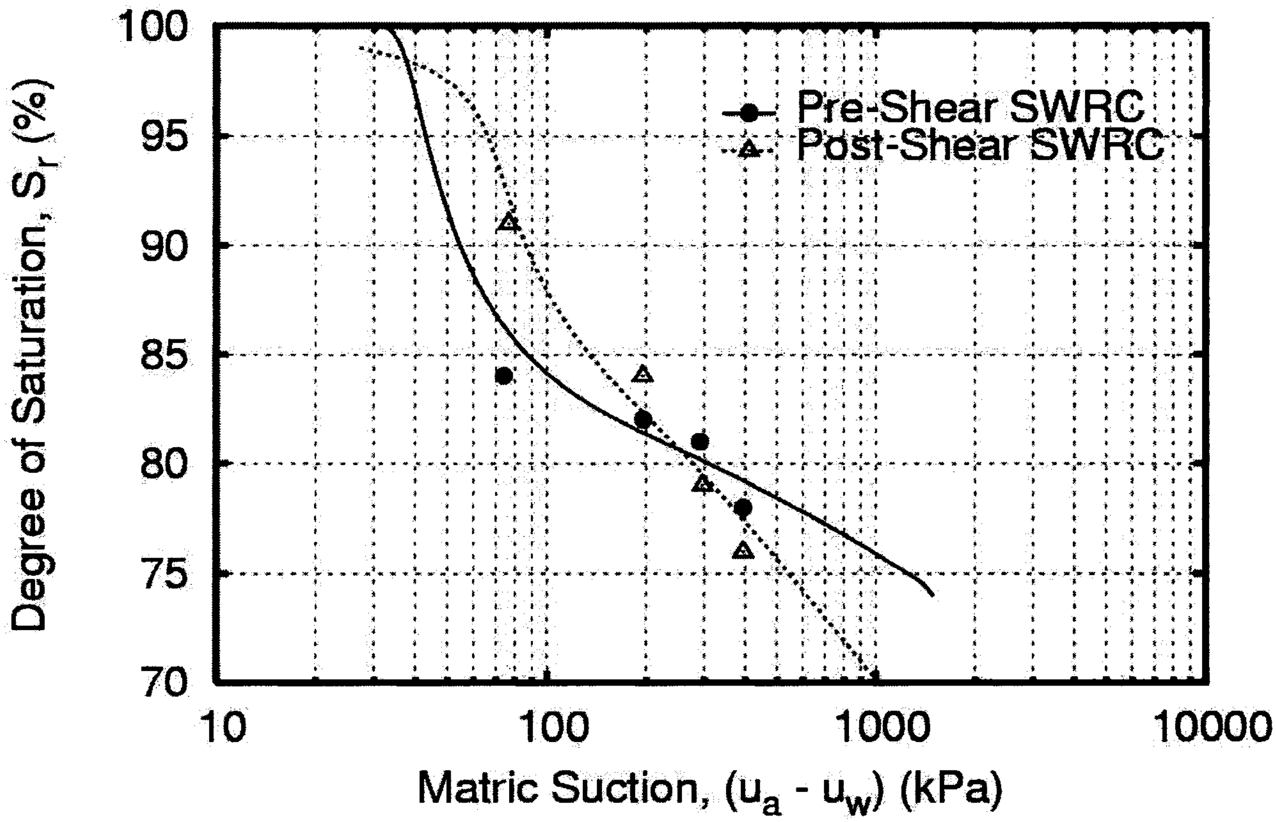

Figure 6.2 Soil-water retention curve data derived from the triaxial shear test results undertaken on Dhanauri clay specimens tested under a confining pressure of 96 kPa.

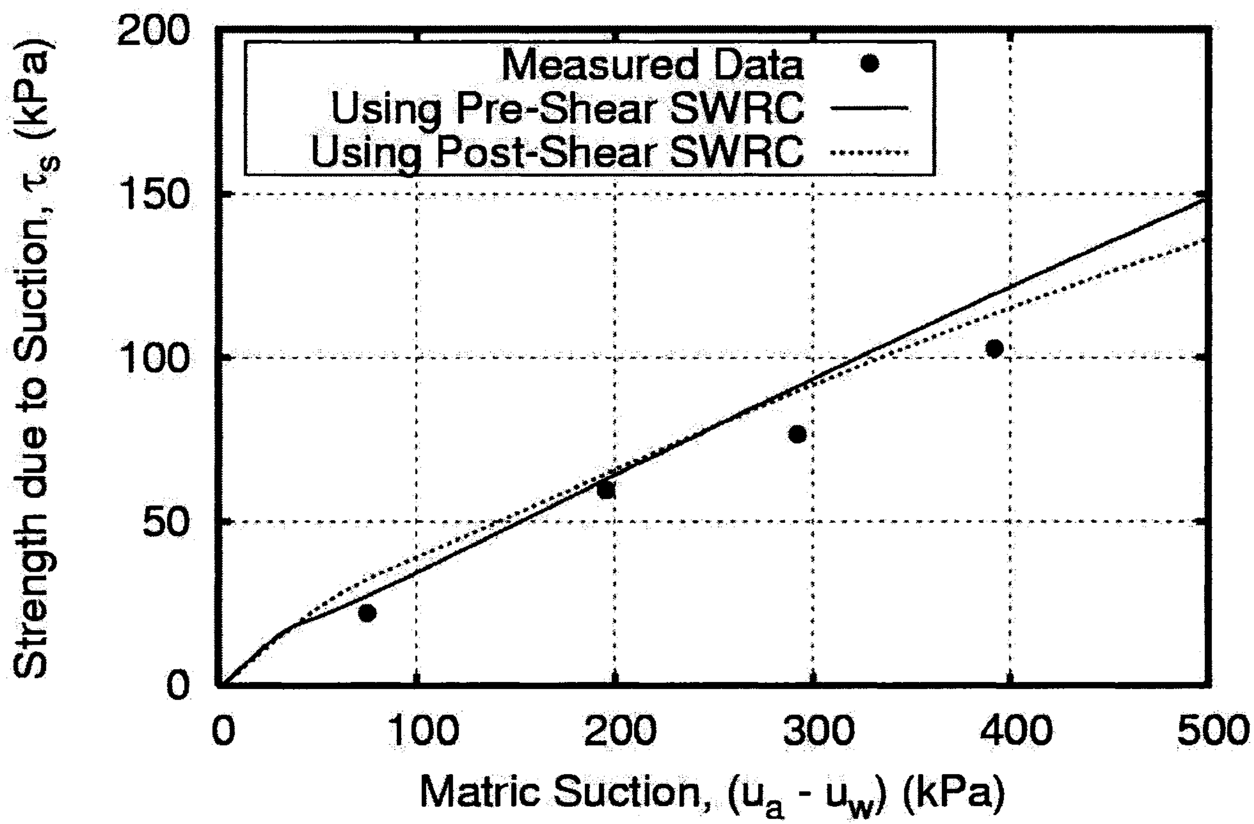

Figure 6.3 Measured and predicted shear strength of Dhanauri clay for a suction range of 0 to 400 kPa and a net confining pressure of 96kPa.

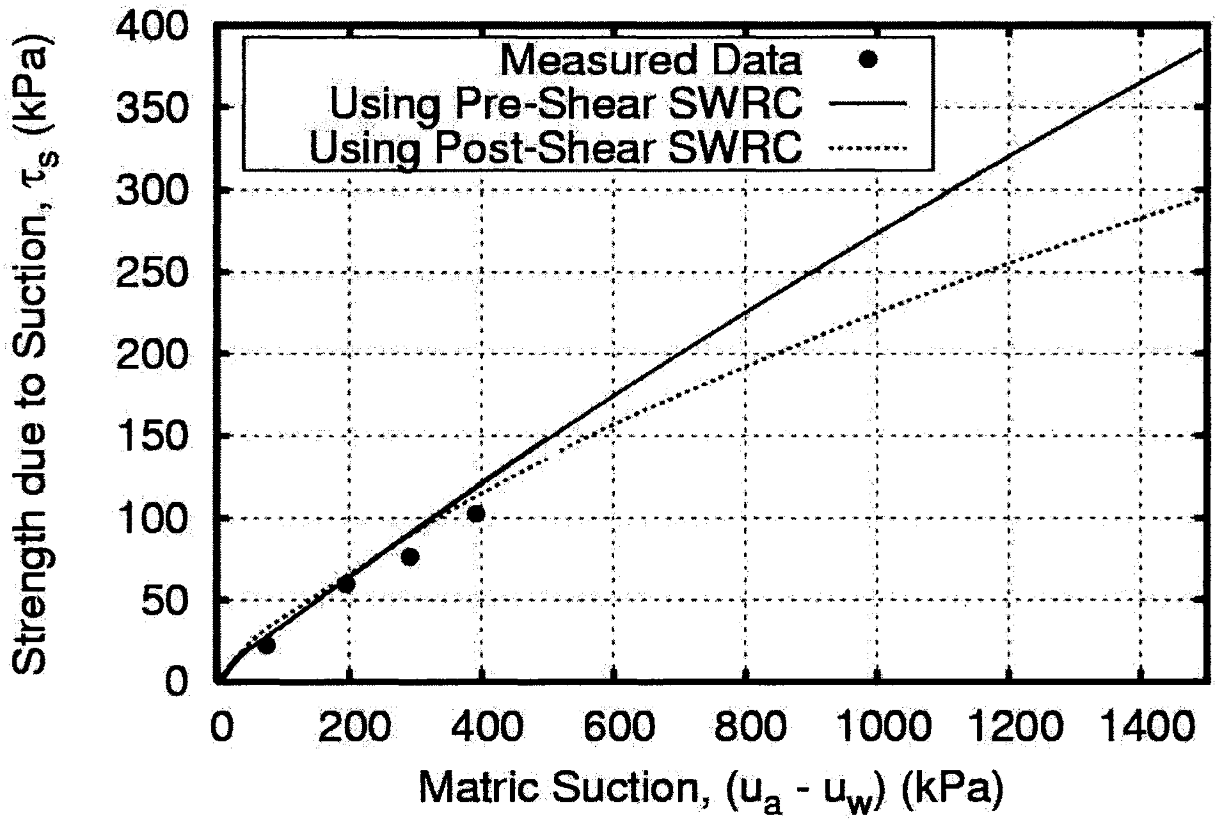

Figure 6.4 Measured and predicted shear strength of Dhanauri clay for a net confining pressure of 96 kPa.

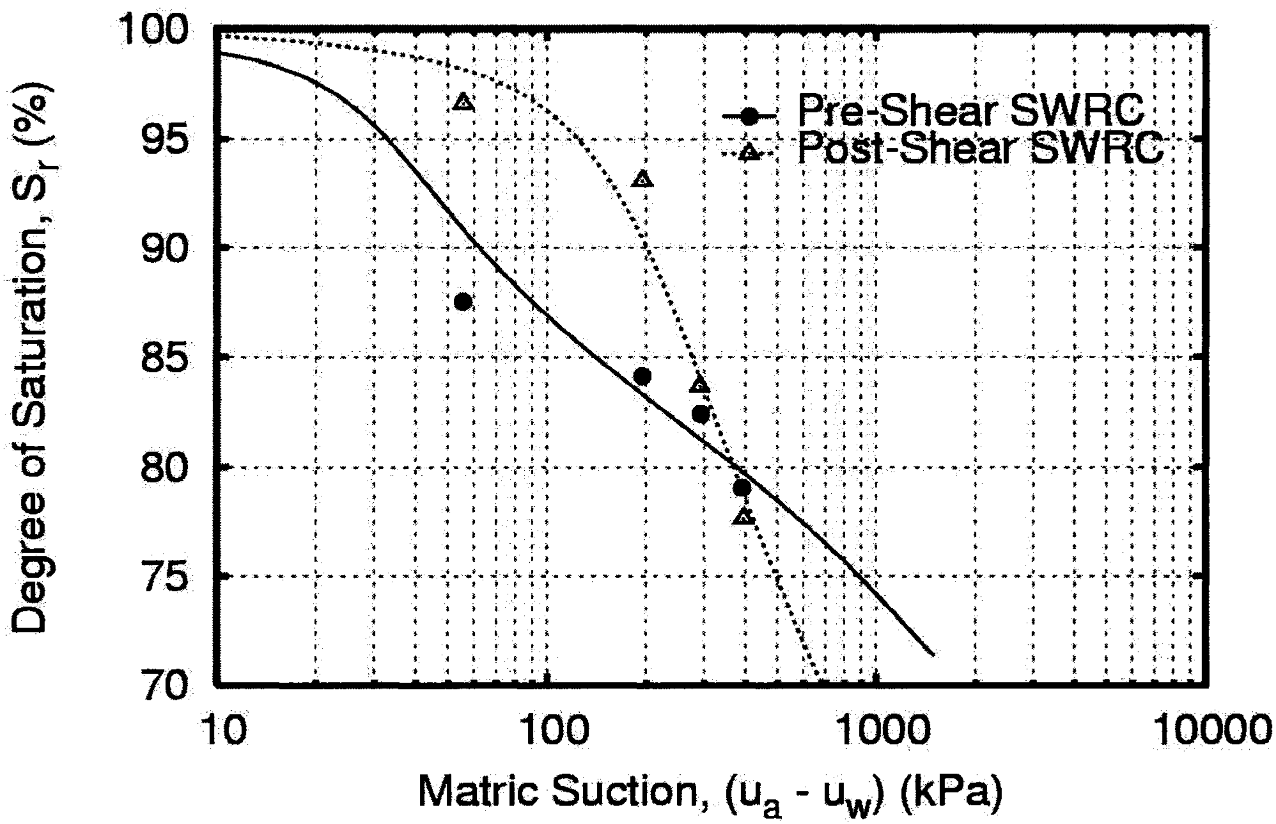

Figure 6.5 Soil-water retention curve data derived from the triaxial shear test results undertaken on Dhanauri clay specimens tested under a net confining pressure of 386 kPa.

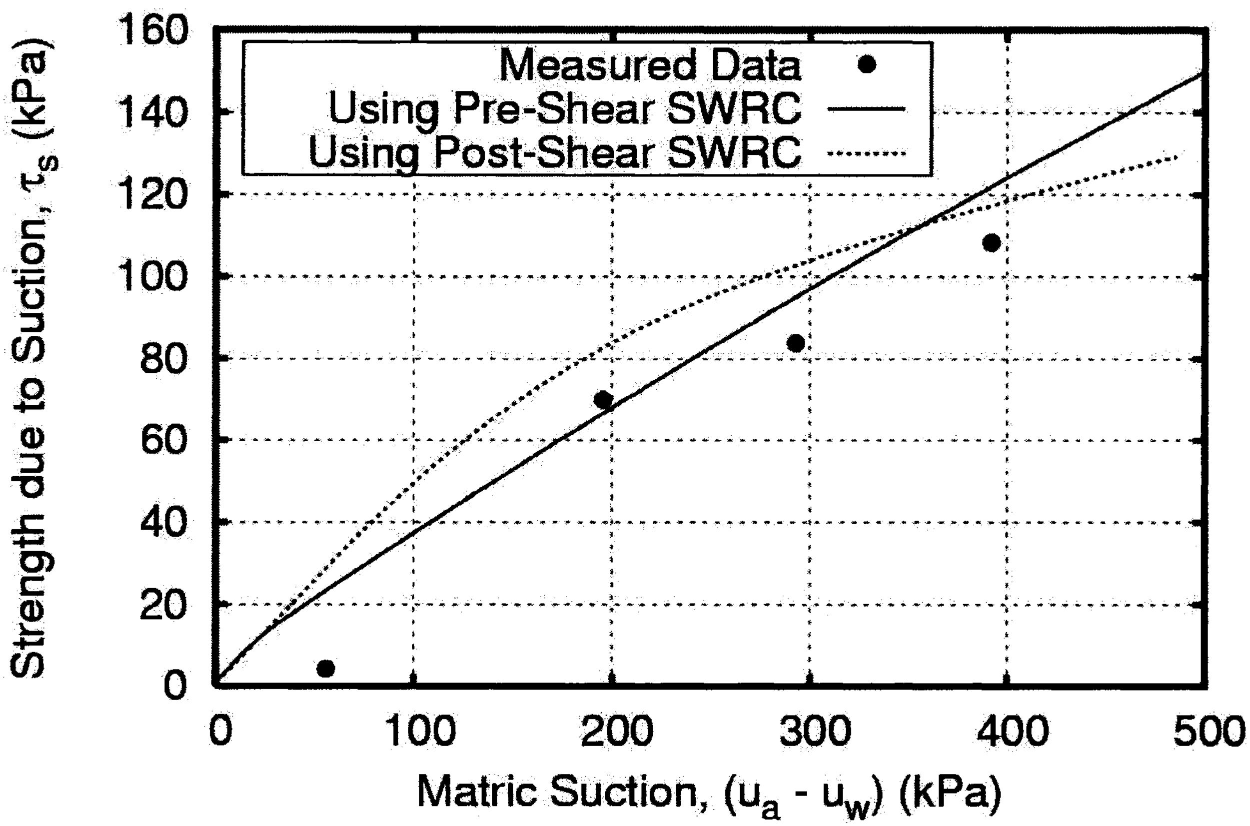

Figure 6.6 Measured and predicted shear strength of Dhanauri clay for a suction range of 0 to 400 kPa and a net confining pressure of 386kPa

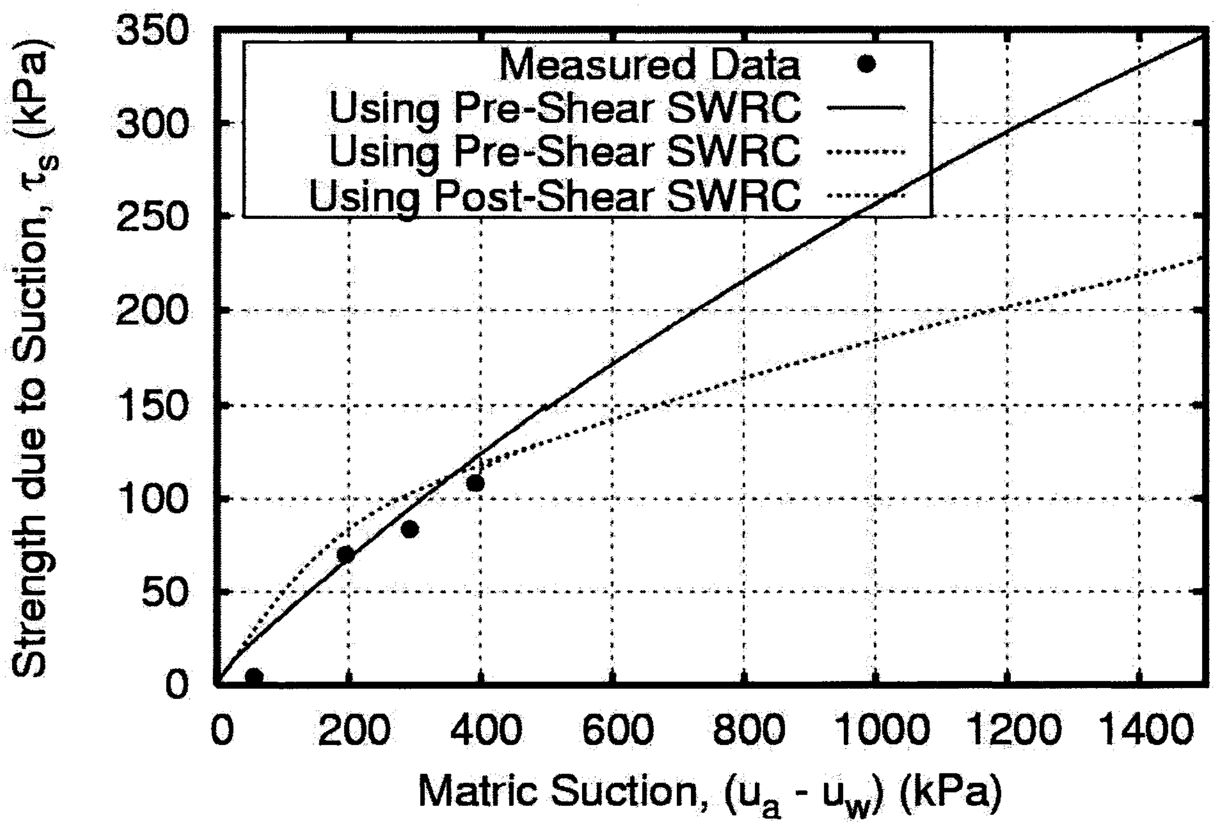

Figure 6.7 Measured and predicted shear strength of Dhanauri clay for a net confining pressure of 386kPa

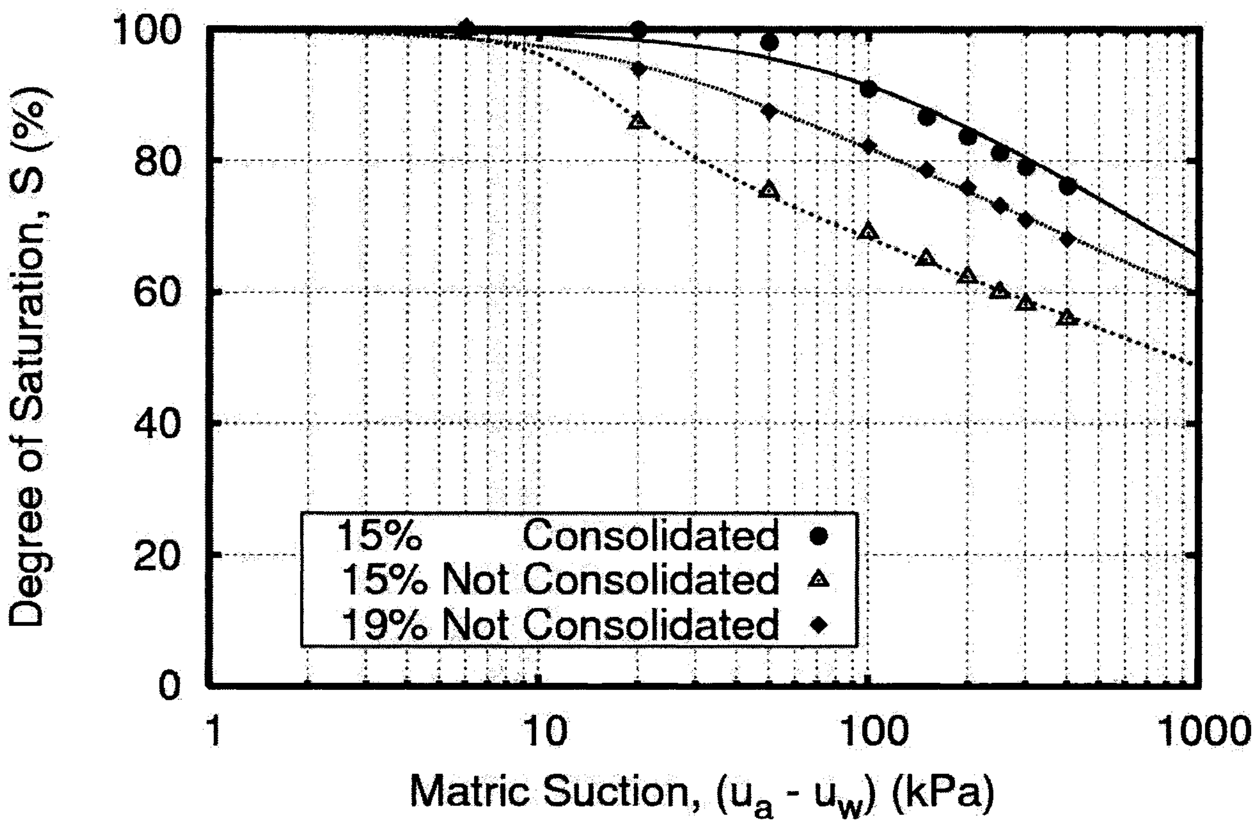

Figure 6.8 SWRC for Indian Head till specimens compacted at 15% and 19% water contents. A series of 15% specimens were consolidated, after saturation, under a normal stress of 150 kPa..

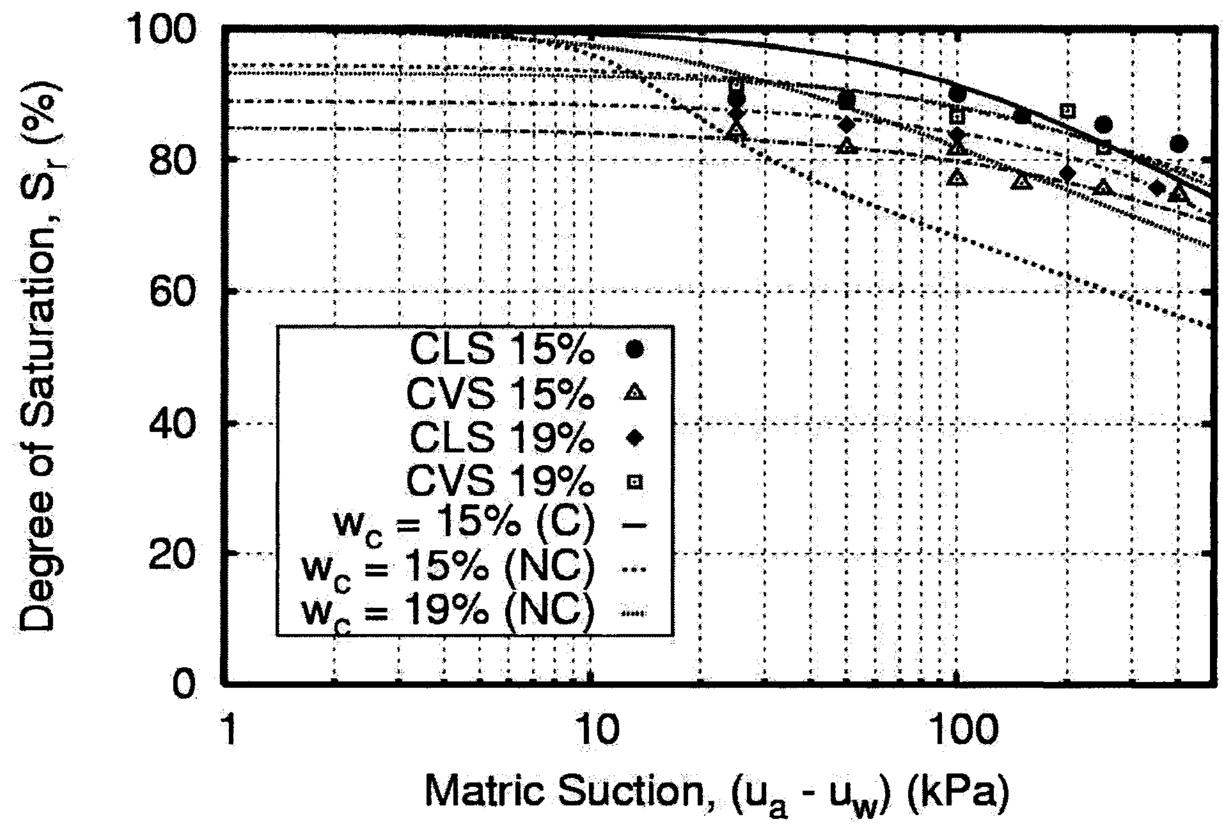

Figure 6.9 SWRC from the sheared specimen compacted at water contents, w_c, of 19% and 15% compared to the consolidated (C) and non-consolidated (NC) SWRC obtained by conventional means on specimens compacted at a water content of 15% and 19% (NC only). The ring shear specimen and consolidated SWRC specimen were consolidated under a vertical stress of 150 kPa.

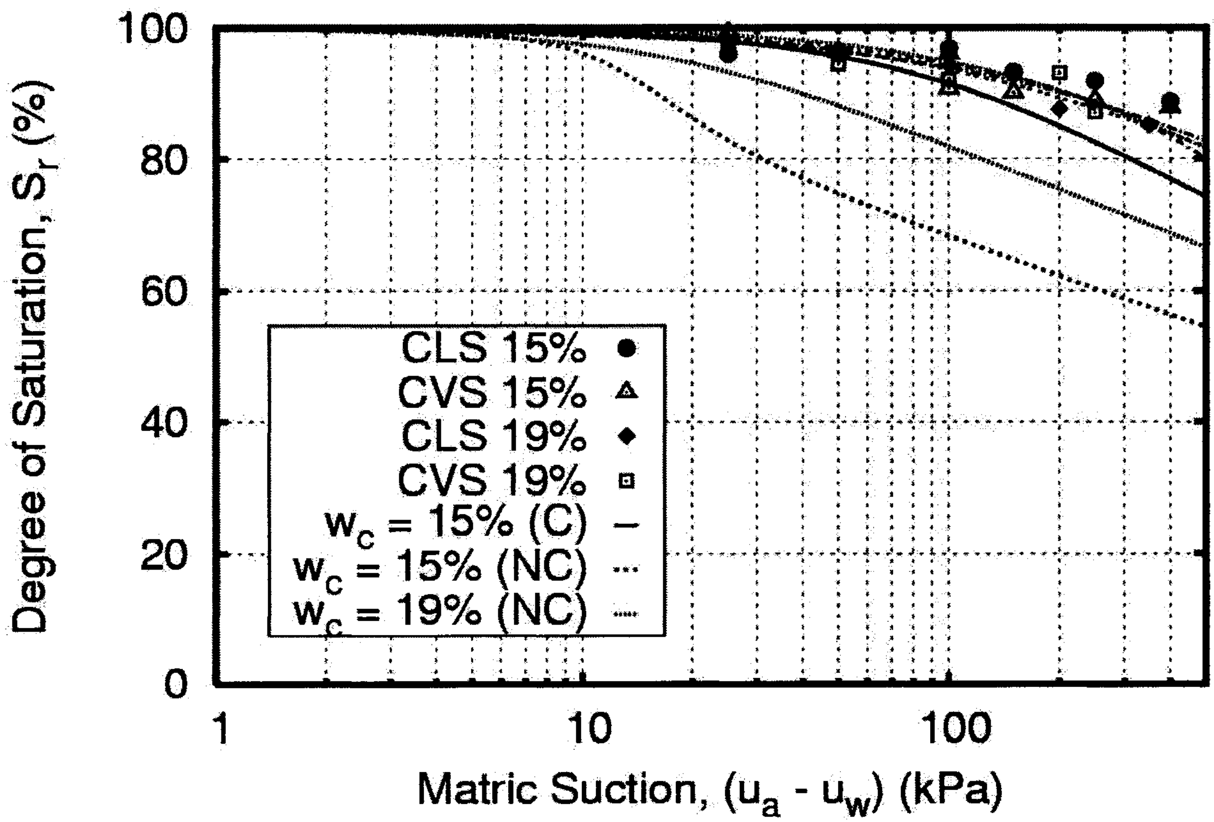

Figure 6.10 Apparent SWRC from the sheared specimen compacted at water contents, w_c, of 19% and 15% compared to the consolidated (C) and non-consolidated (NC) SWRC obtained by conventional means on specimens compacted at a water content of 15% and 19% (NC only). The ring shear specimen and consolidated SWRC specimen were consolidated under a vertical stress of 150 kPa.

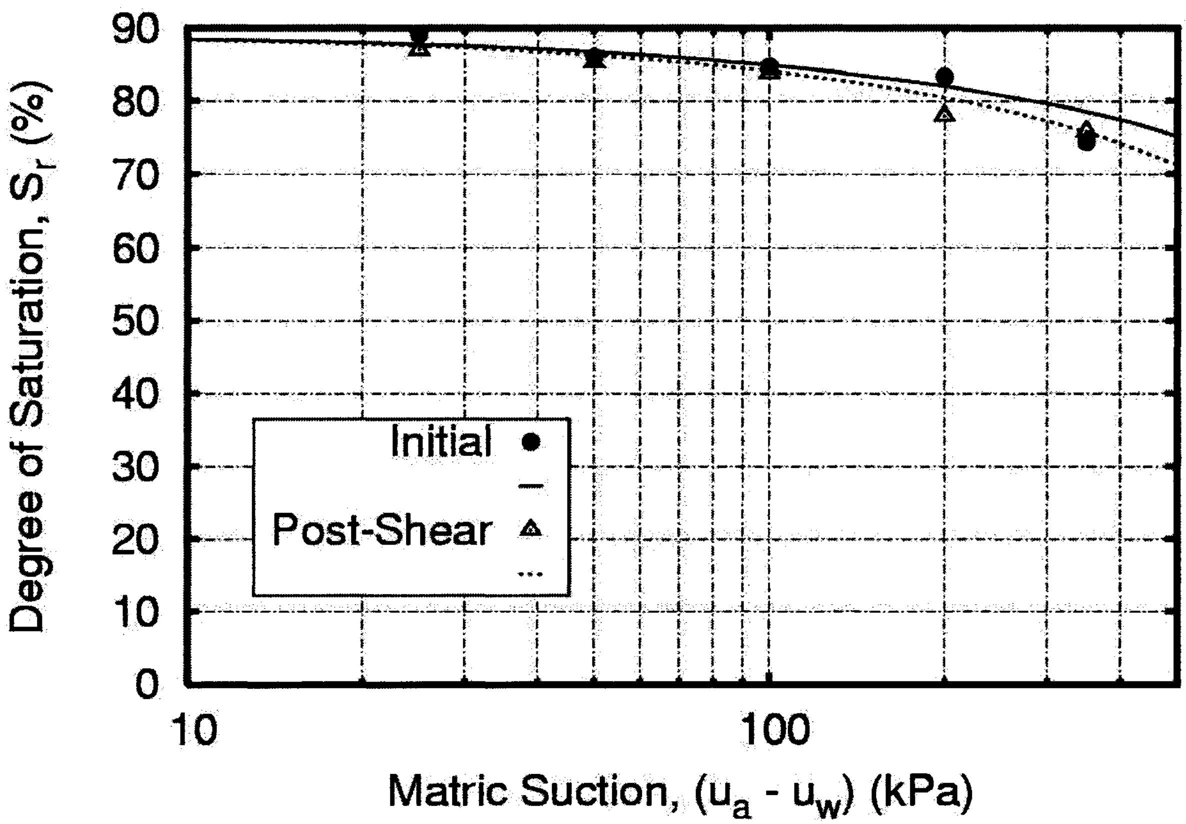

Figure 6.11 SWRC generated from pre-shear and post-shear conditions on a CLS specimen compacted at a water content, w_c, of 19%.

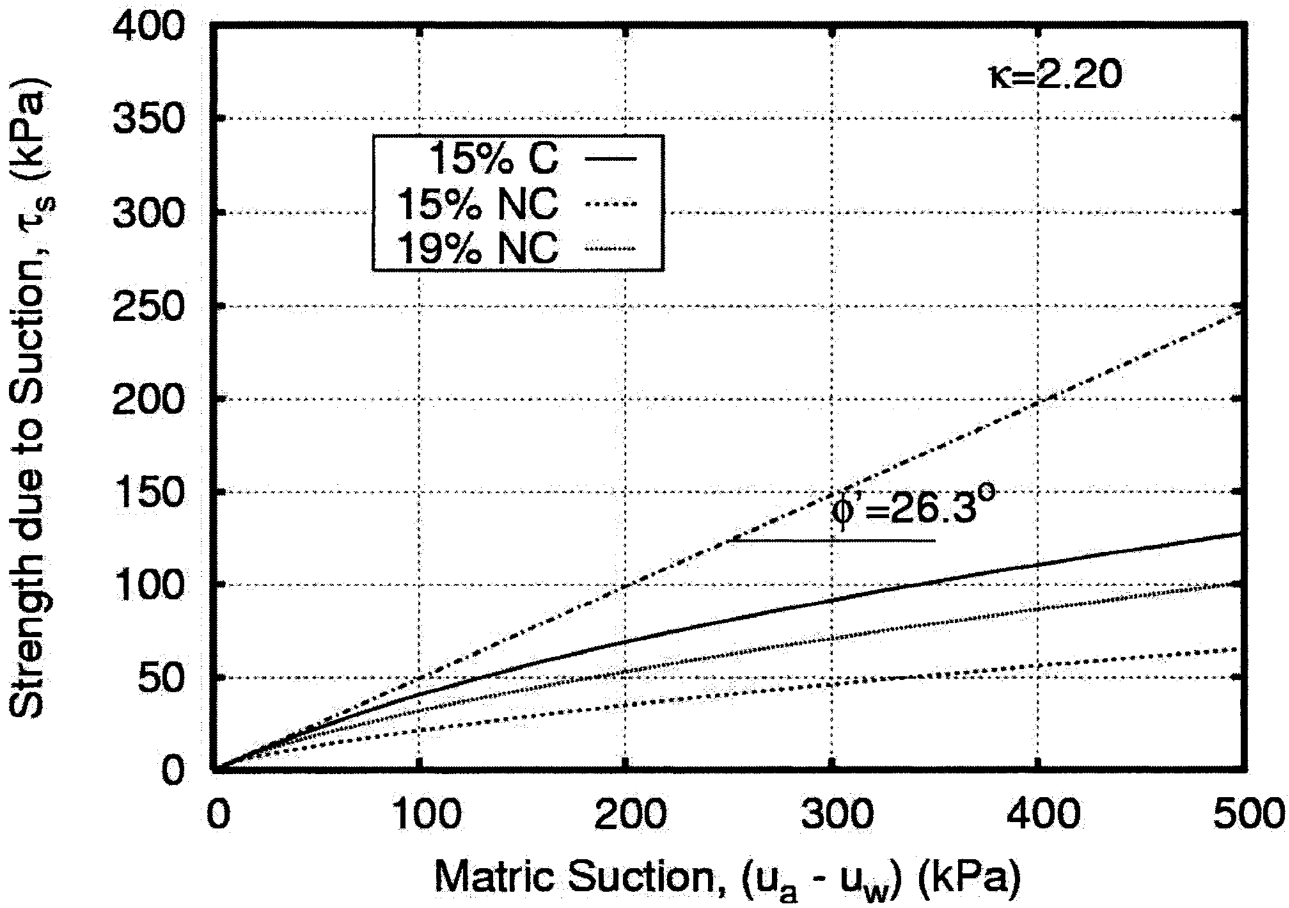

Figure 6.12 Suction contribution due to suction predicted from a κ=2.2 obtained from the plasticity chart, and using conventional SWRC curves.

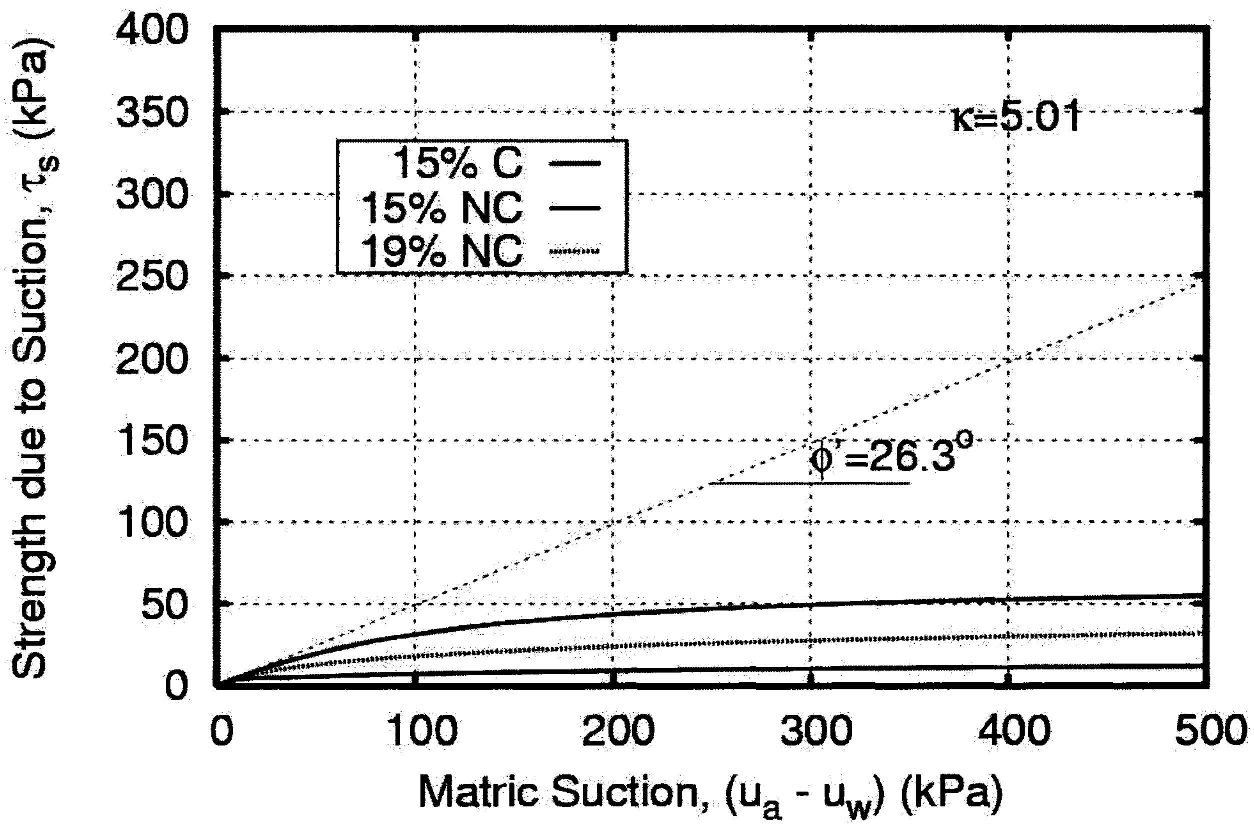

Figure 6.13 Suction contribution due to suction predicted from a κ=5.01 obtained by fitting the data from strength at large deformations, and using conventional SWRC curves.

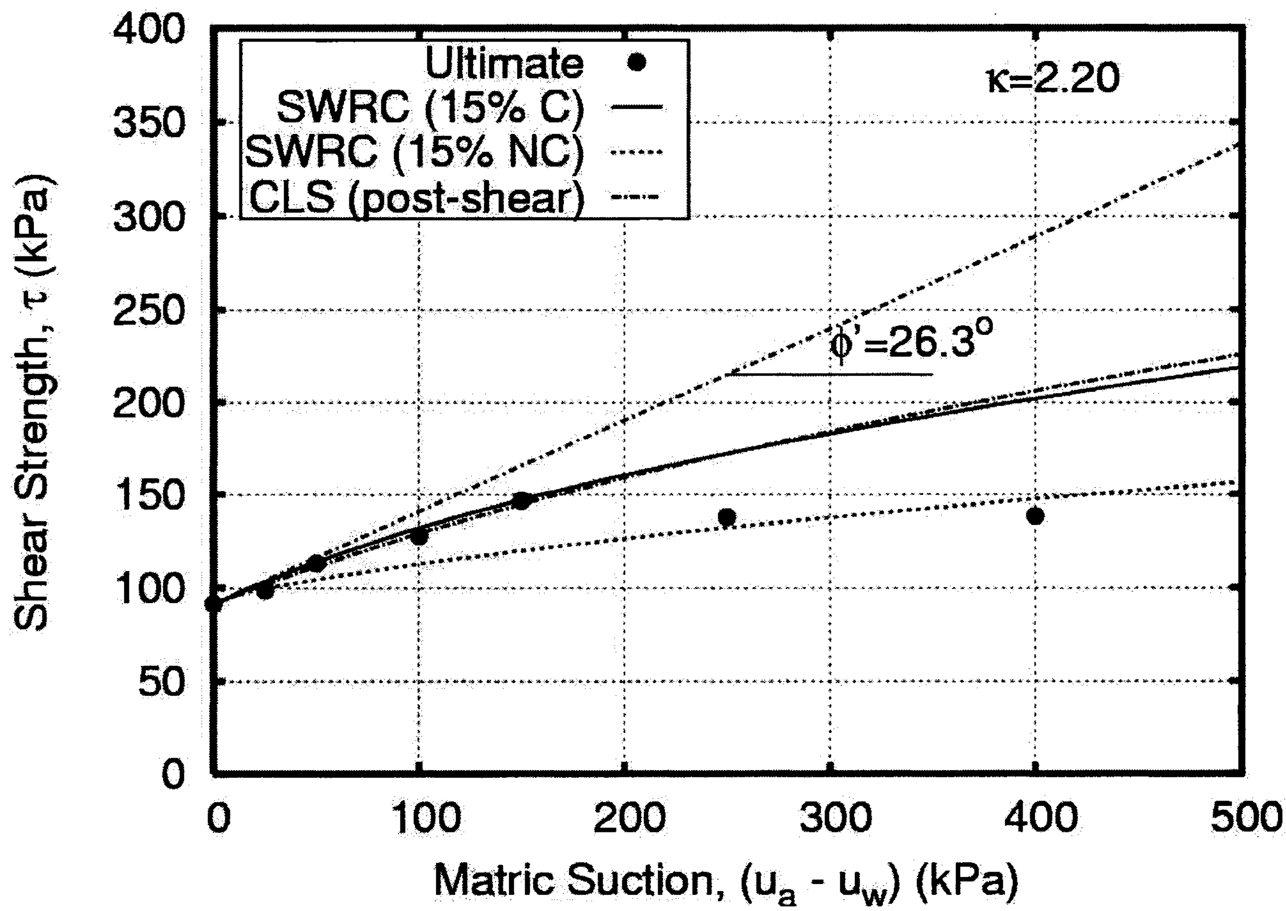

Figure 6.14 Prediction of CLS shear strength of Indian Head till, using conventional SWRC from consolidated (C) and non-consolidated (NC) specimens and using the SWRC generated from post-shear data of a ring shear specimen compacted at a water content, w_c, of 15%. This prediction uses a κ=2.2 from the plasticity chart.

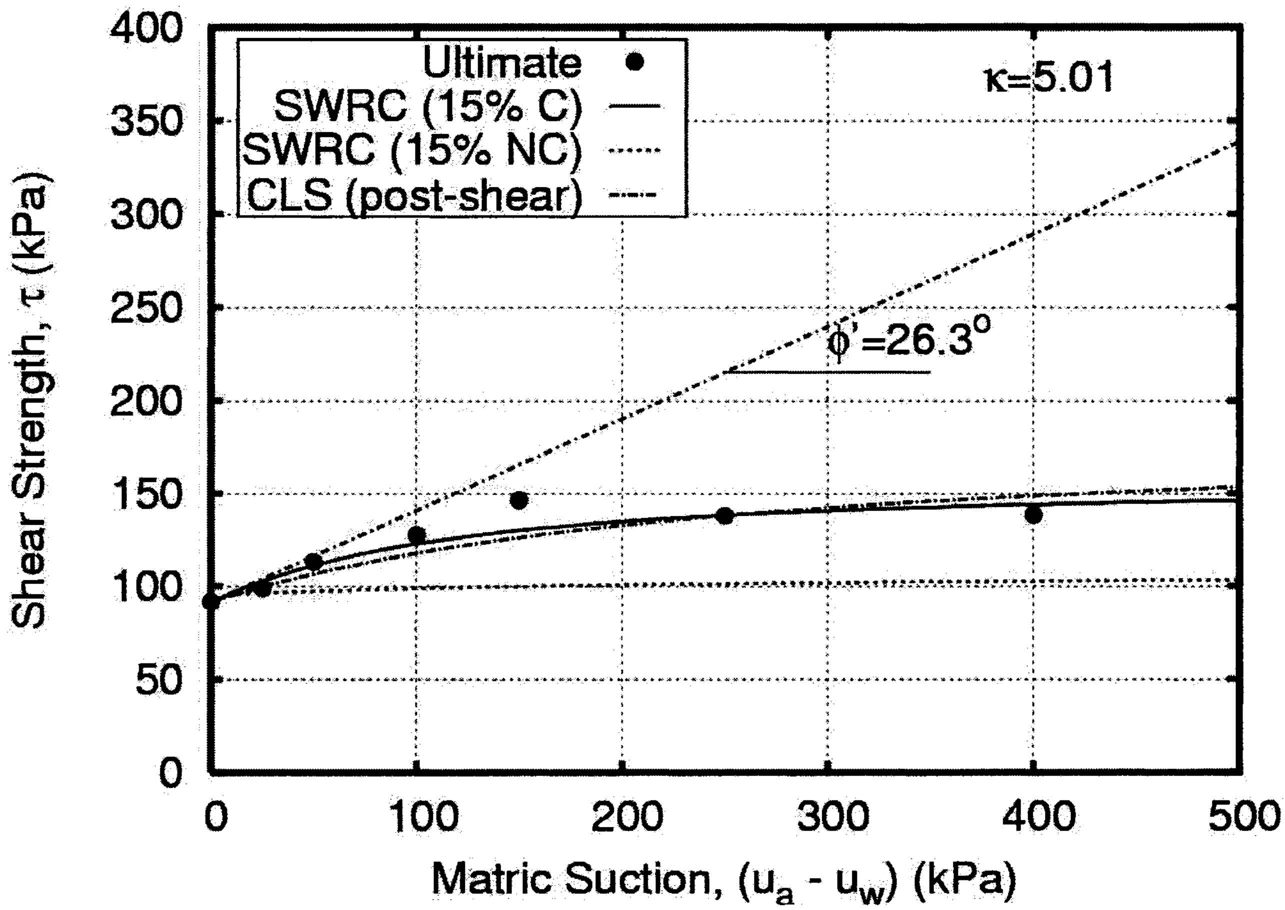

Figure 6.15 Prediction of CLS shear strength of Indian Head till, using conventional SWRC from consolidated (C) and non-consolidated (NC) specimens and using the SWRC generated from post-shear data of a ring shear specimen compacted at a water content, w_c, of 15%. This prediction uses a κ=5.01 fitted from shear strength at large deformations.

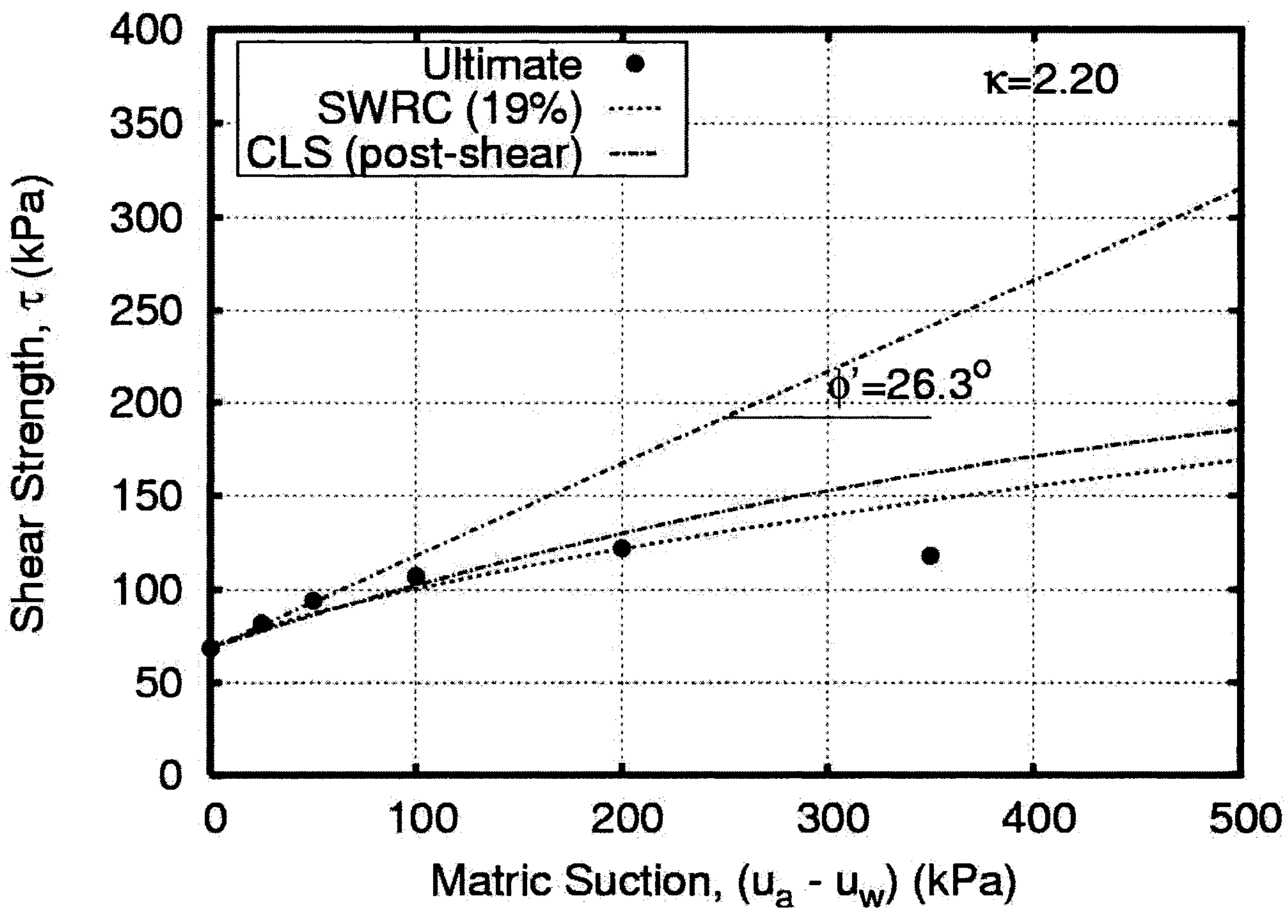

Figure 6.16 Prediction of CLS shear strength of Indian Head till, using conventional SWRC from non-consolidated (NC) specimens and using the SWRC generated from post-shear data of a ring shear specimen compacted at a water content, w_c, of 19%. This prediction uses a κ=2.2 from the plasticity chart.

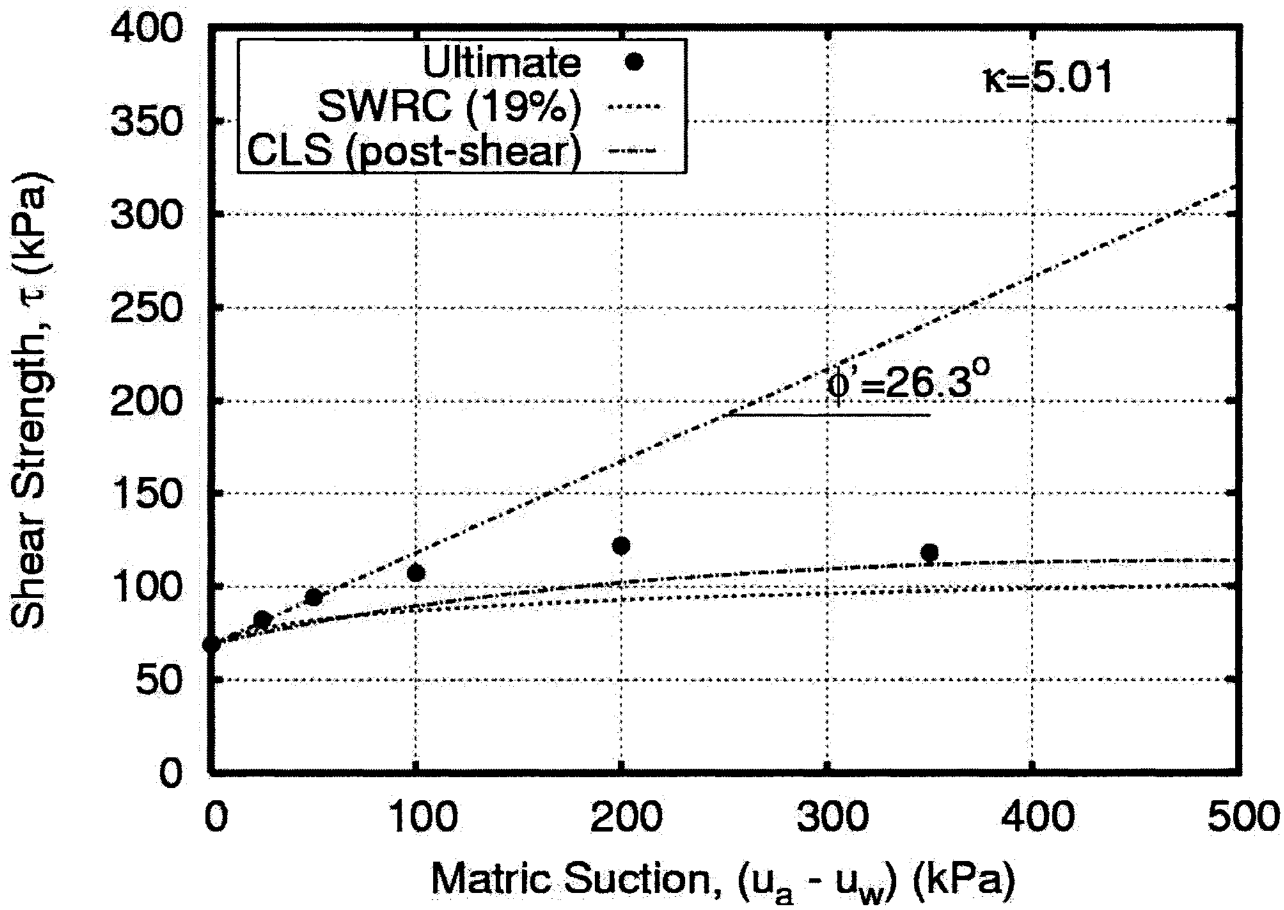

Figure 6.17 Prediction of CLS shear strength of Indian Head till, using conventional SWRC from non-consolidated (NC) specimens and using the SWRC generated from post-shear data of a ring shear specimen compacted at a water content, w_c, of 19%. This prediction uses a κ=5.01 fitted from shear strength at large deformations.

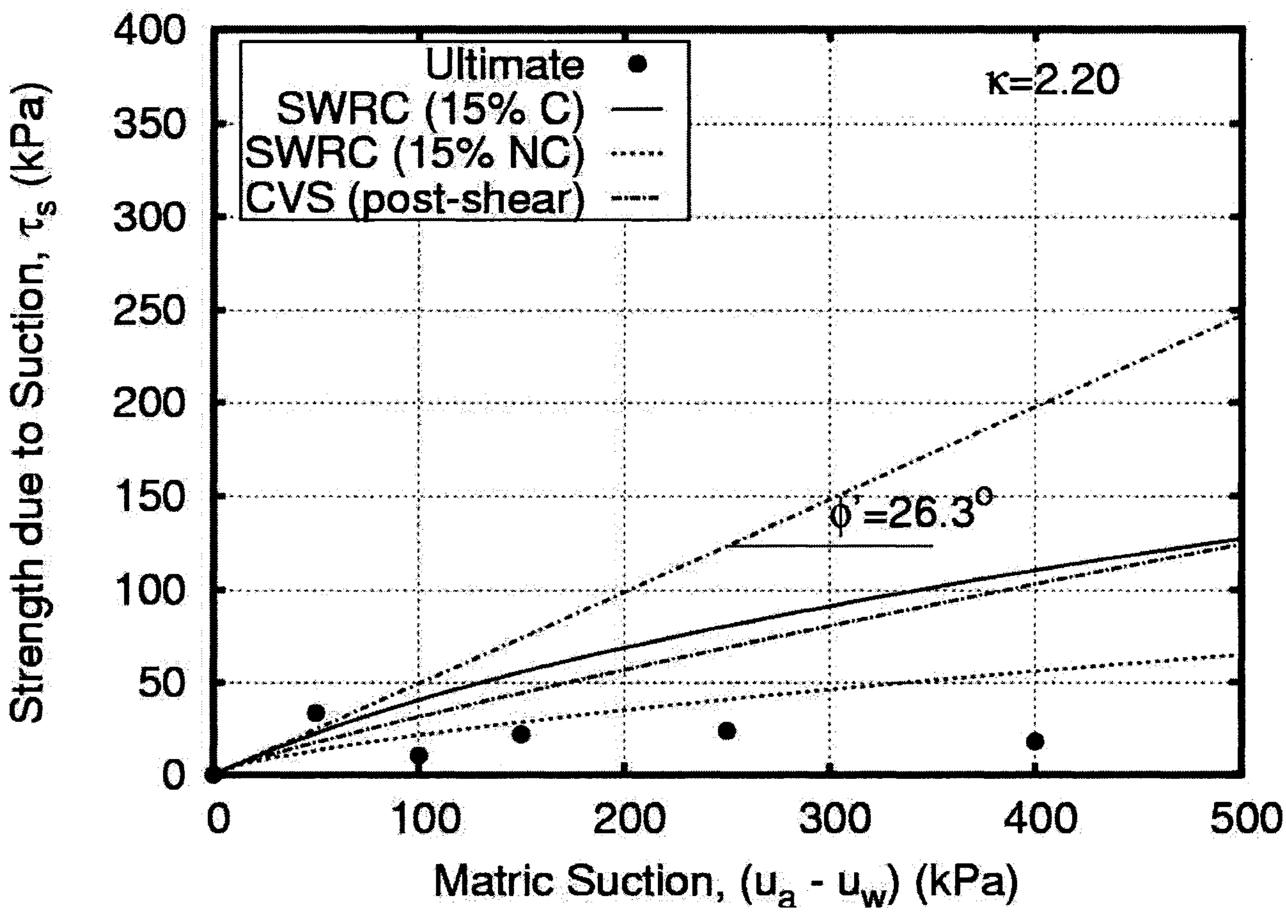

Figure 6.18 Prediction of the contribution of matric suction to the CVS shear strength of Indian Head till, using conventional SWRC from consolidated (C) and non-consolidated (NC) specimens and the SWRC generated from post-shear data of a ring shear specimen compacted at a water content, w_c, of 15%. This prediction uses a κ=2.2 from the plasticity chart.

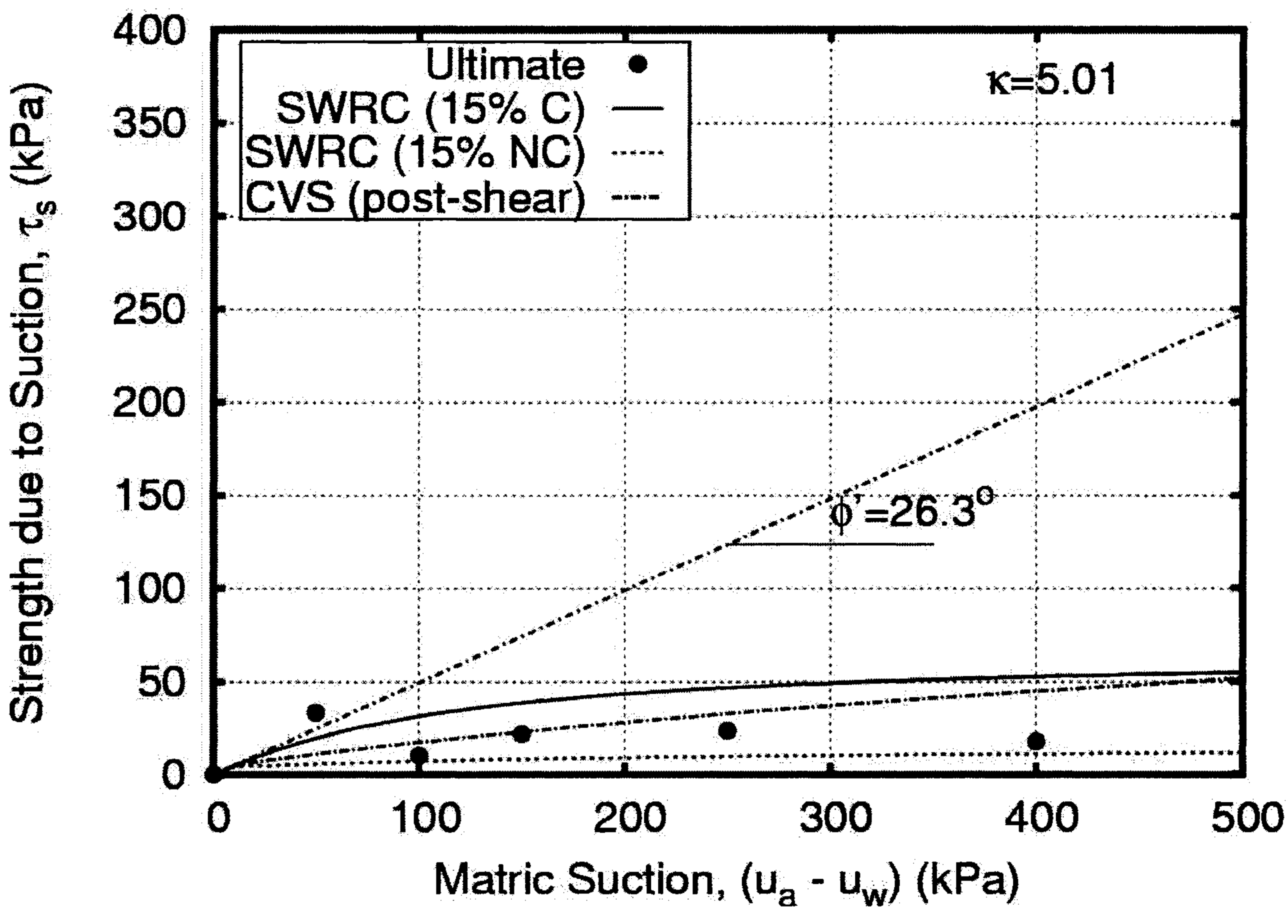

Figure 6.19 Prediction of the contribution of matric suction to the CVS shear strength of Indian Head till, using conventional SWRC from consolidated (C) and non-consolidated (NC) specimens and the SWRC generated from post-shear data of a ring shear specimen compacted at a water content, w_c, of 15%. This prediction uses a κ=5.01 fitted from shear strength at large deformations.

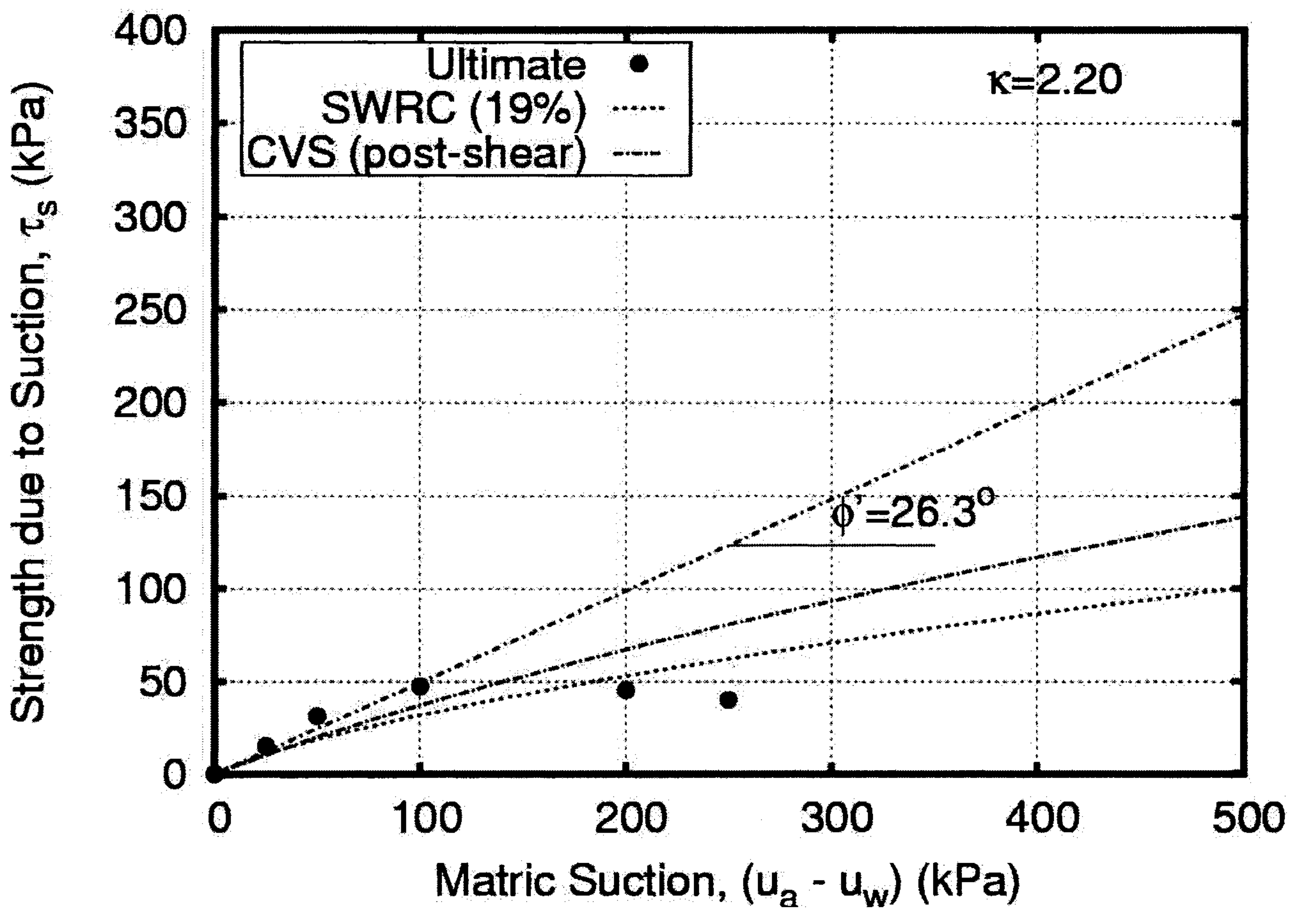

Figure 6.20 Prediction of the contribution of matric suction to the CVS shear strength of Indian Head till, using conventional SWRC and the SWRC generated from post-shear data of a ring shear specimen compacted at a water content, w_c, of 19%. This prediction uses a κ=2.2 from the plasticity chart.

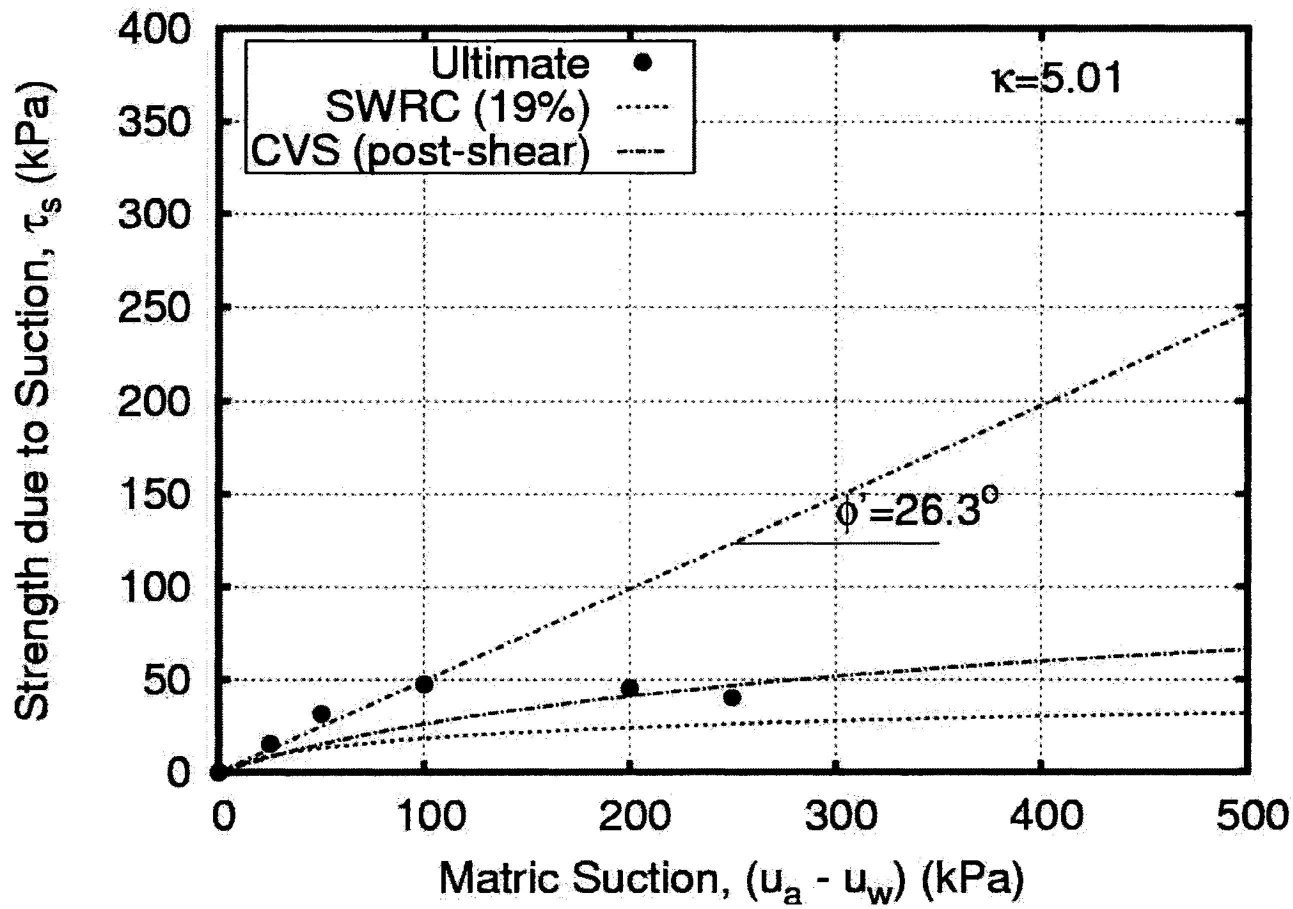

Figure 6.21 Prediction of the contribution of matric suction to the CVS shear strength of Indian Head till, using conventional SWRC and the SWRC generated from post-shear data of a ring shear specimen compacted at a water content, w_c, of 19%. This prediction uses a κ=5.01 fitted from shear strength at large deformations.

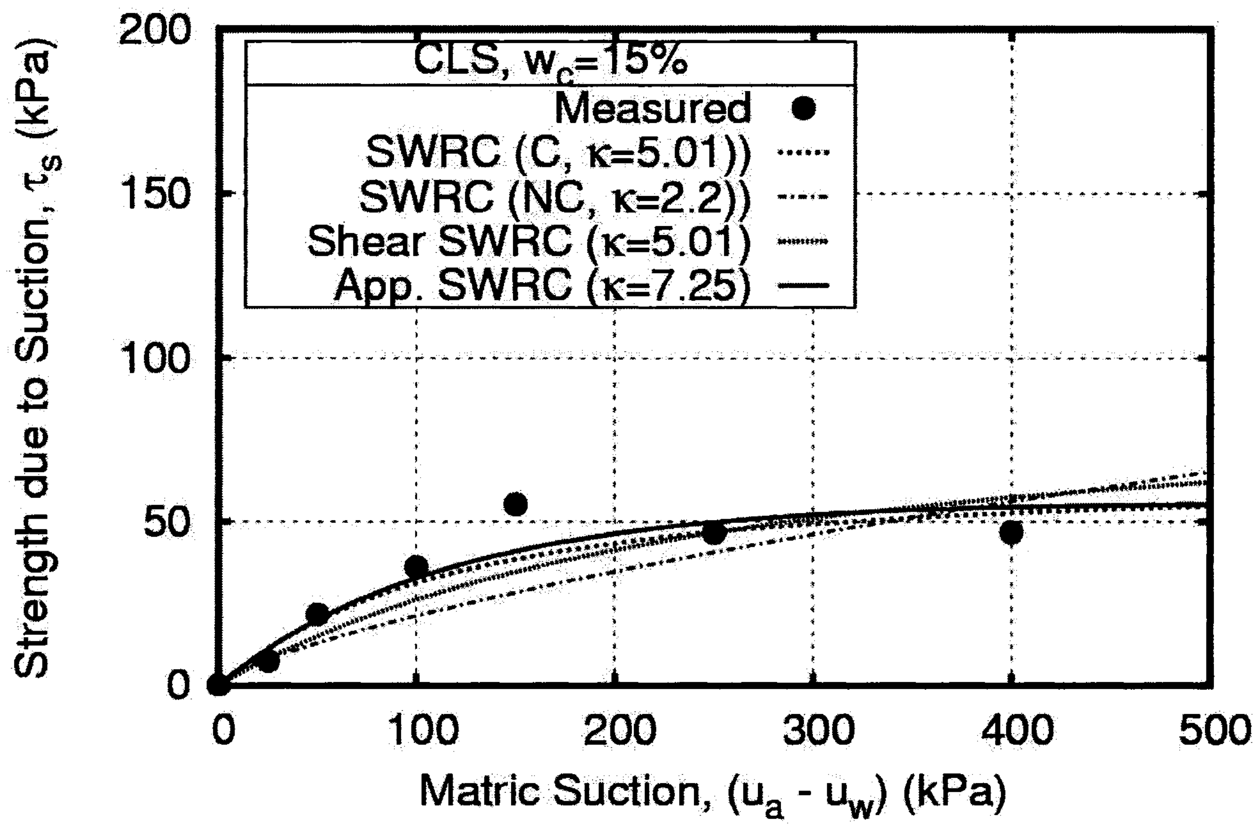

Figure 6.22 Prediction of the contribution of matric suction to the CLS shear strength of Indian Head till, using conventional SWRC from consolidatd (C) and non-consolidated (NC) specimens, and the apparent SWRC generated from post-shear data of a ring shear specimen compacted at a water content, w_c, of 15%.

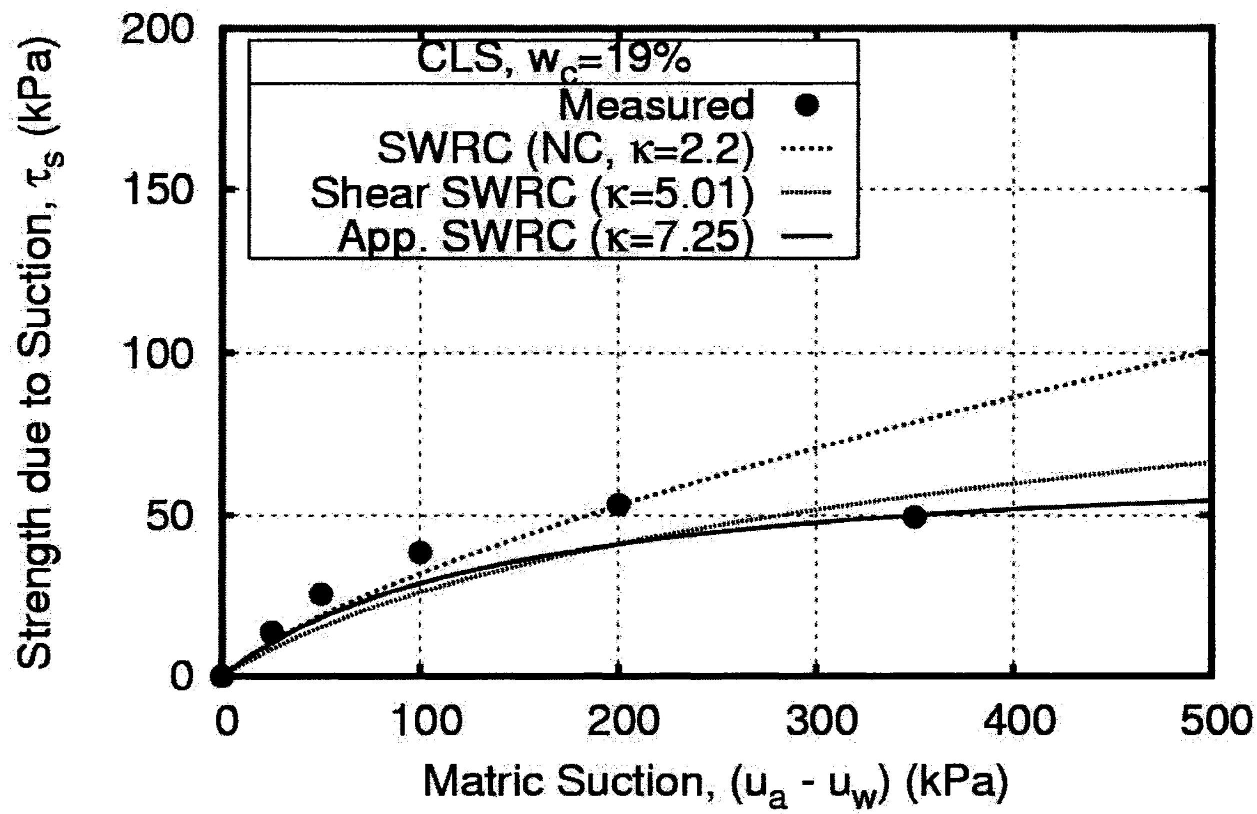

Figure 6.23 Prediction of the contribution of matric suction to the CLS shear strength of Indian Head till, using conventional SWRC and the apparent SWRC generated from post-shear data of a ring shear specimen compacted at a water content, w_c, of 19%.

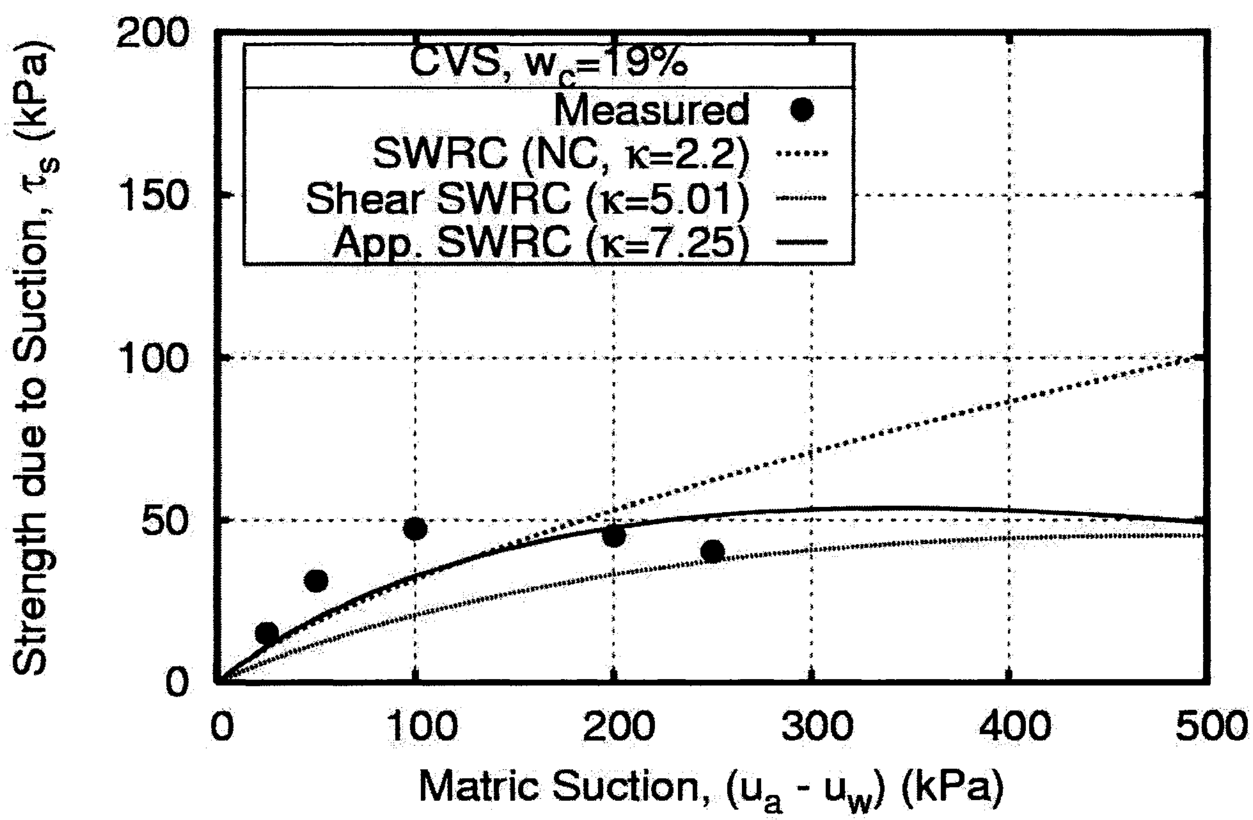

Figure 6.24 Prediction of the contribution of matric suction to the CVS shear strength of Indian Head till, using conventional SWRC and the apparent SWRC generated from post-shear data of a ring shear specimen compacted at a water content, w_c, of 19%.

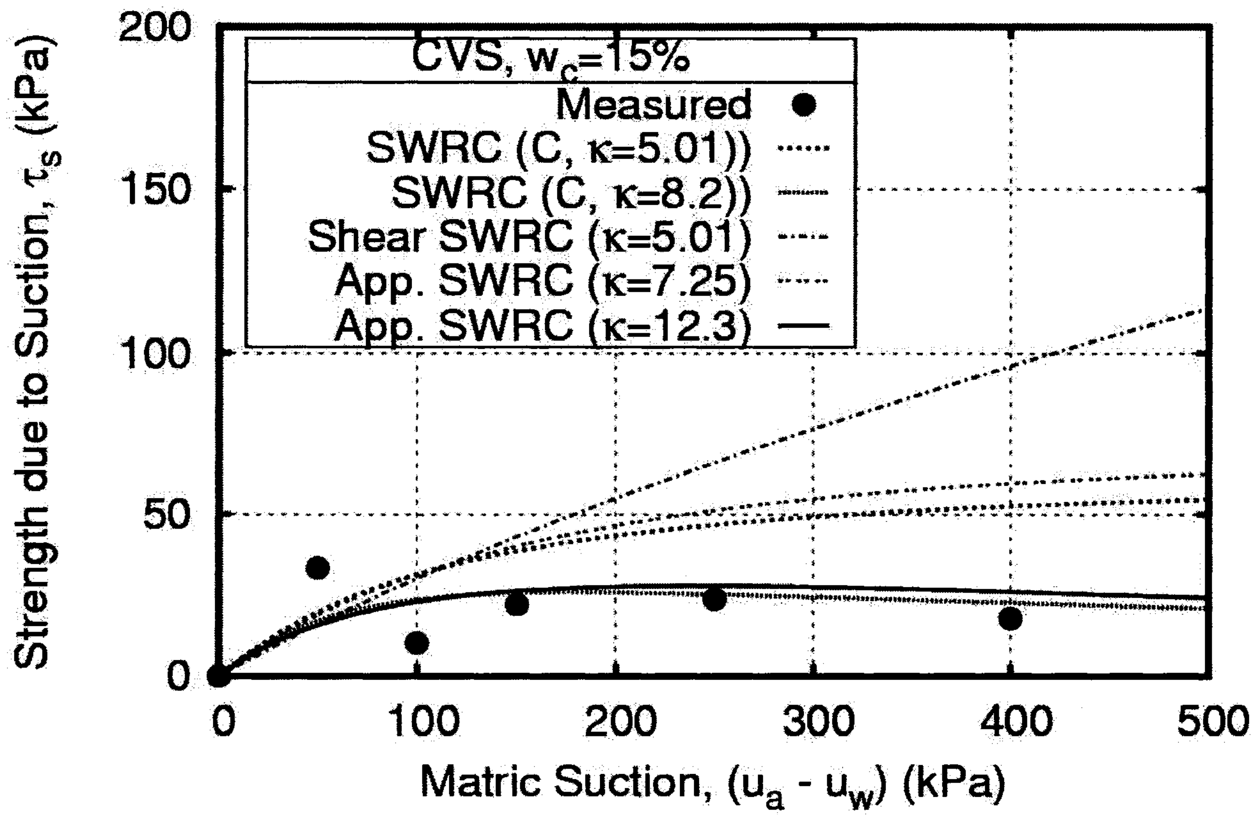

Figure 6.25 Prediction of the contribution of matric suction to the CVS shear strength of Indian Head till, using conventional SWRC and the apparent SWRC generated from post-shear data of a ring shear specimen compacted at a water content, w_c, of 15%.

7 Summary and Conclusions

7.1 Summary

Conventional testing equipment of saturated soils are not suitable to study the hydro-mechanical properties of unsaturated soils. It as therefore necessary design and build laboratory equipment that can be used to properly take into account the hydro-mechanical properties of unsaturated soils. To achieve this objective, a conventional ring shear apparatus was modified for testing of unsaturated soils, with matric suction control, and specimen water volume monitoring capabilities. Using this device, unsaturated soil specimens can be subjected to arbitrarily large deformations, thus permitting the study of the critical state of unsaturated soils.

Using this modified ring shear device, it is possible to determine both the peak (in single stage tests) and critical state shear strength envelopes, with respect to both the net normal stress and the matric suction. The device is also capable of subjecting specimens to various shearing conditions, namely: Constant Load and constant Suction (CLS), Constant Volume and constant Suction (CVS), Constant Load and constant Water content (CLW) and Constant Volume and constant Water content (CVW).

Furthermore, the modified ring shear apparatus can also be used to determine the soil-water retention curve (SWRC) can also be obtained for a single specimen under various conditions. Such conditions include subjecting the specimen to a constant volume, or a constant net normal load. This can be done for specimens that have been subjected to shear as well as specimens that have been simply compacted and consolidated. In addition, a single specimen can be subjected to a multistage shearing sequence and the equivalent SWRC obtained represents the end condition of each shearing stage.

In addition to the shear strength and volumetric properties, the study of unsaturated soils requires the precise monitoring of the changes in specimen water volume. To obtain reliable measurements, however, proper corrections must be applied to account for air diffusion and evaporation (Romero, 1999, 2001; Airò Farulla and Ferrari, 2005). In the current study, a procedure has been outlined to correct the water content readings from the water volume data acquired using an electronic balance connected to the modified ring shear apparatus. Using this data, it is possible to quantify the rate of air infiltration by the combined effect of air diffusion and leakage. The corrections discussed, also included the identification of the rate of moisture exchange between the specimen and the air in the cell through evaporation or condensation.

The investigation program has also included the development of a precise device that combines the volume gauge and the de-airing unit. Such a device can provide precise volumetric data from which both the specimen water content and the diffused air volume may be calculated. The volumetric data is subjected to the same corrections as the readings from the electronic balance used with the ring shear apparatus. It can be used in conjunction with any device that utilizes the axis-translation technique to obtain precise measurements (0.007 ml) of the volumetric changes of the specimen. Greater precision may be achieved by using an inner tube with a finer bore.

Finally, the research program has also included the development of a simple, yet precise pressure gauge that can be used in conjunction with devices that utilize the axis-translation technique. This pressure gauge is reliable, inexpensive, robust, and can be easily be constructed and upgraded if greater precision is required. Its operational characteristics make it well suited for axis-translation applications since for a given gauge tube length, it provides greater precision at lower values of applied pressures (i.e. matric suction), than at the higher values where lower precisions can be tolerated.

7.2 Conclusions

The key conclusions from the testing of Indian Head till using the modified ring shear apparatus are:

1. The rate of change of water content of the CVS tests, although lower than the CLS test, was in the same order of magnitude (0.1 to 0.15 ml as opposed to 0.3 ml for a shear deformation of approximately 20 mm). This behaviour was also clearly identifiable from the plots of water movement with time, while the specimen volume remained constant during the test. Such a behaviour suggests that shearing also affects the SWRC of the soil by means other than the volumetric strain. In particular, this suggests that the distribution of voids is affected by the shearing process.

2. The changes in the water content of the specimen with respect to shear deformation, in both CLS and CVS tests, can vary almost linearly for strain deformations that are considered to be large in the context of the modified triaxial and direct shear testing equipment. The 20 mm shear deformations imposed on most tests of the testing program represents a significant shear deformation for a 20 mm tall specimen such as those that were used in the tests of this research program. The shear strength and the volumetric strain plots demonstrate close to critical state conditions. However, it is only after shear deformation approaching 100 mm that the change of water content with respect to shear strain began showing a curvature. This indicates that a true representation of the ultimate conditions of unsaturated soils may require much larger shearing strains than are commonly applied in geotechnical laboratories. In other words, the condition of a constant degree of saturation must also be included in the definition of the critical state of unsaturated soils. The overall change in the degree of saturation due to shearing was small (in the order of 0.06% to 0.12%). However, given the little difference in water content between the suction increments (in the order of 0.12%) the influence of the shearing process was generally comparable. These results were obtained for specimens that were sheared to shear strains that were insufficient to reach critical state, however. A more extensive testing program, at larger strain deformations for a wider range of soils is required to investigate the full impact of shearing.

3. Shearing under constant volume conditions results in lower changes in water content as a function of shear deformation, than shearing under constant load conditions for a given shear

strain for a specimen compacted at low compaction energies. This is consistent with the fact that the changes in the SWRC during a CLS test are due to both the volumetric changes as to the pore space rearrangement. In CVS tests, the global void ratio remains the same and only pore space rearrangement would contribute to the changes in the SWRC.

4. The choice of SWRC, will have a marked influence on the prediction of the shear strength of unsaturated soils. The error increases as the degree of saturation decreases. The SWRC obtained using conventional procedues can be substantially different from the SWRC obtained from conventional methods. In particular, the maximum degree of saturation of the SWRC generated from shear data is lower than 100%, suggesting that entrapment of air occurs during the shearing process even though the matric suction was changed along the drying path. The calibration of models using SWRC obtained by conventional procedures, can fail to model these changes, and may result in poor prediction of the shear strength.

5. Subjecting the SWRC specimens to a stress history comparable to the stress history of the test specimens before the shearing process can markedly improve the shear strength predictions.

6. The apparent SWRC derived from the sheared specimens, results in a better prediction of the shear strength of the tested soil than the SWRC determined by using directly the degree of saturation of the sheared specimens for the entire range of suctions tested.

7. The modified ring shear apparatus appears to be best suited for the study of the critical state of unsaturated soils due to the apparently much larger strains required to achieve water equilibrium, as opposed to shear strength or volumetric equilibrium. In this respect, the short drainage path of the device gives it an additional advantage.

7.3 Suggestions For Further Research

The conclusions of this research program have underscored the fact that shearing at much larger strains must be conducted to truly assess the critical state of unsaturated soils. Therefore, a series of shear tests at strain deformations in excess of 100 mm should be conducted until water contents become as steady as the shear strength and the volumetric strain. This would permit the establishment of a true CSL for Indian Head till, or any other unsaturated soil.

The observations made in the current study permit the hypothesis that the CSL and continuously disturbed line (CDL) might actually be a single line. If this were true, then the differences in stress path between constant suction and constant water content tests would be the cause that larger strains are required for CLS tests to achieve the critical state. This in turn would cause the different types of tests to generate two parallel lines when conducted under insufficient shear strains. Therefore, to verify this hypothesis, in addition to the generation of true CSL at very large deformations, a full series of constant water content tests should also be undertaken to establish the CDL. This would allow the verification of whether the difference that was observe by Ridley (1995) between the CSL and the CDL, might not in fact be caused by the testing conditions.

Lastly, since the shearing process may have a significant impact on the SWRC of the tested specimen, it is suggested that extensive experimental studies should be undertaken to determine the changes of the SWRC during the shearing process. These changes should be accompanied by the generation of SWRC using conventional means, for soils consolidated at various normal stresses, along the both the drying and wetting paths. Models for the prediction of the changes of the SWRC during shearing would be valuable tool to combined with the equations predicting the shear strength of unsaturated soils using the SWRC.

The fitting parameter κ [Vanapalli and Fredlund (2000)] should be computed for various soils using the SWRC from sheared specimens and the scatter compared to that obtained base on conventional SWRC. Given the dependency of the SWRC on the stress history of the specimen, differences should be expected, with improved regularity at the ultimate state.

8 References

Airò Farulla, C., Ferrari, A., 2005, "Controlled suction oedometric tests: analysis of some experimental aspects", Advanced Experimental Unsaturated Soil Mechanics, Tarantino, Romero & Cui (eds), Trento, Italy: 43-48.

Aitchison, G.D., Donald, I.B. 1956, "Effective Stresses in Unsaturated Soils", Proceedings of the 2nd Australia-New Zealand Conf. Soil Mech. 83-88.

Alonso, E.E., Gens, A., Josa, A. 1990, "A constitutive model for partially saturated soils", Géotechnique, 40(3): 405-430.

Bao, C.G., Gong, B., Zhan, L., 1998, Properties of unsaturated soils and slope stability of expansive soil. Keynote Lecture, UNSAT 98, 2nd International Conference on Unsaturated Soils, Beijing.

Barbour, S.L., 1998, "Nineteeth Canadian Geotechnical Colloquium: The soil-water characteristic curve: a historical perspective", Can. J. Geotech. J., 35: 873-894

Bishop, A.W., 1959, "The principle of effective stress." Teknisk Ukeblad I Samarbeide Med Teknikk, Oslo, Norway: 106(39): 859-863.

Bishop, A.W., G.E. Blight, 1963, "Some aspects of effective stress in saturated and partly saturated soils", Géotechnique 13:177-197.

Bishop, A.., Donald, I.B. 1961, "The experimental study of partly saturated soil in the triaxial apparatus", Proc 5th ICOSMFE, Paris: 13-21.

Blatz, J.A., Graham, J. 2003, "Elastic-plastic modelling of unsaturated soil using results from a new triaxial test with controlled suction", Géotechnique, 53(1): 113-122.

Blight, G.E. 1967, "Effective stress evaluation for unsaturated soils", ASCE Journal of the soil mechanics and foundations division.: 125-149.

Buenfil, C., Romero, E., Lloret, A., Gens, A., 2005, Hydro-mechanical behaviour of a clayey silt under isotropic compression. Unsaturated soils: Experimental studies, T. Schanz (ed), Germany:331-342

Burland, J.B., 1965, "Some aspects of the mechanical behaviour of partly saturated soils" Proceedings of the conference on moisture equilibria and moisture changes in soil beneath covered areas, G.D. Aitchison (ed) London: Buttersworth: 270-278.

de Campos, T.M.P., Carrillo, C.W. 1995, "Direct shear testing on an unsaturated soils from Rio de Janeiro", Unsaturated Soils/Sols Non Saturés, Alonso & Delage (eds): 31-38.

Caruso, A., Tarantino, A., 2004, "A shear box for testing unsaturated soils from medium to high degrees of saturation.", Géotechnique, 54(4):281-284

Casagrande, A. 1936, "Characteristics of cohesionless soils affecting the stability of slopes and earth fills", Contributions to soil mechanics 1925-1940, Boston Society of Civil Engineers.

Castro, G., Poulos, S.J. 1977, "Factors affecting liquefaction and cyclic mobility", J. Geotechnical Engineering, ASCE, 103(6): 501-516.

Chiu, C.F., Ng, C.W.W. 2003, "A state-dependent elasto-plastic model for saturated and unsaturated soils", Géotechnique, 53(9): 809-829.

Croney, D., Coleman, J.D. 1954, "Soil Structure in Relation to Soil Suction", Journal of Soil Science, 5(1): 75-84.

Cui, Y.J., Delage, P., 1996, "Yielding and plastic behaviour of an unsaturated compacted silt.", Géotechnique, 46(2): 291-311.

Delage, P., Audiguier, M., Cui, Y.-J., Howat, M.D. 1996, "Microstructure of a compacted silt", Can. Geotech. J., 33: 150-158.

Delage, P, Fry, J.-J. 2000, "Comportement des sols compactés: apports de la mécanique des sols non saturés", Revue française de géotechnique., 92(3): 18-29.

Escario, V. 1980. Suction controlled penetration and shear test. In Proceedings of the 4th International Conference on Expansive Soils, Denver, Colo. American Society of Civil Engineers, New York 2: 780-797.

Escario, V., Juca, 1989, "Shear strength and deformation of partly saturated soils", Proceedings of the 12th International Conference on Soil Mechanics and Foundation Engineering, Rio de Janeiro, 2:43-46

Escario, V., Sáez, J. 1986, "The shear strength of partly saturated soils", Géotechnique, 36(13): 453-456.

Fredlund, D.G, 1975, "A Diffused Air Volume Indicator for Unsaturated Soils", Can. Geotech. J., 12: 533-539.

Fredlund, D.G., Morgenstern, N.R. 1977. "Stress state variables for unsaturated soils.", ASCE Journal of the Geotechnical Engineering Division, Proceedings, American Society of Civil Engineering (GT5), 103: 447-466.

Fredlund, D.G., Morgenstern, N.R., Widger, R.A. 1978, "The shear strength of unsaturated soils", Can. Geotech. J., 15(3): 313-321.

Fredlund, D.G., Rahardjo, H., 1993, "Soil mechanics for unsaturated soils", Wiley-International: 517

Fredlund, D.G., Rahardjo, H., Gan, J.K-M. 1987, "Nonlinearity of strength envelope for unsaturated soils", Proceedings 6th international conference on Expansive soils, New Delhi: 49-54.

Fredlund D.G., Xing, A. 1994, "Equations for the soil-water characteristic curve", Can. Geotech. J., 31: 521-532.

Gallipoli, D., Gens, A., Sharma, R., Vaunat, J., 2003, "An elasto-plastic model for unsaturated soil incorporating the effects of suction and degree of saturation on mechanical behaviour.", Géotechnique, 53(1): 123-136.

Gan, J.K.M., D.G. Fredlund, 1988, "Multistage Direct Shear Testing of Unsaturated Soils," ASTM, Geotech. Testing J., 11(2):132-138.

Garga, V.K., Infante Sedano, J. A. 2002. Steady State Strength of Sands in a Constant Volume Ring Shear Apparatus, Geotechnical Testing Journal, GTJODJ, 25(4).

Herkal, R.N., Vatsala,A., Srinivasa Murthy, B.R. 1999, "Triaxial compression and shear tests on partly saturated soils", Proc. 1st Int. conf. on Unsat. Soils. Paris.: 109-116.

Hettiaratchi, D.R.P., O' Sullivan, M.F., Campbell, D.J. 1992. A constant cell volume triaxial testing technique for evaluating critical state parameters of unsaturated soils., Journal of Soil Science, 43: 791-806.

Hilf, J.W. 1956, "An investigation of pore water pressure in compacted cohesive soils", US Bureau of Reclamation, Tech. Mem. 654, Denver: US Bureau of Reclamation.

Ho DYF, Fredlund DG 1982. A multi-stage triaxial test for unsaturated soils. ASTM Geotechnical Testing Journal 5 (1): 18-25.

Infante Sedano, J.A. 1998, "Constant volume ring shear test for sand", M.A.Sc. Dissertation, University of Ottawa, Ottawa, Canada.

Infante Sedano, J.A., Garga, V.K.A, Vanapalli, S.K., 2002. Influence of volume change on the prediction of the shear strength of unsaturated soils. Proceedings of the 55th Canadian Geotechnical Conference, Niagara Falls, 1269-1276.

Jennings, J.E.B., Burland, J.B. 1962, "Limitations to the use of effective stresses in partly saturated soils", Géotechnique, 12: 125-144.

Khalili, N., Khabbaz, M.H. 1998, "A unique relationship for c for the determination of the shear strength of unsaturated soils", Géotechnique, 48(5): 681-687.

Likos, W.J., Lu, N., 2003. "Automated humidity system for measuring total suction characteristics of clay." Geotechnical Testing Journal, 26(2): 179-190.

Maatouk, A., Leroueil, S.,Rochelle, P.L.A. 1995, "Yielding, and critical state of a collapsible unsaturated silty soil.", Géotechnique, 45(3): 465-477.

Morgenstern, N.R. 1979, "Properties of compacted soils", Contributions to panel discussion, session IV, Proc. of the 6th Panamerican Conf. Soil Mech. Found. Eng. (Lima, Peru), 3: 349-354.

Murray, E.J. 2002, "An equation of state for unsaturated soils", Can. Geotech. J., 39: 125-140.

Ng, C.W.W., Zhan, L.T., Cui, Y.J., 2002, "A new simple system for measureing volume changes in usnaturated soils", Can. Geotech. J. 39: 757-764.

Öberg, A.L., Sällfors, G. 1997, "Determination of shear strength parameters of unsaturated silts and sands based on the water retention curve", American Society for Testing and Materials.

Poorooshab, H.B. 1989, "Description of flow of sand using state parameters", Computers and Geotechnics, 8: 195-218.

Poulos, S.J. 1981, "The steady state of deformation", J. Geotechnical Engineering, ASCE, 107(5): 553-562.

Rampino, C., Mancuso, C., Vinale, F., 2000, " Experimental behaviour and modelling of an unsaturated compacted soil." Can. Geotech. J., 37: 748-763

Rao, S.M., Revanasiddappa, K. 2003, "Role of soil structure and matric suction in collapse of a compacted clay soil", Geotechnical Testing Journal, GTJODJ, 26(1): 102-109.

Rassam, D.W., Cook, F. 2002, "Predicting the Shear Strength Envelope of Unsaturated Soils", Geotechnical Testing Journal, GTJODJ, 25(2): 215-220.

Rassam, D.W., Williams, D.J. 1999, "A relationship describing the shear strength of unsaturated soils", Can. Geotech. J., 36: 363-368.

Ridley, A.M. 1993, "The measurement of soil moisture suction", Ph.D. dissertation, University of London (Imperial College of Science, Technology and Medicine), London, England.

Ridley, A.M. 1995, "Strength-suction-moisture content relationships for kaolin under normal atmospheric conditions", Unsaturated Soils/Sols Non Saturés, Alonso & Delage (eds): 645-651.

Romero, E. 1999, “Characterisation and thermo-hydro-mechanical behaviour of unsaturated Boom clay: an experimental study”, Tesis doctoral, Universitat Politecnica de Catalynya, Barcelona.

Romero, E., 2001, “Controlled suction techniques”, 4° Simposio Brasileiro de Solos Nao Saturados. W.Y.Y. Gehlding and F. Schnaid (eds), Porto Alegre, Brasil: 535-542

Romero, E., Gens, A., Lloret, A. 1999, "Water permeability, water retention, and microstructure of unsaturated compacted Boom clay", Eng. Geol., 54: 117-127.

Romero, E., Vaunat, J., 2000, “Retention curves in deformatble clays.” Experimental evidence and theoretical approaches in unsaturated soils, A. Tarantinoo and C. Mancuso (eds), Rotterdam: A.A. Balkema: 91-106.

Roscoe, K.H., Schofield, A.N. and Wroth, C.P. 1958, "On the yielding of soils", Géotechnique, 8(1): 22-53.

Satija, B.S. 1978, “Shear behaviour of partially saturated soils”, Ph.D. Thesis, Indian Institute of Technology, Delhi.

Tarantino, A., Tombolato, S., 2005, “Coupling of hydraulic and mechanical behaviour in unsaturated compacted clay.”, Géotechnique, 55(4): 307-317

Tekinsoy, M.A., Kayadelen, C., Keskin, M.S., Soylemez, M. (2004) “An equation for predicting shear strength envelope with respect to matric suction.” *Computers and Geotechnics*, 31(7), 589-593.

Toll, D.G. 1990, "A framework for unsaturated soil behaviour", Géotechnique, 40(1): 31-44.

Vanapalli, S.K. 1994 “Simple test procedures and their interpretation in evaluating the shear strength of an unsaturated soil.”, Ph.D. Thesis, University of Saskatchewan, Saskatoon, Saskatchewan. 351 p

Vanapalli, S.K., Fredlund, D.G 2000, "Comparison of different procedures to predict unsaturated soil shear strength", ASTM Proceedings, Unsaturated Soils, Geo-Denver 2000, Special Publication No. 99: 195-209.

Vanapalli, S.K., Fredlund, D.G., Pufahl, D.E., Clifton, A.W. 1996, "Model for the prediction of shear strength with respect to soil suction", Can. Geotech. J., 33: 379-392.

Vanapalli, S.K., Garga, V.K., Infante Sedano, J.A. 2003. A rigorous approach of predicting the shear strength of unsaturated soils. Proceedings of the 2nd Asian Conference on Unsaturated soils, USAT-ASIA, editors: Karube et al. ,Osaska, Japan, 253-258.

Vatsala, A., Srinivasa Murthy, B.R. 2002, "Suction in compacted states", Géotechnique, 52(4): 279-283.

Wang, X., Benson, C.H., 2003, “Leak-Free Pressure Plate Extractor For Measuring the Soil Water Characteristic Curve”, Geotechnical Testing Journal, GTJODJ,27(2)

Wheeler, S.J. 1988, "The undrained shear strength of soils containing large gas bubbles", Géotechnique, 38(3): 399-413.

Wheeler, S.J. 1991, "Technical Note: An alternative framework for unsaturated soil behaviour", Géotechnique, 41(2): 257-261.

Wheeler, S.J., Sharma, R.S., Buisson, M.S.R. 2003, “Coupling of hydraulic hysteresis and stress-strain behaviour in unsaturated soils.”, Géotechnique, 53(1): 41-54.

Wheeler, S.J., Sivakumar, V. 1995, "An elasto-plastic critical state framework for unsaturated soil.", Géotechnique, 45(1): 35-53.

Wheeler, S.J., Sivakumar, V., 2000, "Influence of compaction procedure on the mechanical behaviour of an unsaturated compacted clay. Part 2: shearing and constitutive modelling.", Géotechnique, 50(4): 369-376.

Xu, Y. F., Sun, D. A., 2001, "Determination of unsaturated shear strength using a fractal model." Fractals, 9(1), 51-60.

Yin, J.H. 2003, "A double cell triaxial system for continuous measurement of volume changes of an unsaturated or saturated soil specimen in triaxial testing", Geotechnical Testing Journal, GTJODJ, 26(3): 353-0.

List of Figures

Figure 2.1 Relationship between the fitting parameter κ and the plasticity index of a soil [from Vanapalli and Fredlund (2000)]. 27
Figure 2.2 Graphical representation of Eq. 2.7 [from Rassam and Cook (2002)]. 28
Figure 2.3 Strength -suction-moisture condition of kaolin at failure [from Ridley(1995)]. 29
Figure 2.4 Yield surfaces in (p,q,s) space [from Alonso et. Al (1990)]. 30
Figure 2.5 Three-dimensional view of the yield surfaces in (p, q, s) stress space [from Alonso et. al (1990)] 31
Figure 2.6 Plots of q versus p'c at critical states from the data of Wheeler and Sivakumar (1995) [from Murray (2002)] 32
Figure 2.7 Ratio between inter-particle forces at suction s and at null suction due to a water meniscus located at the contact between two identical spheres [from Gallipoli et al. 2003]. 33
Figure 2.8 Schematic of the triaxial cell used by Bishop and Donald (1961). 34
Figure 2.9 Triaxial cell used by Ng et al. (2002). 35
Figure 2.10 Triaxial cell used by Wheeler (1988). 36
Figure 2.11 Modified direct shear device used by Gan et al. (1988). 37
Figure 2.12 Direct shear test apparatus used by de Campos and Carrillo (1995). 38
Figure 2.13 Transducer used by Ridley (1993). 39
Figure 2.14 Direction of water movement in a twin burette system with the three-way valves opened to the left, (a), and to the right, (b) [from Fredlund and Rahardjo (1993)]. 40
Figure 2.15 Volumetric pressure plate extractor with hysteresis attachments [Soilmoisture Equipment Corp. (1985)]. 41
Figure 2.16 Bubble pump an air trap [from Bishop and Donald (1961)]. 42
Figure 2.17 Diffused air volume indicator [from Fredlund (1975)]. 43
Figure 2.18 Measurement of the diffused air volume under isothermal conditions [from Fredlund and Rahardjo (1993)]. 44
Figure 2.19 Settlement and water volume change versus time during equalization step [after Airò Farulla and Ferrari (2005)]. 45
Figure 3.1 Conceptual model of the pressure gauge. 59
Figure 3.2 Pressure gauge designed with the aid of Mariotte bottle and a 343 mm long scale. 60
Figure 3.3 Schematic of pressure reading system 61
Figure 3.4. Design of a check valve using a 1 cc syringe and a small spring. 62
Figure 3.5 The operation of the syringe check valve. 63
Figure 3.6 Illustration of the generation of a pressure scale for a number of predetermined gauge pressure values ΔP. 64
Figure 3.7 Interface to the macro program to generate a custom graduated pressure scale. 65
Figure 3.8 Custom horizontal and vertical scales generated for an atmospheric pressure of 101.3, and a trapped air length of 300 mm. 66
Figure 3.9 Calibration of a 430 mm long horizontal gauge tube, with both increasing and decreasing pressures. 67
Figure 3.10 Random samples of the atmospheric pressure taken in Ottawa, Canada, during a period of almost 4 months. Data from Environment Canada. 68

Figure 3.11 Variations of the pressure reading for a gauge of 430 mm trapped air length using either an average atmospheric pressure Po of 101.3 kPa or ± 1 standard deviation (0.87 kPa). 69
Figure 3.12 Relationship of the relative error in measurement at the standard deviation boundaries with respect to gauge pressure ΔP, for different lengths of gauge tube lengths Lo. 70
Figure 3.13 Two valves to atmosphere can be added to facilitate resetting of the pressure gauge. 71
Figure 3.14 Soil water rentention curves for 3 different sands (silty sand, Barahona sand, washed concrete sand), generated using the trapped air column pressure gauge for a range from 1 to 500 kPa. 72
Figure 3.15 View of the flushing system/volumetric gauge apparatus connected to a tempe cell for axis translation technique. 73
Figure 3.16 Schematic view of the flushing/gauge system. 74
Figure 3.17 Inner tube is raised for flushing (a), and lowered for taking readings (b). 75
Figure 3.18 Adding spacers to increase range of readings. 76
Figure 3.19 Calibration of the volume gauge. 77
Figure 3.20 Air outflow (during lowering of inner tube or rise in water level), and inflow (during raising of the inner tube, or decrease of water level). 78
Figure 4.1 Cross-section of the modified ring shear cell. 93
Figure 4.2 Base of the ring shear cell showing details of the flushing system. 94
Figure 4.3 Base of the unsaturated ring shear cell with ceramic discs and inner confining ring stacks in place. 95
Figure 4.4 Dearing groove disposition under the ceramic discs. 96
Figure 4.5 Bottom platen of the modified ring shear test apparatus. 97
Figure 4.6 Torque arm extension. 98
Figure 4.7 Idealized schematic of the de-airing system, including the groove found below the ceramic discs, and the tubes leading to the pump, and the air trap. 99
Figure 4.8 Schematic view of a simple gear pump. 100
Figure 4.9 1 ml syringe used to reset the water level in the air trap, and provide confirmation reading on the volume of removed air. 101
Figure 4.10 Close up view showing the dampening mass added to the lower part of the last segment of the overflow tube. 102
Figure 4.11 Instrumentation of the modified Ring Shear Test apparatus. 103
Figure 4.12 Pressure regulators used to control the normal stress and applied air pressure. 104
Figure 4.13 Actuator converting the air pressure into a normal force. 105
Figure 4.14 Alignment ring. 106
Figure 4.15 Compactor loading block and ring shear cell. 107
Figure 4.16 View showing the uplifted central portion of the loading foot used to align the specimen with the loading rod. 108
Figure 4.17 Static compaction loading frame of a specimen. 109
Figure 5.1 Grain size distribution of the Indian Head glacial till. 135
Figure 5.2 Compaction curves of Indian Head glacial till. Proctor density is compared to static compaction at compaction loads of 750 kPa, and 375 kPa respectively. 136
Figure 5.3 Drill press used to statically compact an oedometer specimen. 137
Figure 5.4 Compaction force applied to a 50 mm diameter oedometer specimen. 138
Figure 5.5 Compaction energy curve for an Indian Head Till specimen compacted at a water content of 15% under a vertical compaction stress of 375 kPa. 139
Figure 5.6 Shear strength envelopes at large deformations of Indian Head glacial till compacted at a

water content of 19%. 140
Figure 5.7 SWRC obtained from specimens compacted at two different water contents . Some specimens were consolidated in saturated conditions under a net normal stress of 150 kPa. Each point represents the average of 3 samples. 141
Figure 5.8 Typical overflow readings during a matric suction increment phase. 142
Figure 5.9 Extracting diffusion rate from recorded water movement data between flushing stages. 143
Figure 5.10 Readings realigned into a continuous curve, as if deairing cycles had not been conducted. 144
Figure 5.11 Illustration of the correction of rate anomalies due to flushing operations. 145
Figure 5.12 The calculated diffusion rate is used to remove the cumulative air diffusion from the continuous readings curve. 146
Figure 5.13 Water mass readings corrected for evaporation/condensation. 147
Figure 5.14 Failure envelope of an Indian Head till specimen sheared under CLS conditions. The compaction water content, wc, was 15% and the applied net normal stress was 150 kPa. 148
Figure 5.15 Failure envelope of an Indian Head till specimen sheared under CLS conditions. The compaction water content, wc, was 19% and the applied net normal stress was 150 kPa. 149
Figure 5.16 Difference between the pseudo peak and the residual failure envelopes with respect to matric suction for a specimen compacted at at water content, wc, of 19%, tested under CLS conditions under a net normal stress of 150 kPa. 150
Figure 5.17 Typical stress/deformation relationship for a CLS test on a ring shear specimen compacted at 15% and consolidated under saturated conditions under 150 kPa normal load. 151
Figure 5.18 Stress-deformation curves for specimens compacted at a water content of 15% and sheared under a constant net normal stress of 150 kPa. 152
Figure 5.19 Stress-deformation curves for specimens compacted at a water content of 19% and sheared under a constant net normal stress of 150 kPa. 153
Figure 5.20 Vertical deformation plots for soils compacted at a water content of 15%, and sheared at a constant normal stress of 150 kPa. 154
Figure 5.21 Typical plot of the change of water mass reading as a function of time. (CLS, wc = 15%, (ua – uw) from 25 kPa to 50 kPa). The two vertical lines indicate the shear period. 155
Figure 5.22 Rate of water overflow in grams per day. The onset of shear is clearly visible as a sudden increase in the water mass rate readings. 156
Figure 5.23 Variation of the water content of a specimen, compacted at a water content, wc, of 15%, during CLS shear at various matric suctions (CLS). 157
Figure 5.24 Variation of the water content of a specimen, compacted at a water content, wc, of 19%, during CLS shear at various matric suctions. 158
Figure 5.25 Variation of the water ratio, ew, of a specimen, compacted at a water content, wc, of 15%, during CLS shear at various matric suctions. 159
Figure 5.26 Variation of the water ratio, ew, of a specimen, compacted at a water content, wc, of 19%, during CLS shear at various matric suctions. 160
Figure 5.27 Water content changes from water content at beginning of shear, Δw, for a specimen, compacted at a water content, wc, of 15%, and sheared in CLS conditions at various matric suctions. 161
Figure 5.28 Variation of the degree of saturation, S, of a specimen, compacted at a water content, wc, of 15%, during CLS shear at various matric suctions. 162
Figure 5.29 Variation of the void ratio for a specimen, compacted at a water content of 15%, and sheared under CLS conditions at a net normal stress of 150 kPa. 163

Figure 5.30 Failure envelope with respect to matric suction for specimens tested under CVS conditions. The compaction water content ,wc,was 15%. 164
Figure 5.31 Failure envelopes for a specimen of Indian Head till tested under CVS conditions. The compaction water content, wc, was 19%. 165
Figure 5.32 Stress-deformation curves for CVS shear tests on soils compacted at a water content, wc, of 15%. 166
Figure 5.33 Variation of the normal stress during CVS tests. 167
Figure 5.34 Vertical deformation plots for till compacted at a water content of 15%, and sheared at a constant normal stress of 150 kPa. 168
Figure 5.35 Void ratio during CVS shear for a specimen compacted at a water content, wc, of 15%. 169
Figure 5.36 Water mass readings as a function of time for a CVS specimen compacted at a water content, wc, of 15%, under a net normal load (σ-ua) of 150 kPa, and a matric suction (ua – uw) of 50 kPa. 170
Figure 5.37 The change of water content for specimen compacted at a water content, wc, of 15%, including CVS (multi-stage and single stage)and CLS tests. The suction values range from 25 to 400 kPa, and the shear rate is either 0.022 mm/min or 0.048 mm/min. 171
Figure 5.38 CVS tests on specimens tested at a matric suction, (ua – uw), of 150 kPa. 172
Figure 5.39 The change of water content for specimen compacted at a water content, wc, of 15%, during CVS tests. The suction values range from 25 to 400 kPa, and the shear rate is either 0.022 mm/min or 0.048 mm/min. 173
Figure 5.40 Comparison of the change in water content in CVS shear test for specimens compacted at a water content, wc, of 15% and sheared to 20 mm, or 95 mm displacements. 174
Figure 5.41 Shear strength versus net normal stress for ring shear tests on unsaturated Indian Head till. 175
Figure 5.42 Shear strength versus matric suction for ring shear tests on unsaturated Indian Head till. 176
Figure 5.43 Relationship between the void ratio and the net normal stress at ultimate conditions from ring shear tests on unsaturated Indian Head till. 177
Figure 5.44 Relationship of the void ratio to the matric suction at ultimate state conditions for ring shear tests on unsaturated Indian Head till. 178
Figure 5.45 Critical state line (CSL) relating gravimetric water content, w, to matric suction, (ua-uw), for Indian Head Till for single stage (SS) and multi-stage (MS) ring shear tests. 179
Figure 5.46 Critical state line (CSL) relating water ratio, ew, to matric suction, (ua-uw), for Indian Head Till for single stage (SS) and multi-stage (MS) ring shear tests. 180
Figure 5.47 Shear strength of unsaturated Indian Head till plotted against an average skeleton stress defined in terms of the degree of saturation, S. 181
Figure 5.48 Shear strength of unsaturated Indian Head till plotted against an average skeleton stress defined in terms of the degree of saturation of the macro-voids, SrM. 182
Figure 5.49 Ultimate shear strength of unsaturated Indian Head till plotted against an average skeleton stress defined in terms of the exponential degree of saturation, Sk. Fitting parameter, κ, is obtained from plasticity chart. 183
Figure 5.50 Ultimate shear strength of unsaturated Indian Head till plotted against an average skeleton stress defined in terms of the exponential degree of saturation, Sk. Fitting parameter, κ, is back-calculated from ring shear test results. 184
Figure 6.1 Fitting parameter κ versus plasticity index, Ip [from Vanapalli and Fredlund, (2000)]. 197
Figure 6.2 Soil-water retention curve data derived from the triaxial shear test results undertaken on

Dhanauri clay specimens tested under a confining pressure of 96 kPa. 198
Figure 6.3 Measured and predicted shear strength of Dhanauri clay for a suction range of 0 to 400 kPa and a net confining pressure of 96kPa. 199
Figure 6.4 Measured and predicted shear strength of Dhanauri clay for a net confining pressure of 96 kPa. 200
Figure 6.5 Soil-water retention curve data derived from the triaxial shear test results undertaken on Dhanauri clay specimens tested under a net confining pressure of 386 kPa. 201
Figure 6.6 Measured and predicted shear strength of Dhanauri clay for a suction range of 0 to 400 kPa and a net confining pressure of 386kPa 202
Figure 6.7 Measured and predicted shear strength of Dhanauri clay for a net confining pressure of 386kPa 203
Figure 6.8 SWRC for Indian Head till specimens compacted at 15% and 19% water contents. A series of 15% specimens were consolidated, after saturation, under a normal stress of 150 kPa.. 204
Figure 6.9 SWRC from the sheared specimen compacted at water contents,wc, of 19% and 15% compared to the consolidated (C) and non-consolidated (NC) SWRC obtained by conventional means on specimens compacted at a water content of 15% and 19% (NC only). The ring shear specimen and consolidated SWRC specimen were consolidated under a vertical stress of 150 kPa. 205
Figure 6.10 Apparent SWRC from the sheared specimen compacted at water contents,wc, of 19% and 15% compared to the consolidated (C) and non-consolidated (NC) SWRC obtained by conventional means on specimens compacted at a water content of 15% and 19% (NC only). The ring shear specimen and consolidated SWRC specimen were consolidated under a vertical stress of 150 kPa. 206
Figure 6.11 SWRC generated from pre-shear and post-shear conditions on a CLS specimen compacted at a water content, wc, of 19%. 207
Figure 6.12 Suction contribution due to suction predicted from a κ=2.2 obtained from the plasticity chart, and using conventional SWRC curves. 208
Figure 6.13 Suction contribution due to suction predicted from a κ=5.01 obtained by fitting the data from strength at large deformations, and using conventional SWRC curves. 209
Figure 6.14 Prediction of CLS shear strength of Indian Head till, using conventional SWRC from consolidated (C) and non-consolidated (NC) specimens and using the SWRC generated from post-shear data of a ring shear specimen compacted at a water content, wc, of 15%. This prediction uses a κ=2.2 from the plasticity chart. 210
Figure 6.15 Prediction of CLS shear strength of Indian Head till, using conventional SWRC from consolidated (C) and non-consolidated (NC) specimens and using the SWRC generated from post-shear data of a ring shear specimen compacted at a water content, wc, of 15%. This prediction uses a κ=5.01 fitted from shear strength at large deformations. 211
Figure 6.16 Prediction of CLS shear strength of Indian Head till, using conventional SWRC from non-consolidated (NC) specimens and using the SWRC generated from post-shear data of a ring shear specimen compacted at a water content, wc, of 19%. This prediction uses a κ=2.2 from the plasticity chart. 212
Figure 6.17 Prediction of CLS shear strength of Indian Head till, using conventional SWRC from non-consolidated (NC) specimens and using the SWRC generated from post-shear data of a ring shear specimen compacted at a water content, wc, of 19%. This prediction uses a κ=5.01 fitted from shear strength at large deformations. 213
Figure 6.18 Prediction of the contribution of matric suction to the CVS shear strength of Indian Head

till, using conventional SWRC from consolidated (C) and non-consolidated (NC) specimens and the SWRC generated from post-shear data of a ring shear specimen compacted at a water content, wc, of 15%. This prediction uses a κ=2.2 from the plasticity chart. 214
Figure 6.19 Prediction of the contribution of matric suction to the CVS shear strength of Indian Head till, using conventional SWRC from consolidated (C) and non-consolidated (NC) specimens and the SWRC generated from post-shear data of a ring shear specimen compacted at a water content, wc, of 15%. This prediction uses a κ=5.01 fitted from shear strength at large deformations. 215
Figure 6.20 Prediction of the contribution of matric suction to the CVS shear strength of Indian Head till, using conventional SWRC and the SWRC generated from post-shear data of a ring shear specimen compacted at a water content, wc, of 19%. This prediction uses a κ=2.2 from the plasticity chart. 216
Figure 6.21 Prediction of the contribution of matric suction to the CVS shear strength of Indian Head till, using conventional SWRC and the SWRC generated from post-shear data of a ring shear specimen compacted at a water content, wc, of 19%. This prediction uses a κ=5.01 fitted from shear strength at large deformations. 217
Figure 6.22 Prediction of the contribution of matric suction to the CLS shear strength of Indian Head till, using conventional SWRC from consolidatd (C) and non-consolidated (NC) specimens, and the apparent SWRC generated from post-shear data of a ring shear specimen compacted at a water content, wc, of 15%. 218
Figure 6.23 Prediction of the contribution of matric suction to the CLS shear strength of Indian Head till, using conventional SWRC and the apparent SWRC generated from post-shear data of a ring shear specimen compacted at a water content, wc, of 19%. 219
Figure 6.24 Prediction of the contribution of matric suction to the CVS shear strength of Indian Head till, using conventional SWRC and the apparent SWRC generated from post-shear data of a ring shear specimen compacted at a water content, wc, of 19%. 220
Figure 6.25 Prediction of the contribution of matric suction to the CVS shear strength of Indian Head till, using conventional SWRC and the apparent SWRC generated from post-shear data of a ring shear specimen compacted at a water content, wc, of 15%. 221

Appendix A

Machine Shop Drawings

Drawings of Modified Ring Shear Cell

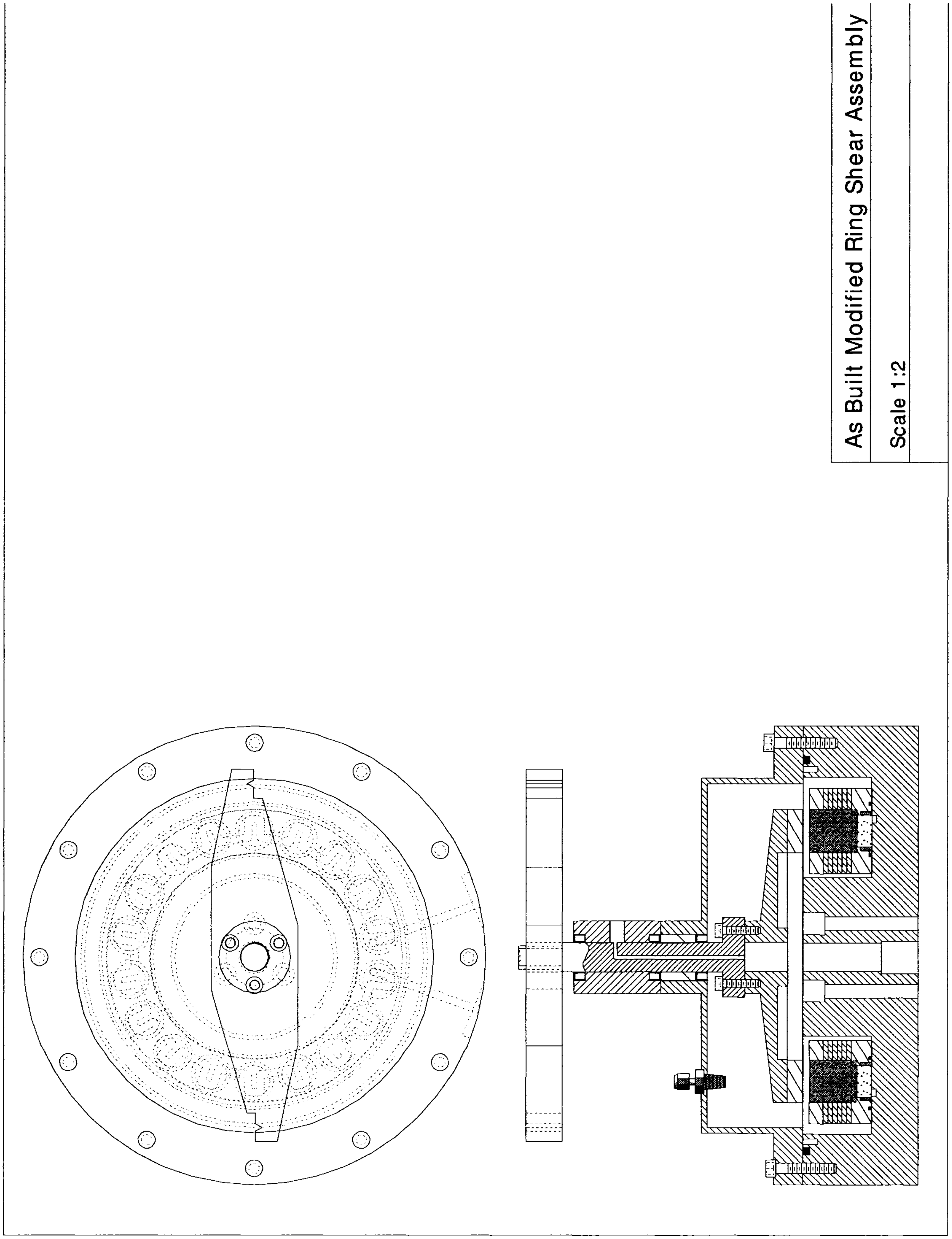
As Built Modified Ring Shear Assembly
Scale 1:2

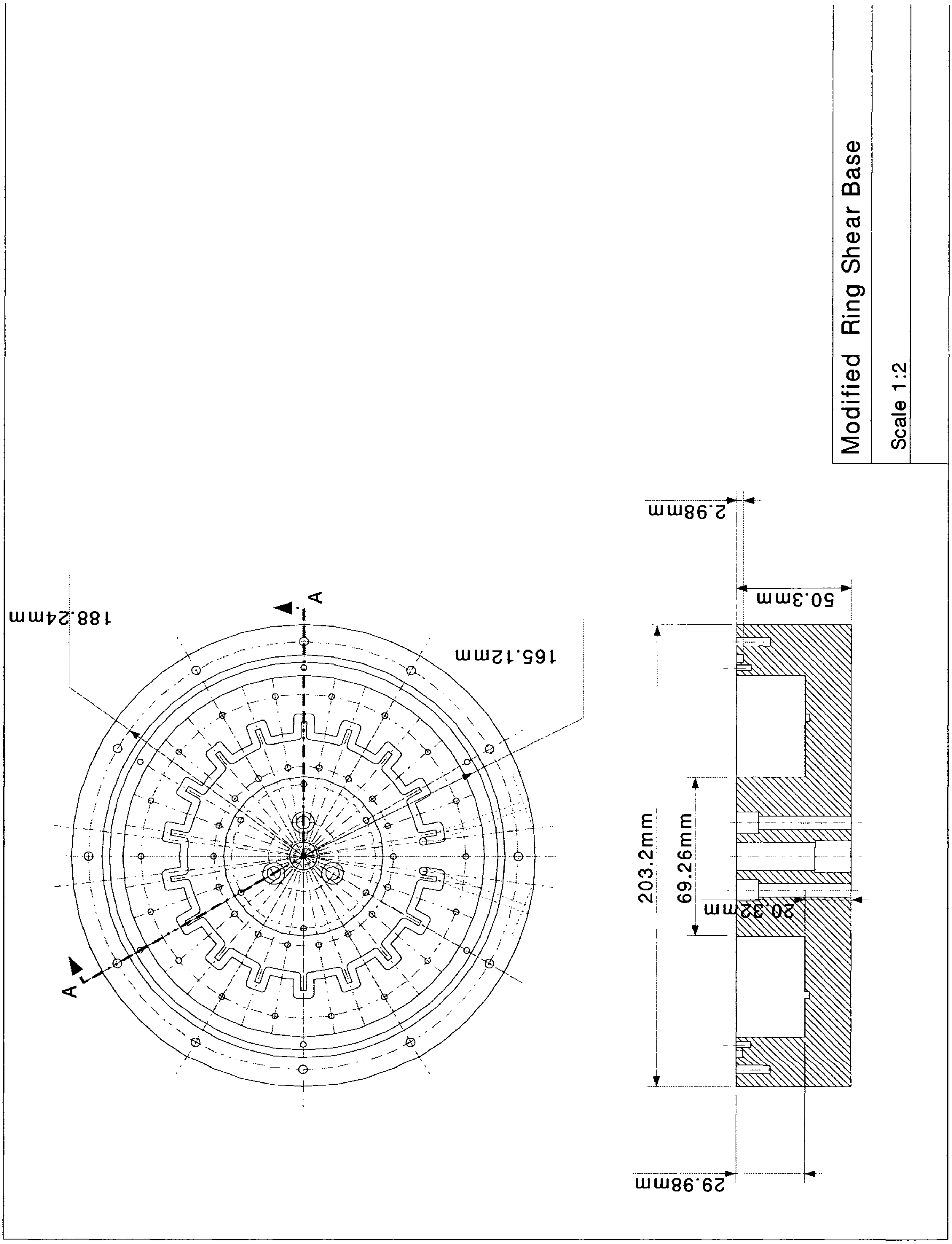
Modified Ring Shear Base
Scale 1:2
188.24mm
165.12mm
A
A
203.2mm
69.26mm
20.32mm
50.3mm
2.98mm
29.98mm

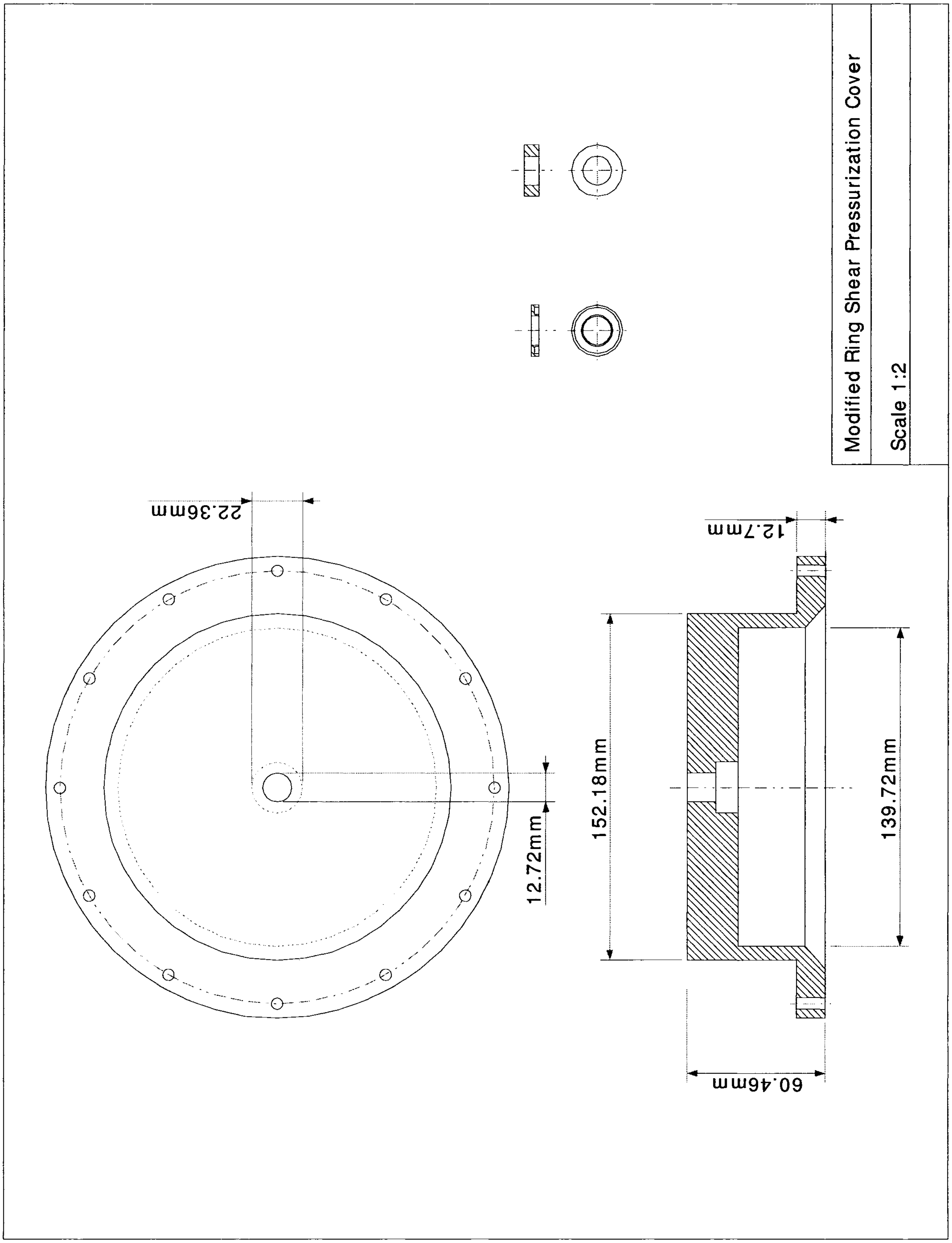
Modified Ring Shear Pressurization Cover
Scale 1:2
22.36mm
12.72mm
152.18mm
139.72mm
12.7mm
60.46mm

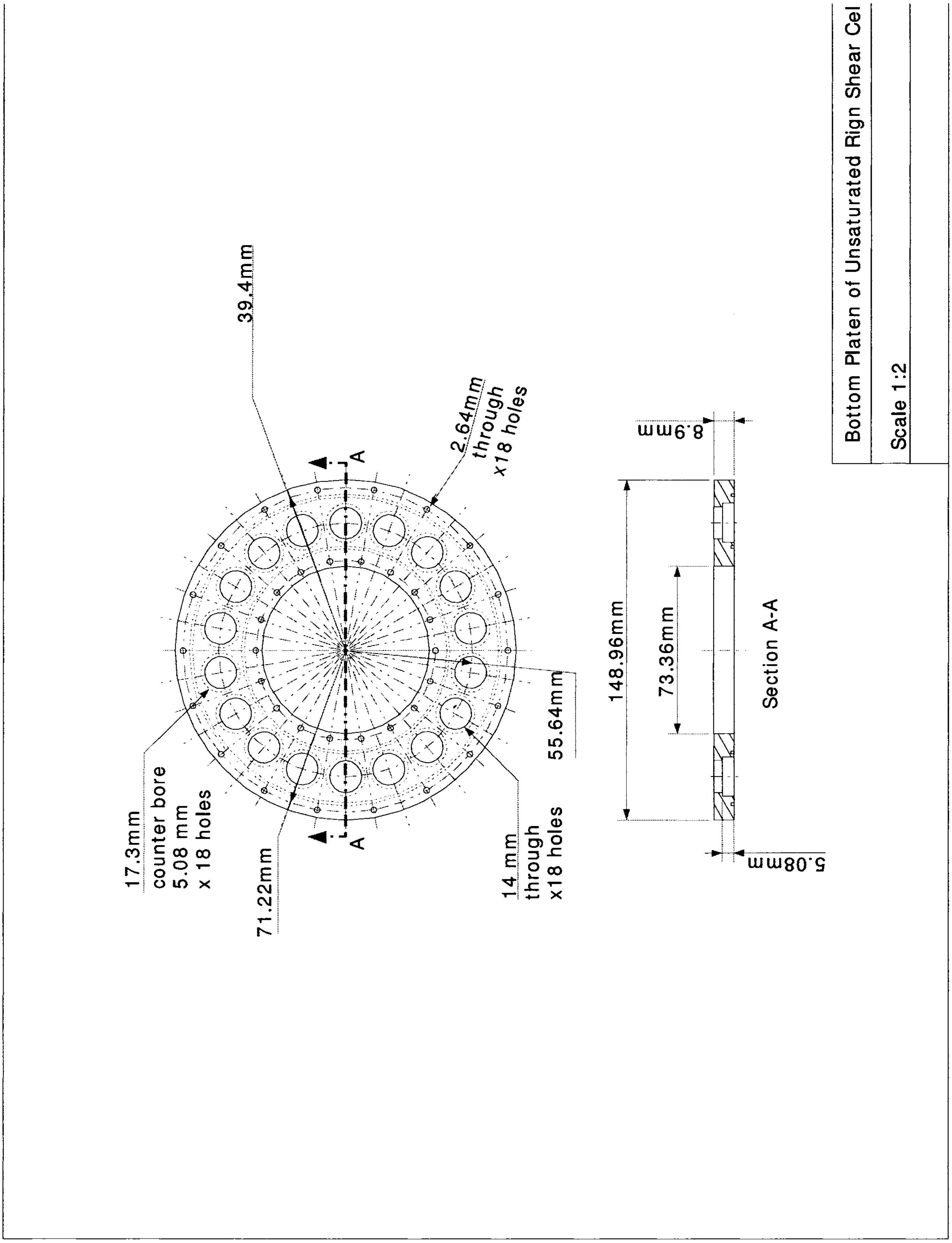
Bottom Platen of Unsaturated Rign Shear Cel
Scale 1:2
39.4mm
2.64mm through x18 holes
A
8.9mm
148.96mm
73.36mm
Section A-A
55.64mm
14 mm through x18 holes
5.08mm
71.22mm
17.3mm counter bore 5.08 mm x 18 holes

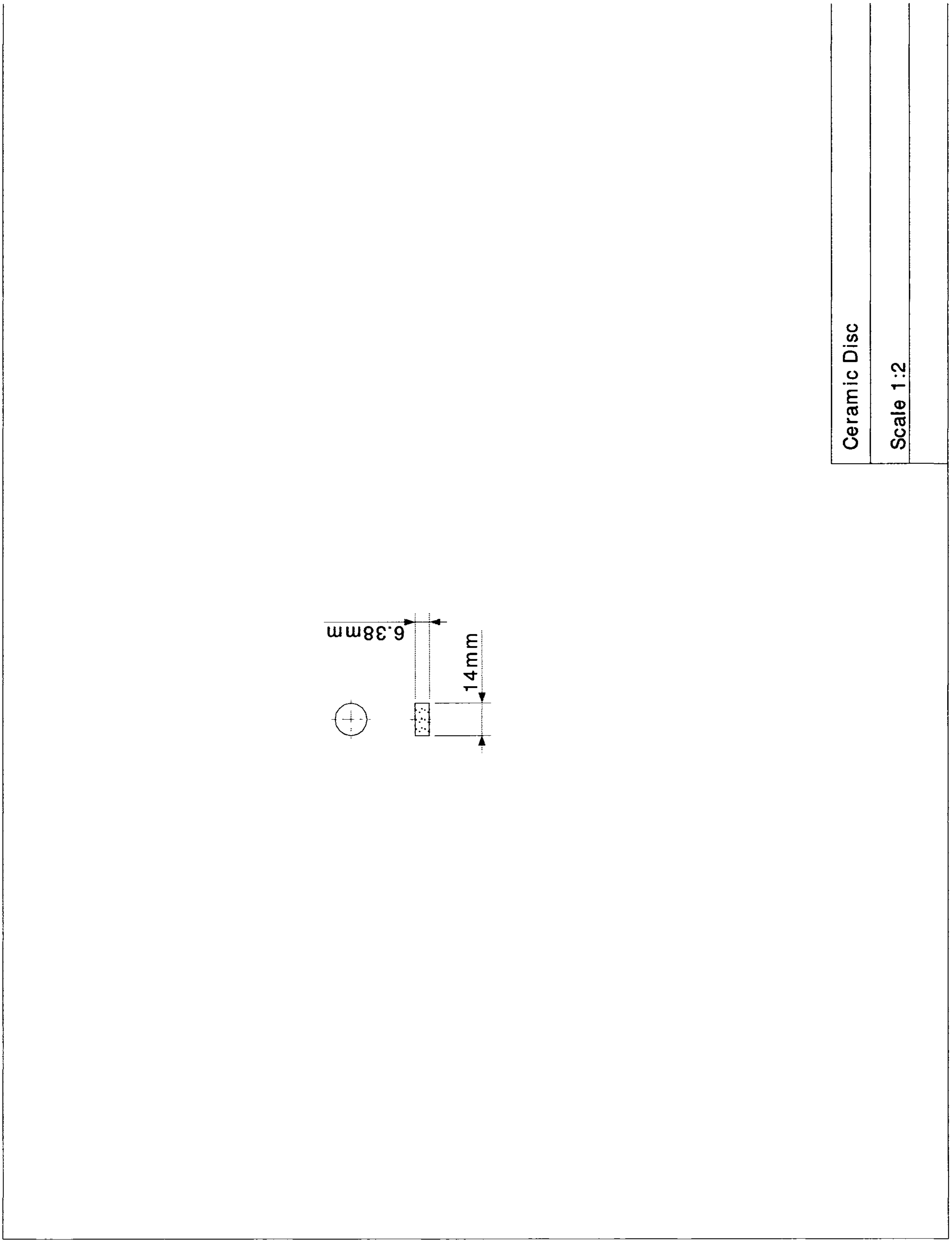

Ceramic Disc
Scale 1:2
6.38mm
14mm

Drawings of original Ring Shear Cell

Appendix A-VIII

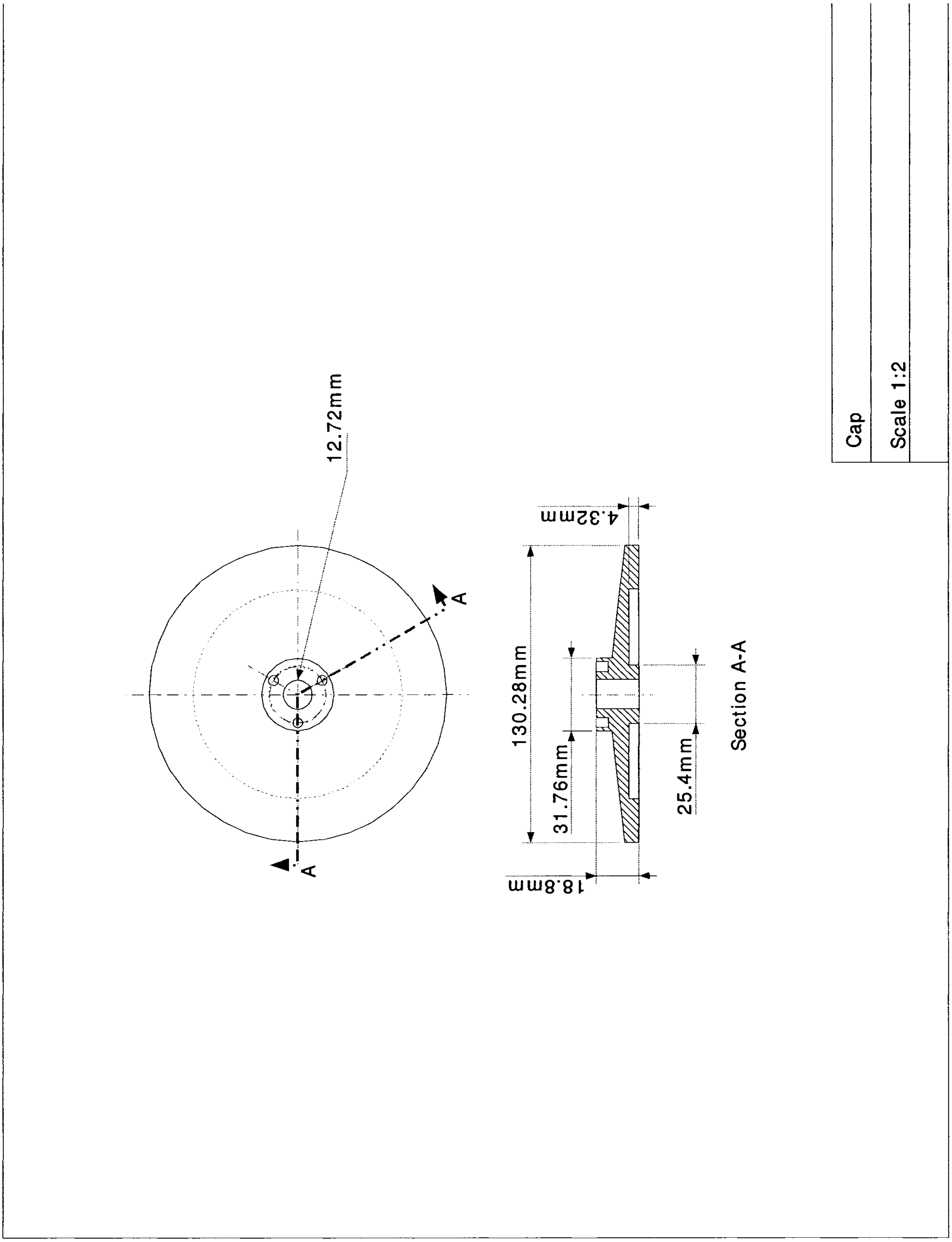

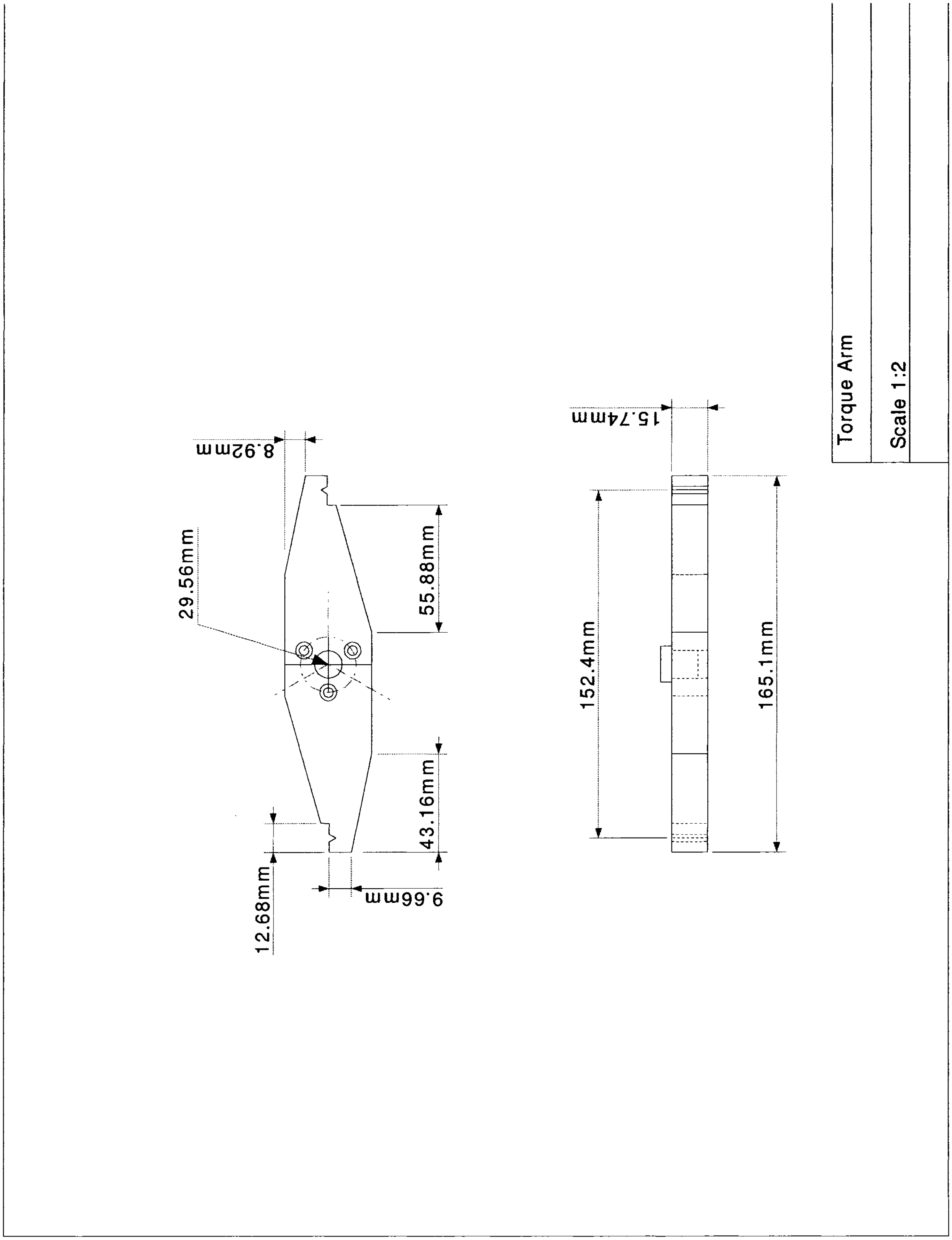
Torque Arm
Scale 1:2
8.92mm
29.56mm
55.88mm
43.16mm
12.68mm
9.66mm
15.74mm
152.4mm
165.1mm

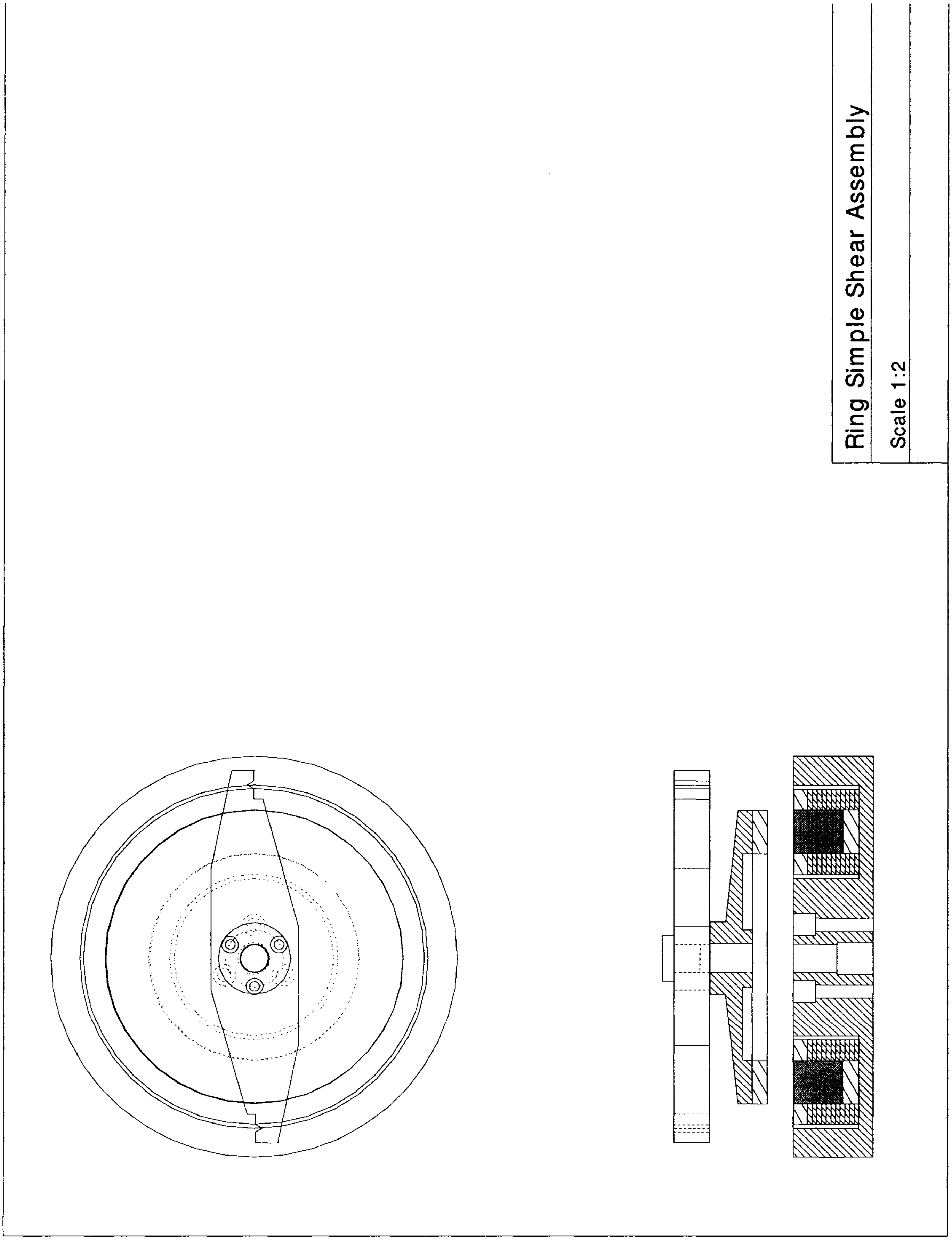
Ring Simple Shear Assembly
Scale 1:2

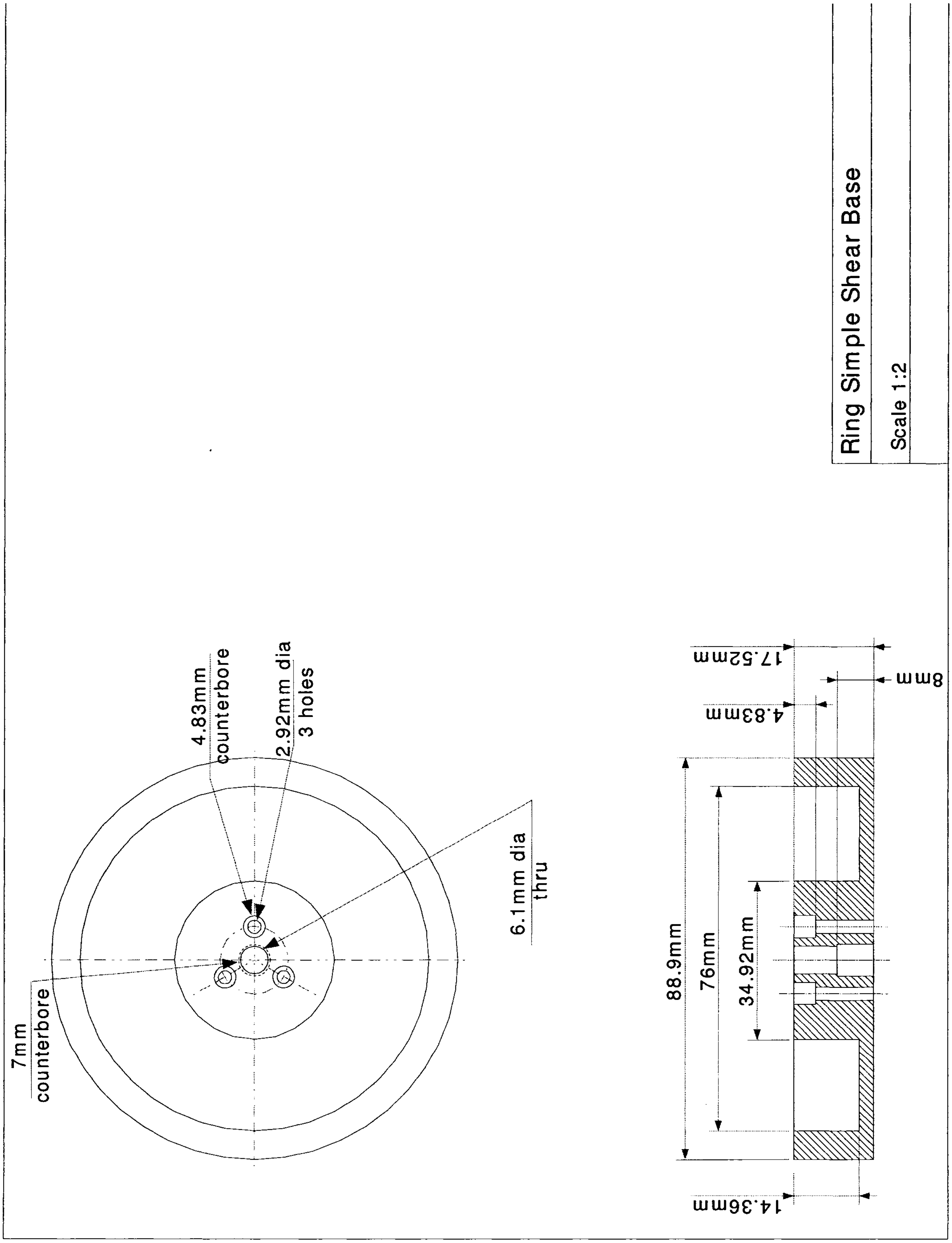
Ring Simple Shear Base
Scale 1:2
4.83mm counterbore
2.92mm dia 3 holes
6.1mm dia thru
7mm counterbore
88.9mm
76mm
34.92mm
17.52mm
4.83mm
8mm
14.36mm

APPENDIX B

PROGRAM SOURCE CODE

The following is the source code to the OpenOffice.org Macro used to generate the scales for the pressure gauge.

```
'****************************************************************************
'**                       PRESSURE Scale                              **
'**                                                                       **
'****************************************************************************
dim MyDocument
dim MyDialog

dim Proceed as boolean

dim mm
dim cm
dim m
dim Pa
dim kPa
dim kg
dim g
dim N
dim kN
dim lb
dim psi
dim inch
dim gw
dim s
dim deg
dim pi


Sub Main
      InitializeUnits
      a=dH(100000,100000,0.3,2)
      set MyDocument = ThisComponent
'     DialogLibraries.LoadLibrary("Standard")
      MyDialog=createUnoDialog(DialogLibraries.Standard.Main_Dialog)
      MyDialog.Execute()
      'end
End Sub

Sub InitializeUnits
      mm = 100.
      cm = 10.*mm
      m  = 100.*cm

      s = 1

      kg = 1.
      g = 0.001*kg

      pi = 4* atn(1)
      deg = pi/180
      N = kg*m/s^2

      Pa =N/m^2
      kPa = 1000*Pa
```

```
      gw = 1000*kg/m^3*9.81*m/s^2
End Sub

Function GetControl(Dialog, ControlName)
      dim Result
      dim Control

      set Control = Dialog.Controls(GetControlIndex(Dialog, ControlName))
      set result = Control.Model
      GetControl = Result
End Function

Function GetControlIndex(Dialog, ControlName)
      dim i
      dim CurrentControl
      dim Done                as boolean
      dim CurrentName


      i = lbound(Dialog.Controls)
      while (i < ubound(Dialog.Controls)+1) and not Done
            set CurrentControl = Dialog.Controls(i)
            CurrentName = CurrentControl.Model.Name
            If lcase(CurrentControl.Model.Name) = lcase(ControlName) Then
                  Done = True
            Else
                  i = i + 1
            End if
      wend
      if Done Then
            GetControlIndex = i
      Else
            GetControlIndex = na()
      End if
End Function

Sub DrawScale
      dim Doc
      dim Drawing
      dim LineElement

      dim Size as new com.sun.star.awt.Size
      dim TextSize as new com.sun.star.awt.Size
      dim Position as new com.sun.star.awt.Point
      dim TextPosition as new com.sun.star.awt.Point
'     dim sampleLine as new com.sun.star.drawing.LineShape
'     'dim TitleBox as new com.sun.star.drawing.TextShape

      dim bundle
      dim smallest_spacing               'in mm smallest spacing of lines to be
            drawn
      dim smallest_pressure              'in kPa, smallest pressure increment to
            be drawn, even if very large at low pressures.
      dim current_pressure_increment     'in mm current division.
      dim ScaleLength
```

```
dim LineWidth
dim LongTickLength
dim ShortTickLength

dim Done as boolean

dim L0
dim P0
dim Theta
dim P
dim potential
dim division_pressure
dim condi as boolean
dim MainLine
dim TickLine
dim TickLabel
dim TickLength

dim ResultString


set Doc = ThisComponent
set Drawing = Doc.DrawPages(0)
set MainLine = Doc.createInstance("com.sun.star.drawing.LineShape")

LongTick = 10*mm
ShortTick = 5*mm
smallest_spacing=1.35*mm
smallest_pressure = 1*kPa

smallest_spacing = GetControl(MyDialog,"TickValue").Value*mm
L0= Getcontrol(MyDialog,"L0Value").Value * mm
P0 = Getcontrol(MyDialog,"PressureValue").Value * kPa
theta =  Getcontrol(MyDialog,"AngleValue").Value * deg
ScaleLength     =     dH(GetControl(MyDialog,"ScaleLengthValue").Value      *
      kPa,P0,L0,theta)
MyDialog.endExecute

Size.Width=1
Size.Height=ScaleLength
Position.X=100*mm
Position.Y=0*mm

with MainLine
      .setSize Size
      .setPosition Position
end with
Drawing.add(MainLine)
TextSize.Width=1 :      TextSize.Height =1

set TitleBox = Doc.createInstance("com.sun.star.drawing.TextShape")
Drawing.add(TitleBox)
with TitleBox
      .TextAutoGrowHeight = TRUE : .TextAutoGrowWidth = TRUE
```

```
		.String = "Reference Atmospheric Pressure = " & P0/kPa & " kPa" & "
"
		.String = .String & "Length of Entrapped Air, L0 = " & L0/mm & " mm" &
"		"
		.String = .String & "Angle of Scale from Horizontal = " & theta/deg &
"o"
		TextPosition.X = MainLine.Position.X + 20 * mm + .Size.Height
		TextPosition.Y = (ScaleLength + .Size.Width)/2
		.RotateAngle=int(90*100)
		.setPosition TextPosition
	End With

	Size.Height = 1
	Size.Width = LongTick
	Position.Y = ScaleLength
	set TickLine  = Doc.createInstance("com.sun.star.drawing.LineShape")
	with TickLine
		.setSize Size
		.setPosition Position
	End With
	Drawing.add(TickLine)
	set TickLabel =  Doc.createInstance("com.sun.star.drawing.TextShape")
	'msgbox TextValue.Dbg_Methods

	'TextValue.Value = "Text"

	TextSize.Width = 1
	TextSize.Height = 1
	Drawing.add(TickLabel)
	with TickLabel
		.setSize TextSize
		'.setPosition TextPosition
		.setString("0")
		.TextAutoGrowHeight = TRUE
		.TextAutoGrowWidth = TRUE

		TextPosition.X = Position.X + LongTick + 2*mm
		TextPosition.Y = Position.Y - 0.5 * .Size.Height
		.setPosition TextPosition
	End With

	gauge_pressure = 0
	P = P0 + gauge_pressure
	Do Until done

		smallest_pressure=dP(smallest_spacing,P,L0,theta)
		potential=(10^(cint(log(smallest_pressure/kPa)/log(10)+0.5)))*kPa
		division_pressure=10*potential

		If smallest_pressure <= 0.5*potential then
			smallest_pressure = 0.5*potential
		Else
			smallest_pressure = potential
		End If
```

```
do
      dope = dP(smallest_spacing,P,L0,theta)
      doperatio=dope/potential
      if dP(smallest_spacing,P,L0,theta) > (0.5*potential) then
            smallest_pressure = potential
      end if
      ResultString=""
      for i = 1 to (division_pressure/smallest_pressure)
            gauge_pressure = gauge_pressure +  smallest_pressure
            ResultString    =    ResultString    &    "Line    at    "    &
(gauge_pressure)/kPa & " kPa" & chr$(13)

            set       TickLine               =       Doc.createInstance
("com.sun.star.drawing.LineShape")
            Drawing.add(TickLine)
            Position.Y  =  ScaleLength  -  dH(gauge_pressure,  P0,  L0,
theta)
            if i = (division_pressure/smallest_pressure) Then
                  TickLength = LongTick
                  set       TickLabel        =       Doc.createInstance
("com.sun.star.drawing.TextShape")
                  Drawing.add(TickLabel)
                  with TickLabel
                        .setString(format(gauge_pressure/kPa+1e-
15,"0"))
                        .TextAutoGrowHeight = TRUE
                        .TextAutoGrowWidth = TRUE

                        TextPosition.X = Position.X + LongTick + 2*mm
                        TextPosition.Y   =   Position.Y   -   0.5   *   .
Size.Height
                        .setPosition TextPosition
                  End With
            Else
                  if i = (0.5*division_pressure/smallest_pressure) then
                        TickLength = 0.75 * LongTick
                  else
                        factor = (i * smallest_pressure)/potential
                        factor = factor - int(factor)
                        if factor < 0.001 then
                              awings/Modified    Ring    Simple    Shear
Assembly.wmffactor = 1
                        end if
                        TickLength = ShortTick * factor
                  end if
            end If
            Size.Width = TickLength
            Size.Height = 1
            with TickLine
                  .setSize Size
                  .setPosition Position
            End With
      next i
      ResultString = ResultString & "Label at " & (gauge_pressure)/kPa
& " kPa"
```

```
                  'MsgBox ResultString
                  CumulativeLength = dH(gauge_pressure,P0,L0,theta)
                  if  CumulativeLength  >= ScaleLength then
                        Done = True
                  End if
                  P = P0 + gauge_pressure
                  condi=(gauge_pressure/potential  mod  (10  *  division_pressure)/
            potential > 0) and (not done)
            loop while condi

      Loop
      'end
'     msgbox "Smallest Pressure = " & smallest_pressure/kPa & " kPa"

      end


'Draw main vertical line
      while not Done
      wend
      end
End Sub



Function dP(dH,P0,L0,theta)
      dP = (P0 * dH)/(L0 - dH)+gw*sin(theta)*dH
End Function

Function dH(dP,P0,L0,theta)
      dim K
      dim b
      if theta =0 then
            dH = (dP * L0)/(P0 + dP)
      else
            K = gw*sin(abs(theta))
            b = -(P0+dP+K*L0)
            dH=(-b - sqr(b^2-4*K*dP*L0))/(2*K)
      endif
End Function
```

```
'*****************************************************************************
'**                              METRIC Scale                               **
'**                                                                         **
'*****************************************************************************

option explicit

dim mm
dim cm
dim m
dim Pa
dim kPa
dim kg
dim g
dim N
dim kN
dim lb
dim psi
dim inch
dim gw
dim s
dim deg
dim pi


Sub Main
      InitializeUnits
      set MyDocument = ThisComponent
      MyDialog=createUnoDialog(DialogLibraries.Standard.Metric_Dialog)
      MyDialog.Execute()
End Sub

Sub InitializeUnits
      mm = 100.
      cm = 10.*mm
      m  = 100.*cm

      s = 1

      kg = 1.
      g = 0.001*kg

      pi = 4* atn(1)
      deg = pi/180
      N = kg*m/s^2

      Pa =N/m^2
      kPa = 1000*Pa

      gw = 1000*kg/m^3*9.81*m/s^2
End Sub


Sub DrawMetricScale
      dim Doc
```

```
dim Drawing
dim LineElement

dim Size as new com.sun.star.awt.Size
dim TextSize as new com.sun.star.awt.Size
dim Position as new com.sun.star.awt.Point
dim TextPosition as new com.sun.star.awt.Point

dim bundle
dim smallest_spacing               'in mm smallest spacing of lines to be
      drawn
dim smallest_pressure              'in kPa, smallest pressure increment to
      be drawn, even if very large at low pressures.
dim current_pressure_increment     'in mm current division.
dim ScaleLength

dim LineWidth
dim LongTick
dim ShortTick

dim Done as boolean

dim MainLine
dim TitleBox
dim TickLine
dim TickLabel
dim TickLength
dim TickCount           as long

dim ResultString
dim   CumulativeLength        as long


set Doc = ThisComponent
set Drawing = Doc.DrawPages(1)
set MainLine = Doc.createInstance("com.sun.star.drawing.LineShape")

LongTick = 10*mm
ShortTick = 5*mm

ScaleLength = GetControl(MyDialog,"ScaleLength").Value * mm

Size.Width=1
Size.Height=ScaleLength
Position.X=100*mm
Position.Y=0*mm

with MainLine
      .setSize Size
      .setPosition Position
end with
Drawing.add(MainLine)
TextSize.Width=1 :      TextSize.Height =1

set TitleBox = Doc.createInstance("com.sun.star.drawing.TextShape")
```

```
Drawing.add(TitleBox)
with TitleBox
      .TextAutoGrowHeight = TRUE : .TextAutoGrowWidth = TRUE
      .String = "MILLIMETRES"
      TextPosition.X = MainLine.Position.X + 20 * mm + .Size.Height
      TextPosition.Y = (ScaleLength + .Size.Width)/2
      .RotateAngle=int(90*100)
      .setPosition TextPosition
End With

Size.Height = 1
Size.Width = LongTick
Position.Y = ScaleLength
set TickLine  = Doc.createInstance("com.sun.star.drawing.LineShape")
with TickLine
      .setSize Size
      .setPosition Position
End With
Drawing.add(TickLine)
set TickLabel =  Doc.createInstance("com.sun.star.drawing.TextShape")
'msgbox TextValue.Dbg_Methods

'TextValue.Value = "Text"

TextSize.Width = 1
TextSize.Height = 1
Drawing.add(TickLabel)
with TickLabel
      .setSize TextSize
      .setString("0")
      .TextAutoGrowHeight = TRUE
      .TextAutoGrowWidth = TRUE

      TextPosition.X = Position.X + LongTick + 2*mm
      TextPosition.Y = Position.Y - 0.5 * .Size.Height
      .setPosition TextPosition
End With

Do Until done
      TickCount=TickCount + 1

      set TickLine  = Doc.createInstance("com.sun.star.drawing.LineShape")
      Drawing.add(TickLine)
      Position.Y = ScaleLength - TickCount*mm

      if (TickCount mod 10) = 0 Then
            TickLength = LongTick

            set           TickLabel           =            Doc.createInstance
      ("com.sun.star.drawing.TextShape")
            Drawing.add(TickLabel)
            with TickLabel
                  .setString(format(TickCount,"0"))
                  .TextAutoGrowHeight = TRUE
                  .TextAutoGrowWidth = TRUE
```

```
                        TextPosition.X = Position.X + LongTick + 2 * mm
                        TextPosition.Y = Position.Y - 0.5 * .Size.Height
                        .setPosition TextPosition
                  End With
            Elseif (TickCount mod 5) = 0 then
                  TickLength = 0.75 * LongTick
            Else
                  TickLength = ShortTick
            End If



            Size.Width = TickLength
            Size.Height = 1
            with TickLine
                  .setSize Size
                  .setPosition Position
            End With
            CumulativeLength = TickCount * mm
            if  CumulativeLength  >= ScaleLength then
                  Done = True
            End if
      Loop
      MyDialog.EndExecute()
End Sub
```

APPENDIX C

COMPARING TRIAXIAL AND DIRECT SHEAR TEST RESULTS ON UNSATURATED SOILS

Triaxial and direct shear tests follow very different stress paths unless the triaxial test is stress path controlled. Typically, a series of triaxial tests on unsaturated soils will be conducted at a constant net normal stress, while the suction is incremented to predetermined values. This generates failure circles similar to those show in Figure C.1.

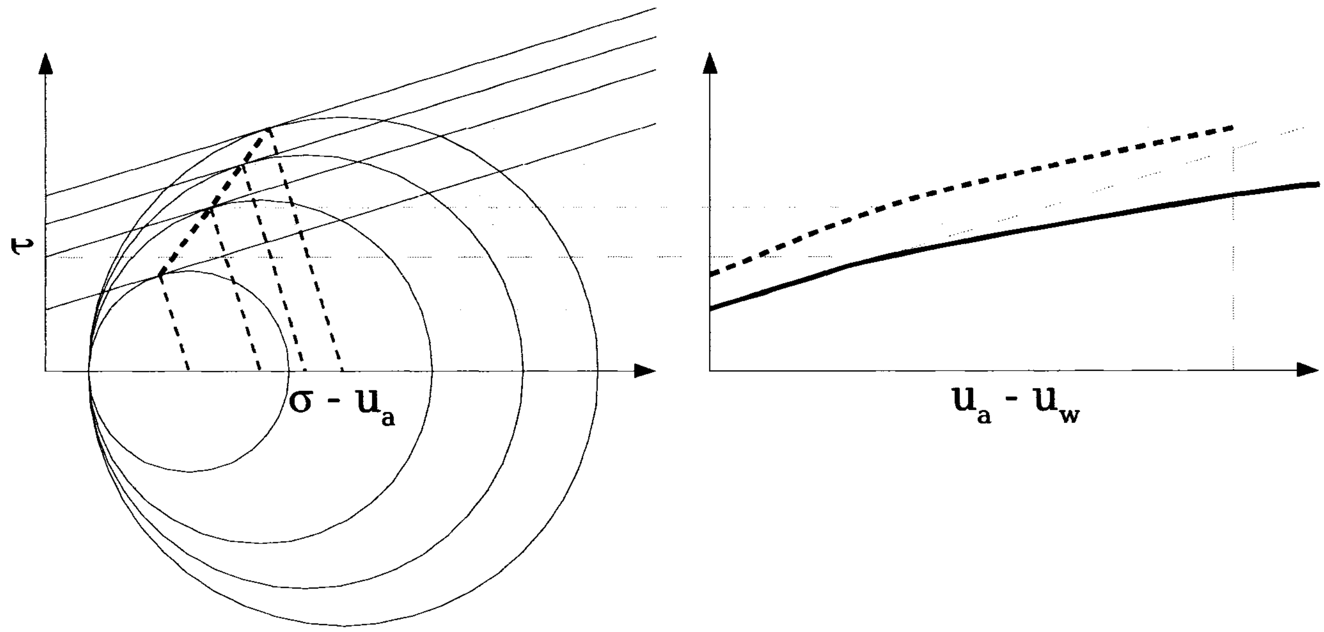

Figure C.1 A series of triaxial tests on an unsaturated soil at the same net confining pressure (σ_3-u_a) for equidistant matric suction increments.

As it can be seen from the figure, the net normal stress on the plane of failure (bold dashed line) is not constant for all tests, although the net confining pressure, (σ_3-u_a), is. Since the net normal stress at failure is not constant, the failure envelope it generates in the matric suction space is not parallel to the failure envelope with respect to suction (continuous black line). Therefore, the triaxial test results do not directly generate a failure envelope in the matric suction versus shear strength axis.

To generate a failure envelope at a constant net normal stress from triaxial data, it is necessary to calculate the contribution to shear strength due to suction only. To do this, we subtract ($c' + (\sigma_n - u_a) \tan \phi'$) from the shear strength on the plane of failure of each Mohr circle (Figure C.2). The dashed failure envelope in the shear strength versus matric suction plane is now parallel to the failure envelope in suction space for a net normal stress of 0 (its intercept is equal to c'). To generate the failure envelope at a given net normal stress (on the plane of failure) it is only necessary to add that single fixed ($c' + (\sigma_n - u_a) \tan \phi'$). Of course, this assumes that the net normal stress acting on the plane of failure has no influence on the failure envelope, since the actual normal stress acting on the plane of failure was different for each test.

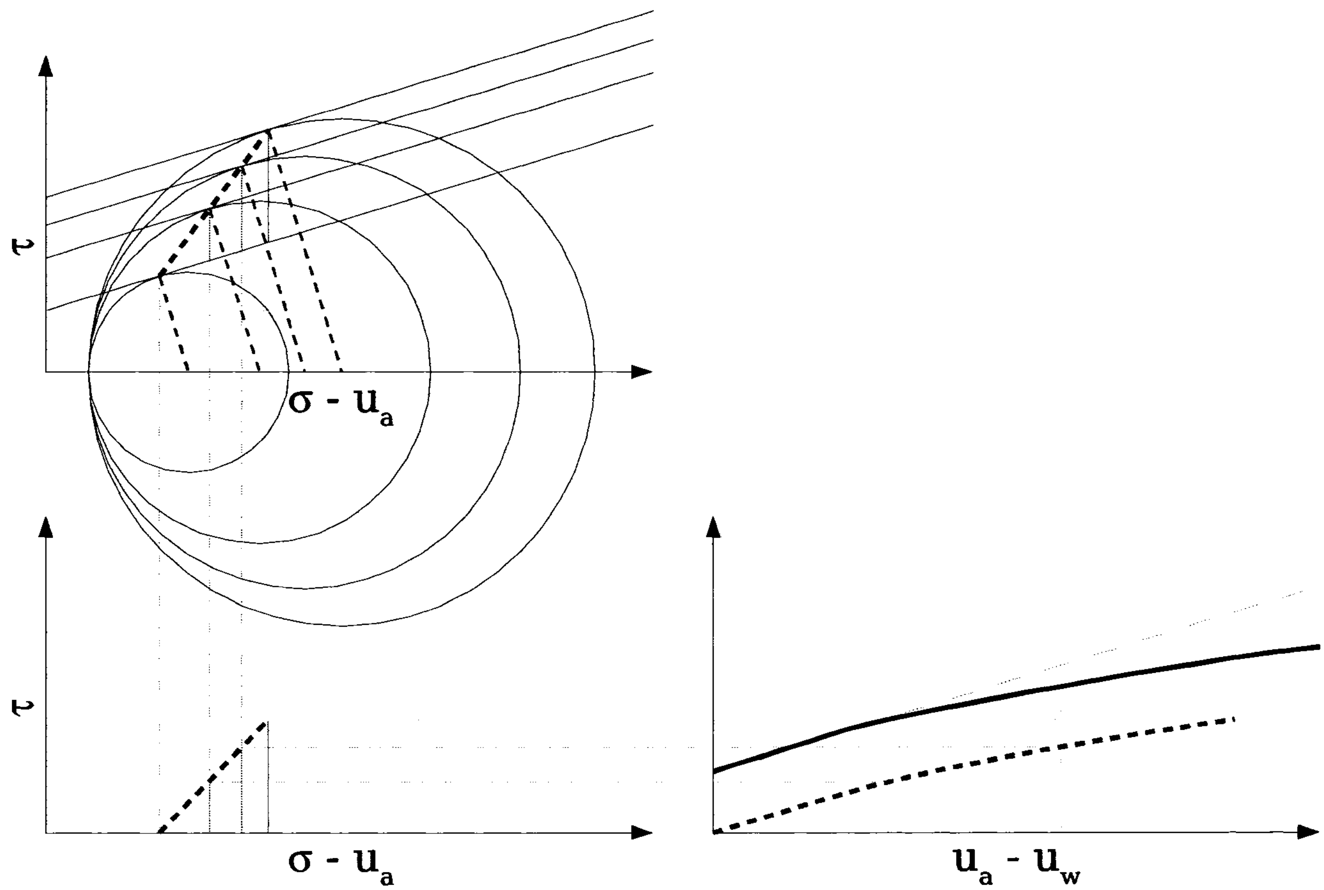

Figure C.2 Isolating the contribution due to suction from a series of triaxial test data.

In the case of the direct shear box, a series of tests with a constant net normal stress is represented in Figure C.3. In this case, the net normal stress on the plane of failure for all tests is the same, therefore the failure envelope generated in the τ vs $(u_a - u_w)$ plane is parallel to the failure envelope at 0 net normal stress. The failure envelope is a true failure envelop in the suction space, and no special construction technique is required to generate it.

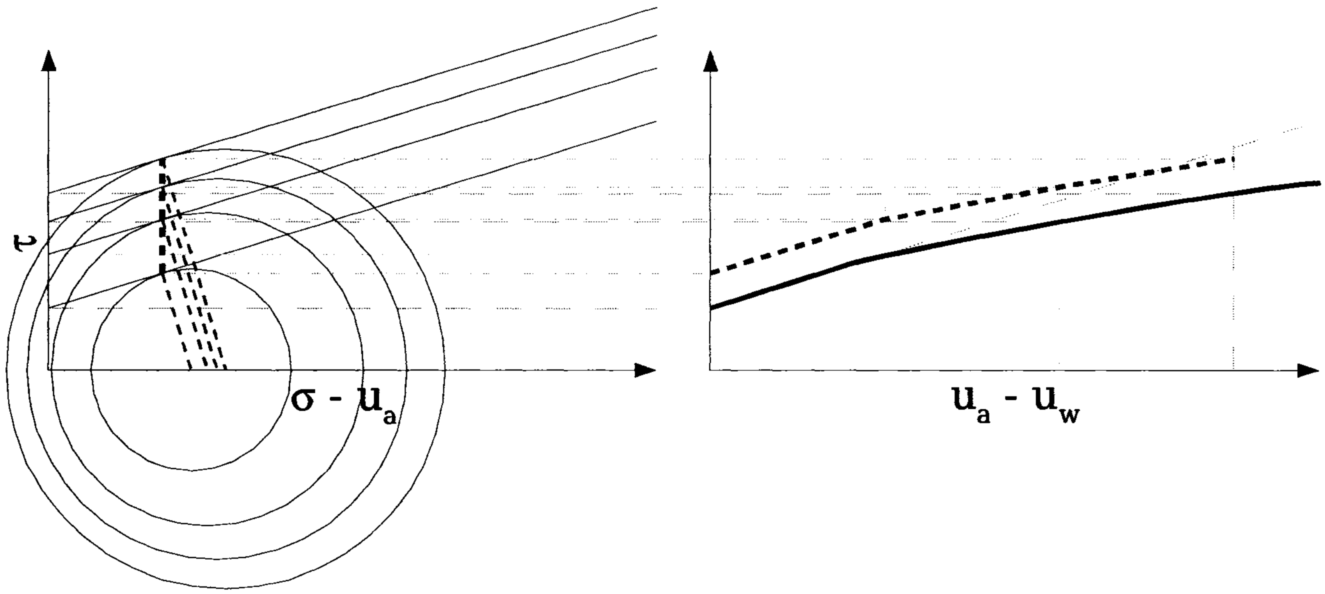

Figure C.3 Generation of a failure envelope in the τ vs ($u_a - u_w$) plane using direct shear tests at a constant net normal stress.

To compare both data sets, the ($c' + (\sigma_n\text{-}u_a)\ tan\ \phi'$) term corresponding to the constant net normal stress of the direct shear test can be added as a constant to the suction contribution to shear strength from the triaxial tests. That will shift the curve up so that it matches the direct shear test results if the two failure envelopes are indeed parallel between them, and with the envelope at net normal stress of 0 (Figure C.4).

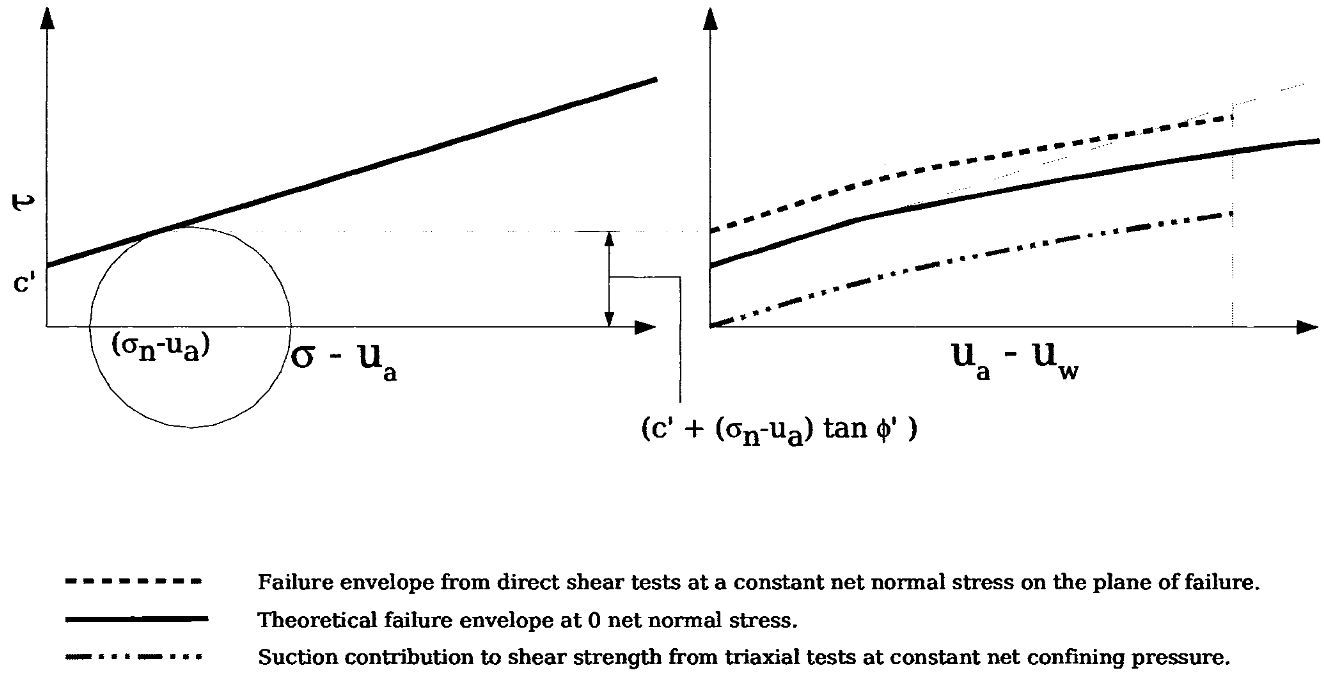

Figure C.4 Combining the results from *triaxial contribution to suction* + (c' + $(\sigma_n$-$u_a)$ *tan* ϕ') from direct shear tests and comparing to direct shear tests results.

If there is no effect of the net confining stress on the failure envelope with respect to matric suction, then the curves generated from direct shear tests and those obtained from the suction contribution to shear from triaxial tests (incremented by ($c' + (\sigma_n$-$u_a)$ *tan* ϕ')) should overlap. If the net normal stress does have an influence then they will not. The direct shear test provides nices slices perpendicular to the τ vs $(\sigma_3 - u_a)$ plane, while the slices produced by the triaxial tests are not perpendicular to this plane, therefore using the construction method described above would not provide a proper failure envelope in the τ vs $(u_a - u_w)$ plane. The 3D failure envelope of the triaxial tests would still be valid of course, and probably using a single confining stress provides a better identical condition, but it would not be correct to use it to generate a virtual slice perpendicular to the τ vs $(\sigma_3 - u_a)$ plane.